PHYSICOCHEMICAL INVESTIGATIONS ON MICROHETEROGENOUS SYSTEMS WITH SPECIAL REFERENCE TO SPECTROSCOPIC STUDIES

A Thesis submitted to the University of North Bengal

For the Award of

Doctor of Philosophy in Chemistry

BY

MOUMITA CHAKRABORTY

GUIDE

DR. AMIYA KUMAR PANDA

Department of Chemistry

University of North Bengal

2013

DECLARATION

I declare that the thesis entitled "PHYSICOCHEMICAL INVESTIGATIONS ON MICROHETEROGENOUS SYSTEMS WITH SPECIAL REFERENCE TO SPECTROSCOPIC STUDIES", has been prepared by me under the guidance of Dr. Amiya Kumar Panda, Associate Professor, Department of Chemistry, University of North Bengal.

No part of this thesis has formed the basis for the award of any degree or fellowship previously.

Moumita Chakraborty

Department of Chemistry

University of North Bengal

Darjeeling-734013

West Bengal, India

CERTIFICATE FROM THE GUIDE

I certify that Ms. Moumita Chakraborty has prepared the thesis entitled "PHYSICOCHEMICAL INVESTIGATIONS ON MICROHETEROGENOUS SYSTEMS WITH SPECIAL REFERENCE TO SPECTROSCOPIC STUDIES", for the award of Ph.D. degree of the University of North Bengal, under my guidance. She has carried out the work at the Department of chemistry, University of North Bengal.

Amiya Kumar Panda

Dedicated to my Parents

ACKNOWLEDGEMENT

The research work, as presented in the dissertation entitled "PHYSICOCHEMICAL INVESTIGATIONS ON MICROHETEROGENOUS SYSTEMS WITH SPECIAL REFERENCE TO SPECTROSCOPIC STUDIES", has been carried out under the supervision of Dr. Amiya Kumar Panda, Department of Chemistry, University of North Bengal. I am immensely grateful to him for his constant inspiration and guidance during the tenure of my PhD work.

I bid my gratitude to the authority of University of North Bengal for providing the facilities and accessibilities related to the research work. Financial supports from the University Grants Commission (UGC), Govt. of India, and Department of Science and Technology, Govt. of India (INSPIRE Fellowship) are gratefully acknowledged.

I convey my sincere appreciation to all the faculty and staff members of the Department of Chemistry, University of North Bengal. Valued guidance, advice and suggestions from Prof. Chien-Hsiang Chang, Department of Chemical Engineering, National Cheng Kung University, Tainan, Taiwan is gratefully acknowledged.

I acknowledge them who have directly and indirectly inspired me to make this work happen. My heartiest thanks go to my fellow colleagues Kausik, Banita, Sujoy, Sudarshana, Pritam, Biplab, Prasant and Gourav for their cooperation and constant support.

The work would not have materialized without the blessings and support of my parents and encouragement of my sister.

Finally, I am ever grateful to my husband Mr. Ratul Chowdhury for his unconditional love, support and patience.

ABSTRACT

The thesis entitled "PHYSICOCHEMICAL INVESTIGATIONS ON MICROHETEROGENOUS SYSTEMS WITH SPECIAL REFERENCE TO SPECTROSCOPIC STUDIES" describes the spectroscopic investigation of dye / probe / aggregates comprising three specific systems viz., soft, flexible and rigid.

The soft system describes the studies on the interaction between an anionic xanthene dye, eosinY with cationic surfactants in aqueous medium.

The second category, i.e., the flexible system describes the interaction of eosinY with three different cationic polymers. This was done in order to understand the nature of interaction involved between the dye and macromolecules.

The third category is associated with two different rigid systems, viz.,colloidal silica and surfactant stabilized colloidal dispersions of silver bromide in aqueous medium. This set of work has been categorized into two:

(a) UV-visible absorption and emission spectral studies in order to identify the characteristics of the excited state H-bonding between colloidal silica and 7-hydroxycoumarin in aqueous medium.

(b) The second category surfactant stabilized silver bromide nanoparticles were synthesized and characterized using different techniques.

Photophysical behaviour of the anionic xanthene dye, eosin Y (EY) was investigated in solvents of different polarity as well as in the presence of aqueous cationic surfactants. By suitably analyzing the spectral data different solvatochromic parameters were analyzed and subsequently interpreted. Effects of aqueous surfactant solution on the spectral behaviour of dye were compared with that of the solvent induced properties of EY. A red shift, both in the absorption and steady state fluorescence spectra, for EY was observed with decreasing solvent polarity. EY tends to dimerize in aqueous medium specially in the higher concentration range (> 10μM). Extent of EY dimerisation depended on solvent polarity. Cationic surfactants hindered the dimerisation process of EY, as evident

from the lower dimerisation constant (K_D) values. Dye-surfactant interaction constants were evluated at different temperatures (298 – 318K) and subsequently the thermodynamic parameters of the interaction process, viz., changes in standard free energy (ΔG^0), enthalpy (ΔH^0) and entropy (ΔS^0) were derived from the spectral data. Stokes shifts were calculated and correlated with the polarity of the medium. A red shift in the fluorescence spectra occurred with the increasing surfactant concentration. Fluorescence of EY was initially quenched by the cationic surfactants in their pre-micellar region. Fluorescence quenching was found to be of Stern-Volmer type where the excited state lifetime of EY remained unchanged in different surfactant media. However, upon further addition of surfactant intensity of the red shifted band increased which eventually attained a continuum. Fluorescence anisotropy value of EY increased non linearly in the post micellar region of surfactants.

In the second part of the thesis absorption and emission spectral behaviour of eosinY was investigated to perceive the nature and extent of interaction with three different cationic polyelectrolytes, viz., poly[diallyldimethyl ammonium] chloride (PDMDAAC), N,N-dimethyl-N-dodecyl derivative of hydroxyl ethyl cellulose (LM200) and N,N-dimethyl-N-methyl derivative of hydroxyl ethyl cellulose (JR400). Both the electrostatic and hydrophobic forces were associated in the interaction processes. Interaction constant and stoichiometry of the dye-polymer aggregates in their ground states were evaluated by analyzing the absorption spectra at different concentration of the polymers (with a fixed dye concentration). Also, the thermodynamic parameters for the interaction process were evaluated. Extent of dye-polymer interaction followed the sequence: PDMDAAC>JR400> LM200. Excited state interaction phenomena were investigated by steady state fluorescence spectroscopy, anisotropy and excited state lifetime measurements. There was no significant change in the excited state lifetime of EY for all the three added polymers. Stern-Volmer quenching constants, also the excited state interaction constant of the dye-polymer aggregates, were calculated using standard method. Orientation of the dye molecule around the polymer matrix could have been predicted from the anisotropy measurements.

Third part of the work describes the absorption and emission spectroscopic investigation, combined with FTIR studies, on the interaction of 7-hydroxycoumarin (7HC) and aqueous nanocolloidal dispersion of silica. Attempts were made to identify the characteristics of excited state H-bond formed between colloidal silica and 7HC. Both the absorption and emission spectra of 7HC depended on the concentration of silica. In the lower concentration range of silica, absorbance of 7HC decreased with increasing silica concentration. On the contrary, in the higher concentration range, there occurred a bathochromic shift in the absorption spectra of 7HC. Fluorescence behaviour followed an opposite trend compared to the absorption spectra. It is proposed that in the lower concentration range, excited state H-bond was formed between 7HC and colloidal silica. In the higher concentration range, decrease in fluorescence intensity was due to the self quenching of adsorbed dye molecules over silica surface following the mechanism of Homo Förster resonance energy transfer (HFRET). Results were correlated with the size and surface charge of colloidal silica as measured by dynamic light scattering and zeta potential studies.

Last part of the work describes the synthesis and characterization of colloidal dispersions of silver bromide (AgBr) in aqueous surfactant medium. AgBr nanoparticles were prepared using a surfactant-assisted synthesis approach with hexadecyltrimethylammonium bromide (CTAB). The surfactant acted both as source of bromide ion as well as the stabilizing agent. Upon progressive addition of silver nitrate to aqueous CTAB solution, stable AgBr dispersions were obtained. Formation of surfactant cation (CTA^+) stabilized AgBr was confirmed by way of XRD, FTIR and NMR studies. Thermal behaviour of the isolated nanoparticles was investigated by differential scanning calorimetry (DSC) and thermal gravimetric analysis (TGA), where the occurrence of phase transition in the surfactant stabilized nanoparticles was observed. Kinetics of the particle growth was investigated by dynamic light scattering measurements, which predicted the formation of surfactant bilayered structures associated with the nanoparticles of AgBr. Band gap of the nanoparticles was determined by suitably analysing the UV-visible spectral data, which concluded that the particles behaved like insulators. Morphology of the particles, studied by TEM

measurements, was found to be spherical. Finally, enthalpy of formation of surfactant stabilized AgBr, determined calorimetrically, was found to be dependent on the concentration of the precursors.

PREFACE

The present dissertation deals with the physicochemical investigations on microheterogenous systems with special reference to spectroscopic studies. The dissertation begins with introduction and corresponding literature survey. The reported information of different microheterogenous systems in a general way have been reviewed followed by a description of the scope and perspective.

Although many reports on the dye-surfactant interactions are available in the literature, however, systematic investigations on the photophysics of an anionic xanthene dye eosinY (EY) in the presence of different cationic surfactants and also in the solvents of different polarity are not common. Therefore, detailed investigations on the spectral behaviour of EY with reference to the above were considered to be important. Studies involving oppositely charged dye-polymer aggregates can shed light in understanding the interaction mechanism and thus explore the yet to be known aspects of different physicochemical decolourisation processes. Several reports are available in literature describing the interaction between silica and a number of dyes. However, studies on the interaction of colloidal silica with 7-hydroxycoumarin are not common. Therefore, a detailed spectral investigation on the absorption and fluorescence spectra of dye-silica aggregates are warranted for better technological applications as well as from the fundamental understanding point of view. Despite manifold applications of AgBr nanoparticles it is difficult to obtain stable colloidal dispersions of AgBr especially in the aqueous medium. A simple one–pot synthesis approach in obtaining stable AgBr nanoparticles in aqueous media in the presence of a cationic surfactant (hexadecyltrimethylammonium bromide) was adopted. Synthesized nanoparticles were characterized by different techniques, viz., XRD, FTIR, NMR, conductometric titration, UV-visible spectroscopy, dynamic light scattering, DSC-TGA, isothermal titration calorimetry and TEM measurements.

The obtained results and the related observations have been summarized followed by conclusions.

The dissertation then follows the basic data and off-prints of the published papers.

TABLE OF CONTENTS

LIST OF TABLES

Item **Page No.**

LIST OF FIGURES AND SCHEMES

CHAPTER 1

INTRODUCTION

INTRODUCTION

1. General overview of dye

A dye is a coloured substance with an affinity to bind on to a substrate on which it is applied. An aqueous medium is usually preferred as dispersion medium for dye formulation and the dyes require mordant to improve the fastness of their adsorption / binding onto the substrate of interest. Dyes can be defined as coloured ionising and aromatic organic compounds with affinity towards the substrate to which they are applied. Dyes are applied to numerous substrates, e.g., textile, leather, plastic, paper, etc. One of the main characteristics of dye is that it must get completely or at least partially soluble in which it is being put to.

There are different ways of classification for dye molecules. Some of them are mentioned below:

i. Organic / inorganic.
ii. Natural / synthetic.
iii. By area and method of application.
iv. Chemical classification: based on the nature of their respective chromophores.
v. By nature of the electronic excitation (i.e., energy transfer contents, absorption colorants and fluorescent colorants).
vi. According to the method of dyeing.

By the nature of their chromophore, dyes can be chemically classified into different categories:

i. Acridine dyes and its derivates
ii. Anthraquinone dyes and their derivates
iii. Arylmethane dyes
iv. Azo dyes: based on -N=N- azo structure
v. Diazonium dyes: based on diazonium salts
vi. Nitro dyes: based on a $-NO_2$ (nitro) functional group
vii. Nitroso dyes: based on a -N=O (nitroso) functional group
viii. Phthalocyanine dyes and derivatives of phthalocyanine

ix. Quinone-imine dyes and derivatives of quinone
x. Thiazole dyes and derivatives of thiazole
xi. Xanthene dyes, derived from xanthene

Dyes have become one of the indispensable ingredients for a variety of applications. From acting as colorants for plastics, textile dyeing industries and the highly sophisticated biotechnology industry, dyes are touching our life everywhere. Dyes are also used by industries for inks and tinting [2]. Other industries where dyes are used in a variety of products include paper and pulp[3], adhesives, art supplies, beverages[4], construction, cosmetics, food[5], glass, ceramics, paints[6], polymers, soap, wax and biomedicine[7], etc. Dyes are also used as probes to understand the microheterogeneity of compartmentalized systems, viz., micelles[8], reverse micelles[9], microemulsion[10], polymers[11], nanoparticles[12], etc. Dye aggregates are useful in developing light-harvesting arrays for artificial photosynthetic systems. Use of such dye aggregates as light-harvesting antennas as well as photosensitizers in photoelectrochemical cells are available in literature[13,14]. Basic understanding of dye aggregation over nanoparticle surface as well as the excited-state interaction with the semiconductor support is important in developing efficient photoelectrochemical solar cells[15].

Xanthene dyes are those containing xanthylium as the chromophore with amino or hydroxyl groups meta to the oxygen as the usual auxochromes. Xanthene dyes are most commonly used synthetic dyes. Xanthene derivatives are used as sensitizers for organic photochemical reactions and in photochemical cells [16]. They are important because of their brilliant hues and shades. They are generally very strong, with much higher oscillator strengths [17]. As a consequence of their rigid chromophoric nucleus, xanthenes are often fluorescent. They are used for the direct dyeing of wool and silk and mordant dyeing of cotton. Paper, leather, woods, food, drugs and cosmetics are dyed with xanthene dyes [18]. Xanthene is the parent heterocycle of fluorescein and its derivatives.

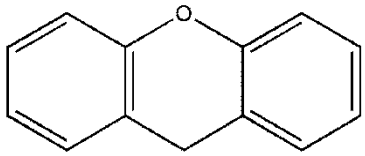

Scheme 1. Schematic representation of xanthene dye.

Xanthene dyes are divided into three subgroups: fluorenes, fluorones and rhodols. Fluorenes and fluorones contain dyes of importance in histotechnology, the rhodols do not.

i. Fluorene dyes: The pyronin subgroup of fluorenes has the general formula shown below. The dyes pyroninY and pyronin B belong to this category of dyes.

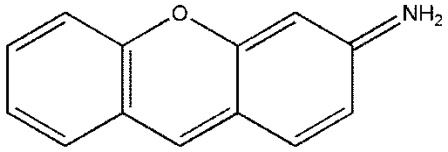

Scheme 2. General formula of pyronin subgroup of fluorene dye.

The rhodamine subgroup of fluorenes (e.g., rhodamine B) has the following general formula:

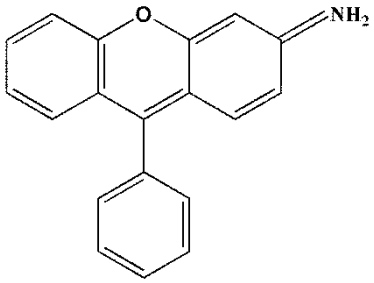

Scheme 3. General formula of rhodamine subgroup of fluorene dye.

ii. Fluorone dyes: Fluorones have the general formula as shown below. The fluorones are sometimes referred to as the eosins, and include many dyes used as counterstains to alum hematoxylin. Their general formula shown above is actually that of fluorescein, from which they are derived.

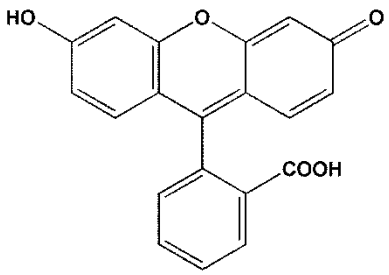

Scheme 4. General formula of fluorone dyes.

1.1. Aggregation of xanthene dye

Aggregation is one of the features of dyes in solution, affecting their colouristic and photophysical properties and is therefore of special interest. Dye molecules possess strong intermolecular van der Waals like attractive forces between them, as a result they generally undergo the process of self-association in solution or at the solid-liquid interface, which is a frequently encountered phenomenon in dye chemistry. The aggregates in solution exhibit distinct changes in the absorption band compared to that of the monomeric species. By suitably analyzing the spectral data formation of different types of aggregates has been proposed. The bathochromically shifted bands are known as J-bands after the name of E.E. Jelley [19]. On the other hand, hypsochromically shifted bands are commonly known as H-bands[20]. Aggregation behaviour of the cyanine dyes have extensively been studied as they are the best known self-aggregating systems. It is

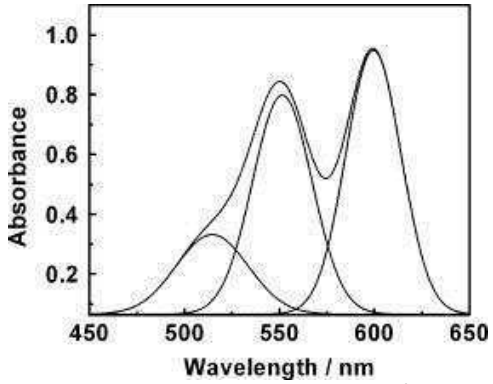

Figure 1. Deconvoluted absorption spectra of 10.0 μmol dm^{-3} PIN in water obtained by fitting the absorbance data with Gaussian multi-peaks function. Three overlapping spectral components were found at 600 nm (for monomer), at 552 nm (for dimer) and at 515 nm (for higher aggregates of PIN) [22].

well known that the amphipathic dyes tend to aggregate even in the dilute regime, leading to the formation of dimer, and sometimes even higher aggregates[21-23]. Dimers as the simplest aggregates are the subject of many studies concerned with the thermodynamics of monomer–dimer equilibrium and photo-physical properties, and therefore being of special interest[21,23-26].

Xanthene dyes are also known to aggregate in aqueous medium when present even in lower concentration (as low as 10μM). Aggregation of these dyes has fundamental consequences in photographic technology, tunable lasers, fluorescence depolarization diagnostics devices and photomedicine[23]. Hence, studies on the aggregation behaviour of xanthene dyes are considered to be significant from the application as well as the fundamental understanding point of view. Geometry of the aggregates can restrict the transition of dye molecules from ground state to excited state. The aggregates in which monomers are stacked in parallel are known as H-aggregates. In this case the transition to the topmost level is allowed.

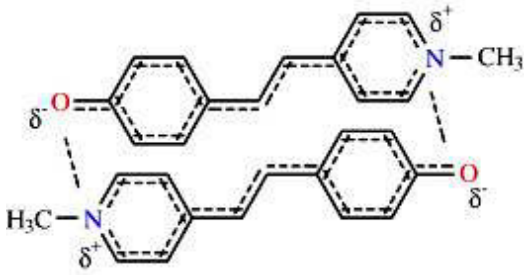

Scheme 5. H-aggregates of merocyanine dye in acetonitrile solvent depending on the type of counterions, adapted from Kolev et al. [27]

The aggregates in which the monomers are arranged in a head-to-tail manner are known as J-aggregates. In this case the only allowed transition is to the lowest split level. In case of aggregates having intermediate geometry, both these transitions are partially allowed and band splitting is observed[26].

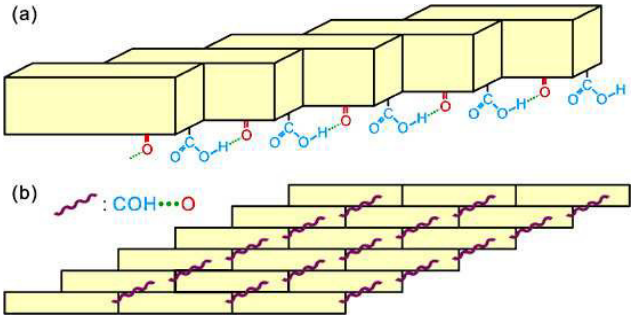

Scheme 6. Merocyanine dye molecules are connected by intermolecular hydrogen bonds (a) and then stacked side-by-side by electrostatic force (b), giving rise to formation of ribbon-shaped J-aggregates [28].

There is always an equilibrium between dimer and monomer. Curve-fitting techniques can be employed to obtain the dimerization constant value of the xanthene dye and to decompose and analyze the absorption spectrum in terms of component bands[21]. At low concentrations, the dye is primarily in the form of monomers and dimers. If we neglect the effect of higher aggregates, the equilibrium between monomer and dimer ($2M \Leftrightarrow D$) is described by the dimerization constant K_D, which is given by the ratio between the molar concentrations of dimers, C_D, and monomers, C_M, at equilibrium:

$$K_D = C_D/C_M^2 \quad (1)$$

Thus, one needs to known values of C_D and C_M, which, in turn, can be determined from the molar absorptivity obtained from the spectral bands of monomeric and dimeric species. The total absorbance of a dye solution per unity of optical length at a given wavelength ($A(\lambda)$) is:

$$A(\lambda) = \varepsilon_M(\lambda).C_M + \varepsilon_D(\lambda).C_D \quad (2)$$

where, ε_M and ε_D represent the molar absorption coefficients of monomeric and dimeric species, respectively, of any band at a wavelength λ.

The monomer and dimer concentrations can be calculated from eq 1 considering the mass balance of dye in the volume dispersion

$$C = C_M + 2\,C_D \quad (3)$$

where, C is the total analytical concentration of dye.

Insertion of eq 1 and 3 into eq 2 affords the following expression:

$$A(\lambda) = \varepsilon_D(\lambda)\left(\frac{C}{2} - \frac{-1\pm\sqrt{1+8.K_D.C}}{8.K_D}\right) + \varepsilon_M(\lambda)\left(\frac{-1\pm\sqrt{1+8.K_D.C}}{4.K_D}\right) \quad (4)$$

By plotting the measured absorbances as a function of dye concentration at any wavelength, the molar absorptivity of monomers, ε_M (λ), and dimers, ε_D (λ), as well as the dimerization constant, K_D, can be calculated using a nonlinear least-squares fitting routine[29].

Solvent effects are important in determining the photophysical properties of dye molecules in solution.

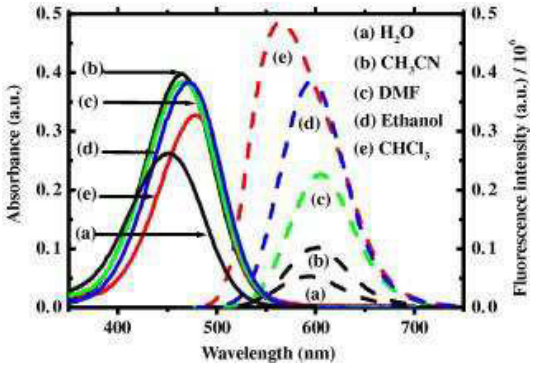

Figure 2. Linear absorption (left) and single-photon fluorescence spectra (right) of trans-4-[p-(N,N-hydroxyethyl) aminino-styryl]-N-methylpyridinium iodide in different solvents at $d_0 = 1 \times 10^{-5}$ mol/l[30].

Aggregation of xanthene dyes is promoted by polar protic solvents while it is impeded by polar aprotic solvents. The hydrogen bonding of solvents also play important role in inducing dye aggregation.

Eosin is a fluorescent red dye resulting from the action of bromine on fluorescein. It is hydroxyl xanthene and can be used to stain cytoplasm, collagen and muscle fibers for examination under the microscope. Structures that stain readily with eosin are termed eosinophilic.

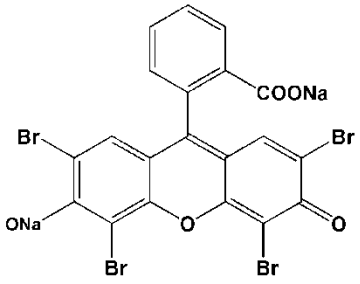

Scheme 7. Structure of eosinY.

There are actually two very closely related compounds commonly referred to as eosin. Most often used is eosin Y. The other eosin compound is eosin B . Eosin Y is a tetrabromo derivative of fluorescein. The spectral behaviour of EY is affected by the solvent polarity, pH of the aqueous medium, surfactant, polymers, colloidal particles, etc.

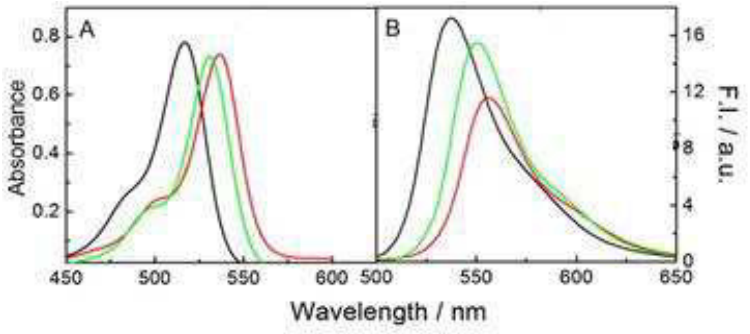

Figure 3. Absorption (A) and steady state emission spectra (B) of eosin Y in ([bmim][MS] ± water)/(Tween 20 + n-pentanol)/n-heptane polar domain-in-oil microemulsion system along with the spectra in pure water and IL + water mixture. Spectra in pure water are shown through the black lines while the green lines correspond to the spectra in IL+water in μE comprising 50mol% IL and $\phi_d = 0.057$ The red lines represent the spectra of eosinY in IL+water mixture[31].

1.2. Brief study on coumarin dyes

Coumarin is a naturally occurring dye, found naturally in many plants. Coumarins owe their class name to 'Coumarou', the vernacular name of the tonka bean (Dipteryx odorata Willd., Fabaceae), from which coumarin itself was isolated back in 1820[32]. Coumarin is classified as a member of the benzopyrone family of compounds, all of which consist of a benzene ring joined to a pyrone ring[33]. There are four main coumarin sub-types: the simple coumarins, furanocoumarins, pyranocoumarins and the pyrone-substituted coumarins. The simple coumarins (e.g. coumarin, 7-hydroxycoumarin and 6,7- dihydroxycoumarin), are the hydroxylated, alkoxylated and alkylated derivatives of the parent compound, coumarin along with their glycosides. As a group, coumarins exhibit interesting fluorescence properties, which include a high degree of sensitivity to their local environment, including polarity and viscosity. This sensitivity has led to their widespread application as sensitive fluorescent probes of a wide range of systems, including homogeneous solvents and mixtures, and heterogeneous materials [34]. Coumarins substituted at position 7 with an electron- donating group are known to

Table 1. Classification of coumarin dyes with features and examples.

Classification	Features	Example
SIMPLE COUMARINS	Hydroxylated, alkoxylated or alkylated on benzene ring.	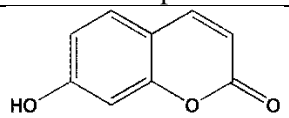 7-Hydroxycoumarin
FURANOCOUMARINS	5-membered furan ring attached to benzene ring. Linear or Angular	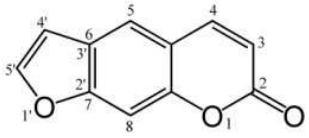 Psoralen
PYRANOCOUMARINS	6-membered pyran ring attached to benzene ring. Linear or Angular	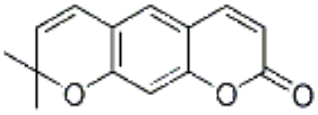 Xanthyletin
PYRONE-SUBSTITUTED COUMARINS	Substitution on pyrone ring, often at 3-C or 4-C positions	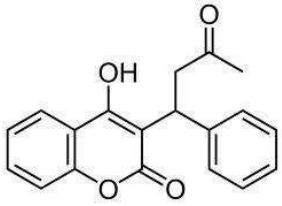 Warfarin

exhibit strong fluorescence [35]. The use of coumarin dimers as photocontrolled molecules opening and closing a silica pore, wherefrom guest molecules are released or in photodegradable polymers has been reported in literature [36].

Coumarin is used in the pharmaceutical industry as a precursor molecule in the synthesis of a number of synthetic anticoagulant pharmaceuticals similar to dicoumarol, the notable ones being warfarin and some even more potent rodenticides that work by the same anticoagulant mechanism. 7-hydroxy coumarin is a widespread natural product of the coumarin family[37]. It is also known as 'Umbelliferone'. Umbelliferone is the parent compound for a large number of natural products. Herniarin (7-O-methylumbelliferone or 7-methoxycoumarin) occurs in the leaves of water hemp (Eupatorium ayapana) and rupturewort. O-Glycosylated derivatives such as skimmin (7-O-β-D-glucopyranosylumbelliferone) occur naturally and are used for the fluorimetric determination of glycoside hydrolase enzymes[38]. There are great similarities between hydroxy derivatives and their ethers. Thus, 7-hydroxy-, 7-methoxy-, and 7-glucoxycoumarin give a family of nearly identical curves[39]. The ultraviolet activity of umbelliferone led to its use as a sunscreen agent, and

an optical brightener for textiles [40]. It has also been used as a gain medium for dye lasers [41]. Umbelliferone can be used as a fluorescence indicator for metal ions [42]. In the majority of human subjects studied, coumarin is extensively metabolised to 7-hydroxycoumarin. The measurement of urinary 7-hydroxycoumarin following an oral dose of coumarin has been employed as a biomarker of human hepatic CYP2A6, the cytochrome P-450 (CYP) isoform which is responsible for coumarin 7 hydroxylation in human liver [43].

2. Surfactant and its classification

The word 'SURFACTANT' is a diminutive form of the phrase "SURface ACTive Agent. Surfactants are usually organic compounds that are amphiphilic, meaning they contain both hydrophobic groups and hydrophilic groups. Therefore, a surfactant contains both a water insoluble component and a water soluble component. Surfactants diffuse in water and adsorb at interfaces between air and water or at the interface between oil and water, in the case where water is mixed with oil. They not only tend to accumulate on the surfaces,but they also alter the properties of the surfaces, being

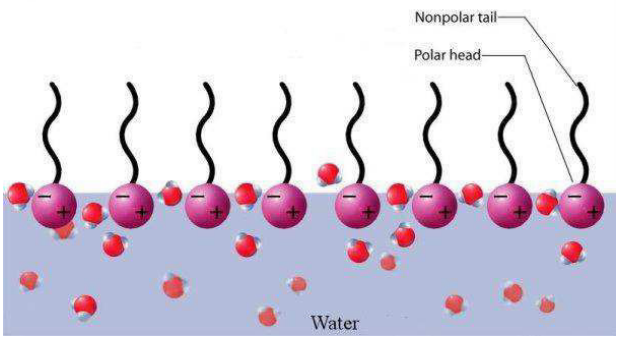

Scheme 8. Schematic representation for the arrangement of surfactant molecules at the air–water interface.

active at the interfaces. In addition, because of their amphipathic structures, they can congregate to form a stabilized entity, called micelle, after the attainment of critical micelle concentration (CMC).

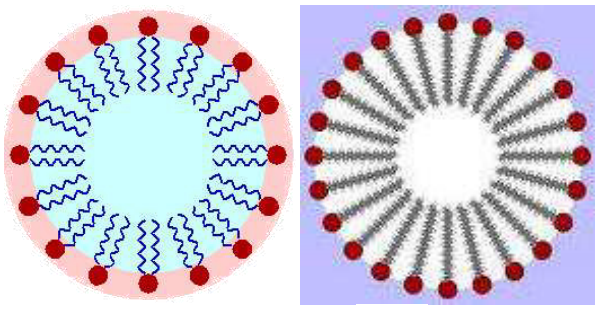

Scheme 9. Schematic representations of normal micelle of (A) double-tailed and (B)single-tailed surfactant in aqueous solution.

Based on the origin, surfactants are classified as follows:

i. **Soap.** Soaps are naturally occurring substances, usually water-soluble sodium or potassium salts of fatty acids. Soaps are made from fats and oils, or their fatty acids, by treating them chemically with a strong alkali [44,45]. They are less soluble in hard water. Examples include sodium palmitate, sodium oleate, sodium cholate, etc.

ii. **Detergent.** Detergents refer to the synthetically prepared surfactants [46]. Alkylbenzenesulfonates, a family of compounds that are similar to soap but are more soluble in hard water, because the polar sulfonate (of detergents) is less likely than the polar carboxyl (of soap) to bind to calcium and other ions found in hard water. Most of the detergents are synthetic. Examples of detergent include sodium dodecylbenzenesulphonate, sodium dodecylsulfate, cetyltrimethylammonium bromide, cetylpyridinium chloride, polyoxyethylene sorbitan monolaurate (Tween 20, Polysorbate 20), etc.

Depending on the chemical constituents attached to the hydrophobic moiety, surfactants are classified as:

i. Anionic: The hydrophilic portion of the molecule bears a negative charge. Alkylbenzene sulfonates (detergents), sodium or potassium salt of fatty acid (soaps), lauryl sulfate (foaming agent), di-alkyl sulfosuccinate (wetting agent), lignosulfonates (dispersants), etc., belong to this category.

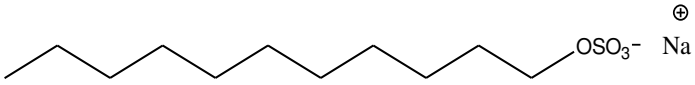

ii. Cationic: In this category the surface active portion of the molecule bears a positive charge. Long chain alkyltrimethylammonium bromide, cetylpyridinium chloride, double tailed alkyldimethylammonium bromide etc., are some of the examples of cationic surfactants.

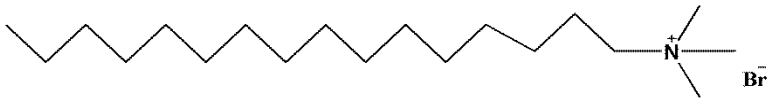

iii. Zwitterionic: If a surfactant contains a head with two oppositely charged groups, it is termed as zwitterionic or amphoteric. 1,2-diacyl-sn-glycero-3-hosphatidylcholine(lecithin), 3(ethyldimethylammonio)propane-1-sulfonate (NDSB-195) are some of the examples of this type of surfactant.

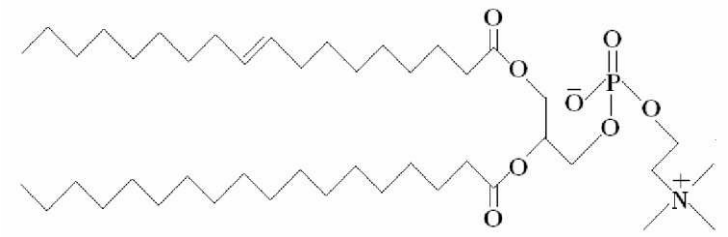

iv. Nonionic: Nonionic surfactants do not have ionisable groups. Examples include polyoxyethylene sorbitan monolaurate (Tween 20), t-octylphenoxypolyethoxyethanol (Triton X100), polyethylene glycol lauryl ether (Brij35), etc.

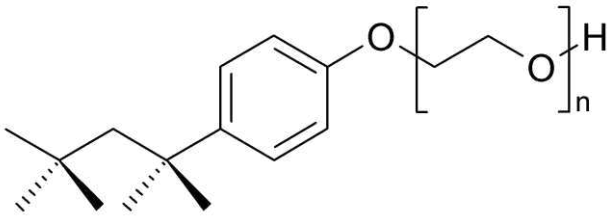

The typical surfactant molecules are composed of a single or double tail connected to a single head group; there are other types of surfactants, which have been developed [47].

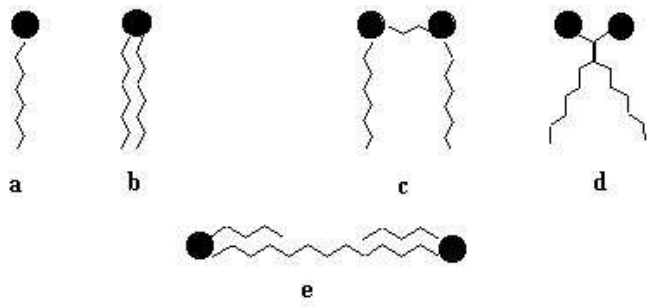

Scheme 10. Schematic representation of different types of surfactants: (a) single-tailed (b) double-tailed (c) and (d) gemini and (e) bolaform.

2.1. Dye-surfactant interaction

Although many studies have been undertaken on the interaction of oppositely charged dyes and surfactants, this area is still important and interesting from the theoretical, ecological and technological point of view. The enhanced energy transfer between dyes in dye-surfactant systems made them good model membrane systems of chloroplast [48,49]. The deformation of the absorption and emission spectra of ionic dyes in the presence of oppositely charged ionic surfactants in aqueous solution proposes the formation of higher aggregates in the surfactant micelle [50-52].

When surfactant interacts with dye, there occurs spectral shift in the bands of the dye with variations in the intensity. The effect becomes significant for oppositely charged dye-surfactant systems. Depending on the nature of aggregates a red or blue shift may occur in the absorption maxima of dye. Red shift in the absorption band of surfactant-dye aggregates with respect to the absorption band of the dye in aqueous solution is attributed to head-to-tail aggregation, i.e., formation of J-aggregates, whereas blue shift occurs due to parallel aggregation, i.e., formation of H-aggregates[53].

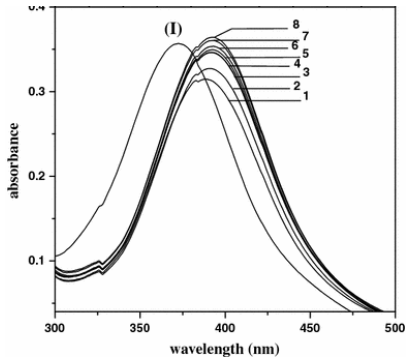

Figure 4. Effect of CTAB on the absorption spectrum of Alizarin Yellow R in aqueous solution at 25°C; I without surfactant; (1) 0.7 mM; (2) 0.8 mM; (3) 0.9 mM, (4) 1.0 mM, (5) 2.0 mM,(6) 3.0 mM, (7) 4.0 mM, and (8) 8.0 mM [53].

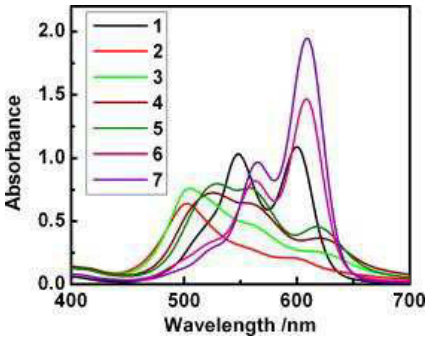

Figure 5. Visible absorption spectra 10 μmol dm^{-3} of PIN in the presence of varying concentration of NaDC in aqueous medium, at 298 K. Concentration of NaDC (mmol dm^{-3}): 1, 0; 2, 1; 3, 2; 4, 3; 5, 5; 6, 8 and 7, 10 [22].

Also, the investigations on the behaviour of different dyes in aqueous surfactant solution can provide useful information about the mechanisms according to which surfactants operate as levelling agents and provide information on the thermodynamics and kinetics of dyeing process. This may directly affect the quality of dyeing, which is one of the goals of textile finishing. Surfactants are also used as solubilizers for water insoluble dyes, to break down dye aggregates in order to accelerate adsorption processes on fiber, as auxiliaries for improving dye adsorption and as dispersing agents[54-56]. The interactions of binary dye-surfactant systems find applications in other scientific fields, including analytical chemistry, photography, luminescence, and lasers, etc. Amphiphilic dyes, for which the concepts of color and surface-active properties coexist within the same molecular framework, are of particular interest [57]. Besides, dye-surfactant interaction studies can effectively determine the critical micelle concentration of surfactants[58,59].

Determination of CMC by spectroscopic probing technique: CMC is one of the most important solution properties exhibited by surfactant molecules. At a fixed environmental condition, most of the physicochemical properties of a surfactant

solution show remarkable changes at the onset of micellization. It is, therefore, worthy to determine the CMC of a surfactant or a mixture of surfactants precisely.

i. **Absorption spectroscopy.** The process is mostly applicable to the surfactants which give one or more absorption peak in the absorption spectrum. In a typical experiment, surfactant solutions of different concentrations are prepared and the absorption values are recorded.

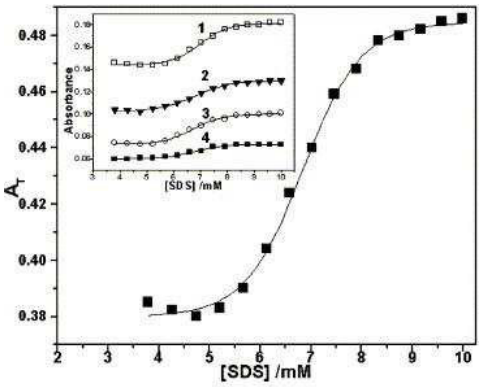

Figure 6. Determination of CMC by absorption spectroscopic method, adapted from Basu Ray et al. [60]

The absorption values are then plotted against [surfactant] in the solution. The break point appeared in the profile is the CMC. For non-absorbing surfactants CMC is determined by absorption spectroscopy by adding a probe into the surfactant solution.

ii. **Fluorescence spectroscopy.** The method is based on the fluorescence spectra of a dye which varies substantially with its environment. In fluorimetry, in the pre-micellar region, the dye (with its negligible aqueous solubility) accommodates itself in water (polar environment) and after micellization it partitions between water and the nonpolar micellar core or the dye may also reside at the palisade layer of the micelle [61]. In a typical experiment surfactant solutions of different concentrations are prepared which varies from below CMC to above CMC having fixed amount of the probe and then from the plot of fluorescence intensity vs. [surfactant] the CMC can be determined.

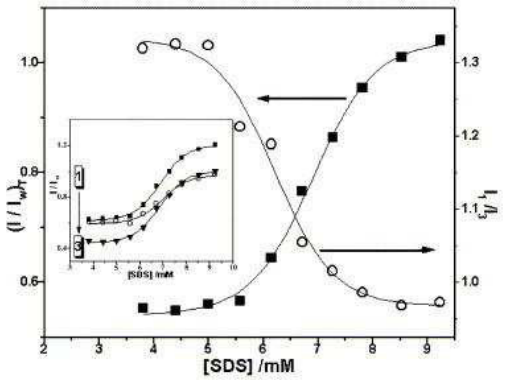

Figure 7. Determination of CMC by fluorescence spectroscopic method, adapted from Basu Ray et al. [60]

Among the various forms of environment, the micellar media can be the best choice to reach a deeper understanding of dye-media interactions as compared to the other solvation systems. According to Göktürk et al. [62], a dye molecule exhibits spectral changes in presence of varying amount of surfactants consistently and there exist sequential equilibria between surfactant monomers, micelles, dye aggregates and pre-micellar dye-surfactant complex, etc. From practical and scientific aspects, the studies in this area are still important and interesting. The interaction of eosin Y with cationic detergents has also been applied to the assay of such detergent[63]. The eosin Y-surfactant complexes is a good model for studying dye adsorption and absorption[64] by surfactants, both of

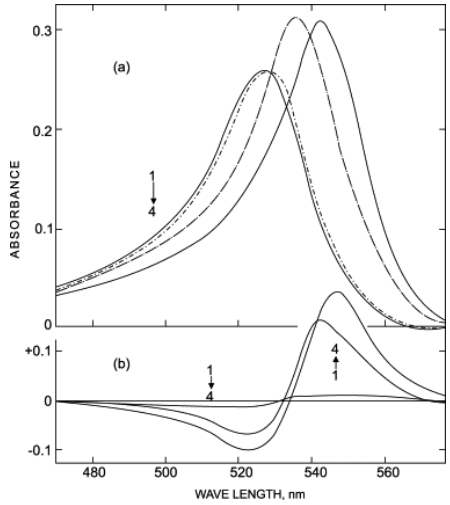

Figure 8. The visible absorption spectra of erythrosin B in water (1), in aqueous solution of anionic surfactant SDS (2), cationic surfactant CTAB (3) and neutral surfactant TX-100 (4) at 298 K, adapted from Bhowmik et al. [24]

which are important in the dyeing industry. Studies of the influence of various nonionic, anionic and cationic surfactants on the fluorescence and absorption spectra of eosin yellow have been reported earlier[65]. The optimum solubilization showing dye‑surfactant interaction can be utilized as separation of dyes from waste dye-stuffs of different textile, paper and pulp industries. The spectral behaviour of some anionic xanthene dyes namely erythrosin B, rose bengal and eosin have been studied in micellar solution of TX-100 (neutral), SDS (anionic) and CTAB (cationic) and the studies have been correlated with the photoelectrochemical studies of these dyes in aqueous solution of these surfactants[24].

In the present work systematic studies on the interaction between EY and different cationic surfactants have been reported. The surfactant head group, chain length, as well as the number of hydrocarbon chains (single or double tailed) have been varied. The surfactants used were cetyltrimethylammonium bromide, cetylpyridinium chloride, didodecyldimethylammonium bromide and didecyldimethylammonium bromide. Dye-surfactant interaction studies are believed to shed information on the polarity of the medium (governed by added surfactants), nature and extent of interactions between dye and surfactant molecules as well as the self-aggregation behaviour of dye in presence of the surfactants.

3. Cursory glance on polymers

The word polymer literally means “many parts”. A polymeric material may be considered to be one that contains many chemically bonded parts or units which themselves are bonded together to form a solid. In other way a polymer is a large molecule composed of repeating structural units or chains typically connected by covalent chemical bonds. While polymer in popular usage suggests plastics, the term actually refers to a large class of natural and synthetic materials with a variety of properties and purposes. Hence, the terms polymer and polymeric material encompass very large, broad classes of compounds, both natural and synthetic, with a wide variety of properties. Because of the

extraordinary range of properties of polymeric materials [66], they play an essential and ubiquitous roles in everyday life[67], from those of familiar synthetic plastics and other materials of day-to-day work and home life, to the natural biopolymers that are fundamental to biological structure and function.

3.1. Classification of polymer:

Polymers are classified in different ways:

1. On the basis of arrangement of monomer unit.
    a) Homo polymers, e.g. polyvinyl chloride.
    b) Co-polymers, e.g. ethylene-vinyl acetate.
2. On the basis of their mode of formation.
    a) Condensation polymer, e.g. polyamide.
    b) Addition polymer, e.g. Saran (plastic) wrap.
3. On the basis of chemical composition.
    a) Organic polymer, e.g. deoxyribonucleotides.
    b) Hetero-organic polymer, e.g. polysiloxanes.
    c) In-organic polymer, e.g. polydimethylsiloxane.
4. On the basis of their occurrence.
    a) Natural polymer, e.g. cellulose.
    b) Synthetic polymer, e.g. polyethylene.

3.2. Polymer properties

Polymer properties are broadly divided into several classes based on the scale at which the property is defined as well as upon its physical basis [68]. The most basic property of a polymer is the identity of its constituent monomers. A second set of properties, known as microstructure, essentially describe the arrangement of these monomers within the polymer at the scale of a single chain. These basic structural properties play a major role in determining bulk physical

properties of the polymer, which describe how the polymer behaves as a continuous macroscopic material. Chemical properties, at the nano-scale, describe how the chains interact through various physical forces. At the macro-scale, they describe how the bulk polymer interacts with other chemicals and solvents.

3.3. Polyelectrolytes

Polymer molecules containing ionizable subunits are known as polyelectrolytes or ionomers. Electrochemically active polymers can be classified into several categories based on the mode of charge propagation. The mode of charge propagation is linked to the chemical structure of the polymer. Polyelectrolytes are polymers whose repeating units bear an electrolyte group. These groups will dissociate in aqueous solutions (water), making the polymers charged. Polyelectrolyte properties are similar to both electrolytes (salts) and polymers (high molecular weight compounds), and are sometimes called polysalts. The adsorption behavior of polyelectrolytes has attracted a lot of attention recently because of the widespread industrial use of these substances for example in papermaking, in mineral processing, in waste water treatments, in paints and in cosmetics[69,70]. In papermaking, polyelectrolytes are used as retention aids to promote retention by flocculation and to improve drainage, as fixing agents to promote aggregation of colloidal material to the fibers and as wet and

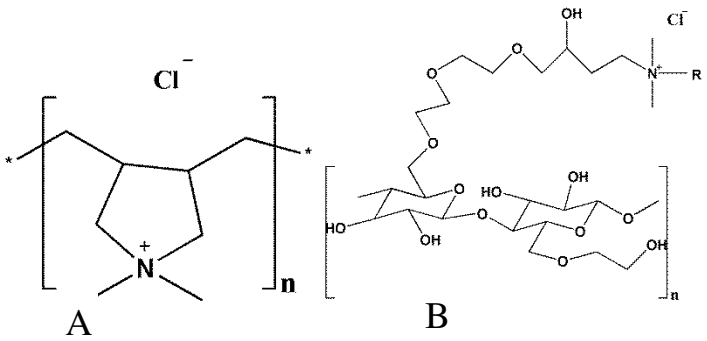

Scheme 11. Schematic representation of (A) poly(diallyldimethyl ammonium) chloride and (B) N,N-dimethyl-N-dodecyl derivative of hydroxyl ethyl cellulose(LM200) / N,N-dimethyl-N-methyl derivative of hydroxyl ethyl cellulose(JR400)[R = $-CH_3$: JR400, R = $-C_{12}H_{25}$: LM200].

dry strength additives to promote the strength of paper[71]. In particular, cationic polyelectrolytes have found widespread industrial application as flocculants in

branches of industry such as mining, water resource management, and papermaking[70,72]. Chemically, these polyelectrolytes are a group of macromolecules where the charges are localized pendant to the hydrophobic carbon backbone, most frequently as quaternary ammonium substituents, and which have molar masses in the order of 106 to 107 g/mol. Cationic polymers play important role in gene delivery for their competency of aggregating the DNA molecules[73]. Cationic polymers have also proven to be successful in the condensation of DNA[74]. Nowadays, hydrophobically modified biocompatible polymers are recognized as an important and attractive class of drug carriers, especially for intravenous administration of hydrophobic drugs[75,76]. The hydrophobically modified cationic polyelectrolytes proved to provide a hydrophobic environment favourable to Rutin partitioning/binding. Further, they allowed discrimination of factors responsible for polymer / Rutin interaction, as the effect of alkyl side chain length and microdomain compactness on the interactions could be ascertained by Bai et al.[77].

3.4. Importance of dye-polymer interaction study

Dye-polymer interaction has several importance. The functional group of a polymer can be detected by using dye-polymer interaction [78]. Different complexes can be formed through different polyelectrolytes assembled with different

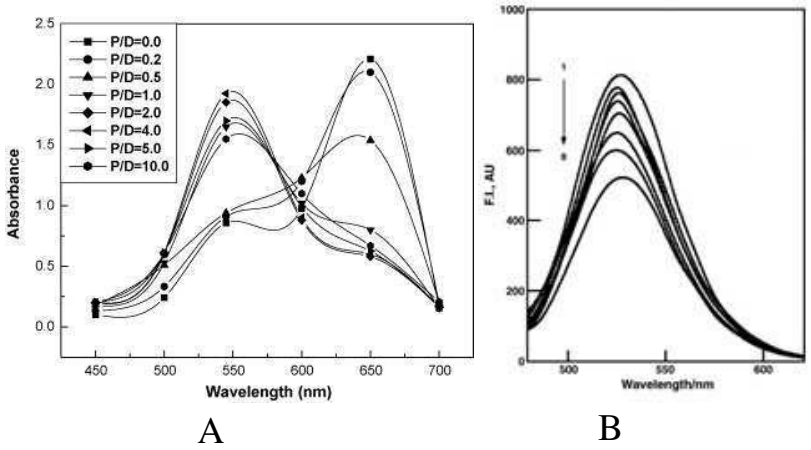

Figure 9. (A) Absorption spectrum of Azure B–NaAlg system at various P/D ratios[1] and (B) Emission spectra of 10^{-5} mol dm^{-3} acridine orange at 303 K in presence of varying amounts of Klebsiella K18 capsular polysaccharide[81].

surfactants or dyes. The complexes can be used in dyeing, liquid crystal displays (LCDs), nonlinear optics, food, medicine, chromatograms, and other new technical fields[79,80]. To identify the molecular geometry of a polymer-dye complex, dye-polymer interaction study is used [82]. The assembly of dyes molecules on metal-polymer complexes is of interest due to their potential applications in photovoltaic cell, separation, and wastewater treatment[83]. Several physiochemical parameters such as molecular weight of each repeating unit, stoichiometry of the dye-polymer complex, binding constant, and other related thermodynamic parameters like free energy, enthalpy, and entropy changes can be evaluated using polymer-dye interactions. Also, the equivalent weight of a polymer can be determined from the dye-polymer interaction studies[84,85]. The rate of isomerisation of azo-dye in some polymer matrices as well as in some solvents depend on dye-polymer interactions[86] i.e., one can control the reaction rate by controlling the properties of the medium. Many reports are available in the literature on dye-polymer interaction studies in controlling the kinetics of photobleaching reactions[87-89]. Information about the dynamics of polymer chains during phase transition could be obtained by investigating the fluorescence properties of the dye embedded into polymer both at the bulk and single molecule levels[90]. Organic dye-doped polymer materials have numerous optoelectronic applications, including frequency conversion of light, waveguiding, optical signal processing, and optical data storage[91,92]and are also established as potential laser media[93]. Dye-polymer interaction is also a suitable tool for the removal of organic compounds form waste water by the method of adsorption[94,95]. Studies on binding of oppositely charged dye to different synthetic and natural polyions have been reported by many researchers [96-99]. The encaging property of polymer highly influences the excited state properties of many xanthenes dyes [100] leading to variations in the spectra. Fluorescence intensity of a dye can get either enhanced or quenched. The usually encountered fluorescence quenching processes are collisional (dynamic) quenching and static (complex formation).

i. Collisional quenching occurs when the excited fluorophore experiences contact with an atom or molecule that can facilitate non-radiative

transitions to the ground state. In the simplest case of collisional quenching, the following relation called the Stern-Volmer equation holds [26]:

$$\frac{F_0}{F} = 1 + K_{sv}[Q] \qquad (3)$$

where, F_0 and F are the fluorescence intensities of EY in the absence and presence of quencher, Q; [Q] = Quencher concentration. K_{SV} = Stern-Volmer quenching constant. Plot of F_0 / F vs. [Q] yields a straight line with a slope equal to K_{SV}.

ii. In case of static quenching a fluorophore form a stable complex with another molecule in the ground state and consequently the number of fluorophores emitting get reduced thus leading to the decrease in the fluorescence intensity.

In such case the dependence of the fluorescence as a function of the quencher concentration follows the relation[101]:

$$\frac{F_0}{F} = 1 + K_a[Q] \qquad (4)$$

where K_a is the association constant of the complex.

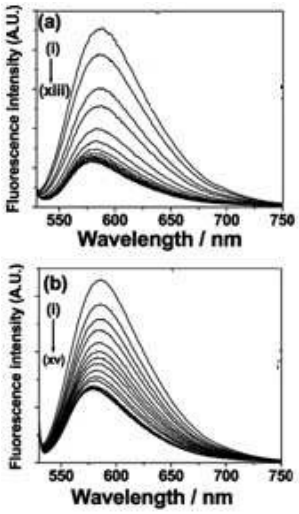

Figure 10. Emission spectra of (a) PSF, and (b) ST, in the presence of different ctDNA *concentrations.* (λ_{exc} = 520 nm). Curves correspond to (a) 0, 6, 9, 13, 21, 37, 47, 71, *and 92 μM of DNA; (b) 0, 4.6, 8.5, 12, 20,* 36.5, 46, 60.5, *75, 90, 102.5, and 114 μM of* DNArespectively[102].

In the present dissertation efforts were made to investigate the interaction of EY with oppositely charged aqueous polyelectrolytes. Also, the variation in the absorption and emission spectral bands as function of polyelectrolyte

concentration was studied. Subsequently, the binding constant of the dye-polymer complex and related thermodynamic parameters were evaluated. The polymers chosen for the interaction studies are structurally different (as shown in scheme 11) so different types of interactions are likely to occur.

4. Colloidal dispersion

Colloidal solutions (also called colloidal suspensions) are the subject of interface and colloid science. This field of study was introduced in 1861 by Scottish scientist Thomas Graham. A colloidal system consists of two separate phases: a dispersed phase (or internal phase) and a continuous phase (or dispersion medium) in which the colloid is dispersed. A colloidal system may be solid, liquid, or gas**.** One property of colloid systems that distinguishes them from true solutions is that colloidal particles scatter light. If a beam of light, such as that from a flashlight, passes through a colloid, the light is scattered by the colloidal particles and the path of the light can therefore be observed. The dispersed particles have a diameter of between approximately 1 and 1000 nanometers[103]. The stability of a colloidal system is the capability of the system to remain as it is. Stability is hindered by aggregation and sedimentation phenomena, which are driven by the colloids tendency to reduce surface energy. Reducing the interfacial tension will stabilize the colloidal system by reducing this driving force.

Nanoparticles are the clusters of 10-1000 atoms with size dependent physical, chemical, electronic, and optical properties[104]. In nanotechnology a particle is defined as a small object that behaves as a whole unit in terms of its transport and properties. Ultrafine particles or nanoparticles are sized between 100 and 1nm. Nanoparticles are of great scientific interest as they are effectively a bridge between bulk materials and atomic or molecular structures[105]. A bulk material should have constant physical properties regardless of its size, but at the nano-scale size-dependent properties are often observed. Thus, the properties of materials change as their size approaches the nanoscale and as the percentage of atoms at the surface of a material becomes significant. Nanoparticles often

possess unexpected optical properties as they are small enough to confine their electrons and produce quantum effects[106]. For example gold nanoparticles appear deep red to black in solution. Nanoparticles of usually yellow gold and grey silicon are red in color[107]. Other size-dependent property changes include quantum confinement in semiconductor particles[108], surface plasmon resonance in some metal particles[109] and superparamagnetism in magnetic materials[110]. Ironically, the changes in physical properties are not always desirable. Ferromagnetic materials smaller than 10 nm can switch their magnetisation direction using room temperature thermal energy, thus making them unsuitable for memory storage[111]. The reasons for the outstanding properties of nanoparticles may be due to their particle size, large specific surface area, strong surface area and change of electronic properties which is supported by the quantum effects of particles less than 10 nm.

Because of a number of special properties exhibited by nanoparticles, they find multifarious applications. Nanoparticles are versatile enough to be used in many types of technological applications from delicate electronics [112] to revolutionary medical procedures [113]. Among the wide range of applications the timeliest one is perhaps in medical applications. Their pathogen sized proportions make them useful in fighting viruses and bacteria in human body and in the production of anti-cancer drugs [114]. Studies of nanoscale noble metal materials are additionally important because these materials have potential as optical filters [115], plasmonic waveguides [116], bio-chemo-sensors [117], and substrates for surface-enhanced spectroscopies [118]. Nanoparticles of magnetic metals find applications as catalysts, nucleators for growth of high-aspect-ratio nanomaterials and toxic waste remediation. Nanomaterials find numerous applications in biology or medicine. They are used as fluorescent biological labels [119], in drug and gene delivery [120], in bio detection of pathogens [121], in detection of proteins [122], in probing of DNA structure [123], in tissue engineering [124], in separation and purification of biological molecules and cells [125], in MRI contrast enhancement [126], in phagokinetic studies [127], etc.

4.1. Colloidal silica

Colloidal silica is a dispersion of fine amorphous, nonporous, and typically spherical silica particles in a liquid phase. Among different semiconductor nanocrystals, silica has got special importance because it can be used in different forms for solute pre-concentration and immobilization of analytical reagents [128]. Besides, silica has got special attention for other specific properties like optical transparency [129], high hydrophilicity [130] and negative surface charge in aqueous media [131]. According to Bonacchi et al. [132], silica nanoparticles have some fascinating properties compared to other conventional

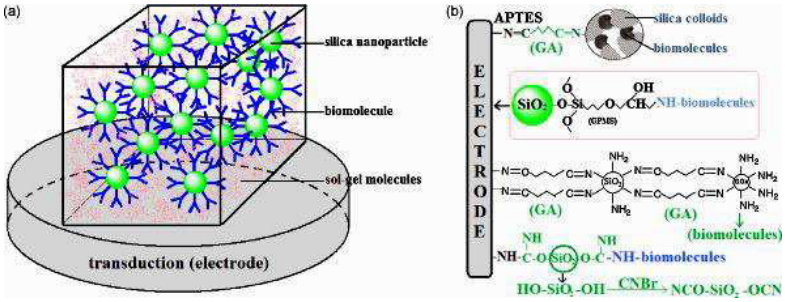

Scheme 12. Schematic representation of a silica nanoparticle-based biosensor fabricated via (a) the entrapment technique and (b) covalent conjugation[133].

nanosystems which include its photophysical inertness, absence of intrinsic toxicity, capability to host a large number of photochemically active species and also to protect the active material segregated inside its pore. These specific properties have additional advantages for silica nanoparticles in the field of bioanalysis and disease diagnostics [134]. They can be used as templates for the formation of ordered mesoporous polymers of tunable pore size[135]. Colloidal silica is mainly used in catalysis, ceramics, paper, textile applications, strength enhancement in rubber, tobacco treatment, and medicine [136]. Also, they find applications in high-temperature bonding, investment casting, refractory fiber bonding, and silicon wafer polishing [137]. Several optimizations can lead to the binding of SiO_2 particles with each other or with other substrates [138]. Ludox® is commercially available spherical shaped silica particles suspended in aqueous medium which find different applications for their specific properties like optical transparency, high hydrophilicity and negative surface charge[139-142]. Therefore,

colloidal silica in the form of Ludox® can be considered as an appropriate model system in investigating its capability to alter (both enhancement and quenching) the absorbance and fluorescence intensity of fluorophores in aqueous medium.

4.1.1. Preparation of colloidal silica

Colloidal silica can be prepared by various methods and starting materials[143]. These methods include ion exchange [144], neutralization or electrodialysis of aqueous silicates, hydrolysis and condensation of silane [145], peptization or milling of silica gel or powder [146], and direct oxidation of silicon [147]. There are four most important methods to prepare colloidal silica from natural ore [148].

The first among them is the preparation of colloidal silica from liquid sodium silicate by the ion exchange process. The sodium silicate is obtained from naturally available silica by melting the silica ore in the presence of alkali flux; subsequently, it is dissolved by heating under pressure to produce liquid sodium silicate, which is commonly known as water glass. The liquid sodium silicate has high viscosity, and therefore, it is diluted to a concentration of 3-5 wt%. Next, it is passed through an ion-exchange resin, and then fed into the alkali solution to form

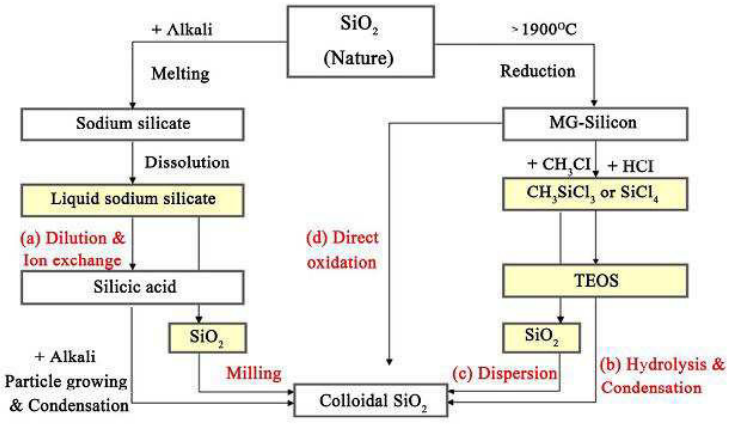

Scheme 13. Various preparation methods for colloidal silica: (a) Ion exchange from sodium silicate; (b) Hydrolysis and condensation from TEOS; (c) Milling or dispersion fromfumed silica; (d) Direct oxidation from silicon[148].

a silica seed, which is then used to grow silica particles. The product is concentrated to 30 wt% to obtain the commercial product.

The second method for preparing colloidal silica is from tetraethoxysilane (TEOS), which is well known as the Stöber method [145]. TEOS is a silane monomer prepared from tetrachlorosilane, which in turn is derived from metallurgical grade silicon. The silicon itself is obtained by the reduction of naturally occurring silica ore at temperature over 1900°C in the presence of carbon.

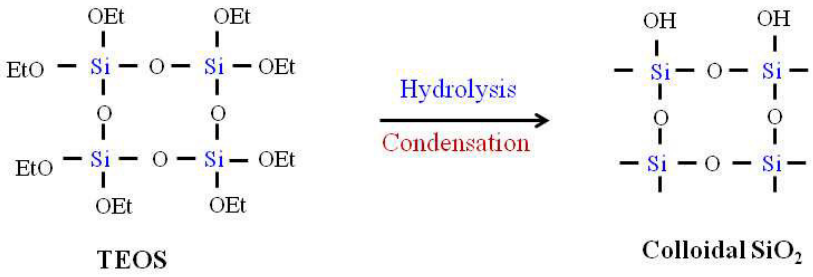

Scheme 14. Schematic representation of preparation of colloidal silica from TEOS.

The third method is that of direct oxidation of silicon wherein colloidal silica is prepared by the direct oxidation of metallurgical grade silicon without using TEOS. The silicon is treated with water in the presence of alkali catalysts to produce silica along with the evolution of hydrogen and heat.

The fourth method for preparing colloidal silica is by milling and peptization of silica that can be found either in the form of silica gel or fumed silica, which consists of preferentially coaccervated or aggregated primary silica particles. The properties of the colloidal silica prepared by this route largely depend not only on the milling and peptization process but also on the properties of the starting silica source such as purity, shape, and aggregation.

Ludox® colloidal silica is an aqueous colloidal dispersion of silica particles. It is an opalescent liquid with a slight-to-moderate bluish cast. Because of their colloidal nature, particles of ludox® have high specific surface area which accounts for the novel properties and wide variety of uses. Du Pont offers seven general grades of Ludox®: HS-40%, HS-30%, TM, SM, AM, AS and LS. Du

Pont also offers a special grade Ludox® CL-X for packaging frictionizing. The particles in Ludox® are discrete uniform spheres of silica which have no internal surface area or detectable crystallinity. They are dispersed in an alkaline medium which reacts with the silica surface to produce a negative charge. Because of the negative charge, the particles repel one another resulting in a stable product.The stabilizing counter ion in Ludox® HS-30%, HS-40%, LS, SM, TM, AM and CL-X is sodium whereas in Ludox® AS the counter ion is ammonium. Most applications of Ludox® colloidal silica depend on the high surface area and reactivity of the suspended particles. The use of sodium aluminate instead of sodium hydroxide in stabilizing Ludox® AM gives it broader stability against variation of pH. In applications where a colloidal silica needs to be incorporated at a neutral or acid pH, Ludox® AM has been the grade of choice [149].

4.1.2. Aggregation between dye and colloidal silica dispersions

Incorporation of dyes in small solid particles instead of bulk solid material is gaining interests[150,151] for many reasons. Small particles reveal interesting optical scattering phenomena, especially in combination with interference effects. Dye-colloidal aggregates are important in the field of waste water treatment [152], lasing property [153], dye-sensitized solar cells [154], photocatalytic reactions [155], etc. Van Blaaderen et al. [150,151] synthesized dye incorporated silica colloids. Such dyed particles enable measurements of particle diffusion by fluorescence recovery after photobleaching[156], and direct imaging of dense colloidal structures by confocal fluorescence microscopy[157]. Among the different fluorescent labels, dye-doped silica nanoparticles show distinct advantages over quantum dots, fluorescent dyes, up-converting phosphors and plasmon resonant particles because of their high quantum yield, photostability, water dispersibility and ease of surface modification with different functional groups for subsequent bioconjugation, due to well-known silica chemistry[158]. According to Ha et al. [159] and Bringley [160] in some cases, fluorescence could even be quenched, compared to the free dye molecules. Therefore, a detailed spectral investigation on the absorption and fluorescence behaviour of dye-silica aggregates is warranted for better technological applications as well as from the fundamental understanding point of

view. Towards this initiative spectroscopic investigations on colloidal silica-7HC aggregates in a wide concentration range of silica were undertaken. Although several reports are available in the literature which include the interaction between silica and a number of dyes [25,161-166], however, reports involving the interaction of Ludox® with 7-hydroxycoumarin are not common in literature. The occurrence of excited state H-bonding between silica and 7-hydroxycoumarin is supposed to be understood in a better way through fluorescence spectroscopic analysis, which could further be investigated via FTIR measurements.

4.2. Synthesis of nanoparticles

4.2.1. In different phases

Methods for preparation of nanoparticles can be divided into physical and chemical methods based on whether there exist chemical reactions. On the other hand, these methods can be classified into gas phase, liquid phase and solid phase methods based on the state of the reaction system.

- Gas phase: The gas phase method includes gas-phase evaporation method (resistance heating, high frequency induction heating, plasma heating, electron beam heating, laser heating, electric heating evaporation method, vacuum deposition on the surface of flowing oil and exploding wire method), chemical vapor reaction (heating heat pipe gas reaction, laser induced chemical vapor reaction, plasma enhanced chemical vapor reaction), chemical vapor condensation and sputtering method.
- Solid phase: This method includes thermal decomposition, solid state reaction, spark discharge, stripping and milling method. The thermal decomposition method is one of the chemical methods that can synthesize well-dispersed NPs with good crystallization. The solventless thermal decomposition method by capping agents like oleate can be used for the preparation pure metal nanoparticles in regulated conditions either spontaneously or in the presence of a reducing gas.
- Liquid phase: Liquid phase method for synthesizing nanoparticles mainly includes chemical reduction, sol gel, hot-soap, solvothermal method,

pyrolysis, and spray pyrolysis methods and methods of using templates like micelles and reverse micelles.

4.2.2. Synthesis of nanocolloidal dispersion in aqueous media

There are different preparative routes for the synthesis of nanoparticles in aqueous media:

1. Monolayer and Langmuir-Blodgett techniques are more effective in controlling the molecular orientation and packing at a molecular level [167]. The Langmuir–Blodgett (LB) technique allows the transfer of nanoparticles from solutions into thin films. Compression of nanoparticles at water interface using monolayer film as the surrounding matrix is one of the commonly used method for preparation of composite films [168]. Not only can Langmuir-Blodgett films fabricate the packing and the thickness of the molecular films in a controlled manner, but also they provide possible templates to control the nucleation and growth of organized inorganic nanoparticles under mild conditions [170]. However, although this method is useful in obtaining a thin film but this is not suitable for obtaining nano-colloidal distributions.

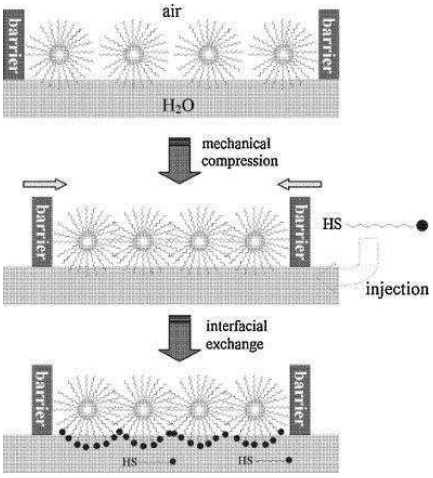

Scheme 15. Schematic of the preparation of Janus nanoparticles based on the Langmuir-Blodgett technique [169].

2. Preparation of nanoparticles in microemulsion media: Synthesis of nanoparticles in microemulsions is an area of considerable current interest.

Among all chemical methods the microemulsion has been demonstrated as a very versatile and reproducible method that allows to control over the nanoparticle size and yields nanoparticles with a narrow size distribution [171]. Depending on the proportion of various components and hydrophilic–lipophilic balance (HLB) value of the used surfactant microemulsions can be classified as water-in-oil (W/O), oil-in-water (O/W) and intermediate bicontinuous structural types that can turn reversibly from one type to the other. Water-in-oil microemulsions have been used to prepare nanoparticles for more than two decades, and a wide variety of materials has been synthesised by these methods [172-174]. The preparation procedure of metallic nanoparticles in W/O microemulsion commonly consists of mixing of two microemulsions containing metal salt and a reducing agent respectively. After mixing two microemulsions, the exchange of reactants between micelles takes place during the collisions of water droplets result of Brownian motion, the attractive van der Waals forces and repulsive osmotic and elastic forces between reverse micelles. Successful collisions lead to coalescence, fusion, and efficient mixing of the reactants. The reaction between solubilizates results in the formation of metal nuclei. Growth then occurs around this nucleation point where successful collision occurs between a reverse micelle carrying a nucleus and another one carrying the product monomers with the arrival of more reactants due to intermicellar exchange. The nucleation reaction and particle growth take place within the micelles and the size and morphology of as-prepared nanoparticles depend on the size and shape of the nanodroplets and the type of the surfactant, whose molecules are attached on the surface of the particles to stabilize and protect them against further growth [172]. However, this method also has limitations. Particles as synthesized cannot be directly used for practical applications as they are confined within the oil medium. They need to be isolated for further use which is not always feasible.

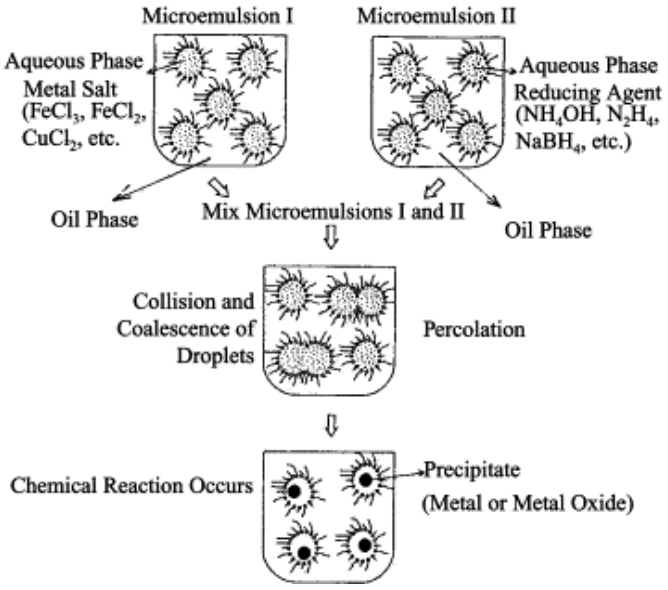

Scheme 16. Proposed mechanism for the formation of metal particles by the microemulsion approach[174].

3. Preparation of nanoparticles in micellar media: In aqueous media, the nanosized particles are primarily separated by the ionic repulsion forces produced due to adsorption on their surface. In this perspective, stabilization of the nanoparticles by surfactants in aqueous solution has been proved to be one of the most effectual methods. The size, shape and other surface properties of the nanoparticles can be altered by different surfactants depending on the latter's molecular structure, i.e., nature of head group, length of hydrophobic tail and type of counterions. Diffusion and attachment rates of surfactants on the nanoparticle surface control the termination of the particle growth [175]. The preparation method consists of simple addition of aqueous metal salt solution and aqueous surfactant solution by controlling the concentration of the surfactant and the molar ratio of surfactant to metal salt in the reaction solution [176].

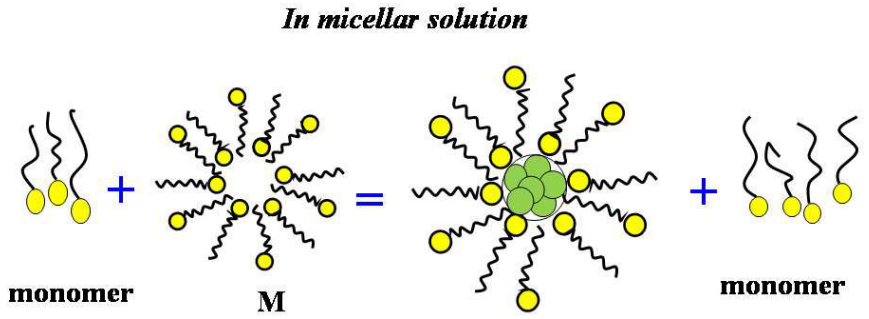

Scheme 17. Schematic representation of surfactant-capped nanoparticles in micellar medium.

4.3. Advantages of nanoparticle synthesis in aqueous surfactant solution

In comparison to their bare counterparts, nanoparticles capped by surfactants stay well dispersed in solution for a longer time. Surfactant stabilized aqueous nano entities offer a unique environment for inorganic reactions, i.e., they act not only as a micro-reactor for hosting the reaction but also as a steric stabilizer to inhibit aggregation. The main advantages of this method are that (i) it is a soft technique, i.e., it does not require extreme conditions of temperature and pressure, (ii) the particle size, shape, and distribution can be controlled by simply varying the composition and dynamics, and (iii) these surfactant stabilized nanoreactors are capable of compartmentalization which in turn alters the ground transition, product states and reduces the reaction dimensionalities [177,178].

4.4. Importance of silver bromide nanoparticles

Nanoparticles of silver bromide serve as model material to study the quantum confinement effects of indirect band gap semiconductors [179], sensitive photographic material for high-speed photography [180], and efficient photocatalyst for hydrogen generation from a solution of methanol and water [181]. Silver bromide nanoparticles serve as a source of strongly biocidal but nontoxic Ag+ ions[182]. On the other hand, the importance of silver halides in photochemistry has shown how these materials are unique. This compound can absorb photons in the visible and shorter wavelengths to generate photoelectron and photohole pairs. The electrons subsequently combine with interstitial silver ions to form silver atoms under continuous irradiation [183].

Synthesis and characterization of silver halide nanoparticles have gained huge research interest over past few decades[181,184-187]. They have been widely used in optoelectronics [188,189], catalysis [190,191], surface-enhanced Raman scattering [192] and more recently surface enhanced fluorescence[193]. Jeunieau et al.[194] prepared silver bromide nanoparticles by typically carrying out a reaction upon mixing two identical microemulsions, each containing one of the reactants forming the precipitate. Rosseti et al.[195] explained the particle size dependence of the excited state electronic properties of silver iodide and silver bromide as a consequence of electron and hole localization in the small crystallites. Ohde et al.[196] have synthesized silver halide nanoparticles in super critical carbon dioxide utilizing a water-in-CO_2 microemulsion. Koh et al.[197] synthesized silver haide nanocomposites using amphiphilic graft copolymer as the template. Silver halide fibers are flexible, water insoluble, non-toxic, and have good transmission in the mid-infrared region, therefore they can be used in many applications such as fiber-optic infrared spectroscopy, radiometry, and transmission of CO_2 laser power for medical purposes[198]. The water-insoluble cationic polymer/silver bromide nanoparticle composites form good coatings on glass and exhibited long-lasting antibacterial properties toward both airborne and waterborne bacteria [184]. Preparation of AgBr nanoparticles has also been reported in water-in-oil microemulsion media by Husein et al.[186]. They have prepared AgBr nanoparticles in water-in-oil microemulsion where the existence of bulk water was possible for which the nanoparticles got precipitated in that water pool. Nanoparticles have inherent tendency to coalesce in solution[199]. Hence, to form stable dispersions of nanoparticles, stabilizing agents that bind to the nanoparticle surface are essential. It has been reported earlier that capping agents comprising a reactive head and a hydrophobic tail acts as a good stabilizing agent for the synthesized silver bromide nanoparticles[200]. Many researchers have used cetyltrimethylammonium bromide (CTAB) as a capping agent to form stable dispersions of nanoparticles[176,201-203]. CTAB adsorbs on the surface of the nanoparticles and forms a bilayer structure which is favourable to enhance the stability of the nanoparticles[176]. Bai et al.[204] have prepared and characterized AgBr nanoparticles in poly(vinylpyrrolidone) matrix. CTAB acts as a stabilizer in seed mediated

growth of silver nanodisks in aqueous media [205]. He et al.[187] have prepared novel layered AgBr based nanocomposite stabilized by CTAB. Sui et al.[201,202] have used CTAB as a stabilizer in preparing positively charged silver nanoparticles.

In the present dissertation, attempts have been made to synthesize nanocolloidal dispersions of silver bromide (AgBr) by way of simply adding silver nitrate to aqueous cetyltrimethylammonium bromide (CTAB) solution. CTAB served both as stabilizing agent as well as the source for bromide ion. AgBr nanoparticles are proposed to get stabilized by the layered structured surfactant cation assemblies. Although there are previous reports on the synthesis and characterization of AgBr nanoparticles[176,206,207], however, studies on such a system in solution phase are not so common in the literature. Keeping in mind about the multifaceted application potentials, AgBr were prepared and characterized in aqueous CTAB solution in the concentration range (10^{-6}-10^{-5}M), well above its solubility limit.

4.5. Characterization of nanoparticle

Nanoparticles can be characterized by a number of techniques for example XRD, FTIR, NMR, conductometry, UV-vis spectroscopy, dynamic light scattering studies, DSC, TGA, isothermal titration calorimetry, electron microscopy, etc.

XRD: X-ray diffraction method is a useful tool for characterization of nanoparticles. From the XRD data, one can obtain the material composition, structure (three-dimensional coordinates of atoms, chemical bonding, molecular conformation and three-dimensional conformation, the electron density value, etc.) and the information on the interaction between molecules.

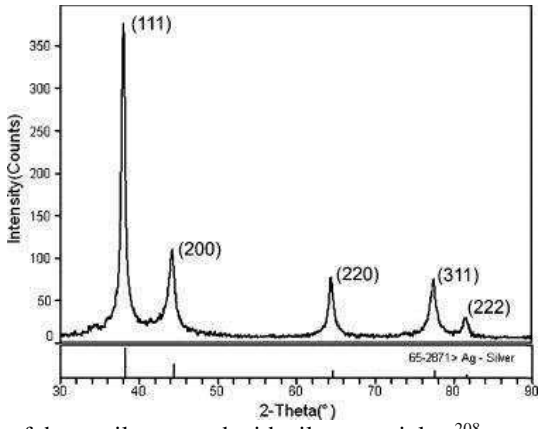

Figure 11: XRD pattern of the textiles coated with silver particles [208].

FTIR: From the IR spectrum, one can observe the absorption and emission due to the molecular vibration and rotation in the electromagnetic wave infrared region (15000~10 cm^{-1}). It reveals the unknown composition qualitatively according to the bands characteristic frequency, determines a component content of the sample (quantification) according to band intensity. It can also reveal the molecular structure (such as functional group, bond), identify isomer, and determine structures of compounds.

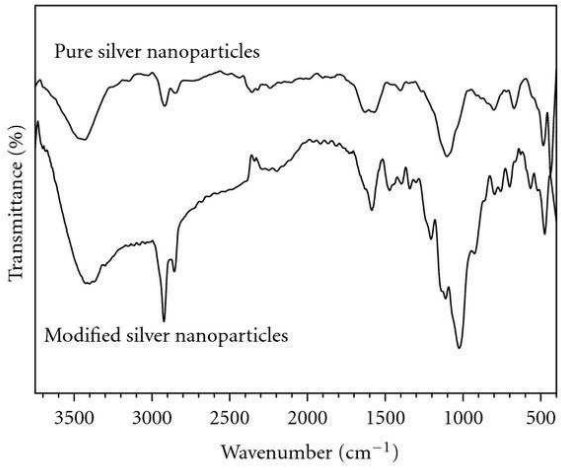

Figure 12: FTIR spectra for the pure and modified silver nanoparticles [209].

NMR: It can be a very selective technique, distinguishing among many atoms within a molecule or collection of molecules of the same type but which differ only in terms of their local chemical environment. NMR spectroscopy is used to unambiguously identify known and novel compounds, and as such, is usually

required by scientific journals for identity confirmation of synthesized new compounds.

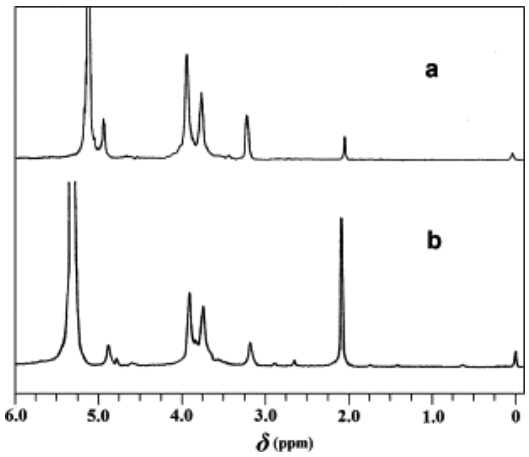

Figure 13. ^{1}H NMR spectra of: (a) chitosan and (b) Cholesterol-modified chitosan conjugate with succinyl linkages [210].

Conductometry: Conductometry has notable application in analytical chemistry, where conductometric titration is a standard technique. Conductometric titration is a type of titration in which the electrical conductivity of the reaction mixture is continuously monitored as one reactant is added. The equivalence point is the point at which the conductivity undergoes a sudden change.

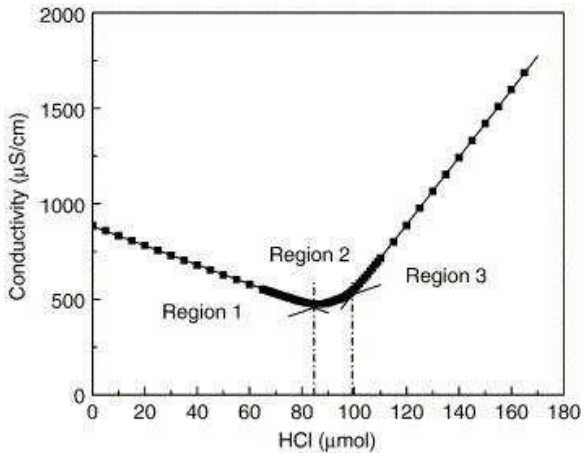

Figure 14. Conductometric titration of oxidative-acid-treated diamonds (nominal size ~100 nm). In this titration, an excessive amount of NaOH was first added into the nanodiamond suspension and then neutralized with 0.1 N HCl. The first region in the plot corresponds to neutralization of solution OH^- groups and the second region corresponds to neutralization of surface $-COO^-$ group [211].

.**UV-Visible spectroscopy** is one of the most widely used techniques for the characterization of nanoparticles. This technique is used in the study of nanomaterials as a diagnostic of nanoparticle formation. Used in conjunction with affinity labeling, UV-visible spectroscopy often provides the means of choice to gauge response in an analysis using nanoparticles. It has been further suggested that the spectroscopic properties of nanoparticles can provide an indicator of their size distribution by fitting the position of the surface plasmon resonance (SPR) to a simple wavelength function[212].

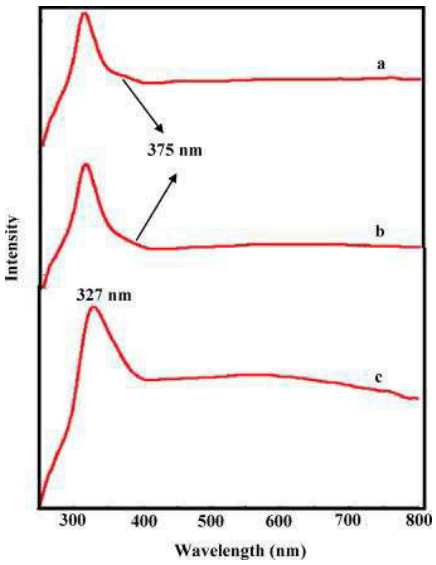

Figure 15: UV–vis diffuse reflectance spectra of (a) 0.02AgCl/Ag/MCM-41, (b) 0.1AgCl/Ag/MCM-41 and (c) 0.2AgCl/Ag/MCM-41[213].

Dynamic light scattering (DLS) studies: The size and surface charge (zeta potential) of the nanoparticles can be measured by DLS measurements. DLS is used to measure particle and molecule size. This technique measures the diffusion of particles moving under Brownian motion, and converts this to size and a size

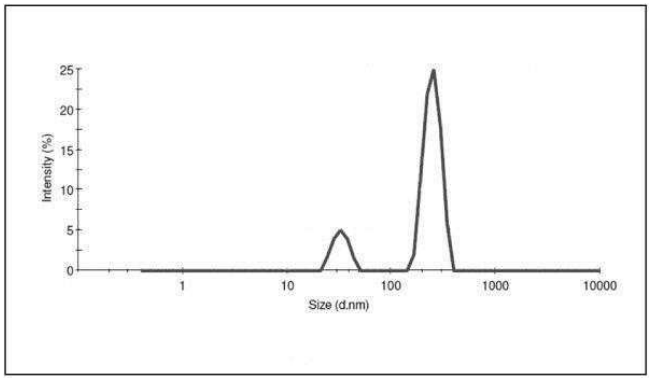

Figure 16. DLS size distribution graph of AuNPs synthesized using chitosan as reductant [215].

distribution using the Stokes-Einstein relationship. The technique is suitable for the characterization of colloidal particles over a wide range of sizes from a few nanometers to several micrometers. If the system is monodisperse, the mean effective diameter of the particles can be determined. This measurement depends on the size of the particle core, the size of surface structures, particle concentration, and the type of ions in the medium [214].

Differential Scanning Calorimetry (DSC) and Thermogravimetric Analysis (TGA): DSC profiles of heating and cooling of the systems can also help in confirming the monolayer or bilayer structure of the surfactant protected nanoparticles. DSC is a thermal analysis apparatus measuring how physical properties of a sample change, along with temperature against time. In other words, the device is a thermal analysis instrument that determines the temperature and heat flow associated with material transitions as a function of time and temperature. During a change in temperature, DSC measures a heat quantity, which is radiated or absorbed excessively by the sample on the basis of a temperature difference between the sample and the reference material[216].

In TGA the % weight losses of the components are found out between a wide range of temperatures. The information regarding the thermal decompositon of the components helps in predicting the structure of the aggregates.

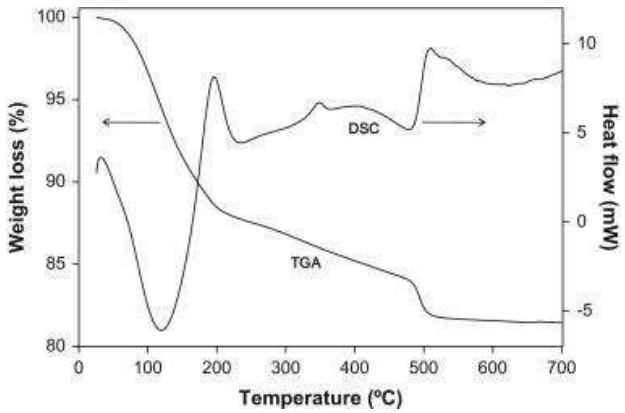

Figure 17. (a) TGA/DSC curves for as-synthesized Mn oxide precipitated in ethanol (heating rate = 10 °C/min under a stream of air) [217].

Isothermal Titration Calorimetry can provide information about the standard enthalpy of formation of the nanoparticles and hence various thermodynamic parameters can be calculated. From such a plot one can determine the enthalpy of formation of a reaction involved in precipitation which is otherwise impossible. Similarly, when such a parameter is estimated in aqueous micellar media at different concentrations the extrapolated value can provide the absolute enthalpy of formation for a reaction associated with precipitation.

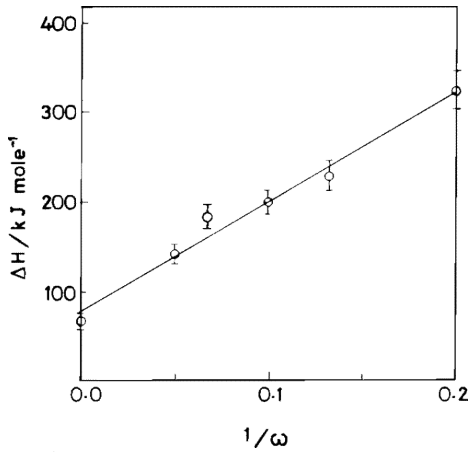

Figure 18. *Plot of* ΔH_f *vs* ω^{-1} for the formation of $Cu_2[Fe(CN)_6]$ in H_2O/AOT/heptane w/o microemulsion at 303 K [218].

Transmission Electronic microscopy is a useful technique in the characterization of nanoparticles. It is one of the most important tools in determining the morphology, crystal orientation, modulations in chemical identity, etc., of the systems. In this microscopy technique a beam of electrons is transmitted through an ultra-thin specimen, interacting with the specimen as it passes through. An image is formed from the interaction of the electrons transmitted through the specimen, which is then magnified and focused onto an imaging device.

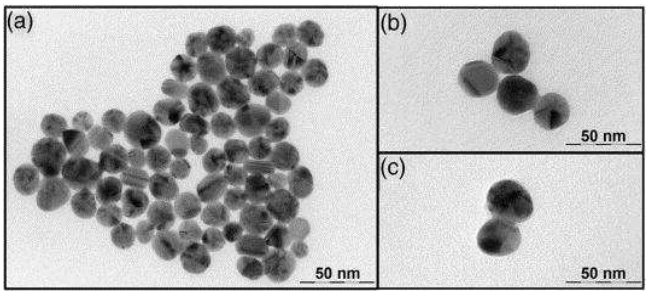

Figure 19. TEM images of silver nanoparticles synthesized using different molar concentration of tannic acid (a) 2.9 µM of tannic acid, average particle size 19.5 ± 3 nm, (b) 5.9 µM of tannic acid, average particle size 25.4 ± 2.8 nm, (c) 23.5 µM of tannic acid, average particle size 29.7 ± 4.3 nm[219].

Borrowing the concept from X-ray diffraction, the electron diffractogram in TEM is the diffracted intensity I as a function of either the scattering angle θ or the scattering vector q. Diffractogram sometimes is also called one dimensional (1-D) diffractogram, while a diffraction pattern is occasionally called two dimensional (2-D) diffractogram. Therefore, in some cases, the Fourier transform of the image intensity distribution can also called the diffractogram of the image.

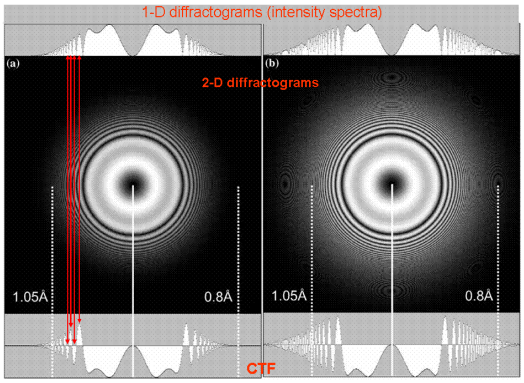

Figure 20. (a) and (b) CTFs and diffractograms obtained based on two different TEM systems [220].

By considering the aforementioned discussions and associated literature review it was palpable that in spite of extensive literature in various aspects of dye-surfactant / polymer / nanoparticle interaction as well as the synthesis of the inorganic nanomaterials, further scopes are there as they all have several lacunae. This has motivated the researcher to undertake the following investigations:

i. Systematic investigations on the photophysics of eosin Y (EY) in different cationic surfactants and also in the solvents of different polarity.

ii. Comprehensive studies on the interaction of three cationic polymers with EY have been done.

iii. A detailed physico-chemical studies on the interactions of imperfect nanocolloidal dispersion of silica with 7-hydroxycoumarin (7HC) have been undertaken.

iv. And finally a simple one–pot synthesis of stable AgBr nanoparticles in aqueous media and their characterization have been reported.

AIMS AND SCOPES OF THE PRESENT STUDY

AIMS AND SCOPES OF THE PRESENT STUDY

Studies on the photophysical behaviour of dye molecules in microheterogenous media have gained special attention because of their multifarious application potentials. Dye-surfactant interaction studies are considered to be significant as they can provide useful information about the altered environment of the medium induced by surfactants. Besides, such systems are mimetic to the compartmentalized systems like cell membrane, vesicles, etc. Information on the conformational aspects of polyelectrolytes in the solution phase can be investigated through dye-polymer interaction studies. Besides, such studies are considered to be mimetic to host-guest or drug-biomolecular aggregates. Physicochemical studies on dye-colloidal aggregates would have been equally important in the field of waste water treatment, lasing property, dye-sensitized solar cells, photocatalytic reactions, etc.Considering the diverse applications, it is worthy to have sufficient information on the dye-surfactant/polymer/nanoparticle aggregates at the molecular level. Synthesis and characterization of silver bromide nanoparticles in aqueous medium have practical applications which augmented the significance of the study. The specific aims and scopes of the works, as described in the present dissertation, are summarized below:

1. Although many reports on dye-surfactant interaction studies are available in the literature, however, systematic investigations on the photophysics of eosin Y (EY) in different cationic surfactants and also in the solvents of different polarity are not plenty. Thus interaction of EY with different cationic surfactants, by spectroscopic techniques, is considered to be significant. Such studies with the variation of surfactant head group, chain length, as well as the number of hydrocarbon chains are also considered to shed further light in this area of research. Solvent polarity can significantly control the photophysical characteristics of a dye. Hence spectroscopic investigations on dye molecules in solvents of different polarity can

provide information involving the solvation capacity of the dye molecules and their aggregation behaviour.

2. Studies involving oppositely charged dye-polymer aggregates are important in order to understand the interaction mechanism and thus explore the yet to be known aspects of different physicochemical decolourisation processes. Although there are several reports on the interaction of cationic dyes with anionic polyelectrolytes, however, use of polycation in dye-polymer interaction studies are rare.
3. A detailed spectral investigation on the absorption and fluorescence spectra of dye-silica aggregates are warranted for better technological applications as well as from the fundamental understanding point of view. Till date, many reports are available in literature involving the interaction between silica and a number of dyes, but reports on the interaction of colloidal silica with 7-hydroxycoumarin (7HC) are not common. Such a study will help in understanding the extent of interaction and occurrence of excited state H-bonding between silica and 7HC in a better way.
4. Nanoparticles of silver bromide serve as model material to study the quantum confinement effects of indirect band gap semiconductors, sensitive photographic material for high-speed photography, and efficient photocatalyst for hydrogen generation from a solution of methanol and water. Also, they serve as a source of strongly biocidal but nontoxic Ag+ ions. Despite manifold applications of AgBr nanoparticles, it is difficult to obtain stable colloidal dispersions of AgBr especially in the aqueous medium. Therefore, a one–pot synthesis of stable AgBr nanoparticles by simple addition of $AgNO_3$ solution to cetyltrimethylammonium bromide solution in aqueous media will prove to be essential for practical purposes.

CHAPTER 1

Spectral behaviour of Eosin Y in different solvents and aqueous surfactant media

Abstract

Photophysical behaviour of the anionic xanthene dye, eosin Y (EY) was investigated in solvents of different polarity as well as in the presence of aqueous cationic surfactants. From the correlation between $E_T(30)$ and Kosower Z values of EY in different solvents, subsequent parameters for EY were determined in the presence of surfactants. A red shift, both in the absorption and emission spectra of EY, was observed with decreasing solvent polarity. Dimerization of EY was found to be dependent on solvent polarity. Cationic surfactants retarded the process of dimerization, which were evident from the lower dimerization constant (K_D) values, compared to that of in pure water. Dye-surfactant interaction constants were determined at different temperatures (298 – 318K) and subsequently the thermodynamic parameters, viz., ΔG^0, ΔH^0 and ΔS^0 were evaluated using the interaction constant values. The fluorescence spectra of EY followed the same trend as in the absorption spectra, although with lesser extents. Stokes shifts were calculated and correlated with the polarity of the medium. Fluorescence of EY was initially quenched by the cationic surfactants in their pre-micellar region, which then followed a red shift with intensity enhancement. Fluorescence quenching was found to be of Stern-Volmer type where the excited state lifetime of EY remained unchanged in different surfactant media. However, the anisotropy value of EY was changed in the post micellar region of surfactants.

Spectrochim. Acta A **2011,** 81, 458-465.

1. Introduction

Surfactants have a tendency to accumulate at the air-liquid interface and thus they can change the properties of interface. In addition, because of their amphipathic structures, they can congregate to form a stabilized entity, called micelle, after the attainment of critical micelle concentration (CMC) [221]. Among the different industrial applications, surfactants are used in dye industry as they can wet [222] and help in the dispersion of dyes, especially which are poorly soluble. Examples include industrial cleaners, cosmetics, plasticizers in cements and concretes, etc [223,224]. Thus the study of dye-surfactant interaction is important from the fundamental understanding point of view as well as industrial applications. Photophysical studies of dyes in aqueous surfactant solution are also important to understand the mimicking bio-membranous interfaces [225]. According to Bhowmik and Ganguly [225], dye molecules form 1:1 charge transfer complex with oppositely charged surfactants. Surfactants are also used as solubilizers for water insoluble dyes, as disaggregating agent for dyes, which accelerates the adsorption of dye on fibres [226]. Besides, dye-surfactant interaction studies can effectively determine the critical micelle concentration of surfactants [58,59].

EosinY (EY) belongs to the xanthene group of dyes and studies on the interaction of surfactant with different xanthene dyes have been performed for a substantial period of time[225,227-229]. EY is a xanthene derivative and finds many applications, viz., in solvent polarity determination [227], lasers, CMC determination [58], the characterization of super conductors, etc. [230]. EY sensitized nanoparticles can produce hydrogen by photocatalytic decomposition of water [231]. Although several studies have been made involving dye-surfactant interactions, yet this particular field of research is still important for improvised dyeing process in terms of theoretical, technological, environmental as well as economic point of view [232]. According to Göktürk et al. [62], a dye molecule exhibits spectral changes in presence of varying amount of surfactants consistently and there exist sequential equilibria between surfactant monomers, micelles, dye aggregates and pre-micellar dye-surfactant complex, etc. Solvents also play important role on the spectral and aggregation behaviour of dye molecules, which subsequently find

many applications as described by De et al. [227]. Effect of solvent polarity on the aggregation behaviour of EY has been studied by De et al. [227], where a significantly high concentration of dye was used (as high as 10^{-3}M). However, practical applications, which count for economy, environmental issues and lesser usage of dye molecule, photophysical studies of EY in the dilute region, is believed to be more important. In addition to this, a systematic investigation on the photophysical behaviour of EY in a variety of solvents is also not common in literature. Photophysical studies of EY in presence of different surfactants are also not very common [225,227].

The present study deals with the photophysical behavior of EY in solvents of different polarities and cationic surfactants. The endeavour was to undertake a physico-chemical investigation on the effects of different solvents (protic and aprotic) on EY. The solvents used were water, methanol, ethanol, n-propanol, n-butanol, n-propanol, n-butanol, n-pentanol, DMF and DMSO. Also, systematic studies on the interaction between EY and different cationic surfactants were undertaken with the variation of surfactant head group, chain length, as well as the number of hydrocarbon chains. The surfactants used were hexadecyltrimethylammonium bromide, hexadecylpyridinium chloride, didodecyldimethylammonium bromide and didecyldimethylammonium bromide. As the polarity of a solvent controls the photophysical characteristics of a dye at the molecular level, hence such studies are assumed to provide information involving the solvation capacity of the dye molecules and their aggregation behaviour. These parameters could directly be estimated using the Kosower Z values, dielectric constants and the refractive indices of the media. Effect of solvent polarity on the self-aggregation of dye molecules can also be estimated from such studies. Dye-surfactant interaction studies are believed to shed information on the polarity of the medium (governed by added surfactants), nature and extent of interactions between dye and surfactant molecules as well as the self-aggregation behaviour of dye in presence of the surfactants.

2. Experimental section

2.1. Materials

The anionic xanthene dye, 2-(2, 4, 5, 7-tetra bromo-6-oxido-3-oxo-3H-xanthen-9-yl) benzoate, disodium salt (eosin Y, EY) was a product from Sigma-Aldrich, USA. The cationic surfactants, hexadecyltrimethylammonium bromide (CTAB, Aldrich, Germany), hexadecylpyridinium chloride (CPC, SRL, India), didodecyldimethylammonium bromide (DDAB) and didecyldimethylammonium bromide (DeDAB, Fluka, Switzerland) of >99% purity were used. Solvents used, viz., methanol (MeOH), ethanol (EtOH) and n-butanol (ButOH) (sd fine chem. Ltd India); n-propanol (PrOH) (SRL, India); n-pentanol (PentOH) (Lobe Chemie Pvt. Ltd. India); dimethyl formamide (DMF) and dimethyl sulphooxide (DMSO) (E. Merck, India) were of HPLC grade. A.R. grade glycerol was a product from SRL, India. Water used in this study was deionised and doubly distilled.

2.2. Methods

A stock solution of 1.0 mM EY was prepared to perform the experimental works after proper dilution as per requirement. The visible absorption spectra were recorded on a UVD-2950 spectrophotometer (Labomed Inc., USA). Spectra were recorded in the range 400-600nm using a matched pair of quartz cuvette of 1.0 cm path length. The fluorescence spectroscopic measurements were performed using a bench-top spectrofluorimeter (Quantamaster-40, Photon Technology International Inc., NJ, USA). Fluorescence data were recorded at controlled room temperature. The excitation wavelength for EY was set at 500nm (λ_{ex}) and the emission spectra were recorded in the range of 500-650nm. Fluorescence anisotropy measurements were performed at an emission wavelength of 540nm (λ_{em}^{max}). Steady state fluorescence anisotropy (r) was determined according to the expression,

$$r = \frac{(I_{VV} - G.I_{VH})}{(I_{VV} + 2G.I_{VH})} \qquad (1)$$

where, G = I_{VV} / I_{HH}. I_{VV} corresponds to the intensity obtained when the excitation and the emission polarizers are oriented vertically. I_{VH} is the intensity obtained for vertical excitation polarizer and horizontal emission polarizer. I_{HV} and I_{HH} refer to similar parameters as above for the horizontal positions of the excitation polarizer [233].

Fluorescence lifetime measurements of EY were recorded with the same fluorimeter where a nano LED (Photon Technology International Inc.) of 505nm wavelength was used to excite the dye. Fluorescence decays were obtained by ströbe technique [234].

3. Results and discussion

3.1. Absorption spectra of EY

3.1.1. Effect of dye concentration on the absorption spectra of EY

Figure1A describes the visible absorption spectra of aqueous EY at different concentrations (2 – 20 μM). The aqueous solution of EY exhibits an intense band at 517nm with a shoulder at 496nm. The present observation was found to be comparable with previous reports [58,227]. The band at 517nm corresponds to the monomeric form of EY while the shoulder at 496nm is due to the dimeric form of EY. According to De et al. [227], EY dimerizes through the stacking of two monomers (Type A), alternately known as H-aggregates. With the increasing

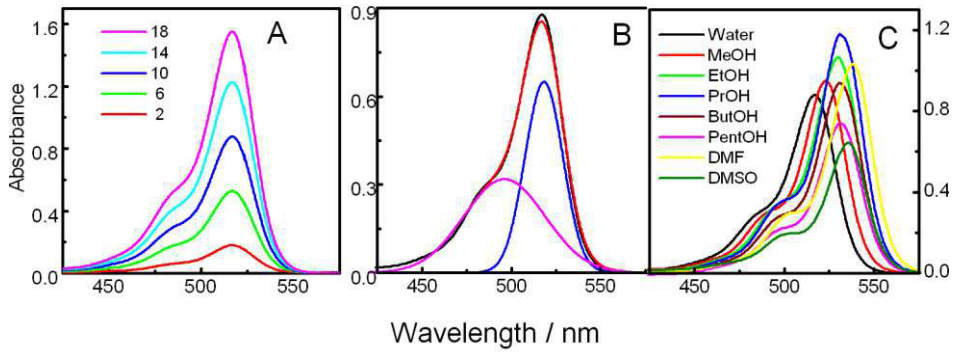

Figure 1. (A) *Absorption spectra of EY in water at different concentrations (in μM, mentioned inside the figure). (B) Resolved absorption spectra of 10 μM EY in* H_2O (purple and blue), the red and black lines represent the reconstituted and original spectra of EY respectively. (C) Absorption *spectra of 10 μM EY in different solvents (as mentioned in the figure). Temperature 298K.*

concentration of the dye in water, intensity of both the bands increased. However, the relative enhancement in the intensity of 496nm shoulder was found to be higher than that of the 517nm peak. Results clearly suggest that with increasing EY concentration in water the process of dimerization through the stacking of monomers increases. Thus the ground state population of the dimeric form increases with increase in dye concentration[22,232]. As in the present study, the maximum concentration of dye in water was 20μM, therefore, no higher aggregates, other than the dimers were expected [227]. The absorption spectra of EY were resolved using principal component analysis method, as detailed in different publications of Estelrich et al. [232] and De et al. [227]. Briefly, the spectra were fitted to two overlapping Gaussian curves with the help of Gaussian curve fitting, as shown in Figure 1B. As already stated, the resolved spectra of EY in water comprise of two peaks. Therefore, it could be assumed that there exists equilibrium between the monomer (M) and the dimer (D) at a particular temperature. If we consider the following equilibrium (ignoring the existence of higher aggregates other than the dimer):

$$2M \Leftrightarrow D \tag{2}$$

then the equilibrium constant (K_D) could be expressed as:

$$K_D = C_D / C_M^2 \tag{3}$$

where, C_D and C_M stand for molar concentration of dimeric and monomeric form of EY.

Thus, the total absorbance of EY at a particular wavelength A(λ) is contributory effect of both the monomeric and dimeric form of EY. Therefore one can make a following expression:

$$A(\lambda) = \varepsilon_M(\lambda)\, C_M + \varepsilon_D(\lambda)\, C_D \tag{4}$$

The term '$\varepsilon(\lambda)$' stands for the molar absorption co-efficient at a particular wavelength (λ). The ultimate solution for resultants of equation takes the following form as:

$$A(\lambda) = \varepsilon_D(\lambda)\left(\frac{C}{2} - \frac{-1 \pm \sqrt{1 + 8.K_D.C}}{8.K_D}\right) + \varepsilon_M(\lambda)\left(\frac{-1 \pm \sqrt{1 + 8.K_D.C}}{4.K_D}\right) \quad (5)$$

K_D can suitably be determined by iterative method as described by Estelrich et al. [232]. If one plots the molar absorbance, A(λ), as a function of dye concentration (C) at any wavelength, one can determine the molar absorptivity of monomer, $\varepsilon_M(\lambda)$, dimer, $\varepsilon_D(\lambda)$ and the dimerization constant, K_D. The non-linear least square regression analysis of the above equation was done using Microsoft Excel (Solver)[TM] program. Initially, some hypothetical value of $\varepsilon_M(\lambda)$ and $\varepsilon_D(\lambda)$ were provided to the solver. The molar absorptivity of the lowest concentration of the dye was approximated for the monomeric form while that of the dimeric form was considered as highest concentration. The iterative method of using MS Excel (Solver)[TM] minimises all the values and hence K_D can be determined. K_D value of aqueous EY in the studied concentration range (2 – 20 μM) was found to be 9.7 x 10^4 M^{-1}. The present result for the K_D value was found to be higher than that reported by De et al. [227] (3.0 x 10^4 M^{-1}). In their study, the concentration range of EY was much higher than the present concentration range, where the probability of higher aggregate formation was less than the reported systems of De et al. [227].

3.1.2. Effect of solvent polarity

Solvent polarity plays a great role on the spectral behaviour of a dye molecule. Therefore, by suitably analysing the spectral behaviour of a dye molecule, a solvent can be characterized in terms of its polarity and solvation power. Spectra of EY were recorded in a number of solvents of different polarity. Two categories of solvents were used, viz., protic (water, methanol, ethanol, n-propanol, n-butanol and n-pentanol) and aprotic (DMF and DMSO). It may be mentioned that due to its ionic nature, EY was insoluble in solvents like n-alkanes, cyclo-alkanes, chloroform, carbon tetrachloride, etc. The absorption maximum (λ_{max}^{abs}) of EY was shifted to higher wavelength (red shift) with the decrease in solvent polarity. The λ_{max}^{abs} for EY followed the order: water < methanol < ethanol < n-propanol ≈ n-butanol ≈ n-pentanol < DMSO < DMF. Spectra of EY in different solvents have also been shown in Figure1 C.

The solvent polarity parameter, $E_T(30)$, of EY was evaluated using the following formula [235,236]:

$$E_T(30) = 28591 / \lambda_{max}^{abs} \quad (6)$$

Another parameter called Kosower Z value is also used as standard of solvent polarity [237], which are readily available in the literature.

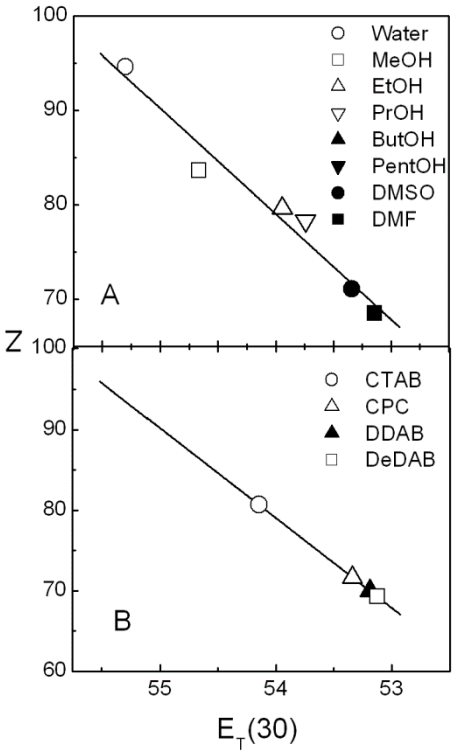

Figure 2. Kosower Z vs. $E_T(30)$ profile for *10μM EY in (A) solvents of different polarity* and (B) surfactants at 298K. Solvents and surfactants are mentioned inside the figure.

It was found that the Kosower Z value decreases linearly with the decrease in solvent polarity as shown in Figure 2A. $E_T(30)$ values of EY in presence of different surfactants were also calculated using equation (6) (spectral behaviour of EY in presence of surfactants will be discussed later). A good linear co-relation between the Kosower Z and $E_T(30)$ values for EY and different surfactants were also observed as shown in Figure 2B. Table 1 summarises the results of the spectral analyses of EY in different solvents and aqueous surfactant solutions.

While considering the process of dimerization (the method of K_D determination has previously been described in detail), it was found that the K_D value decreased with the decrease in solvent polarity. This was as predicted. It is

Table 1. Spectral parameters of EY in presence of different solvents and surfactants at 298K.

Solvent/system	$E_T(30)$	Z	K_D x 10^4 /lit.mol $^{-1}$	$\bar{\nu}_a$/cm^{-1}	$\bar{\nu}_f$/cm^{-1}	$\Delta\bar{\nu}$/ cm^{-1}
Water	55.3	94.6	9.7	19342.4	18518.5	823.9
MeOH	54.7	83.6	9.8	19120.5	18416.2	704.3
EtOH	53.9	79.6	9.1	18867.9	18248.2	619.7
PrOH	53.7	78.3	7.1	18797.0	18018.0	779.0
ButOH	53.7	77.7	6.8	18797.0	18115.9	681.1
PentOH	53.7	77.6	5.5	18797.0	18115.9	681.1
DMSO	53.3	71.1	7.5	18656.7	17921.2	735.5
DMF	53.1	68.5	5.5	18587.4	18148.8	438.6
CTAB (15)	54.1	80.7	7.9	18939.4	18248.2	691.2
CPC (15)	53.8	77.3	6.1	18832.4	18214.9	617.5
DDAB (0.03)	53.3	71.7		18656.7	18115.9	540.8
DeDAB (0.2)	53.1	69.4		18587.4	18115.9	471.4

Parentheted values indicate the surfactant concentration in mM. 10 μM EY was used for study.

expected that with the decrease in solvent polarity the process of dimerization (formation of H-aggregates) will be hindered. As surfactant in water also lead to the decrease in polarity, hence the K_D value of EY in surfactant medium should decrease compared to the K_D value in pure water. Besides, coulombic interaction of EY with oppositely charged surfactant retards the process of dimerization. Analysis of Table 1 reveals that the dimerization constant of EY was almost the same in water and methanol. Protic solvents favoured the process of dimerization than the aprotic solvents. The trend leads to the conclusion that the dielectric constant of the medium plays an important role in dye aggregation. Thus, hydrophobic interaction of dye molecules will be strong enough to overcome the electrostatic repulsion between the anions. Also, the –OH group present in water and alcohols promote aggregation, as hydrogen bonding plays an important role which is revealed by near similarity of K_D values for water, methanol and ethanol.

3.1.5. Effect of surfactants

Figure 3 describes the effect of the surfactants (CTAB, CPC and DDAB) on the absorption spectra of 10μM EY in water. The intensity of EY absorption decreased and subsequently the absorption maximum of EY was also shifted to higher wavelengths with the progressive addition of cationic surfactants. After a

certain concentration of the surfactant was attained, there was no shift in the peak position (except didodecyldimethylammonium bromide). However, there was increase in the absorbance value which eventually attained maximum. Such spectral shift in presence of surfactants is not uncommon [225,227]. In presence of CTAB, CPC and DDAB, the absorption maxima were red shifted to 528, 531 and 536nm respectively (for pure EY in water the value was at 517nm), indicating electrostatic interaction between EY and oppositely charged cationic surfactants[225,238]. Between CTAB and CPC, CPC exhibited stronger interaction with EY, as

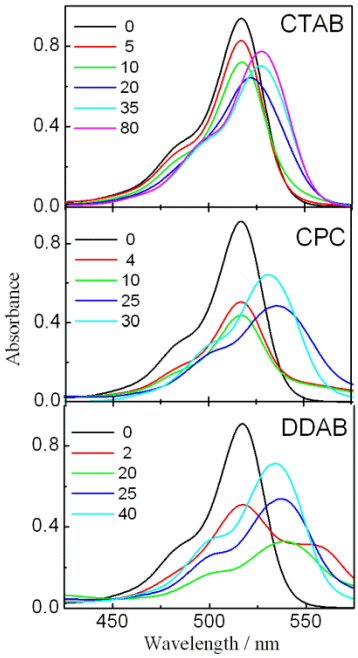

Figure 3. *Absorption spectra of 10μM EY in* water in the presence of different concentrations of surfactants at 298K. *Surfactants and their concentrations (in μM)* are mentioned in the figure.

it required lesser amount to cause significant spectral change. Both CPC and CTAB have similar hydrocarbon chain length, but the hydrophilic-lipophilic balance (HLB) value of CPC being higher [239,240], its hydrophilic interaction (which was prevalently electrostatic in nature) with the dye is higher. A surfactant having higher HLB value implies its stronger affinity towards water and vice versa. Besides, the presence of a planar pyridinium ring favours better stacking of the dye with CPC. A significant spectral change was also observed in case of the doubled tailed surfactant, DDAB. In fact, the hydrophobic interaction is definitely higher in case of DDAB compared to the other single tailed surfactants. Also, vesicle formation could play some role in this case [24,241,242]. Similar were the

observations for DeDAB (spectra not shown). The spectral data with a fixed concentration of EY and varying concentrations of the cationic surfactants (CTAB, CPC, DDAB and DeDAB) have been utilized to calculate the binding constant (K_b) of the dye with the surfactants using Rose and Drago's absolute method [243] :

$$\frac{(C_D.C_S)}{(A-A_0)} = \frac{1}{[K_b.L(\varepsilon_{DS}-\varepsilon_D)]} + \frac{C_S}{[L(\varepsilon_{DS}-\varepsilon_D)]} \quad (7)$$

where, C_D = initial concentration of the dye, C_S = initial concentration of the surfactant, A_0 = absorbance of the pure dye solution at λ_{max}^{abs}, A = absorbance of the dye-surfactant solution at λ_{max}^{abs}, K_b = binding constant of the dye with surfactant, ε_D = molar absorption coefficient of the dye, ε_{DS} = molar absorption coefficient of the dye-surfactant complex, L = optical path length of the solution. The values of $(C_D.C_S)/ (A-A_0)$ were plotted against C_S and a straight line was constructed (figure not shown to save space). From the slope and intercept of the linear plots, the binding constant, K_b was calculated. The K_b values for the surfactants were calculated at five different temperatures (298, 303, 308, 313 and 318K). From the K_b values, the thermodynamic parameters like the standard Gibbs free energy change (ΔG^0), the standard enthalpy change (ΔH^0) and the standard entropy change (ΔS^0) for the dye-surfactant complex formation were determined using standard thermodynamic expressions [244]:

$$\Delta G^0 = - RT \ln K_b \quad (8)$$

Changes in the standard enthalpy, ΔH^0, were evaluated by the van't Hoff equation:

$$\left[\frac{\partial(\Delta G^0)}{\partial(1/T)}\right] = \Delta H^0 \quad (9)$$

In the present study, ΔG^0 vs. T profile was found to follow a 2^0 polynomial equation as [245]:

$$\Delta G^0 = a + bT + cT^2 \quad (10)$$

where a, b and c are the polynomial coefficients**.**

The polynomial coefficients thus helped in determining the ΔH^0 values described in the following expression:

$$[\frac{d(\Delta G^0/T)}{d(1/T)}] = a - cT^2 = \Delta H^0 \quad (11)$$

The standard entropy change (ΔS^0) for the dye-surfactant complex formation was then evaluated according to the following expression:

$$\Delta S^0 = (\Delta H^0 - \Delta G^0)/ T \quad (12)$$

Table 2. Thermodynamic parameters for the interaction of EY with different surfactants.

Surfactants	T/K	K_b x10^4	(-)ΔG^0/kJmol$^-$	ΔH^0/kJmol$^-$	ΔS^0/JK$^-$
CTAB	298	4.62	26.69	-16.38	34.62
	303	3.67	26.56	-35.28	-28.77
	308	2.94	26.43	-54.49	-91.12
	313	1.94	25.77	-74.02	-154.16
	318	1.15	24.80	-93.87	-217.19
CPC	298	13.52	29.36	-78.54	-165.03
	303	7.16	28.25	-63.74	-117.12
	308	6.69	28.54	-48.69	-65.41
	313	3.99	27.65	-33.39	-18.33
	318	3.83	27.99	-17.85	31.90
DDAB	298	6.75	27.06	-37.08	-31.70
	303	5.70	27.67	-11.30	54.03
	308	4.57	27.56	14.91	137.90
	313	8.73	29.70	41.55	227.64
	318	8.53	30.11	68.62	310.48
DeDAB	298	2.35	25.02	-53.48	-95.53
	303	1.68	24.59	-35.87	-37.21
	308	1.48	24.67	-17.96	21.79
	313	1.38	24.88	00.25	80.27
	318	1.45	25.41	18.74	138.86

10 *μM EY was used for study.*

Thermodynamic parameters for the formation of the dye-surfactant complexes have been summarized in Table 2. Analysis of the table reveals that

with the increase in the temperature, the binding constant (K_b) values decrease, revealing the binding process to be exothermic in nature. Negative ΔH^0 values also support this, although few exceptions were observed in case of DDAB and DeDAB at higher temperatures. ΔG^0 values reveal that the spontaneity of the dye-surfactant binding process is maximum at 298K in case of single tailed surfactants. Also, the higher values of free energy change indicate the dye-surfactant interaction process to be governed both by electrostatic and hydrophobic forces[225,238].

3.2. Fluorescence spectral studies

3.2.1. Effect of dye concentration

When excited at 500nm, an aqueous solution of 2μM EY emits maximum radiation at 535nm (λ_{em}^{max}). Unlike the absorption spectra EY did not exhibit any significant shoulder in its emission spectra. Figure 4A reveals that with the increasing EY concentration in water, the fluorescence intensity was enhanced and the λ_{em}^{max} was progressively shifted to higher wavelengths up to 545nm. However, in case of absorption spectra no spectral shift occurred with increasing dye concentration. The enhancement in the fluorescence intensity (F.I.) with increasing dye concentration and the absence of any significant dimeric band in the emission spectra proves that the excited state is predominantly populated with the monomeric form of EY and therefore, excited state aggregation is not permitted. In the case of absorption spectra, absorbance vs. concentration profile for EY at λ_{abs}^{max} was linear. But in aqueous medium, F.I. vs. [EY] plot was linear up to 10μM, beyond which a negative deviation from linearity was noted in all the cases. Such phenomenon was probably due to the self quenching of the dye molecules.

3.2.2. Effect of solvent and surfactant on the emission spectra of EY

Emission spectral shift in different solvents followed the same sequence as in the absorption spectra. Emission spectra of EY in different solvents have been present in Figure 4B.

Stokes shift ($\Delta\bar{\nu} = \bar{\nu}_a - \bar{\nu}_f$,where, $\bar{\nu}_a$ and $\bar{\nu}_f$ are the frequencies of the corresponding absorption and fluorescence maximum respectively) for EY in different environments was also evaluated using the standard procedure[246-248]. In the present case, Stokes shift has been found to increase with increasing solvent polarity. Results are summarised in Table 1 alongwith other spectral data. In case of alcohols, behaviour of n-propanol, n-butanol and n-pentanol did not follow the generalization. Stokes shift value decreased for methanol, compared to water, which also decreased further in case of ethanol. In case of n-propanol, the value was increased. The value did not change systematically among n-propanol, n-butanol and n-pentanol. The results indicate that the increasing hydrophobicity of the higher alcohols could not significantly and systematically control the spectral shift of EY. The anomalous behaviour in the presence of higher alcohols could also be due to the limited solubility. However further studies are warranted to make a final conclusion in this regard. Increase in Stokes shift with increasing solvent polarity indicates stronger solvation of EY. EY, being ionized, is expected to be better solvated with a solvent of higher polarity (exceptions being n-propanol and DMF). Results also suggest that excited state dipole moment was

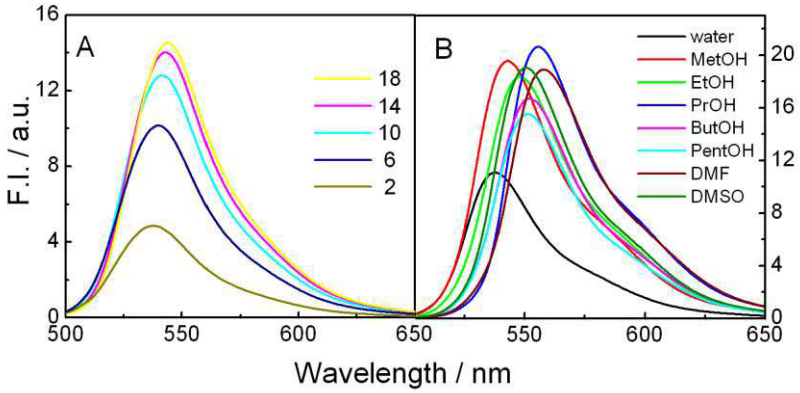

Figure 4. (A) Emission spectra of EY *in water at different concentrations (in μM, as mentioned in the figure). (B) Emission spectra of 10 μM EY in different solvents (mentioned inside the figure). Temperature: 298K;* λ_{ex} = 500nm.

increased in solvents of higher polarity. Larger magnitudes of Stokes shift also indicate the difference between the excited state and the ground state geometry [248].

Similar to the absorption spectroscopic studies, effect of cationic surfactants on the fluorescence spectra of 10μM EY were also undertaken. Results are graphically presented in Figure 5 for CTAB, CPC and DDAB. Unlike the absorption spectra, the emission spectral shift was less induced by cationic surfactants. Emission maximum of EY was only significantly shifted above the critical micelle concentration of all the four surfactants. Surfactants quenched the fluorescence of EY in their pre-micellar region. The cationic surfactants could bind to the anionic dye by way of electrostatic interaction, which finally led to the decrease in fluorescence. Quenching was found to be of Stern-Volmer type, assuming that the fluorescence quenching of EY is due to the formation of the excited state complex with the oppositely charged surfactants. Stern-Volmer constant (the interaction constant between dye and surfactant in the excited state)

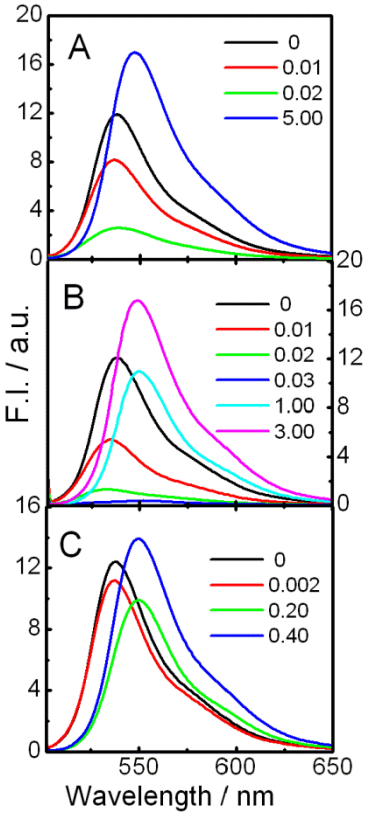

Figure 5. *Fluorescence spectra of 10μM EY in* the presence of different concentrations of (A), CTAB; (B), CPC and (C), DDAB at 298K. Surfactant concentrations (in mM) have been mentioned in the figure.

has been calculated using standard method [227] and also the relation $K_{SV} = k_q \cdot \tau_0$ (k_q = quenching constant and τ_0 = lifetime of the fluorophore), was found to be valid for all the four studied surfactants. As, τ_0 did not significantly change within the studied concentration range for a particular surfactant, hence the product of k_q

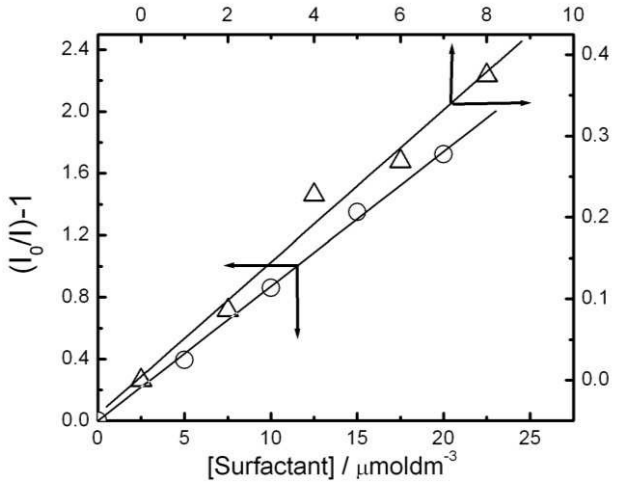

Figure 6. Stern-Volmer *Plot for the fluorescence quenching of 10 μM EY in water by (O),* CTAB *and (Δ), DDAB at 298K.* λ_{ex} = 500nm.

and τ_0 remained constant, i.e., K_{SV} could easily be calculated from the slope of F_0 /F vs. [Q] plot. Stern-Volmer plot for CTAB and DDAB have been shown in Figure 6 as representative. Related results for all the surfactants are summarized in Table 3. Although the excited state lifetime did not change significantly among the four different surfactants, however, the dynamic quenching constants (k_q) varied among the surfactants significantly. For CPC, the value was higher than that of CTAB. Due to the presence of pyridinium ring in CPC there occurred better stacking of EY over CPC, which was not so favourable in case of CTAB. For the double tailed surfactants, the values of k_q were found to be lower even

Table 3. Fluorescence data of aqueous EY solution in the presence of different cationic surfactants at 298K.

Surfactants	10^{-4} x K_{sv} /M^{-1}	τ_0/nS	10^{-13}x k_q/$M^{-1}S^{-1}$
CTAB	8.81	2.50	3.52
CPC	9.41	2.52	3.73
DDAB	4.68	2.60	1.80
DeDAB	4.85	2.54	1.90

10 μM EY was used for study. λ_{ex} *= 500nm.* λ_{em}^{max} = 540nm.

than CTAB. Results indicate retarded interaction between the surfactant head group and EY. Presence of two hydrocarbon tails may hinder the surfactants to be in the proximity of EY. It, therefore, could clearly be concluded that the excited state interaction between dye and oppositely charged surfactants were governed by coulombic interactions [225,249].

3.2.3. Fluorescence lifetime measurements

Time-resolved fluorescence studies were carried out to determine the emission decay parameters for EY in different solvents and surfactants. 10μM EY exhibited a lifetime 2.50 nS. The lifetime did not change significantly with the variation of solvent polarity and surfactant concentration. Similar results were observed by other researchers [227]. The fluorescence decay curve of EY was found to be single exponential in water and in the presence of all the surfactants used (as shown in Figure 7).

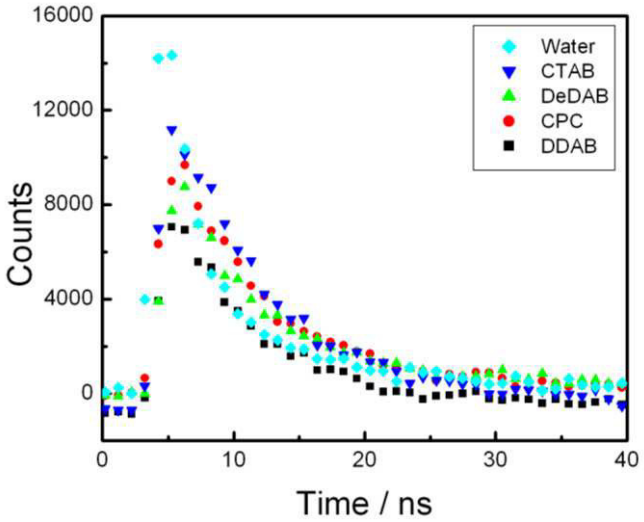

Figure7. *Fluorescence decay curves of 10μM EY in water and different surfactants (mentioned in the figure).* λ_{ex} = 500nm.

3.2.4. Steady-state fluorescence anisotropy

Fluorescence anisotropy provides important information about the micro-viscosity of the medium around a fluorescent dye molecule [238,250]. When a dye molecule binds to oppositely charged micelle, the micro-viscosity of the dye-micelle interface gets significantly changed [251]. Variation of fluorescence

anisotropy with the surfactant concentration has been shown in Figure 8. Pure EY in water has an anisotropy value of 0.057. A mild increase in the anisotropy value was observed in aqueous salt solution (0.057 in water to 0.067 in 1.0mM NaCl solution). The increase in the fluorescence anisotropy with increasing salt concentration was a direct consequence of viscosity enhancement of aqueous salt solution. Among the different alcohols, anisotropy increased with increasing alcohol chain length (data not shown). DMF and DMSO exhibited similar behaviour as that of water. Surfactants could significantly alter the anisotropy value of EY in water. A significant increase in the fluorescence anisotropy of EY was noted in the post-micellar region. Hence, one could employ the anisotropy measurement technique as a tool to determine the critical micellar concentration of surfactant. As already have been mentioned that there is a direct correlation between the fluorescence anisotropy and viscosity of the medium [233,251], therefore, one needs to correlate the anisotropy with viscosity. In the inset of Figure 8, anisotropy dependence of EY on glycerol concentration in water has been shown

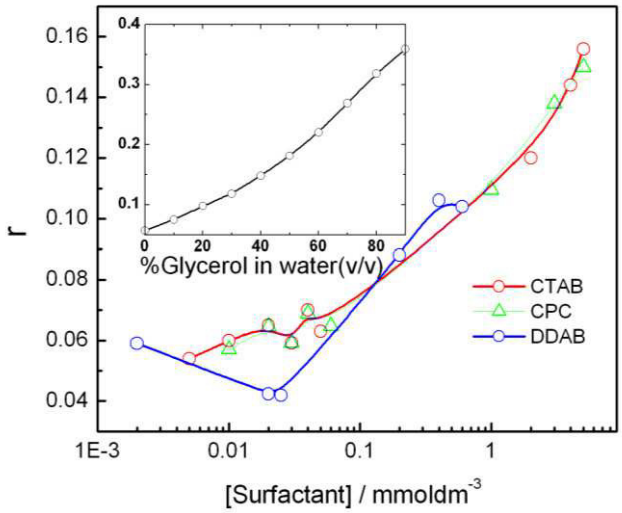

Figure 8. Variation of fluorescence anisotropy (r) of EY with the concentration of surfactant *[surfactant] in water at 298K. A 10 μM EY in water was used.* λ_{ex}*=500nm and* λ_{em}=540nm. Inset: anisotropy – concentration profile of EY in glycerol-water mixture is shown for comparison. Surfactants are mentioned inside the figure.

as reference. It is believed that EY could electrostatically bind at the micellar interface, which restricts the segmental motion of the dye molecule. Hence, the micro viscosity around dye-micelle interface becomes significant than the

viscosity when the dye just binds electrostatically to a surfactant in its pre-micellar region.

4. Summary and Conclusions

Absorption and emission spectral behaviour of the anionic xanthene dye, EY was investigated in the solvents of different polarities as well as in different aqueous cationic surfactant solution. By suitably analysing the spectral data of EY in presence of surfactants in their pre-micellar region, dye-surfactant interaction constant values were determined both in the ground and excited states. Stokes shifts were calculated and correlated with the polarity of the medium. Steady state fluorescence anisotropy values were evaluated in the pre- and post- micellar regions of surfactants in aqueous medium. A significant change in the anisotropy values was observed for EY.

Based on the experimental results the following conclusions could be drawn:

(1) The ground state is predominantly populated with the dimeric form of EY as revealed from the absorption spectra On the contrary, emission spectra of EY prove that the excited state is predominantly populated with the monomeric form of EY and hence excited state aggregation is not permitted.

(2) Dimerization constant (K_D) values in different media reveal that the process is more favoured in protic solvents than the aprotic solvents. The solvent-dye hydrogen bonding plays an important role in the aggregation of the dye molecules.

(3) The dye-surfactant binding process is exothermic in nature and is controlled both by electrostatic and hydrophobic forces, as revealed from the thermodynamic parameters.

(4) A red shift in the absorption spectra of EY with the decrease in solvent polarity was observed. Stokes shifts were found to be correlated with the

polarity of the medium. Larger magnitudes of Stokes shift indicate that the excited state geometry could be different from that of the ground state.

(5) The excited state interaction between EY and surfactants is dependent the nature of the surfactant head group, type and number of hydrocarbon chains, although it is primarily governed by coulombic forces.

(6) Important information regarding the micro-viscosity of the medium around EY could be obtained from the fluorescence anisotropy measurements. Also, this measurement technique could be used as a tool to determine the critical micellar concentration of surfactants.

CHAPTER 2

Molecular Basis of the Binding of Dye to Polycations: Absorption and Emission Spectral Studies

Abstract

Absorption and emission spectral behaviour of an anionic xanthene dye, eosinY was investigated to perceive the nature and extent of interaction with three different cationic polyelectrolytes. The formation of dye-polymer aggregates was found to be associated with two types of interactive forces: electrostatic and hydrophobic forces. The binding constants and stoichiometry of the dye-polymer aggregates in their ground states were determined by suitably analyzing the absorption spectra by varying the concentration of the polymers. Subsequently, the thermodynamic parameters for the interaction processes were evaluated. The interaction parameters followed the sequence PDMDAAC>JR400> LM200. The excited state interaction phenomena were studied from the fluorescence data. Change in the excited state lifetime of the fluorophore was insignificant in all the three cases. Consequently, Stern-Volmer quenching constants of the dye-polymer aggregates were calculated using the standard method. Significant information about the changes on the degree of motion of the fluorescent molecule around the polymer matrix was obtained from the anisotropy measurements.

Communicated to Indian Journal of Chemistry, Section A.

1. Introduction

Studies on the solution behaviour of biologically relevant macromolecules are considered to be important for their multifarious application potentials which cover almost all segment of human life[90], e.g., food, pharmaceutical technology[252,253]. Functionalised organic molecules like dye, when added to polyelectrolyte, also find many applications, viz., textile, film imaging, drug delivery[251,254], etc. Towards proper understanding of the behaviour of polymer, studies on their solution behaviour is necessary[255]. In most of the practical applications polymers are mixed with different additives; the most common example involves the use of dye in textile industry[256-258]. Dye molecules find several industrial applications which cover textiles, paper, plastics, cosmetics and leather. In all the cases dyes are used for aesthetic purpose[259]. According to Chatterjee et al.[238], more than $8x10^5$ tonnes of textile dyes are used annually, whereby, ten percent of them are discharged as effluents. Presence of these colorants in water is not only aesthetically undesirable but also has serious environmental impact[259]. Most of the textile dyes have additional photostability and chemical inertness for which their removal from waste water becomes difficult[260]. Among different physico-chemical decolourisation processes the flocculation / coagulation technique using oppositely charged polyelectrolytes are considered to be more effective[261]. However, the detailed mechanism involved in this process is still not clear. It is therefore, believed that studies involving oppositely charged dye-polymer aggregates would shed further light in understanding the interaction mechanism.

Eosin Y, a xanthene dye, has multiple applications[262]. Although many studies on the dye-polymer interactions have been done so far[263-265], however, studies on interaction of eosin Y with cationic polymers are not so common.

The cationic polymer poly(diallyldimethyl ammonium) chloride; PDMDAAC, is known to be used as a coagulating agent for waste water treatment. Recently Mukherjee et al.[266] have studied the interaction of PDMDAAC with anionic surfactants using a number of techniques. N,N-

dimethyl-N-dodecyl derivative of hydroxyl ethyl cellulose (LM200) and N,N-dimethyl-N-methyl derivative of hydroxyl ethyl cellulose (JR400) are important constituents of the composition for the oxidative dyeing of keratin based fibres[267,268]. They also find wide applications in the formulation of shampoo as they could intensify the degree of accumulation of shampoos[269,270]. The present research group is involved in understanding the solution behaviour of anionic polysaccharides isolated from different bacterial strains of gram negative bacteria Klebsiella[11,84,271]. Also there are several reports involving the interactions of cationic dyes with anionic polyelectrolytes[272-274]. However, use of polycation in dye-polymer interaction studies is not so common. It is believed that such studies would be beneficial specially in waste water treatment[275], ink jet inks[276], textile dyeing[277], fluorescence tuning[278]. Besides, such studies are also considered to be important from the fundamental understanding point of view. The absorption and emission spectroscopic measurements are considered to be the convenient ways in understanding dye polymer aggregates as the dye concentration requirement is usually low. A significant change in the intensity or absorption maxima of dye in the presence of polymer indicates the interaction to take place among the dye and polymer[11]. Formation of a dye-polymer aggregate can be mediated through electrostatic and / or hydrophobic interactions. Different physicochemical parameters, for example, the average mass and charge per repeating unit, stoichiometry of the dye-polymer aggregates and thermodynamic parameters of the binding process can easily be evaluated from such studies. Besides, the tertiary conformation of the macromolecules in solution can also be predicted[11].

The present study involves the interaction of eosin Y with three different cationic polymers. The choice of these three polymers is intentional. Structure of the dye and three polymers have been shown in Scheme1. PDMDAAC has an average molar mass of 162g per repeating unit. It, therefore, can be assumed that the anionic dye eosin Y will prevalently interact with the polymer through electrostatic attraction. And also the degree of motion of the dye molecule bound to the polymer chain is considered to be nearly uniform. However in the case of other two polymers, having structural differences from PDMDAAC as well as

among themselves, would definitely interact differently. Beside electrostatic attraction, hydrophobic interactions are also expected to be involved in case of other two polymers.

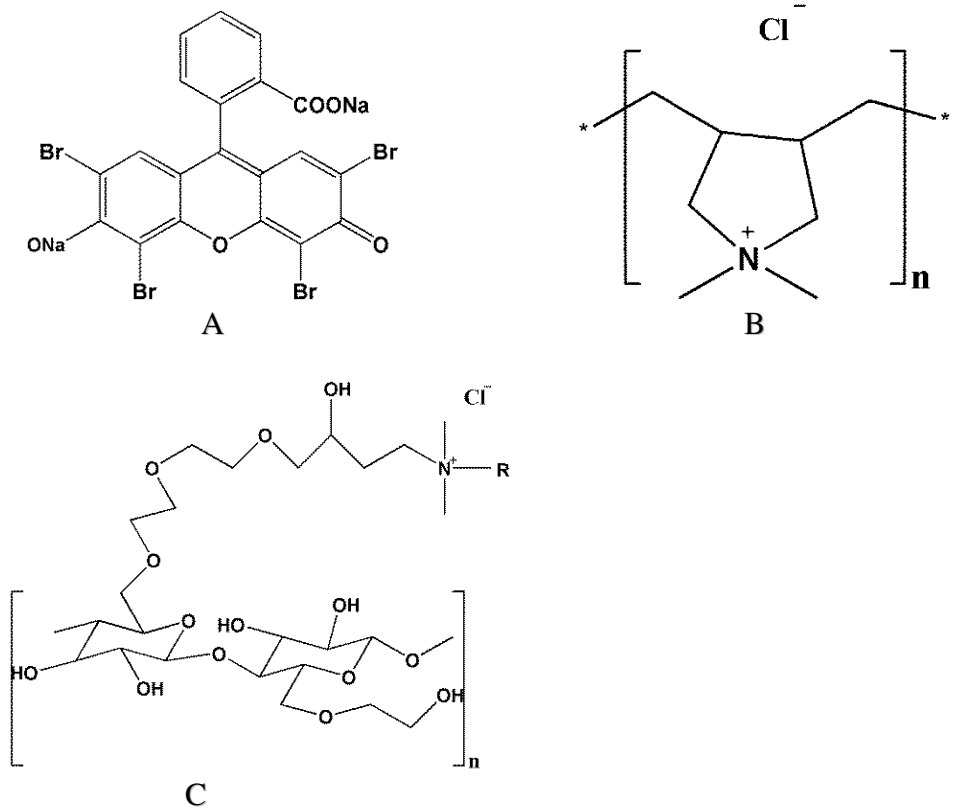

Scheme1. Structures of A, eosinY; B, PDMDAAC and C, JR400 / LM200 (R = $-CH_3$: JR400, R = $-C_{12}H_{25}$: LM200).

The absorption spectral studies were endeavoured to determine the binding constants and stoichiometry of the dye-polymer aggregates in the ground state. The excited state dye-polymer binding constants were evaluated from the fluorescence spectra. Anisotropy measurements can furnish significant information about the changes in the degree of motion of the dye molecule around the polymer matrix.

2. Experimental Section

2.1 Materials

The anionic xanthene dye, 2-(2,4,5,7-tetrabromo-6 oxido-3-oxo-3H-xanthen-9-yl) benzoate, disodium salt (eosin Y, EY) and the cationic polymer poly(diallyldimethyl ammonium) chloride, PDMDAAC, were purchased from Sigma-Aldrich, USA. While the other two cationic polymers N,N-dimethyl-N-dodecyl derivative of hydroxyl ethyl cellulose,LM200 and N,N-dimethyl-N-methyl derivative of hydroxyl ethyl cellulose, JR400 were procured from Amerchol, Union Carbide Chemicals and Plastics Co., USA. The chemicals were stated to be more than 99.5% pure and were used as received. Double distilled water with a conductance of 2-4 μScm^{-1} was used in preparing the solutions.

2.2 Methods

1.0mM aqueous solution of EY and the polymers (PDMDAAC, LM200, and JR400) were prepared using double distilled water. The solutions were then properly diluted as required. The visible absorption spectra were recorded on a UVD-2950 spectrophotometer (Labomed Inc., USA). Spectra were recorded in the range 400 – 600nm using a matched pair of quartz cuvettes of 1 cm path length. Spectra were recorded at five different temperatures (298, 303, 308, 313, and 318 K). The fluorescence spectroscopic studies were carried out in a bench-top spectrofluorometer (Quantamaster-40, Photon Technology International Inc., NJ, USA). EY was excited at 500nm and the emission spectra were recorded in the range 500 – 650nm. Steady state fluorescence anisotropy (r) was determined according to the expression[262]:

$$r = \frac{(I_{VV} - G.I_{VH})}{(I_{VV} + 2G.I_{VH})} \quad (1)$$

where, $G = I_{VV} / I_{HH}$; I_{VV} corresponds to the intensity obtained when the excitation and the emission polarizers are oriented vertically. I_{VH} is the intensity obtained for vertical excitation polarizer and horizontal emission polarizer. I_{HV} and I_{HH} refer to similar parameters as above for the horizontal positions of the excitation polarizer.

Fluorescence lifetime measurements of EY were recorded with the same fluorometer using a nano LED (Photon Technology International Inc.) of 505nm wavelength. The emission data were recorded at 535nm.

3. Results and discussion

3.1 Absorption spectral studies

Aqueous solution of pure EY exhibits a monomeric band at 517nm and a dimeric band at 496nm. Results are in conformity with the previously published reports[262,279]. Effect of polymers in their lower concentration range (0 – 18µM) on the visible absorption spectra of 10µM EY are shown in Figure1. With increasing concentration of PDMDAAC solution, intensities of both the bands of EY decrease with the gradual disappearance of the dimeric band (Figure1A). Appearance of an isosbestic point at 532nm indicates the formation of 1:1 charge-transfer complex between the dye and polymer[22,238]. This also reveals the existence of equilibrium in the binding process. Negatively charged dye, after binding stoichiometrically to the positive centres of the polymer, can stack to each other laterally as two dye molecules are in immediate vicinity of each other as shown in Scheme 2. Similar model has been proposed earlier by Yu et al.[280] The decrease in band intensities is attributed to the electrostatic interaction between the anionic dye and cationic polymer. Attainment of charge neutralization leads to increase in hydrophobicity of the medium around the dye molecule and thus the

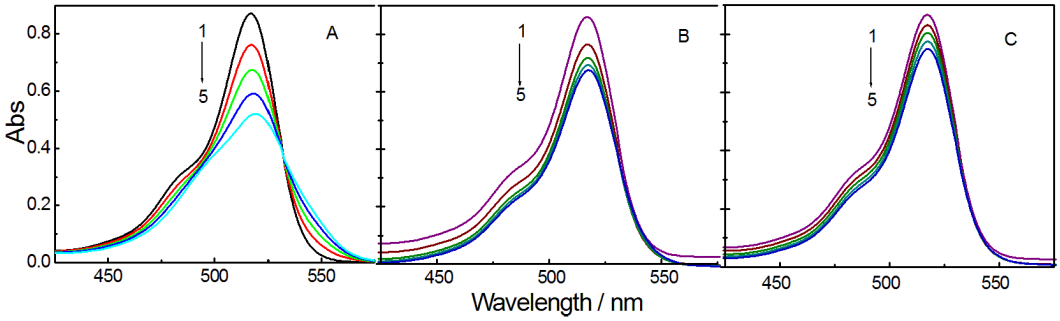

Figure 1. *Absorption spectra of 10µM EY in presence of polymers at different polymer / dye ([P] / [D]) molar ratio.* (A) PDMDAAC, (B) LM 200 and (C) JR 400. [P] / [D] values: (A) 1, 0; 2, 0.2; 3, 0.4; 4, 0.7 and 5, 0.9. For (B) and (C) 1, 0; 2, 0.4; 3, 1.1; 4, 1.4 and 5, 1.8. Temperature: 298K.

band shifted to higher wavelength. Decrease in the intensities of the bands were also observed for LM200 (Figure1B) and JR400 (Figure1C) although to lesser extents. No shifts were observed in the present concentration range in both the cases.

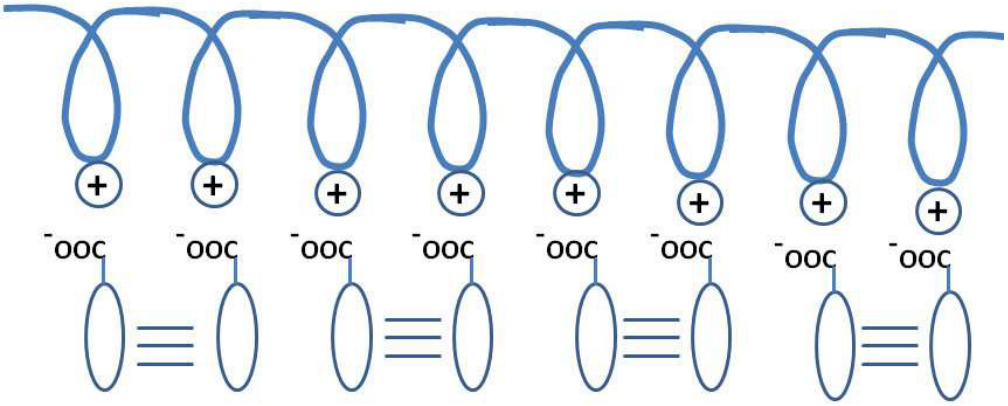

Scheme 2. Proposed model for the stacking of dye at the positive charge centres of polymer.

Effect of polymers on the absorption spectra of EY in higher polymer concentration range was further investigated. Results are summarized in Figure2. In all the three cases there occurred bathochormic shift in the absorption spectra of EY upon the addition of polymers. After the attainment of a certain polymer/dye ratio, no further spectral shift was observed. Such shifts in the peak position are due to encaging of dye into the polymer matrix involving both electrostatic and hydrophobic interactions[1]. However, in case of PDMDAAC the

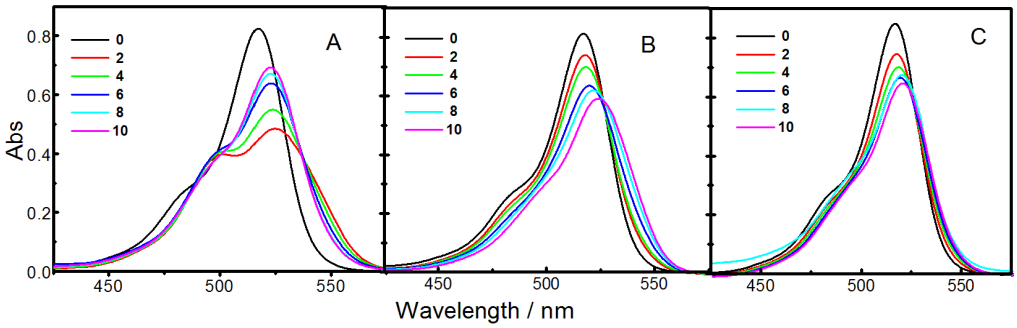

Figure 2. *Absorption spectra of 10μM EY in presence of polymers at different polymer / dye ([P] /* [D]) molar ratio in the higher range. (A) PDMDAAC (B) LM 200 (C) JR 400. [P] / [D] values are mentioned in the figure. Temperature: 298K.

absorbance value increases gradually with the increasing polymer/dye ratio at shifted wavelength (Figure 2A) contrary to LM200 (Figure 2B) and JR400

(Figure2C), where the absorbance decrease with the increasing polymer concentration in the studied range. This is due to higher charge density of PDMDAAC in comparison to LM200 and JR400. Between LM200 and JR400 the former seems to exhibit stronger shift in the band position than the latter due to higher hydrophobicity. It was established in our previously published reports[262] that the absorption maximum shifts to higher wavelength with increasing hydrophobicity of the medium. In the present case due to charge neutralization, the dye molecule experiences less polarity (localized) in the surrounding medium.

The spectral data with a fixed concentration of EY and varying concentrations of the polycations were suitably processed in determining the interaction constant between the dye and the polymers. For PDMDAAC-EY system, the binding constant was calculated using the Benesi-Hildebrand equation[238]:

$$\frac{C_D}{A - A_0} = \frac{1}{\varepsilon_m - \varepsilon_0} + \frac{1}{K_b(\varepsilon_m - \varepsilon_0)C_P} \quad (2)$$

For LM200 and JR400 ground state interaction constants (K_b) of the dye with the polymer at were determined using modified form of Benesi-Hildebrand formalism[281]:

$$\frac{C_D}{A_0 - A} = \frac{1}{\varepsilon_m - \varepsilon_0} + \frac{1}{K_b\ \varepsilon_m - \varepsilon_0\ C_P} \quad (3)$$

where, C_D = concentration of dye, C_P = concentration of polymer, A_0 = absorbance of dye in absence of polymer. A = absorbance of dye in presence of polymer. ε_0 = molar absorption coefficient of the dye in absence of polymer, ε_m = molar absorption coefficient of dye-polymer aggregates. Representative plots of C_D / (A_0-A) vs. 1 / C_P have been shown in Figure 3 for PDAC, LM200 and JR400. From the ratio of intercept and slope the binding constants were calculated. The K_b values show that JR400 undergoes stronger binding with EY than LM400. This was as expected; although the stacking of dye was higher in case of LM200 due to higher hydrophobicity, however, the electrostatic interaction was strong in

case of JR400 due to less steric hindrance of smaller hydrocarbon tail. In the present case the electrostatic interaction precedes over hydrophobic forces.

Two different equations have been used in the study because the spectral pattern of EY-PDMDAAC system was different from that of EY-LM200 and EY-JR400 systems. In case of PDMDAAC, there was bathochromic shift in the spectra of EY in the higher polymer concentration range which then underwent gradual increase in the absorbance with increasing polymer concentration. However, in the cases of LM200 and JR400, the reverse phenomena happened.

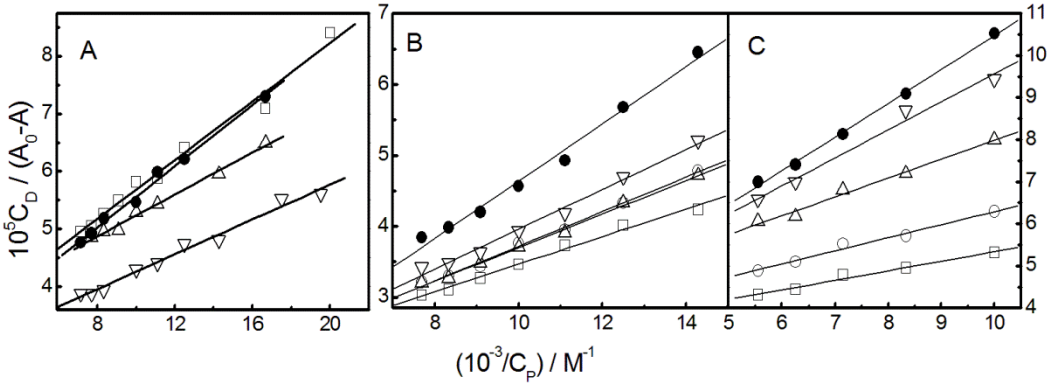

Figure 3. Plot of C_D / (A_0-A) vs. 1 / C_P according to Benesi-Hildebrand formalism to determine *the interaction constant of EY (10 μM)* - polymer aggregates. Polymers: (A) PDMDAAC, (B) LM 200, and (C) JR 400. Temp (in K): □, *298; o, 303; Δ, 308; ▽, 313 and* ●, *318.*

Straight lines were obtained (Figure 3A) from C_D / (A_0-A) vs. 1 / C_P plots and from the ratio of intercept and slope the interaction constants, K_b were calculated. From the K_b values, the thermodynamic parameters like the changes in the standard Gibbs free energy (ΔG^0), the standard enthalpy change (ΔH^0) and the standard entropy change (ΔS^0) for the dye-polymer aggregate were determined using the following thermodynamic expressions[282]:

$$\Delta G^0 = - RT \ln K_b \qquad (4)$$

Changes in the standard enthalpy (ΔH^0) were evaluated by the van't Hoff equation[262]:

$$\left[\frac{\partial(\Delta G^{0})}{\partial(1/T)}\right] = \Delta H^{0} \quad (5)$$

In the present study, ΔG^0 vs. T profile was found to follow a 2^0 polynomial equation as[283]:

$$\Delta G^0 = a + bT + cT^2 \quad (6)$$

where, a, b and c are the polynomial coefficients**.**

The polynomial coefficients thus helped in determining the ΔH^0 values according to the following expression[283]:

$$\left[\frac{d(\Delta G^{0}/T)}{d(1/T)}\right] = a - cT^{2} = \Delta H^{0} \quad (7)$$

The standard entropy change (ΔS^0) for the dye-polymer complex formation was then evaluated according to the following expression[262]:

$$\Delta S^0 = (\Delta H^0 - \Delta G^0)/ T \quad (8)$$

Thermodynamic parameters for the formation of the dye-polymer aggregate have been summarized in Table 1. The results show that with increasing temperature, the binding constant (K_b) values decrease except for PDMDAAC, where the binding is not systematic with the increasing temperature. For this particular system, K_b value passes through a maximum at 308K. This is similar to biologically relevant processes where optimum interaction among the different components occurs at 310K. For LM200 and JR400 results imply that with the rise in temperature the stability of the dye-polymer aggregates decrease as the systems become unstable. Increase in the negative values of enthalpy change with increasing temperature proves the exothermicity of the binding process. The involvement of dual interactions (hydrophobic and electrostatic) is also supported by the higher values of the free energy change. The results of the thermodynamic parameters were found to be comparable with the reversible biological processes[11].

Table 1. Thermodynamic parameters for the interaction of EY with different polymers

Polymer*	T/K	K_b x10^{-3} /M^{-1}	(-)ΔG^0/kJmol^{-1}	(-)ΔH^0/kJmol^{-1}	(-)ΔS^0 /JK^{-1}mol^{-1}
PDMDAAC[a]	298	12.33	23.41	-75.06	-330.43
	308	18.78	25.28	4.88	-66.24
	313	17.59	25.52	45.83	64.9
	318	10.98	24.67	87.45	197.39
LM 200[b]	298	7.80	22.27	-20.32	-142.94
	303	5.29	21.66	18.18	-11.51
	308	5.66	22.19	57.32	114.04
	313	4.12	21.73	97.11	240.83
	318	1.49	19.38	137.53	371.55
JR 400[b]	298	13.50	23.64	35.82	40.88
	303	10.27	23.34	48.41	82.74
	308	7.82	23.03	61.21	123.99
	313	4.34	21.86	74.23	167.30
	318	3.03	21.26	87.45	208.14

*Polymer concentration range (μM): PDMDAAC = 50 – 150.
LM200 = 70 – 150.
JR400 = 100 – 200.

A 10μM EY was used in each study

a) K_b was determined using Benesi-Hildebrand equation [238].
b) K_b was determined using modified Benesi-Hildebrand equation [281].

3.2 Fluorescence spectral studies

Aqueous solution of EY, when excited at 500nm, emits at 535nm. Figure 4 shows that at lower polymer/dye ratio, the fluorescence intensity of the dye is quenched with the gradual addition of polymers. However, quenching efficiency is dependent on the type of polymer. Quenching is more significant in case of PDMDAAC (Figure 4A) compared to LM200 (Figure 4B) and JR400 (Figure 4C). Results reveal that the electrostatic binding is stronger in case of PDMDAAC compared to the other two as the electrostatic binding subjects the probe molecule to the bulk aqueous phase and thus aids the interaction with the quencher [238]. The presence of hydrocarbon tail especially in LM200 renders more hydrophobic forces compared to electrostatic forces. The excited state lifetime of the fluorophore does not change significantly (in the studied concentration range)

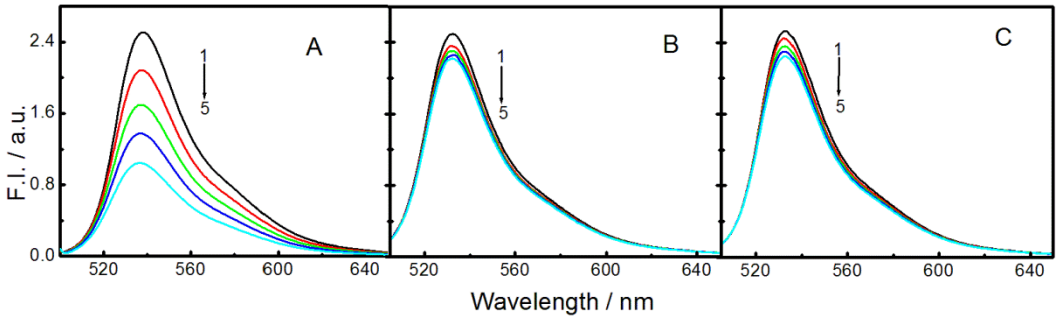

Figure 4. *Fluorescence spectra of 10μM EY in presence of polymers at different polymer / dye* ([P] / [D]) molar ratio. A, PDMDAAC; B, LM 200 and C, JR 400. [P] / [D] values: (A) 1, 0; 2, 0.2; 3, 0.4; 4, 0.7 and 5, 0.9 (B) and (C) 1, 0; 2, 0.4; 3, 1.1; 4, 1.4 and 5, 1.8. Temperature: 298K. λ_{ex} = 500nm.

in all the three cases and the Stern-Volmer quenching constants were calculated using the following method [227]:

$$\frac{F_0}{F} = 1 + K_{sv}[Q] \qquad (9)$$

where, F_0 and F are the fluorescence intensities of EY in the absence and presence of quencher, Q; [Q] = Quencher concentration (herein the polymers). Here K_{SV} is the static quenching and can be expressed as:

$$K_{SV} = K_q \, . \, \tau_0 \qquad (10)$$

where, K_q is the quenching constant and τ_0 is the lifetime of the fluorophore of the quencher.

The product of probe-quencher interaction constant (k_q) and fluorescence lifetime (τ_0) remained constant, i.e., K_{SV} could easily be calculated from the slope of F_0 / F vs. [Q] plot which produced a straight line with unit intercept (figure not shown) proving that the quenching is a static one.. The Stern-Volmer quenching constant (K_{SV}) values are represented in Table 2.

Similar to the absorption spectroscopic studies, fluorescence spectroscopic studies were also carried out at higher polymer / dye ratio (Figure 5). But unlike the absorption spectra, no significant spectral shifts were observed suggesting the fact that the excited state dye-polymer aggregates do not lead to significant

change in polarity. In presence of PDMDAAC (Figure 5A) the fluorescence intensities of EY increases with the increasing polymer / dye ratio. Excited state dye-polymer interaction constant (K) was calculated from the fluorescence using the Benesi-Hildebrand equation[233]:

$$\frac{F_\infty - F_0}{F_x - F_0} = 1 + (K[L])^{-1} \qquad (11)$$

where, F_0 = fluorescence intensity of the dye in absence of polymer, F_x= fluorescence intensity at an intermediate polymer concentration, F_∞= fluorescence intensity at a polymer concentration where the interaction is complete, L= total polymer concentration. Results are summarized in Table 2.

Table2. *Excited state interaction constant of 10 μM EY*-polymer aggregates at 298K.

Polymer	$K_{sv}^{(a)}$ x 10^{-4} /M^{-1}	$K^{(b)}$ x 10^{-5} / M^{-1}
PDMDAAC	11.1	8.5
LM200	1.3	-
JR 400	1.3	-

(a)Values were determined from Stern-Volmer plot [227].
(b)Values were determined from Benesi Hildebrand formalism [233].

While in presence of LM200 (Figure 5B) and JR400 (Figure 5C) no systematic changes were observed.

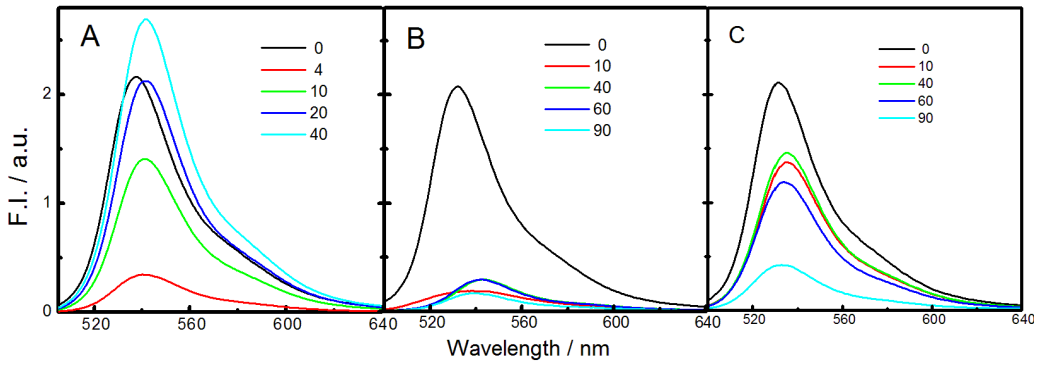

Figure 5. *Fluorescence spectra of 10μM EY in presence of polymers at different polymer / dye* ([P] / [D]) molar ratio in the higher range. (A) PDMDAAC (B) LM 200 (C) JR 400. [P] / [D] values are mentioned in the figure. *Temperature: 298K.* λ_{ex} = 500nm.

This shows that the process of dye-polymer binding for LM200 and JR400 in the excited state is unfavourable at higher polymer / dye ratio.

When the fluorescence data were recorded the background was corrected with respect to the individual polymers. It is worthwhile to mention that in the present study polymers did not exhibit significant absorption in the studied range.

3.3 Steady-state fluorescence anisotropy

Fluorescence anisotropy measurements were carried for all the three systems. Such studies are believed to enlighten ideas on the micro-viscosity of the medium around a fluorophore. Variation of fluorescence anisotropy with the polymer concentration has been shown in Figure 6. The anisotropy value of pure EY in water is 0.06[262], which increases with the increasing polymer concentration and then attain constancy. The increase in the anisotropy value attributes to the increase in the rigidity of the environment surrounding the dye molecule[238] leading to its decrease in the degree of freedom and when all the dye molecules are entrapped within the polymer matrix, the anisotropy values become constant.

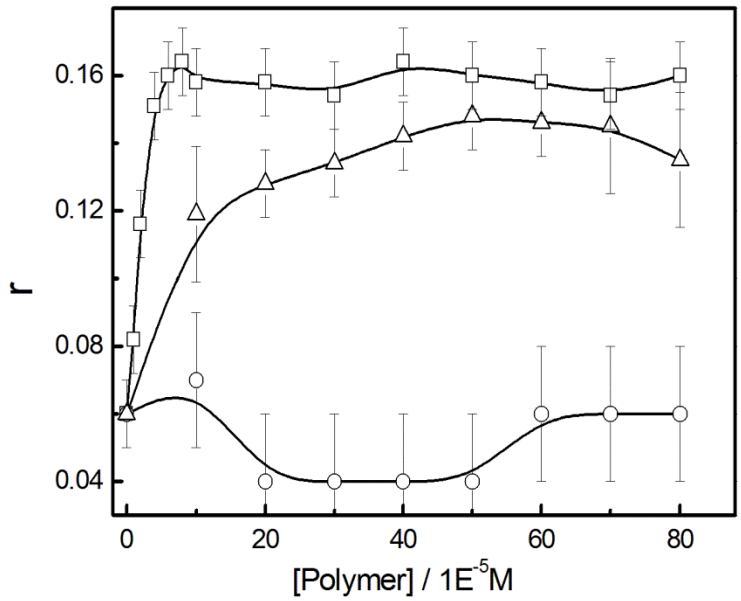

Figure 6. *Variation in the fluorescence anisotropy (r) of 10 μM EY with polymer concentration* ([P]) in aqueous medium at 298K. Polymers: □, *PDMDAAC; Δ, JR 400 and o,* LM 200. λ_{ex}=*500nm and* λ_{em}=535nm.

In case of PDMDAAC, a sharp increase is observed upto polymer / dye ratio value of 10 and after which it did not change significantly, i.e., the rigidity of the environment becomes unchangeable after 100μM PDMDAAC. For JR400, the increase is low in comparison to PDMDAAC. And no significant changes in the anisotropy value with the increasing concentration of LM200 are observed. This again proves that the electrostatic interaction of the dye with LM200 is weak in comparison to JR400.

4. Conclusions

The present work reports comprehensive studies on the interaction of three cationic polymers with an anionic xanthenes dye eosin Y. The dye molecules are held around the polymer matrix both by way of electrostatic and hydrophobic forces. Interaction of EY with PDMDAAC is stronger compared to JR400 and LM200 and also an equilibrium exists in the binding process. In case of JR400, electrostatic interaction precedes over hydrophobic forces, compared to LM200, as evidenced from the binding constant values. The binding processes are exothermic in nature and the stability of the systems is hindered with the rise in temperature. Fluorescence spectral studies suggest that the excited state dye-polymer aggregates do not lead to significant change in polarity. Also, in the excited state, the binding of EY with LM200 and JR400 is unfavourable at higher polymer / dye ratio. The anisotropy results propose the entrapment of the dye within the polymer matrix. However, in order to confirm the complete entrapment of dye molecules further studies are required, which is considered as the future perspective.

CHAPTER 3

Effect of Colloidal Silica on the Spectral Behaviour of 7-Hyroxycoumarin in Aqueous Medium

Abstract

Absorption and emission spectroscopic studies, in combination with FTIR measurements, were carried out for 7-hydroxycoumarin (7HC) and nanocolloidal dispersion of silica. Attempt has been made to identify the characteristics of excited state H-bond formed between colloidal silica and 7HC in aqueous medium. Both the absorption and emission spectra of 7HC was found to be dependent on the concentration of silica. At lower silica concentrations, the absorption spectra decreases with increasing silica concentration, on the other hand, at higher concentration a bathochromic shift occurs in the absorption spectra of 7HC. Fluorescence behaviour followed the opposite trend in comparison to the absorption spectra. It is proposed that at lower silica concentration, excited state H-bond was formed between 7HC and silica dispersions. At higher concentration, the decrease in fluorescence intensity is attributed to the self quenching of adsorbed dye molecules over silica surface following the mechanism of Homo Förster resonance energy transfer (HFRET). Results were correlated with the size and surface charge of colloidal silica as measured by dynamic light scattering and zeta potential studies.

Spectrochim. Acta A **2012,** 97, 722-727.

1. Introduction

Semiconductor nanoparticles have gained importance for their multifarious applications as they posses favorable optical properties, viz., high quantum yield, enhanced photostability, capability of cell imaging [284], etc. Among different semiconductor nanocrystals, silica has got special importance because it can be used in different forms for solute pre-concentration and immobilization of analytical reagents [285]. Besides, silica has got special attention for other specific properties like optical transparency [129], high hydrophilicity [158] and negative surface charge in aqueous media [131]. According to Bonacchi et al. [132], silica nanoparticles have some fascinating properties compared to other conventional nanosystems which include its photophysical inertness, absence of intrinsic toxicity, capability to host a large number of photochemically active species and also to protect the active material segregated inside its pore. These specific properties have additional advantages for silica nanoparticles in the field of bioanalysis and disease diagnostics[134]. According to Parida et al. [163], silica surface can be modified into various functionalities because of the presence of active –OH groups which make silica suitable for different purposes as mentioned above. Traditional organic fluorophores are usually photosensitive which could be overcome by conjugating with silica nanoparticles [134]. However, the process of conjugation between an organic dye and silica nanoparticles is not straightforward. While silica is highly hydrophilic, organic dyes are usually hydrophobic, which makes the aggregation process less favorable. There are several reports on the synthesis and characterization of silica coated fluorescent nanoparticles [132,286]. Although, fluorescent/fluorescent doped/fluorescent conjugated silica nanoparticles have several advantages, however, such systems suffer some limitations which are strongly dependent on their size and concentration [134]. According to Ha et al. [287] and Bringley [160] in some cases, fluorescence could even be quenched, compared to the free dye molecules. Therefore, a detailed spectral investigation on the absorption and fluorescence spectra of dye-silica aggregates are warranted for better technological applications as well as from the fundamental understanding point of view. Towards this

initiative we have undertaken the spectroscopic investigations on colloidal silica-7HC aggregates in a wide concentration range of silica. In addition to the aforementioned point of interest, it is believed that physicochemical studies on dye-colloidal aggregates would have been equally important in the field of waste water treatment [152], lasing property [153], dye-sensitized solar cells [154], photocatalytic reactions [155], etc. Ludox® is commercially available spherical shaped silica particles suspended in aqueous medium which find different applications [139,140,142,154,288,289]. Therefore, colloidal silica in the form of Ludox® can be considered as an appropriate model system in investigating its capability to alter (both enhancement and quenching) the absorbance and fluorescence intensity of fluorophores in aqueous medium. The dye 7-hydroxycoumarin, commonly known as "Umbelliferone", is a natural product of the coumarin family [290]. It is known to have antioxidant properties [291,292]. The ultraviolet activity of 7-hydroxycoumarin led to its use as a sunscreen agent and an optical brightener for textiles [238,247,293,294]. It is used as laser dyes and also as fluorescent indicator [247,295]. Although several reports are available in the literature which include the interaction between silica and a number of dyes [25,161,163-166,296], however, reports involving the interaction of Ludox® with 7-hydroxycoumarin are not common in literature. The occurrence of excited state H-bonding between silica and 7-hydroxycoumarin is supposed to be understood in a better way through fluorescence spectroscopic analysis, which could further be investigated via FTIR measurements.

The present study aimed at understanding the extent of interaction between 7-hydroxycoumarin and Ludox® (commercial form colloidal silica) through absorption and fluorescence spectroscopy, fluorescence lifetime and FTIR studies. Finally, size and zeta potential measurements using dynamic light scattering technique were carried out in order to understand the stacking behavior of dye molecules over the silica surface.

2. Experimental Section

2.1. Materials

The dye, 7-hydroxychromen-2-one (7-hydroxycoumarin, 7HC), was a product from Chem Service, West Chester, USA (99% pure) and was used as received. Colloidal dispersion of silica (Ludox AM-30 colloidal silica, 30 wt.% suspension in water) was procured from M/S Sigma Aldrich, USA. HPLC grade acetonitrile from E. Merck, Germany was used for FTIR measurements. Double distilled water with a conductance of 2 - 4 μS/cm was used in preparing the solutions.

2.2. Methods

A stock solution of 7HC (1.0 mM) was prepared as described elsewhere[297] using double distilled water. This stock solution was diluted within the range 1-20μM. 30 wt.% of the supplied Ludox® solution was diluted to 10 wt.%, which was used as the stock solution. This stock solution was heated at 80ºC for 2 hrs. The heating is supposed to cause defects / imperfections in the microcrystalline silica particles as reported by Banerjee et al. [298]. This solution was then diluted to required concentrations. This preheated colloidal suspension was used throughout all the experiments unless specifically mentioned. Henceforth, colloidal silica means silica microcrystalline suspensions comprising imperfections / defects.

DLS and zeta potential measurements of Ludox®, the dye (7HC) and the dye-Ludox® system were carried out by a Nano ZS 90 (Malvern, U.K.). A He-Ne laser of 632.8 nm wavelength was used and the data were recorded at a scattering angle of 90°. Steady state electronic absorption spectra were recorded on a UVD-2950 spectrophotometer (Labomed Inc., USA). Spectra were recorded within the range 200-400 nm using a matched pair of quartz cuvette of 1 cm path length, while the steady state fluorescence spectra were recorded in a bench-top spectrofluorometer (Quantamaster-40, Photon Technology International Inc., NJ, USA). The dye, in the presence and absence of Ludox®, was excited at 375 nm while the emission spectra were recorded in the range 400-600 nm. Fluorescence

lifetime of the dye in the absence and presence of Ludox® was recorded at 450 nm using 310 nano LED as the light source. The fluorescence decay was found to be single exponential in nature and the χ^2 value was found to be greater than 1.0.

FTIR absorption spectra were recorded in the range of 400-4000 cm^{-1} with a Shimadzu 83000 spectrometer (Japan) using a CaF_2 -IR crystal window (Sigma-Aldrich) equipped with presslock holder with 100 number scans and spectral resolution of 4 cm^{-1}. All the measurements were carried out at ambient but controlled temperature.

3. Results and discussion

3.1. Characterization of Ludox® in the absence and presence of 7HC

3.1.1. Dynamic light scattering (DLS) and zeta potential measurements

Pure Ludox® within the range 0.004-0.02 wt.% exhibited an average particle size of 27 nm as obtained by dynamic light scattering measurement. Effect of heating was insignificant on the size of Ludox suspension. The size variation in the presence of 7HC was found to be insignificant. Zeta potential measurements were carried out to understand the electrostatic interactions between 7HC and Ludox® in aqueous medium. If there occurs such an electrostatic interaction, it is expected that the zeta potential of Ludox® would change with the addition of 7HC. Pure silica exhibited an average zeta potential of -35mV in aqueous medium in absence of 7HC. Ludox suspension, without heating possesses a lower zeta potential value (-14 mV) compared to the thermally treated Ludox suspension. The increase in negative zeta potential value was due to the formation of defects which led to the generation of electron rich centers [299]. However, when Ludox® was added progressively to 10µM 7HC, a variation in the zeta potential was noted as summarized in Table 1. At lower concentration (within 0.004 – 0.02 wt.%) with the progressive addition of Ludox® to the dye, initially the zeta potential value was found to be -23mV, which eventually attained the value for pure Ludox®. When Ludox® is heated above 80˚C it leads to the formation of defects, which are rich in electrons.

These point defects are capable of forming H-bonds with 7HC. Thus 7HC, through the process of adsorption on the defective sites, can delocalize the electron density on Ludox® surface. As a result, there occurs a decrease in the zeta potential for Ludox® on the addition of 7HC. After the complete adsorption of all the dye molecules over the silica surface, no variation in the zeta potential value occurred. Variations and subsequent attainability of the constancy followed the same trend as observed in the absorption and emission spectroscopic

Table 1. Hydrodynamic diameter and zeta potential data for thermally treated colloidal silica *nanoparticles, Ludox®, in the absence and presence of 10 μM 7HC at 298 K.*

Wt % of colloidal silica	**d_h / nm**		**Z.P. / mV**	
	Silica	Silica-7HC	Silica	Silica-7HC
0.004	25	25	-35	-23
0.008	27	27	-35	-29
0.012	25	27	-34	-33
0.016	-	26	-	-35
0.02	-	28	-	-35

measurements. The explanation for the constancy of the size in the presence and absence of 7HC remains unexplored. This needs further experiments which could be considered as future perspective.

3.1.2. Absorption and fluorescence spectral studies

Absorption and emission studies of 7HC within the range 2-20μM are shown in Figure1. Upon increasing the concentration of the dye, both absorption and emission intensities increased linearly in the studied concentration range. The molar absorption coefficient of 7HC at 324 nm was found to be $1.035\times10^4 M^{-1}cm^{-1}$. This linear increment in the absorption and emission spectra revealed that no aggregation occurred in the studied concentration range. No spectral shifts were also recorded, confirming the absence of dimer or higher aggregates in the solution.

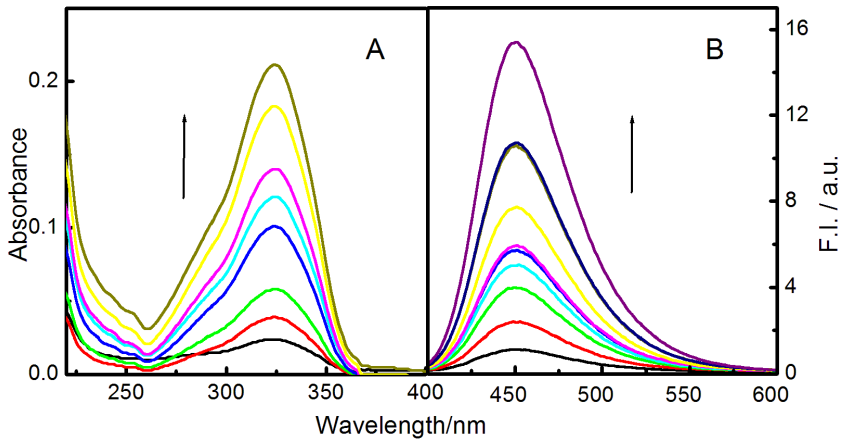

Figure 1. (A) Absorption and (B) emission spectra of 7HC in water at different concentrations at *298K. Concentration of 7HC/ μM: 1,2; 2,4; 3,6; 4,10; 5,12; 6,14; 7,16 and 8,20:* λ_{ex} = 375 nm.

While considering the spectral behavior of Ludox® it is noted that the absorption and emission spectra are featureless for Ludox® upto 0.02 wt.% in water. However, Ludox® at higher concentration range upto 2 wt.% exhibited an absorption peak at 205 nm which is due to the oxygen free radical present in defective SiO_2 moiety. Above this concentration the absorption spectra of Ludox® became noisy with progressive red shifts (spectra not shown). This was due to the scattering of aggregated silica at higher concentration range. Effect of Ludox® on the spectral behavior of 7HC is shown in Figure2. The present study on the interaction of Ludox® and 7HC are divided into two parts: a) lower concentration range, i.e., 0 - 0.02 wt.% of silica and b) higher concentration range, i.e., 0.02 – 9.00 wt.% of silica. In the dilute range of Ludox®, the spectra of pure Ludox® were featureless. However, on the progressive addition of Ludox® to 10μM 7HC solution, absorbance of 7HC is suppressed. Absorbance at 324 nm, characteristic of 7HC, decreased linearly with Ludox® concentration (Figure2A). The linearity is not observed when the Ludox® concentration exceeds the concentration of 0.02 wt.%. The systematic linear decrease at 324 nm on progressive addition of Ludox® at lower concentration range was due to uniform adsorption of 7HC over the colloidal Ludox® surface whereby monolayer of dye molecules were formed [300]. The noisy and non-systematic decrease in the absorption spectra of 7HC in the presence of higher amount (<0.02 wt.%) of

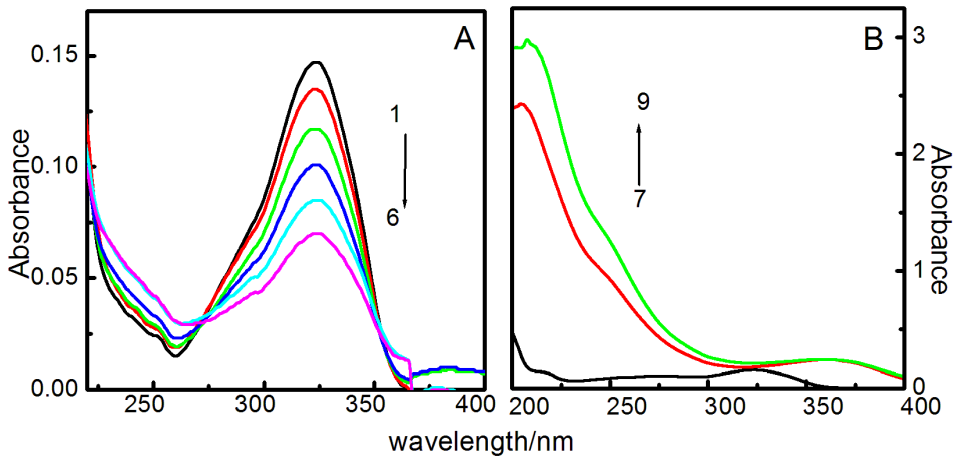

Figure 2. Absorption spectra 10µM 7HC in the presence of varying amount of Ludox® at 298 K. Ludox® was used in the two different concentration (wt.%) ranges. A: 1, 0; 2, 0.004; 3, 0.008; 4, 0.012; 5, 0.016 and 6, 0.02. In panel B spectra of 7HC is shown in the presence of 7, 0.0; 8, 2; and 9, 3 wt.% of Ludox®. Note the differences in the units of absorbance axis in two panels.

Ludox® was due to the irregular adsorption of the dye over Ludox® surface. While considering the absorption spectra in the higher concentration range (Figure 2B), the spectra of 7HC was red shifted to 360 nm due to the irregular stacking of dye molecules over the silica surface whereby fine precipitates were found to settle down at the bottom of the vial, visible through naked eye. The complete adsorption of 7HC leads to the featureless spectra and the formation of precipitates. In Figure 2B, the same spectra of 7HC (spectrum 7), as shown in Figure 2A (spectrum 1), has also been presented for comparison. Due to the large difference in the absorbance values for two different systems (for panel A the absorbance scale is 0 – 0.17 while for panel B it is 0 – 3.25), the spectra of 7HC (as shown in panel B) appears insignificant compared to that of Ludox® at higher concentration. A 2 wt.% silica, when excited at 375 nm, emits at 430 nm. Another shoulder appeared at 450 nm (Figure 3). Again, at higher concentration the spectra became noisy which is due to the irregular scattering of the colloidal aggregates. Contrary to the absorption spectra of silica-dye system in the low concentration range, the fluorescence intensity (F.I.) of 7HC increased linearly with the increasing Ludox® concentration upto 0.02 wt.% as shown in Figure 4A. Upon further increase in the concentration of Ludox® the F.I. decreased in a non-linear fashion (shown in Figure4B). The significant enhancement in the F.I. of7HC in the lower concentration range of Ludox® was due to the excited state

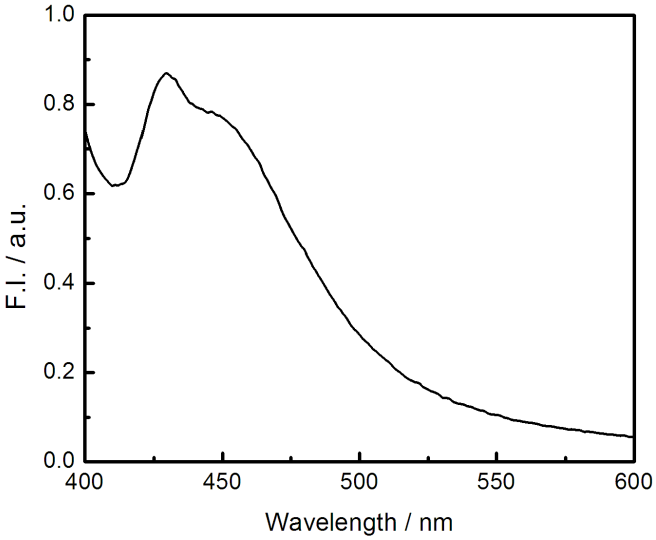

Figure 3. *Emission spectra of 2 wt.% Ludox® in water. Temperature: 298K;* λ_{ex} = 375 nm.

H-bonding between the defects incorporated into silica nanoparticle (resulted by heating) and the OH group of 7HC as shown in Scheme 1 [301]. The formation of H-bond was further established by FTIR measurements (to be discussed and shown in the subsequent section). The non-linear decrease in the F.I. of 7HC at higher concentration range was due to the irregular adsorption and subsequent precipitation of 7HC over the Ludox® surface. According to Chen et al. [134], the quenching mechanism was due to the involvement of non-radiative processes. When the fluorophores are closely packed within the solid matrix of Ludox®, the

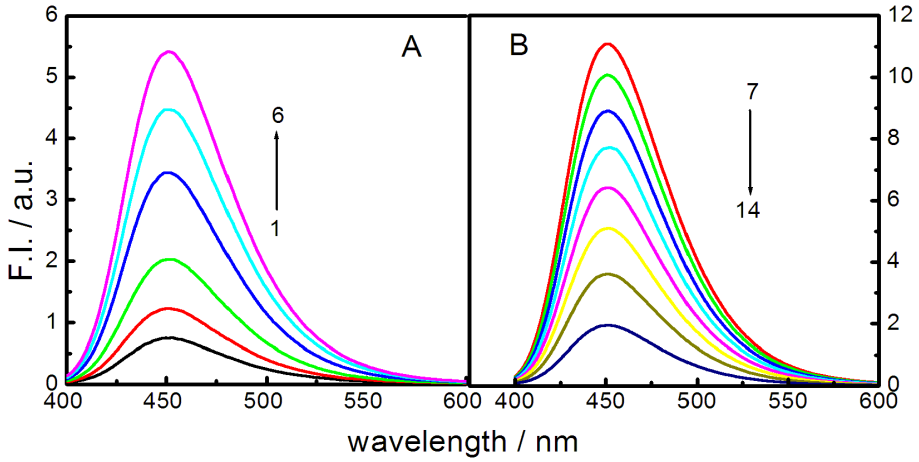

Figure 4. Emission spectra of 10μM 7HC in the presence of (A) lower wt.% (1, 0; 2, 0.004; 3, 0.008; 4, 0.012; 5, 0.016 and 6, 0.02) and (B) higher wt.% (2, 3, 4, 5, 6, 7, 8 and 9 wt.%) of Ludox® at 298K. Note: in the lower concentration range of Ludox®, fluorescence of 7HC increased (Panel A) while the fluorescence of 7HC was quenched in the presence of higher amount of Ludox® (Panel B).

intermolecular energy transfer process becomes more favourable. In the present study, a fast Homo Förster resonance energy transfer (HFRET) among the fluorophores (herein 7HC) become significant, which eventually lead to self quenching process [302]. The process becomes remarkable when no prominent Stokes shift occur for the fluorophores in the absence and presence of silica [303]. The change in fluorescence of a dye molecule in close proximity to a second molecule is attributed to Förster resonance energy transfer (FRET). FRET is a mechanism which describes energy transfer between two chromophores, one in the excited state and the other in its ground state [304]. When the transfer of energy occurs between two identical molecules the phenomenon is known as Homo Förster resonance energy transfer (HFRET) [302]. In the present study, at higher

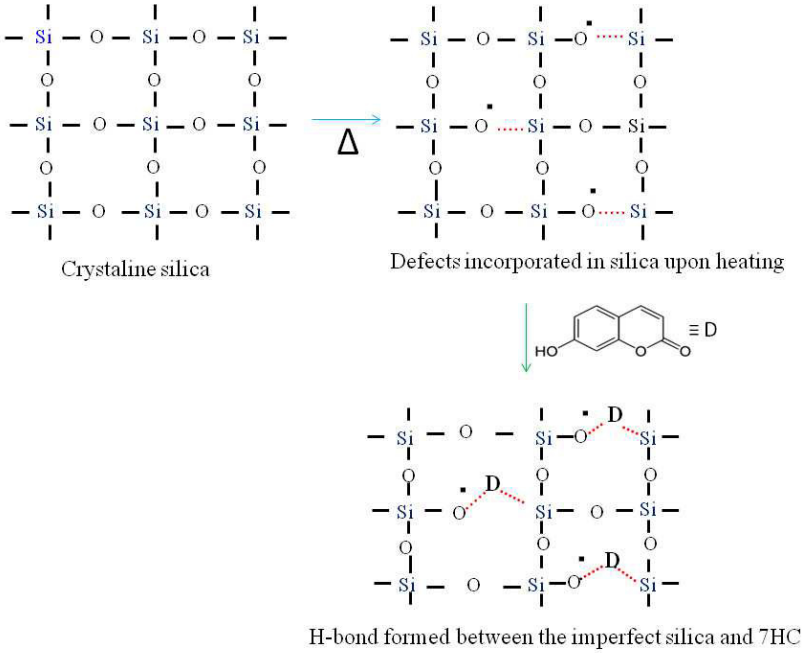

Scheme1. H-bond formation between the imperfect silica and 7HC.

Ludox® concentration, the dye molecules are very rigidly bound around the silica surface for which there are possibilities of energy transfer from an excited dye molecule to another dye molecule in the ground state. It is to be mentioned that the lifetime of 7HC (5.35 ns) was not significantly changed in presence of Ludox®. The Stern-Volmer quenching phenomena help in understanding the kinetics of a photophysical intermolecular deactivation process. Stern-Volmer

quenching process is usually valid for the systems where the lifetime of a probe does not change significantly in the presence of quencher[262]. However, in the present case, the decrease in the F.I. with added Ludox® did not follow Stern-Volmer equation [262]:

$$\frac{F_0}{F} = 1 + K_{sv}[Q] \qquad (1)$$

where, F_0 and F are the fluorescence intensities of 7HC in the absence and presence of quencher, Q; [Q] = Quencher concentration. Had there been a quenching of 7HC by Ludox®, the plot of F_0 / F vs [Q] would be a straight line, which was not observed in the present case.

3.1.3. Infrared spectroscopic study

The IR spectral band of water in the OH stretching frequency region (~ 3100 to 3750 cm^{-1}) is usually very broad and structureless due to the continuum water structures with varying hydrogen bond strength. Anticipating that neat water, therefore, may not provide precise information of the dynamics of water via conventional IR spectroscopy, dilute water is employed for measurement in the present study. Assuming the concentration of neat water to be 55.5M, sufficient amount of CH_3CN was added to water to make it 1.0M because under this condition, water molecules are mostly solvated by CH_3CN and no water aggregates (even low order aggregates) are present [305]. Figure 5 shows the IR spectra of 7HC (1.0M) and water (1.0M) in CH_3CN on CaF_2 plates. The peaks corresponding to the vibration of OH symmetric stretching of the weakly hydrogen bonded (3542cm^{-1}) and nonbonded (3627 cm^{-1}) species of 7HC with CH_3CN are resolved. These peaks are exactly superimposed on the peaks of dilute water (1.0M) in CH_3CN as observed previously (not shown here) [305]. On the other hand, Ludox ® in dilute water yields a broad OH stretching band at 3602 cm^{-1}.

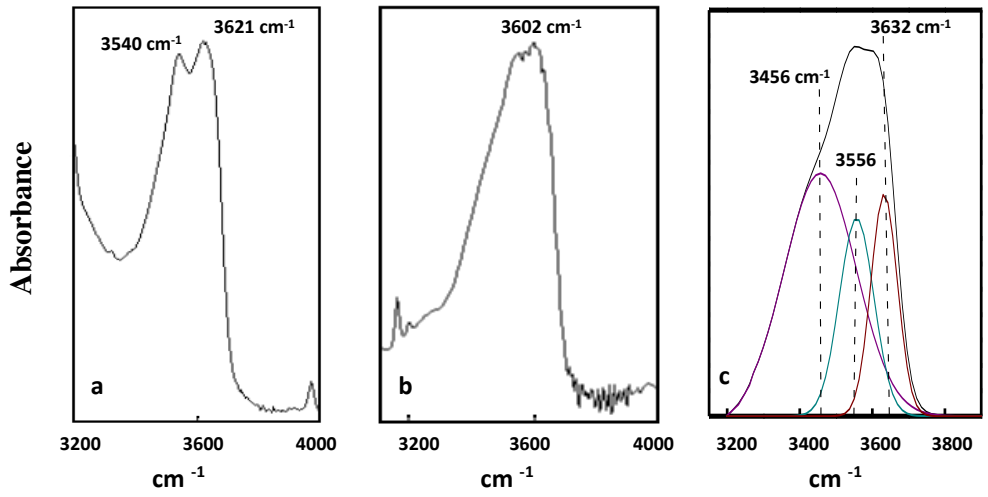

Figure 5. (a) IR spectra of 7-HC (1.0M) and H_2O (1.0M) in acetonitrile, (b) IR spectra of SiO_2 (1.0M) and H_2O (1.0M) in acetonitrile, (c) IR spectra of 7-HC (1.0M), H_2O (1.0M) and SiO_2 (1.0M) in acetonitrile and Gaussian components from least squares fitting.

The IR spectra of the mixture of 7HC (1.0M), water (1.0M), and SiO_2 (1.0M) in CH_3CN is interesting. For the quantitative evaluation, the spectra are deconvoluted into Gaussian profiles, which clearly yield three peaks at 3456 cm^{-1}, 3556 cm^{-1} and 3632 cm^{-1} respectively [175]. It seems apparent that both the components of the OH stretching mode of 7HC are only slightly shifted to 3556 cm^{-1} and 3632 cm^{-1} respectively while that of the hydrated silica is blue shifted to a great extent and resonate at 3456 cm^{-1}. This shows that silica-OH donates proton to the OH oxygen of 7HC acceptor site in forming strong hydrogen bond between the two [160]. However, to make final conclusion on the morphology of Ludox® in the absence and presence of 7HC through electron microscopic measurements are narrated. Besides, the adsorption kinetics of 7HC over silica surface, as measured by quartz crystal micro balance (QCM) studies would further highlight the detailed mechanism. These above mentioned components are considered to be the future perspectives of the present work.

4. Summary and Conclusions

Physico-chemical studies on the interactions of the imperfect nanocolloidal dispersion of silica (Ludox®) with 7HC have been undertaken with

the aid of electronic absorption, emission and vibrational spectroscopic measurements. While the absorption and emission intensities of 7HC were increased with increasing dye concentration in the range of 0-20μM, the enhancement of fluorescence intensity is brought about at the low concentration of silica. This enhancement of the fluorescence intensity of 7HC has been related to the strengthening of excited state H-bonds formed between Ludox® and 7HC. It may be noted that the radiationless deactivation can dramatically influence the regulation of electronic states by H-bonding interactions and the fluorescence of chromophores in H-bonded surroundings may be quenched or enhanced by H-bonds [306]. At high concentration range of silica, strong and irregular adsorption of 7HC onto silica surface led to a red shift in the absorption spectra. The intermolecular fluorescence quenching, under the prevailing condition, is governed by the Homo Förster resonance energy transfer formalism. The size of the colloidal dispersion was independent of the concentration of silica and 7HC. Due to the stacking of dye molecules onto silica surface, negative zeta potential values of Ludox® was suppressed compared to the systems without the dye. The adsorption kinetics of 7HC over silica surface, as measured by quartz crystal microbalance (QCM) studies would further highlight the detail mechanism. Besides, Raman spectroscopic studies are considered to more informative in understanding the exact nature of H-bonding between Ludox® and 7HC in aqueous medium. These components are considered to be the future perspectives of the present work.

CHAPTER 4

CHAPTER 4

Surfactant-assisted Synthesis and Characterization of Stable Silver Bromide Nanoparticles in Aqueous Media

Abstract

Colloidal dispersions of silver bromide (AgBr) in aqueous surfactant medium have been prepared using a surfactant-assisted synthesis approach with hexadecyltrimethylammonium bromide (CTAB). The surfactant acts both as source of bromide ion as well as the stabilizing agent. Upon progressive addition of silver nitrate to aqueous CTAB solution, stable AgBr dispersions were obtained. Formation of surfactant cation (CTA^+) stabilized AgBr was confirmed by way of XRD, FTIR and NMR studies. Thermal behaviour of the isolated nanoparticles was investigated by differential scanning calorimetry (DSC) and thermal gravimetric analysis (TGA), where the occurrence of phase transition in the surfactant stabilized nanoparticles was observed. Kinetics of the particle growth was investigated by dynamic light scattering measurements, which predicted the formation of surfactant bilayered structures associated with the nanoparticles of AgBr. Band gap of the nanoparticles was determined by suitably analysing the UV-visible spectral data, which concluded that the particles behaved like insulators. Morphology of the particles, studied by TEM measurements, was found to be spherical. Finally, enthalpy of formation of surfactant stabilized AgBr, determined calorimetrically, was found to be dependent on the concentration of the precursors.

Langmuir **2012**, 28, 7282-7290

1. Introduction

Because of their fascinating properties and multifaceted application potentials, research interests in the physicochemical investigations on synthesis and characterizations of nanoparticles are ever increasing since last few decades[307,308]. Nanoparticles find applications in various fields, viz., semiconductor[60,189,309,310], superconductor[42,280,311-313], magnetic materials[235,314], opto-electronic devices[189,315-317], catalysts[158,191], paint[295,318], electrochemistry[307,308,319], biomedical devices[320,321], etc. As the nanomaterials have larger surface area than the bulk material, they become more reactive. The nanoparticles can be considered as a bridge between the bulk material and atomic / molecular entities[322].

There has been a significant increase in the synthesis and characterization of silver halide (AgX) nanoparticles due to their specific properties[307,308]. Silver halides are being used as photographic material for a long time[238,280,307,320]. According to Sambhy et al.[320], AgBr nanoparticles have microbicidal activity. Composite materials of AgCl and polymethylmethacrylate can be used as separation membranes[238]. Because of their high conductivity, AgX are used as solid ionic conductors[323]. However, the most important property of silver halides is their enhanced band gap emission in the nano range compared to the bulk material[324]. Besides the aforementioned properties silver halides are also used as catalysts[181,325,326]. Taking into account of different application potentials of nanoparticles of AgX, it is worth pursuing to study the convenient ways to prepare a stable dispersion of AgX. It has been reported that when present in pure crystalline form, silver halide salts are unstable[185]. Detailed mechanism for the degradation of Ag^+ ions into metallic silver has been explained by Proudfoot[327]. However, if AgX salts are in a dispersed state, they become stable[181]. This has motivated the authors to undertake the investigations on the synthesis and characterization of colloidal silver bromide in aqueous surfactant medium. It has been reported by Lahtinen et al.[200] that quaternary ammonium ion comprising a long hydrocarbon chain could stabilize the synthesized AgBr nanoparticle with a protective coating.

Cetyltrimethylammonium bromide (CTAB) is one of the cationic surfactants that has been used by many researchers as stabilizers or templates for the synthesis of various novel materials[307,308,328]. Sui et al.[308] have used CTAB as a stabilizer in preparing positively charged silver nanoparticles. Chen et al.[238] have used CTAB as a stabilizer, where seed mediated growth of silver nanodisks in aqueous media has been reported. Reports of Sui et al.[308] and Nikhoobakt et al.[329] have suggested that CTAB could act as a passivating agent in stabilizing the colloidal nanoparticles. Likewise, Liu et al.[307] have proposed that hexadecyltrimethylammonium ion could form a bilayer like structure around colloidal AgBr particles, which was very much mimetic to vesicles.

Because of the manifold applications of AgBr nanoparticles, a number of reports are available in the literature[181,185,186,320,330,331]. He et al.[331] have prepared novel layered AgBr based nanocomposite stabilized by CTAB. Lahtinen et al.[200] have reported the preparation of surfactant monolayer protected silver bromide nanoparticles. Bai et al.[204] have prepared and characterized AgBr nanoparticles in poly(vinylpyrrolidone) matrix. Photocatalytic activity of the synthesized AgBr nanoparticles as polymer composites has been reported by different authors[185,332]. Preparation of AgBr nanoparticles has also been reported in water-in-oil microemulsion media by Husein et al.[186]. They have prepared AgBr nanoparticles in water-in-oil microemulsion where the existence of bulk water was possible for which the nanoparticles got precipitated in that water pool. In their case, basically formation of AgBr nanoparticles occurred in the confined water pool of water-in-oil microemulsion. However, in the present case, our proposition is different. We believe that AgBr nanoparticles are formed in aqueous medium first which then get stabilized by surfactant monolayers / bilayers. However, in all the cases, the wide applications of AgBr were not convenient because of the limited stability of AgBr nanoparticles as colloidal dispersions. Moreover, reports on the use of AgBr nanoparticles in the dilute concentration range (of the order of milli to micromolar) are not plenty in literature.

As already mentioned, although AgBr nanoparticles have many application potentials, it is difficult to obtain stable colloidal dispersions of AgBr, especially in the aqueous medium.

In this paper, the synthesis and characterization of colloidal dispersions of silver bromide using a very simple but novel approach are reported. Upon progressive addition of silver nitrate to aqueous CTAB solution, colloidal dispersions of AgBr are formed in the aqueous medium. The surfactant acts both as a stabilizing agent as well as the source for bromide ion. The colloidal dispersions of AgBr were stabilized by the layered structured surfactant cation assemblies. Although there are previous reports on the synthesis and characterization of AgBr nanoparticles, the studies in solution phase are not so common, which are essential for practical purposes. In the present case, the nanocolloidal dispersions of AgBr were found to be stable in the studied concentration range (10^{-6}-10^{-5}M) up to a year. Formation of nanoparticles of AgBr was confirmed by the way of XRD, FTIR and NMR studies. Band gap of the nanoparticles in the dispersed state was investigated by UV-visible spectral measurements. Growth kinetics of the surfactant-protected nanoparticles (SPN) was studied by dynamic light scattering method. Thermal behaviour of SPN was also studied by DSC / TGA analysis. Morphological studies were performed by TEM measurements. Our endeavour was to undertake a simple but novel one-pot synthesis of stable AgBr nanoparticles and its application in aqueous media.

2. Experimental section

2.1. Materials

The cationic surfactant hexadecyltrimethylammonium bromide (CTAB) was a product from Sigma-Aldrich, USA. The surfactant was stated to be >99% pure and was used as such. A.R grade silver nitrate ($AgNO_3$) was purchased from S.D. Fine Chemical Ltd., India. All the chemicals were used as received. Double distilled water with a specific conductance of 2-4 μS cm^{-1} at 298K was used for preparing the solutions.

2.2. Methods

A stock solution of 1mM $AgNO_3$ was prepared in water with which experimental works were carried out. 5.0mL of colloidal dispersions of AgBr particles were prepared in 0.4mM CTAB solution at five different concentrations (10, 20, 30, 40 and 50μM). Quantitative amount of 1mM $AgNO_3$ was added in 100 steps with constant stirring to obtain AgBr in the above mentioned concentrations. It may also be mentioned that we had prepared and studied the AgBr nanoparticles in the concentration range of 10-50 μM with an interval of 5 μM. By the method of trial and error it was found that a 0.4mM CTAB solution was the optimum concentration in obtaining a stable dispersion of AgBr up to 50μM (shelf life = 1 year). Above the 0.4mM concentration there is excess of Br^- ions which would cross the solubility limit and thus failed to stabilize the system despite of large amount of CTAB. On the contrary, there is deficiency of CTA^+ ions to stabilize the system when the concentration of CTAB solution is below 0.4mM. Henceforth, all the preparations would mean for a 0.4mM CTAB solution in water. A stock solution of 1mM CTAB was used for the study.

Surfactant stabilized nanoparticles of AgBr were isolated in two ways. Firstly, the method of Liu et al.[307] was adapted to isolate AgBr from its aqueous dispersion. A 10ml 20mM aqueous $AgNO_3$ solution was added dropwise to 100ml 6mM CTAB solution under rigorous stirring and the dispersion thereby obtained, which was not as stable as the aforesaid preparation (stable upto 2 hours), was centrifuged at 10000 rpm and the sediment was washed with water. It was then vacuum dried at 80°C. This isolate was termed as "aqueous extract". In another method, surfactant stabilized AgBr colloidal dispersion was extracted into chloroform layer and then the organic layer was dried under vacuum. The second category was termed as "chloroform extract". XRD, FTIR, DSC and TGA analyses were done on both the extracts.

The diffraction patterns of the isolated nanoparticles and the precursors were recorded in a RINT 2000, Rigaku diffractometer (Japan) using $CuK\alpha_1$ (0.15418 nm) radiation operated at 40 kV and 40 mA in the range of 5° to 70° at

the rate of 3° / min. The FTIR spectral data were recorded in a Shimadzu 8300 FT-IR spectrometer (Japan) by taking the samples in the form of KBr pellets using standard procedure[307]. ^{1}H-NMR spectra were recorded in a 300 MHz FT-NMR by Bruker-Advance (5mm BBO Probe) spectrometer (Switzerland) using tetramethylsilane (TMS) as an internal standard. The conductance measurements were undertaken by Eutech Instruments con 510 conductivity/TDS/°C/°F meter. The UV-visible absorption spectra were recorded on a UVD-2950 spectrophotometer (Labomed Inc., USA) using a matched pair of quartz cuvette of 1 cm path length. Size of nanoparticles was determined by dynamic light scattering method using a dynamic light scattering spectrometer Nano ZS 90 (Malvern, U.K.). A He-Ne laser of 632.8 nm wavelength was used and the data were recorded at a scattering angle of 90°. Samples were filtered using Millipore ^{TM} hydrophobic membrane filter of 0.25μ pore size. Thermal gravimetric analysis (TGA) of the isolated nanoparticles as well as CTAB was carried out on Mettler H10, Neo-Pharma Instruments Corp. from 50 to 325°C and the differential scanning calorimetry (DSC) measurements were done on Pyris 6 DSC (Perkin Elmer, USA). The samples were heated at a rate of 10°C / min from 50 to 140°C and the cooling was done at 5°C / min. The instrument was calibrated with Indium before each experiment. The enthalpy changes for the formation of nanoparticles were measured in an OMEGA isothermal titration calorimeter (ITC) (Microcal Inc., Northampton, MA, USA). 1.8 and 1.325 mL CTAB solutions were taken in the reference and reaction cell, respectively. In the ITC experiment, enthalpy change associated with the interaction process was calculated under constant temperature accurately within 0.01°C. As prepared samples of AgBr nanoparticles in surfactant medium were used for morphological studies by TEM. TEM images were recorded with an H-7500, transmission electron microscope (Hitachi, Japan), with an acceleration voltage of 80 kV. A drop of nanocolloidal dispersion of AgBr was dried on carbon coated copper grid using the standard procedure[308].

3. Results and discussion

3.1. X-Ray Diffraction studies: Characteristic X-ray diffraction patterns of CTA^+ stabilized AgBr nanoparticles, isolated in two different ways, along with the precursors CTAB and $AgNO_3$ are shown in Figure1. X-ray diffractograms of CTAB and chloroform extracted CTA^+ stabilized AgBr bear the same features. Aqueous extract exhibited differences, although not so significantly. Pure CTAB bearing higher crystalinity exhibited sharp and intense peaks at 2θ values of 10.1, 13.4, 18.2, 20.3, 21.4, 23.9, 27.4, 30.8 and 38.1 degrees respectively.

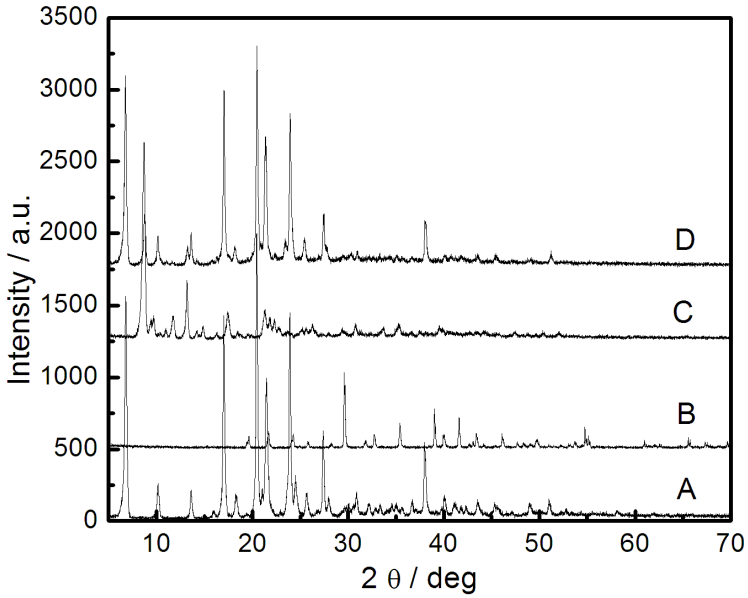

Figure 1. XRD patterns of (A) CTAB, (B) silver nitrate, (C) CTA^+ coated silver bromide nanoparticles isolated from water and (D) CTA^+ coated silver bromide nanoparticles isolated using chloroform.

Nanoparticles extracted by two different methods did not exhibit any characteristic peak for $AgNO_3$. This suggests the complete conversion of $AgNO_3$ to AgBr, which was not unexpected. Maximum concentration of added $AgNO_3$ was 50μM in presence of 0.4mM CTAB. Therefore, it could be expected that all the Ag^+ ions would be in the form of AgBr. Diffractograms of the nanoparticles isolated directly from aqueous media did not exhibit distinct, specific and intense peak for AgBr. The less intense diffractograms of any nanoparticle is not uncommon[269,307,320]. Particles in the nanodimensions are less crystalline and hence their x-ray diffractograms have fewer features than the corresponding bulk

materials[322]. Additionally, formation of lesser amount of AgBr compared to the amount of CTAB present resulted in the masking of AgBr diffractograms by CTAB. CTA^+ coated AgBr nanoparticles exhibited its characteristic peaks at 32.0, 49.0 and 67.5 degrees respectively. The results mildly deviated from the reported values[181,204,320] which is possibly due to the differences in the experimental conditions. In the present case, while obtaining the representative peaks for AgBr nanoparticles, we performed the analysis by expanding the corresponding zones. Individually expanded zones are presented in the Figure 2. The interplanar distances corresponding to the above-mentioned peaks were 2.9, 2.0 and 1.7Å respectively. Corresponding crystal planes (hkl) were (200), (220) and (400) respectively[204].

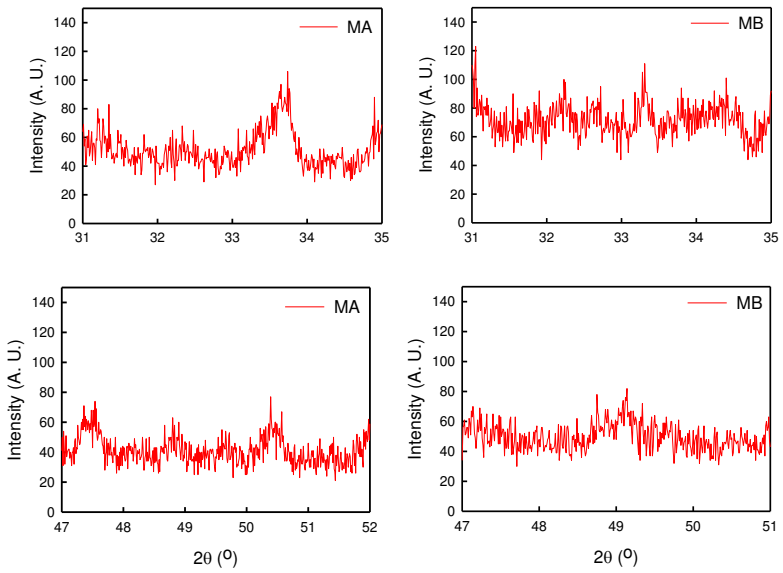

Figure 2: Expanded X-ray diffractograms of (MA) aqueous and (MB) chloroform extract of CTAB stabilized AgBr nanoparticles.

Results confirmed the formation of crystals bearing the same structure as of cubic face centered bromargyrite (www.webmineral.com/MySQL/xray.php). Formation of AgBr was therefore established from the X-ray analysis.

3.2. Fourier Transform Infrared Spectra: In order to further establish the formation of CTA^+ coated AgBr nanoparticles, FTIR spectral measurements were carried out. The representative results are shown in Figure 3. The symmetric and asymmetric $–(CH_2)–$ vibrations of pure CTAB appear at 2849 and 2917 cm^{-1}

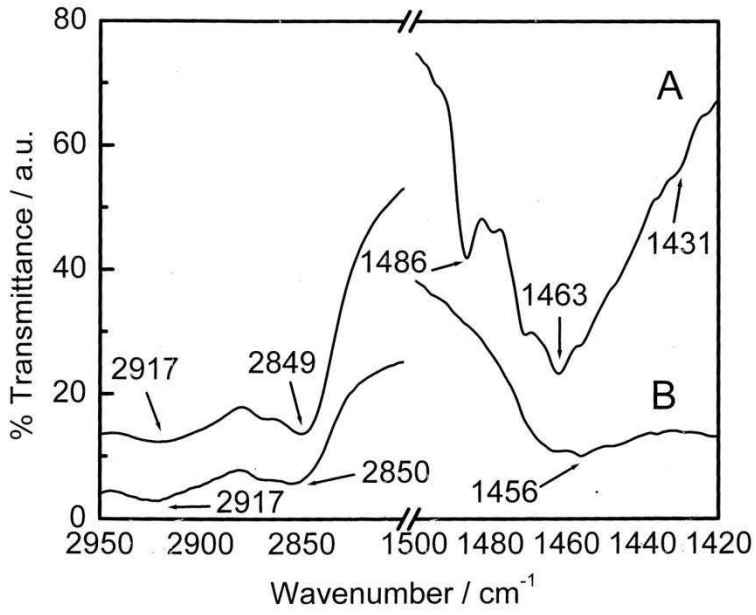

Figure 3. FTIR spectra of (A) pure CTAB and (B) aqueous extract of CTAB stabilized AgBr nanoparticles.

respectively. Isolated nanoparticles also bear the same fingerprint, which indicates the direct non-involvement of hydrocarbon chains in stabilizing the AgBr nanoparticles. The observed peaks at 1486 and 1431 cm^{-1} for pure CTAB were due to the asymmetric and symmetric –C-H vibration of the quarternary ammonium moiety[307,308]. In case of isolated nanoparticles the peak at 1486cm^{-1} was broadened and shifted to 1456cm^{-1} and the peak at 1431cm^{-1} was not present. Results suggest that AgBr clusters influenced the $(CH_3)_3N^+$ vibration.

3.3. NMR spectroscopic studies: Coating ability of CTA^+ over AgBr clusters was further evidenced through ^1H NMR measurements[308,333-335]. Spectral data of NMR studies are summarized in Table 1 and spectra are shown in Figure 4. Peaks for pure CTAB appeared as follows: δ = 3.6ppm (α-CH_2-), δ = 3.47ppm ($(CH_3)_3N^+$), δ = 1.8ppm (β-CH_2-), δ = 1.36ppm (γ-CH_2-), δ = 1.25ppm (-$(CH_2)_n$-) and at δ = 0.88ppm (terminal –CH_3). For surfactant stabilized nanoparticles, no shift in the terminal –CH_3 and -$(CH_2)_n$- protons occurred, which indicates that AgBr clusters could not perturb the terminal –CH_3 protons. All the other proton signals were down shifted (approx. 0.13 ppm) indicating the partial attachment of the surfactant head group to AgBr nanoparticle[308,333-335].

Table 1: ^{1}HNMR data of CTAB and CTA^{+} coated AgBr nanoparticles

System	Terminal-CH_3	-(CH_2)-$_n$	γ-(CH_2)-	β-(CH_2)-	$(CH_3)_3N^{+}$-CH_2-
CTAB	0.88 (3H, m)	1.26 (24H, s)	1.36 (2H, s)	1.8 (2H, br)	3.47-3.6 (11H, m)
Aqueous extract of CTA^{+} coated AgBr	0.88 (3H, m)	1.26 (24H, s)	1.36 (2H, s)	1.76 (2H, br)	3.46-3.54 (11H, m)
$CHCl_3$ extract of CTA^{+} coated AgBr	0.88 (3H, m)	1.25 (24H, s)	1.34 (2H, s)	1.76 (2H, br)	3.38-3.47 (11H, m)

s, m and br, s denote singlet, multiplet and broad singlet. $CDCl_3$ was used as solvent

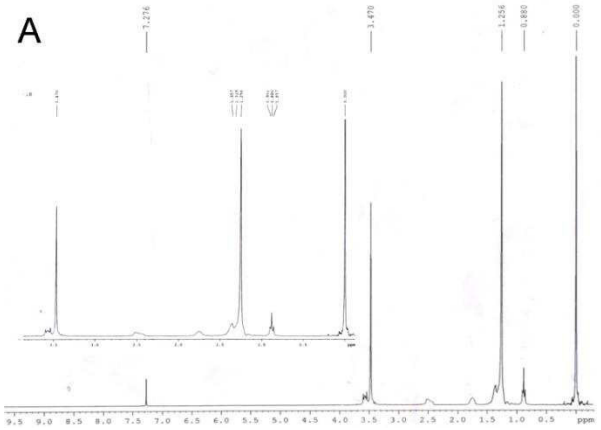

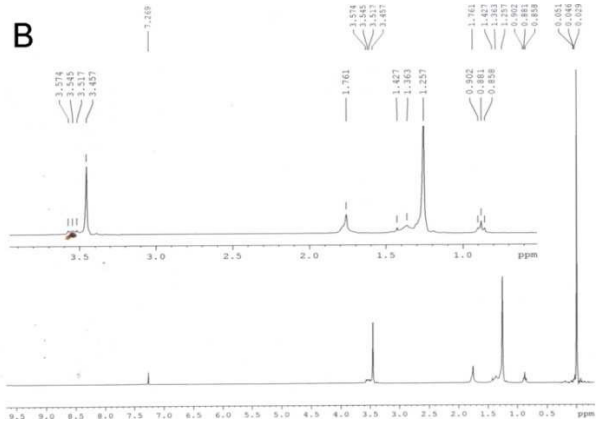

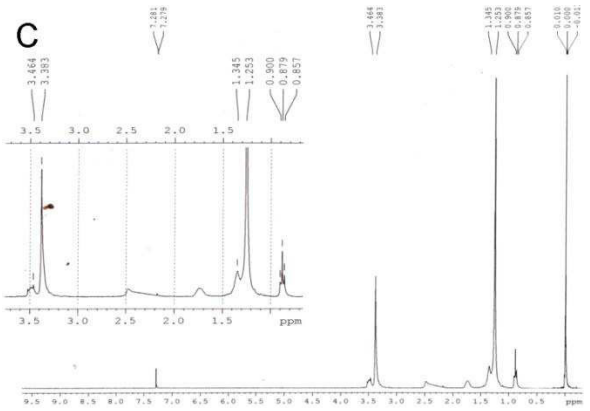

Figure 4: NMR spectra of (A) pure CTAB, (B) aqueous and (C) chloroform extract of CTAB stabilized AgBr nanoparticles.

3.4. Conductometric titration: Conductometric titration of an aqueous solution of 0.4mM CTAB by $AgNO_3$ is graphically presented in Figure 5. Similar titration with 0.4mM KBr is also shown for comparison. With the progressive addition of silver nitrate into the aqueous KBr solution, conductivity monotonously decreased. After the neutralisation point, a further increase in conductance was noted. When $AgNO_3$ solution was progressively added to KBr solution, instantaneous formation of AgBr particles occurred which remained as suspension. Usually, such titration leads to the replacement of Br^- ions with the NO_3^- ions alongwith the formation of insoluble component, AgBr. Conductivity of NO_3^- ions is almost similar to that of Br^- ions[336]. Therefore, there should not be any significant change in the conductance before the neutralisation point. However, suspended AgBr colloids might hinder the mobility of the ions present in solution, which ultimately led to the decrease in conductance.

Conductance profile for CTAB solution followed the similar trend, although to lesser extent. The appearance of neutralisation point at a lower concentration and also lesser conductance in the pre-neutralisation point, compared to KBr, was not unexpected. CTA^+ ions are involved in stabilizing the AgBr nanoparticles in the form of layers (to be discussed in detail later on). The conductivity of CTA^+ ions is less compared to the K^+ ions. Therefore, the conductometric titration curves for CTAB would always maintain a lower profile

than KBr. According to Almgren and Rydholm[337], CTAB micelles have much higher surface charge and hence a larger electric field for which Br^- ions can bind

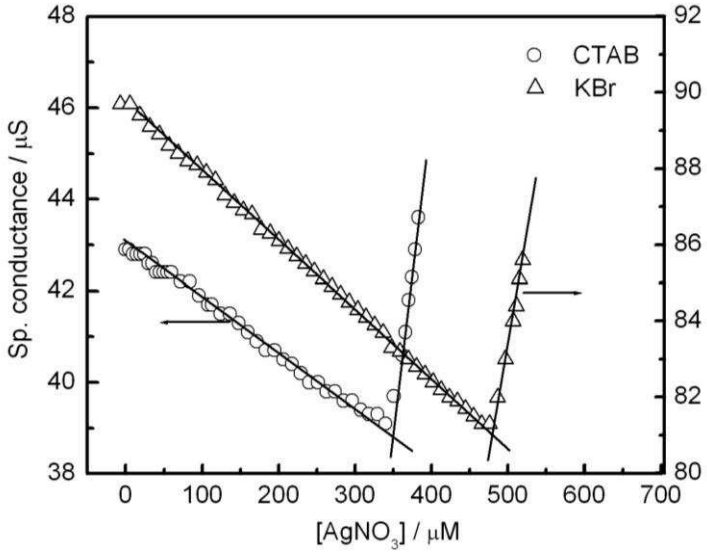

Figure 5: *Conductance profile of (Δ) CTAB and (o) KBr against concentration of $AgNO_3$* (in μM). Initial concentrations of both CTAB and KBr = 0.4mM.

strongly as counterions to the micelles. Subsequently, the average mobility of the ionic species is decreased. In the previously published report[308], surfactant ions could stabilize the nanoparticles through the formation of bilayer structures around them. Br^- ions would thus act as counterions, which lessen their availability compared to KBr solution of identical strength. However, it is to be mentioned that due to the formation of vesicle like entities the fraction of counterion dissociation would be higher compared to the CTAB micelles.

3.5. UV-visible spectroscopy: UV-visible spectra of colloidal AgBr, dispersed and stabilized in / by aqueous CTAB solution, were recorded in the range 200-350nm at different concentrations of AgBr (viz., 10, 20, 30, 40 and 50 μM, some of which are shown in Figure 6). Colloidal dispersions exhibited a strong and intense peak at 212nm against CTAB as blank. Absorbance at 212nm increased with increasing AgBr concentration. The peak at 212nm corresponds to the absorption of CTA^+ coated AgBr in aqueous solution. Increase in intensity with increasing AgBr concentration implies the accumulation of CTA^+ around AgBr

nanoparticles. Results clearly indicate the clustering of the surfactant molecules which eventually stabilizes the nanoparticles. The exact orientation of surfactant

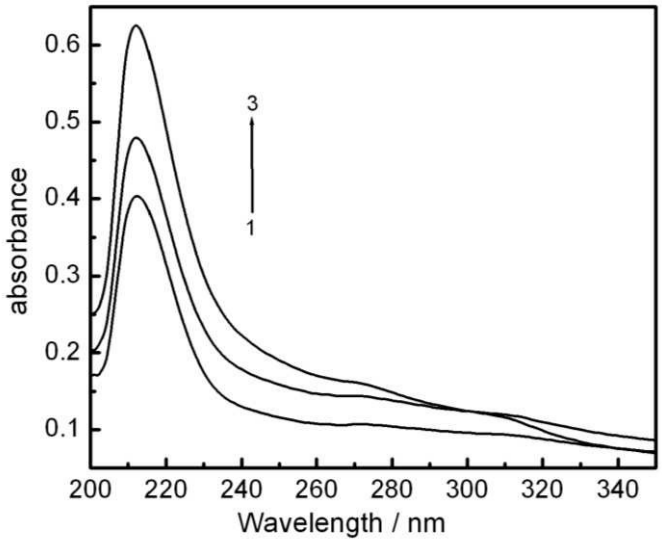

Figure 6. UV-visible absorption spectra of CTA^+ coated AgBr nanoparticles in aqueous medium *at 25ºC. Concentrations of AgBr [in μM]: (1) 20, (2) 30 and (3) 50. A 0.4mM CTAB solution was* used as blank.

molecules around AgBr nanoparticles will be discussed later on. Although not so sharp, another faint shoulder appeared at 270nm which corresponds to AgBr nanoparticles[186,307]. The shoulder at 270 nm appeared faint in comparison to previously published reports[186,307] because in the present case lower concentrations were used. It is also to be mentioned that pure AgBr in bulk state or in its vapor state appears light green [338]. However, in the present case we have failed to detect the corresponding peak in the visible region as the concentration of AgBr was in the micromolar range. Besides, the existence of larger amount of CTAB could have masked the greenish appearance of AgBr. The stabilizing agent, CTAB also protects the AgBr colloids from reduction to Ag metals, which is otherwise common for silver halides in their bulk state.

The absorbance-concentration profile at 212nm obeyed the Beer's law and the molar absorption coefficient of CTA^+ stabilized AgBr was found to be $6.88\times10^{-3}M^{-1}cm^{-1}$ at 212nm. Such kind of report for AgBr is not available in the literature. The spectral data were further analysed to determine the optical band

gap (ε_g) of CTA^+ stabilized AgBr nanoparticles in aqueous medium using the Tauc relation[339]:

$$(\varepsilon h\nu)^{1/n} = C\,(h\nu - \varepsilon_g) \qquad (1)$$

where, ε, h, and ν are the molar absorption co-efficient, Planck's constant and frequency of light respectively and C is a constant. The exponent depends on the type of transition for direct allowed transition (here n = ½). Liu et al.[307] have prepared AgBr nanoparticles using the present approach where the concentration of AgBr was fairly high, for which, the colloidal suspension exhibited peaks in the range 250–320 nm. According to them, the spectra correspond to the direct band gap of AgBr. We also have extended this approach to determine the direct band gap in the range 219–226 nm. From the linear portion of the plot of $(\varepsilon h\nu)^2$ against hν (as shown in Figure 7), the band gap was determined from the ratio of the intercept and slope of the linear part. On an average, the band gap was found to be 5.35 eV for a 30μM AgBr dispersion. With increasing AgBr concentration the band gap decreased, attained a minima at 40 μM AgBr (inset of Figure 7) which again increased up to 50μM AgBr. Dispersions comprising higher than

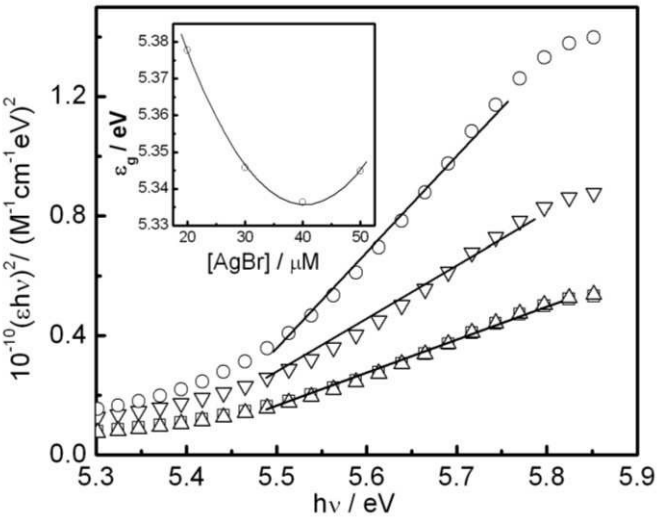

Figure 7. *Plot of $(\varepsilon h\upsilon)^2$ vs. hυ for the determination of the band gap of silver bromide* nanoparticles. Concentrations of AgBr (μM): O, 20; *▽, 30;* □*, 40 and Δ, 50. Inset: Band gap* - silver bromide concentration profile.

60μM AgBr became unstable. For bulk AgBr the reported direct band gap is 4.29eV[340]. Higher band gap value for AgBr nanoparticles was attributed to the

size confinement effect. It is not unexpected for the band gap to increase with the decrease in particle size[339]. The decrease in band gap with increasing AgBr concentration was due to the formation of larger particles. After the attainment of 40μM AgBr concentration, smaller clusters are formed for which a further increase in the band gap occurred.

3.6. DLS studies and zeta potential measurements: The kinetics for the growth in particle size as functions of $AgNO_3$ concentration and time were studied by dynamic light scattering method. Also, during the same studies, surface charges of the colloidal dispersions of CTA^+ coated AgBr were investigated through zeta potential measurements. Results are summarized in Figure 8. With the increase in time, particles grew upto 24 hours and then the size attains constancy. This implies that the growth process is completed within 24 hours. Initially the size was around 50nm. Within 6 hours, there occurred a two-fold increase in size. It is believed that initially randomly oriented CTA^+ ions stabilized the colloidal particles of AgBr through the formation of monolayer, in the manner as shown in the Scheme 1A. However, the kind of orientation, as shown in Scheme 1A, is not stable from both the thermodynamic and kinetic point of view, for which an enlarged bilayer like structure is formed around the AgBr nanoparticle (shown in Scheme 1B), which becomes stable. The CTA^+ bilayer formation in stabilizing

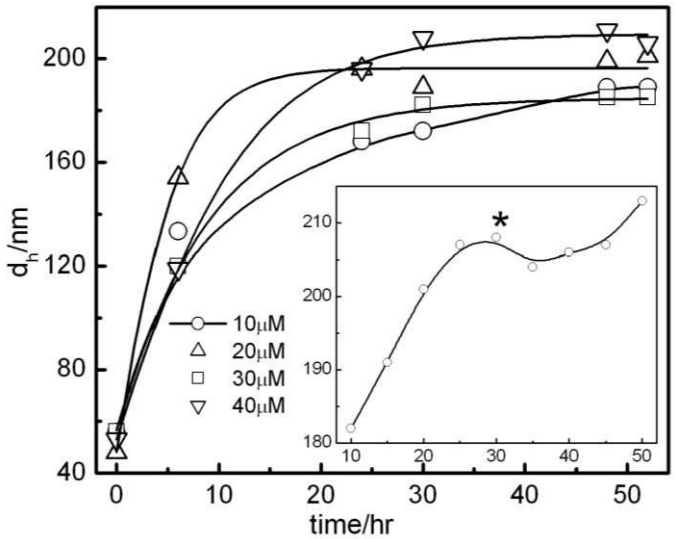

Figure 8. d_h vs. time profiles for silver bromide nanoparticles. Inset: d_h vs. [AgBr] profile after52 hours of the particle formation.

nanoparticles has been reported earlier[307,308,329]. Therefore, the increase in the hydrodynamic diameter of CTA^+ stabilized nanoparticles is a contribution of colloidal growth of AgBr as well as the size enhancement due to the bilayer structure formation. Additionally, the increase in the bilayer density could contribute to the size enhancement of the surfactant stabilized dispersion of silver bromide. The zeta potential values were found to increase with increasing time

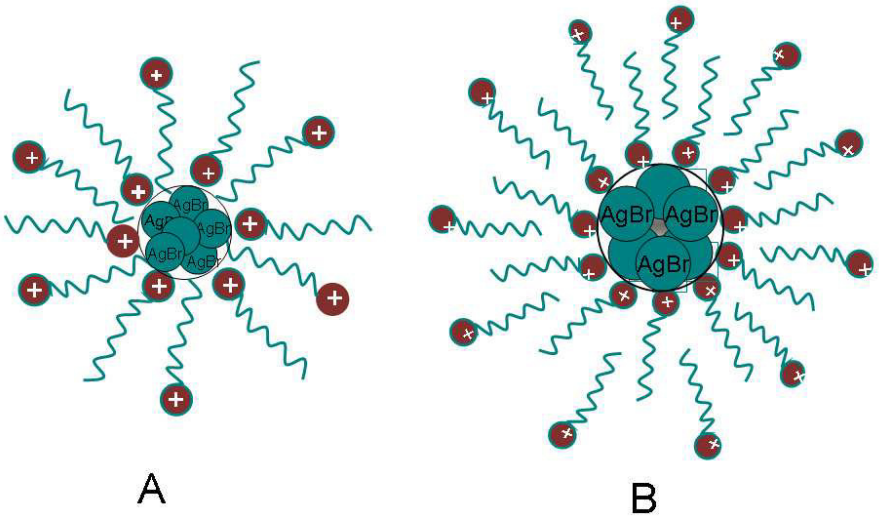

Scheme 1. Schematic diagrams for (A) surfactant monolayer protected AgBr NPs and (B) AgBr NPs stabilized by CTA^+ bilayer.

which subsequently attained constancy (data not shown to save space). Initially, the nanoparticles were stabilized by surfactant molecules through a monolayer coating with an irregular orientation (as shown in the Scheme 1A), with lower zeta potential value. However, after the bilayer-like structures were formed, the extent of dissociation of the counter ions (bromide) increased and hence the zeta potential also increased. When the formation of the bilayer-like structures was completed, the zeta potential values attained constancy (data not shown). The formation of bilayer-like structures would lead to the creation of bigger entities as shown in Scheme 1. Hence, overall charge density would be less compared to the pure micelles. Accordingly, the extent of dissociation would be higher for the bilayer-like entities than the pure micelles of CTAB. As a result, the zeta potential for the bilayer stabilized nanoparticle system will be higher than the corresponding micellar entities.

The size of the AgBr colloids stabilized by CTA^+ was also found to be dependent on the concentration of $AgNO_3$, as shown in the inset of Figure 8. An increase in the size of the particle was observed up to 25μM AgBr dispersion, which then decreased mildly, followed by a further linear increase after 45μM. Precipitation occurred when the final AgBr concentration exceeded 60μM. It is therefore evident that the optimum concentration to get a stable colloidal dispersion of AgBr in 0.4mM aqueous CTAB solution is 30μM as marked with an asterisk in the inset of Figure 8. With increasing concentration of AgBr initially the particles grow bigger with a smaller number of nuclei. This is possible because of the presence of relatively larger amount of stabilizing agent CTAB. When a certain concentration is reached (25 - 30μM) formation of a larger number of nuclei of nanoparticles of AgBr supersedes the growth processes. The growth rates of smaller nuclei were thus smaller than the growth rate of AgBr at lower concentration. At lower concentrations, number density of nanoparticles was low; the stabilizing agent was relatively abundant compare to the formed nanoparticles which results in the formation of fairly stable and larger aggregates. When the concentration of AgBr exceeds 40 μM, there would not be enough supply of the stabilizing agent for the growth of so many nuclei, resulting in smaller nanoparticle formation. Hence, number density of nuclei would increase. Subsequently, collision probability and formation of localised clusters would increase.

The rate of the particle growth was evaluated as the rate process followed a first order kinetics. As the concentration of CTAB was much higher than the $AgNO_3$ concentration, use of first order kinetics is justified. The following first order rate expression could therefore be used [221]:

$$t = \frac{2.303}{k} \log \frac{d_f - d_i}{d_f - d_t} \qquad (2)$$

where, t = time, k = first order rate constant, d_i = initial particle size, d_t = particle size at time t, d_f = final particle size.

There was no significant difference in the growth rate for different concentrations of $AgNO_3$. The average rate constant for the particle growth was found to be 5.63 x 10^{-3} hr^{-1}.

3.7. DSC-TGA analysis: Figure 9A denotes the TGA curves for pure CTAB, aqueous and chloroform extracts of CTA^+ stabilized AgBr nanoparticles. For pure CTAB, two weight loss steps were observed at 160-170 and 170-240°C of 10 and 77%, respectively[201]. The thermal decomposition of aqueous extract of CTA^+ stabilized AgBr was reflected through four weight loss steps at 140-190, 190-220, 220-270 and 270-290°C of 10,6,16 and 24%, respectively. On the contrary, the chloroform extract of CTA^+ coated AgBr was decomposed through two weight loss steps of 15 and 39% at 140-200 and 200-230 °C, respectively. The weight loss for the aqueous extract was higher than that for the corresponding chloroform extract, which was obvious; for the nanoparticles stabilized by bilayered structures, there would be a larger number of surfactant molecules than the corresponding monolayer protected systems (chloroform extract). The weight losses are due to the thermal decomposition of CTAB (150-300 °C)[228] by a self combustion process[221]. According to Mukherjee et al.[221] and others[341] when CTAB undergoes thermal decomposition there occurs formation of some solid carbon for which the attainment of 0 wt. % in TGA analysis was not observed. In case of aqueous extract there is a bilayer of CTA^+ around the AgBr nanoparticles, which makes the system more stable compared to chloroform extract and hence the weight loss takes place at higher temperature. Also, the % weight loss in case of surfactant coated AgBr nanoparticles was less than pure CTAB. Pure CTAB undergoes thermal decomposition in this range of temperature whereas the surfactant coated AgBr decomposes at a much higher temperature. The results suggest two different states of CTA^+ around AgBr nanoparticles and the formation of CTA^+ bilayers on the AgBr clusters. The two different states of CTA^+ ion around the AgBr nanoparticles correspond to the two different orientations: first kind includes the CTA^+ ions where the head groups are oriented towards the nanoparticles while for the other, the surfactant head groups are protruding out of the nanoparticles. It is believed that extracting the CTA^+ coated

nanoparticles in chloroform eliminates the bilayer structure and the CTAB molecules contributing to the second layer will be collected as part of the solid phase when the chloroform is evaporated.

DSC profiles for heating and cooling of the pure CTAB and isolated nanoparticles in the temperature range of 40-140°C are shown in Figure 9B. In

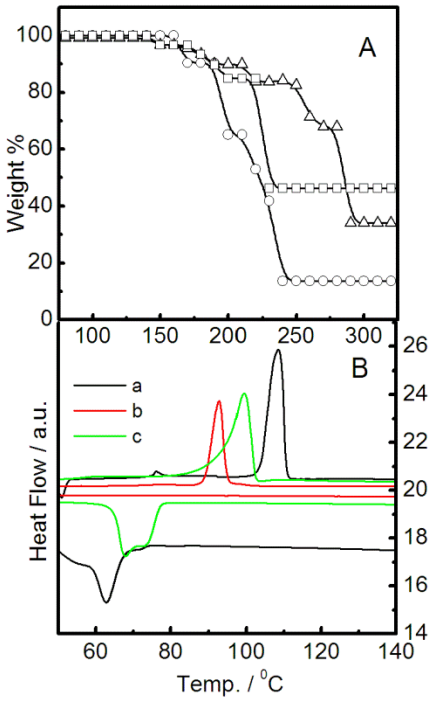

Figure 9. *(A) TGA data of pure CTAB (o),* CTA^+ coated AgBr nanoparticles isolated from *water (Δ) and chloroform (□). (B) DSC curves* of pure CTAB (a), CTA^+ coated AgBr nanoparticles isolated from water (b) and chloroform (c). Upper curves indicate heating while the lower curves were obtained during cooling.

the studied temperature range, pure CTAB exhibited a sharp endothermic peak at 108°C, whereas, the endothermic peaks for the aqueous and chloroform extracts appeared at 93°C and 100°C. These endothermic peaks, in the three cases, are not the result of any weight losses. Rather, these very observations attribute to the melting of the ordered regions of hydrocarbon chains in free CTAB and CTA^+ bilayers[308,342]. The AgBr nanoparticles isolated from chloroform showed the endothermic peak in between pure CTAB and aqueous extract. The reason could be the formation of monolayer-protected nanoparticles, which make them more rigid, compared to those isolated from the aqueous media, thereby having a higher melting point than the aqueous extract but lower than pure CTAB. On the other

hand, during cooling, only pure CTAB and chloroform extracted nanoparticles exhibited peaks within the temperature range of 60-80°C.

3.8. Isothermal Titration Calorimetry (ITC): Isothermal titration calorimetry has been found to be a very sensitive tool in estimating the enthalpy of formation of nanoparticles. It has previously been reported[221] that when otherwise water insoluble materials were synthesized in nano dimension using compartmentalized system, the problem of precipitation could easily be avoided. Not many reports are available in literature on these aspects of nanomaterials. Advantage of ITC studies to estimate the formation of nanoparticles at different precursor

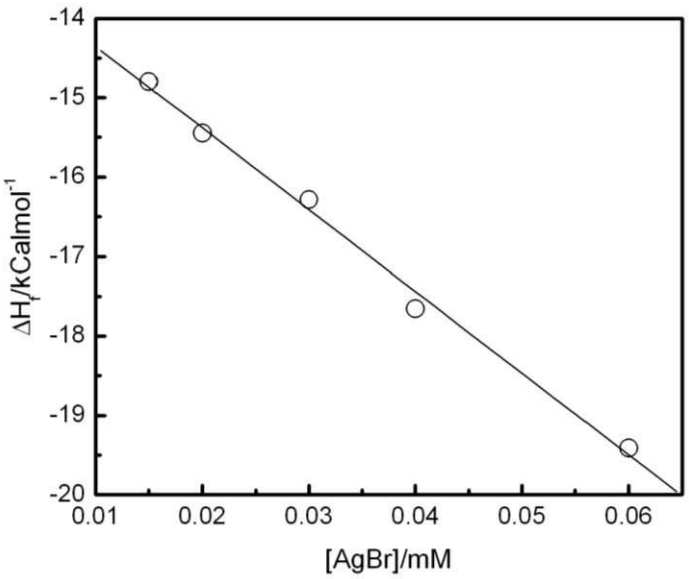

Figure 10. *Plot of* ΔH_f vs. [$AgNO_3$] for the formation of AgBr in presence of 0.4mM CTAB solution.

concentrations lies in the fact that, with suitable processing, the parameters related to the precipitation could easily be avoided. Results of the microcalorimetric titration of aqueous $AgNO_3$ (taken in the syringe against aqueous CTAB solution) for different initial $AgNO_3$ concentrations are shown graphically in Figure 10. It has been observed that with the increasing concentration of AgBr, there is a decrease in the enthalpy change. The decrease is attributed to the formation of a larger number of crystals. ΔH_f vs. [$AgNO_3$] profile was linear in nature. The study was carried out at five different concentrations and then the plot was extrapolated

to zero. The enthalpy change for formation of AgBr nanoparticles was thus found to be 13.24 kcal mol^{-1}. The exothermic nature of the reaction is proved by the negative values of the enthalpy change.

3.9. Transmission Electron Microscopy: Representative TEM images of the nanocolloidal dispersions of silver bromide, stabilized by CTAB, are shown in Figure 11. Particle morphology was found to be strongly dependent on the concentration of AgBr. Particles were spherical in shape although in some cases rice grains like morphologies were also observed (at 10 and 30μM AgBr concentrations). Particles were mostly clustered whereby the size increased with increasing AgBr concentration up to 30μM, beyond which a decrease in the particle size was again observed. In case of 50μM AgBr dispersion, smaller particles were found to be clustered. The observation in dynamic light scattering studies was thus further confirmed by TEM studies. It is to be mentioned here that EDX measurements carried out on the same spot exhibited the absence of artefacts.

At very low concentrations of AgBr, particle density was low, as observed in Figure 11A. With increased AgBr concentration, particles grew bigger. However, beyond 30μM AgBr concentrations, a size constriction effect was observed. When AgBr concentration was sufficiently high, the surfactants failed to provide proper protection. Additionally, with the increased $AgNO_3$ concentration, the rate of AgBr formation became faster. These two combined effects led to the formation of smaller particles in the higher concentration range. Size analysis of Figure 11B reveals the particle to be about 60nm. The shape of the 30μM AgBr was like rice grains. As shown in Figure 11E, the particles were clustered together, suggesting their formation following the same mechanism as in Figure 11D, but with a higher rate. The clustering of smaller particles (as in Figure 11E) was due to the process of Ostwald ripening. When the samples were irradiated with high energy electron beam some Ag^+ ions could have been reduced to Ag^0. However, this reduction did not lead to any significant morphological changes. In the present case, chances of decomposition of AgBr by

electron beam radiation are less, as AgBr particles enjoy additional protection from the surfactant bilayer-like entity. Similar method of TEM measurements has

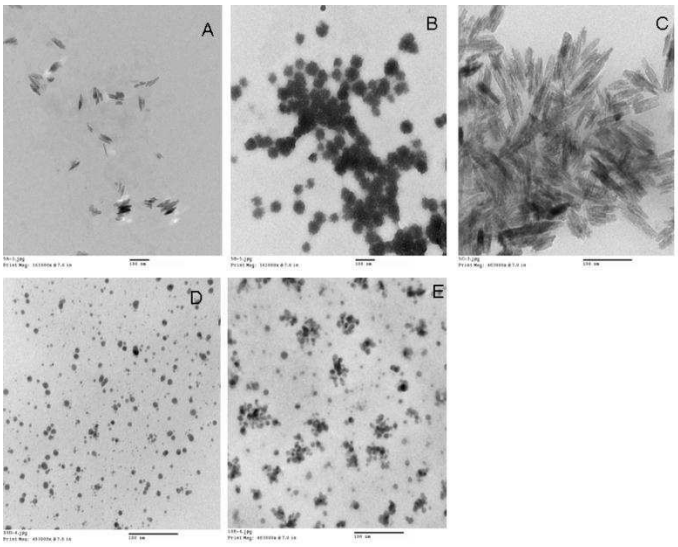

Figure 11. TEM images of different concentrations: A=10μM, B=20 μM, C=30 μM, D=40 μM and E=50 μM of silver bromide nanoparticles. Scale bars: 100 nm.

previously been reported by Liu et al.[307] However, it is noteworthy that the morphological characterization by low energy SEM would have been more reliable, which is considered as the future perspective.

4. Conclusions

Surfactant stabilized colloidal dispersions of AgBr have been prepared and characterized. The optimum concentration of CTAB used was 0.4mM. To obtain the stable colloidal dispersions, the molar ratio of $AgNO_3$ to CTAB was maintained in the range of 1:40 – 1:8. The formation of the nanocolloidal dispersions has been supported by the conductometric and the calorimetric studies. The formation process was found to be exothermic in nature. The complete conversion of $AgNO_3$ to AgBr has been established from the XRD measurements. Formation of CTA^+ coated AgBr nanoparticles was established from XRD, TEM, FTIR, NMR and UV-visible spectral studies. The DSC-TGA analysis confirms two different states of CTA^+ around AgBr nanoparticles and the formation of the CTA^+ bilayer like structure was thus ensured. The formation of

the bilayer like structure was further confirmed from the DLS results, where a two-fold increase in size occurred within few hours from the time of the formation of the nanocolloidal dispersions. The morphology of the nanocolloidal dispersions was examined by TEM measurement and the particles were mostly found to be spherical in shape except for 10 and 30 μM AgBr solutions where the shape is rice-grain like.

SUMMARY

AND

CONCLUSION

In the present dissertation spectroscopic investigation on dye / probe / aggregates comprising three specific systems viz., soft, flexible and rigid have elaborately been carried out.

The soft system described the studies on the interaction between an anionic xanthene dye, eosinY with cationic surfactants in aqueous medium.

The second category, i.e., the flexible system described the interaction of eosinY with three different cationic polymers. This was done in order to understand the nature of interaction involved between the dye and macromolecules.

The third category is associated with two different rigid systems, viz., colloidal silica and surfactant stabilized colloidal dispersions of silver bromide in aqueous medium.

This set of work had been categorized into two:

(a) UV-visible absorption and emission spectral studies in order to identify the characteristics of the excited state H-bonding between colloidal silica and 7-hydroxycoumarin (7HC) in aqueous medium.

(b) The second category described the synthesis and characterization of surfactant stabilized silver bromide nanoparticles. Synthesized nano colloidal dispersions were characterized by number of techniques, viz., XRD, FTIR, NMR, calorimetry, conductometry, DLS studies, UV-visible spectroscopy and TEM measurements.

In **Chapter 1**, UV-visible absorption and fluorescence spectroscopic studies on the anionic xanthene dye, EY were undertaken in solvents of different polarity as well as in the presence three different cationic surfactants in aqueous medium. The absorbance data of EY in presence of surfactants in the pre-micellar region were analyzed to determine the interaction constant of dye-surfactant aggregates. Fluorescence spectroscopic data provided the information on the

interaction between the dye and surfactant in its excited state. Stokes shifts were calculated and correlated with the polarity of the medium. Steady state fluorescence anisotropy values were evaluated in the pre- and post- micellar regions of surfactants in aqueous medium. It could be well wrapped up from the study that probability of formation of aggregated species was less in the excited state as monomeric form of EY was prevalent in the excited state. On the other hand the ground state was predominantly populated with dimeric form of EY. An equilibrium existed between the dimer and monomer of EY in solution. Dimerization constant (K_D) values in different media revealed that the process was more favourable in protic solvents. The binding process between dye and surfactant molecules was exothermic in nature and both electrostatic and hydrophobic forces influenced the interaction process. A disparity in the excited state and ground state geometry was indicated from larger magnitudes of stokes shift. Excited state dye-surfactant interaction was found to be dependent on the surfactant head group, nature and number of hydrocarbon chains. Fluorescence anisotropy measurement was used as a tool to determine the critical micelle concentration of surfactants.

In **Chapter 2** comprehensive studies on the interaction of three cationic polymers with an anionic xanthene dye eosin Y were carried out. The polymer matrix was surrounded by the dye molecules both by electrostatic and hydrophobic forces. Interaction of EY with PDMDAAC was stronger compared to JR400 and LM200 and also an equilibrium existed in the binding process. The binding constant values showcased that electrostatic interaction preceded over hydrophobic forces in case of JR400, compared to LM200. The binding processes were exothermic in nature and the stability of the systems was hindered with increasing temperature. Fluorescence spectral studies suggested that the excited state dye-polymer aggregates did not lead to significant change in polarity. Also, in the excited state, the binding of EY with LM200 and JR400 was unfavourable at higher polymer / dye ratio. The anisotropy results proposed the entrapment of the dye within the polymer matrix. However, in order to confirm the complete

entrapment of dye molecules further studies are warranted, which is considered as the future perspective.

In the third part (**Chapter 3**), physico-chemical studies on the interaction of imperfect nanocolloidal dispersion of silica (Ludox®) with 7-hydroxycoumarin (7HC) have been undertaken implementing electronic absorption, emission and vibrational spectroscopic measurements. While the absorption and emission intensities of 7HC were increased with increasing dye concentration in the range of 0-20μM, the enhancement of fluorescence intensity was brought about at the low concentration of silica. This enhancement of the fluorescence intensity of 7HC was related to the strengthening of excited state H-bonds formed between Ludox® and 7HC. Radiationless deactivation can influence the regulation of electronic states by H-bonding interactions and the fluorescence of chromophores in H-bonded surroundings is either quenched or enhanced by H-bonds. In the high concentration range of silica, strong but irregular adsorption of 7HC onto silica surface led to a red shift in the absorption spectra. The intermolecular fluorescence quenching, under the prevailing condition, was governed by the Homo Förster resonance energy transfer formalism. The size of the colloidal dispersion was independent of the concentration of silica and 7HC. Due to stacking of dye molecules onto silica surface, negative zeta potential values of Ludox® was suppressed compared to the systems without the dye. The adsorption kinetics of 7HC over silica surface, as measured by quartz crystal microbalance (QCM) studies would further highlight the detail mechanism. Besides, Raman spectroscopic studies are considered to more informative in understanding the exact nature of H-bonding between Ludox® and 7HC in aqueous medium. These components are considered to be the future perspectives.

The final part (**Chapter 4**) of the dissertation reports the synthesis and characterization of surfactant stabilized colloidal dispersions of AgBr. The cationic surfactant cetyltrimethylammonium bromide (CTAB) was used for this purpose. The surfactant served two purposes:

i. bromide anion for the formation of AgBr was availed from the surfactant, and

ii. the surfactant acted as the capping agent.

The optimum concentration of CTAB used was 0.4mM. To obtain the stable colloidal dispersions, the molar ratio of $AgNO_3$ to CTAB was maintained in the range of 1:40 – 1:8. Conductometric and calorimetric studies supported the formation of nanocolloidal dispersions and the formation process was found to be exothermic in nature. XRD measurements established complete conversion of $AgNO_3$ to AgBr. Formation of CTA^+ coated AgBr nanoparticles was established from XRD, TEM, FTIR, NMR and UV-visible spectral studies. The DSC-TGA analysis confirms two different states of CTA^+ around AgBr nanoparticles and the formation of the CTA^+ bilayer like structure was thus ensured. The formation of the bilayer like structure was further confirmed from the DLS results, where a two-fold increase in size occurred within few hours from the time of the formation of the nanocolloidal dispersions. The morphology of nanocolloidal dispersions was examined by TEM measurement and the particles were mostly found to be spherical in shape except for 10 and 30 μM AgBr solutions where the shape is rice-grain like. Studies on the antibacterial and catalytic activity of AgBr nanoparticles could have many applications in biotechnology and bioengineering, which are future perspectives.

References

(1) Nandini, R.; Vishalakshi, B. Orbital: Electron. J. Chem. **2009**, 1, 255.

(2) Otis Jr, D. R.; Petersen, D. W.; Michael, D. L.; Google Patents: 2003.

(3) Asgher, M.; Bhatti, H.; Ashraf, M.; Legge, R. Biodegradation **2008**, 19, 771.

(4) Chigurupati, N.; Saiki, L.; Gayser Jr, C.; Dash, A. K. Int. J. Pharm. **2002**, 241, 293.

(5) Mane, V. S.; Mall, I. D.; Srivastava, V. C. Dyes Pigments **2007**, 73, 269.

(6) Busnot, S.; Macaudiere, P.; Google Patents: 2000.

(7) Wainwright, M. In Photosensit. Biomed.; John Wiley & Sons, Ltd: 2009, p 13.

(8) Shirota, H.; Tamoto, Y.; Segawa, H. J. Phys. Chem. A **2004**, 108, 3244.

(9) Majhi, S.; Sharma, Y. C.; Upadhyay, S. N. Environ. Technol. **2009**, 30, 879.

(10) Paul, R.; Solans, C.; Erra, P. Colloids Surfaces A **2005**, 253, 175.

(11) Dasgupta, S.; Nath, R. K.; Biswas, S.; Hossain, J.; Mitra, A.; Panda, A. K. Colloids Surfaces A **2007**, 302, 17.

(12) Song, X. M.; Wu, J. M.; Yan, M. Thin Solid Films **2009**, 517, 4341.

(13) Khazraji, A. C.; Hotchandani, S.; Das, S.; Kamat, P. V. J. Phys. Chem. B **1999**, 103, 4693.

(14) Das, S.; Kamat, P. V. J. Phys. Chem. B **1998**, 103, 209.

(15) Barazzouk, S.; Lee, H.; Hotchandani, S.; Kamat, P. V. J. Phys. Chem. B **2000**, 104, 3616.

(16) Hawn, D. D.; Armstrong, N. R. J. Phys. Chem. **1978**, 82, 1288.

(17) Qin, P.; Yang, X.; Chen, R.; Sun, L.; Marinado, T.; Edvinsson, T.; Boschloo, G.; Hagfeldt, A. J. Phys. Chem. C **2007**, 111, 1853.

(18) Wight, P. In Kirk-Othmer Encyclo. Chem. Technol. ; John Wiley & Sons, Inc.: 2000.

(19) Jelley, E. E. Nature **1936**, 138, 1009

(20) Brooker, L. G. S.; White, F. L.; Heseltine, D. W.; Keyes, G. H.; Dent, S. G.; Vanlare, E. J. J. Photogr. Sci. **1953**, 1, 173.

(21) Sabaté, R.; Estelrich, J. Spectrochim.Acta A **2008**, 70, 471.

(22) Manna, K.; Panda, A. K. Spectrochim. Acta A **2009**, 74, 1268.

(23) Lin, C. T.; Mahloudji, A. M.; Li, L.; Hsiao, M. W. Chem.Phys.Lett. **1992**, 193, 8.

(24) Bhowmik, B. B.; Ganguly, P. Spectrochim. Acta A **2005**, 61, 1997.

(25) Cestari, A. R.; Vieira, E. F. S.; Vieira, G. S.; Almeida, L. E. J. Colloid Interface Sci. **2007**, 309, 402.

(26) De, S.; Das, S.; Girigoswami, A. Spectrochim. Acta A **2005**, 61, 1821.

(27) Kolev, T.; Koleva, B. B.; Stoyanov, S.; Spiteller, M.; Petkov, I. Spectrochim.Acta A **2008**, 70, 1087.

(28) Keiichi, I. AIST Today **2005**, 5, 19.

(29) Sabate, R.; Gallardo, M.; de la Maza, A.; Estelrich, J. Langmuir **2001**, 17, 6433.

(30) Qin, C.; Zhang, W.; Wang, Z.; Zhou, M.; Wang, X.; Chen, G. Opt. Mater. **2008**, 30, 1607.

(31) Paul, S.; Panda, A. K. Colloids Surfaces A **2013**, 419, 113.

(32) Jain, P. K.; Joshi, H. J.Appl. Pharm. Sci. **2012**, 2, 236.

(33) Ojala, T. PhD Thesis, University of Helsinki,Helsinki, Finland **2001**.

(34) Wagner, B. D. Molecules **2009**, 14, 210.

(35) Chun-feng, Y.; He-ping, Z. Chem. Res. Chinese Universities **2011**, 27, 599.

(36) Härtner, S.; Kim, H.-C.; Hampp, N. J.Photochem.Photobiol. A **2007**, 187, 242.

(37) Venugopala, K. N.; Rashmi, V.; Odhav, B. BioMed. Res. Int.**2013**, 2013, 14.

(38) Satyanarayana, P.; Subrahmanyam, P.; Kasai, R.; Tanaka, O. Phytochem. **1985**, 24, 1862.

(39) Goodwin, R. H.; Pollock, B. M. Arch. Biochem. Biophys.**1954**, 49, 1.

(40) Hu, X.-R.; He, J.-B.; Wang, Y.; Zhu, Y.-W.; Tian, J.-J. Electrochim. Acta **2011**, 56, 2919.

(41) Shank, C. V. Reviews of Modern Physics **1975**, 47, 649.

(42) Goddard, J.-P.; Reymond, J.-L. Curr. Opin. Biotechnol. **2004**, 15, 314.

(43) Lacy , A.; O'Kennedy, R. Curr. Pharm. Design **2004**, 10, 3797.

(44) Nelson, A. F. J. Chem. Edu. **1948**, 25, 379.

(45) Snell, F. D. J. Chem. Edu.**1942**, 19, 172.

(46) Llenado, R. A.; Neubecker, T. A. Anal. Chem.**1983**, 55, 93R.

(47) Bunton, C. A.; Robinson, L. B.; Schaak, J.; Stam, M. F. J. Org. Chem. **1971**, 36, 2346.

(48) Usui, Y.; Saga, K. Bull. Chem. Soc. Japan **1982**, 55, 3302.

(49) Sato, H.; Kusumoto, Y.; Nakashima, N.; Yoshihara, K. Chem.Phys. Lett. **1980**, 71, 326.

(50) Valdes-Aguilera, O.; Neckers, D. C. Acc.Chem. Res.**1989**, 22, 171.

(51) Rohatgi, K. K.; Mukhopadhyay, A. K. Chem.Phys. Lett. **1971**, 12, 259.

(52) Peterson, O. G.; Tuccio, S. A.; Snavely, B. B. Appl. Phys. Lett. **1970**, 17, 245.

(53) Nazar, M.; Shah, S.; Khosa, M. J Surfact. Deterg. **2010**, 13, 529.

(54) Akbas, H.; Iscan, M. Turk. J. Chem. **1994**, 18, 80.

(55) Misselyn-Bauduin, A. M.; Thibaut, A.; Grandjean, J.; Broze, G.; Jérôme, R. Langmuir **2000**, 16, 4430.

(56) Sudbeck, E. A.; Dubin, P. L.; Curran, M. E.; Skelton, J. J. Colloid Interface Sci. **1991**, 142, 512.

(57) Barni, E.; Savarino, P.; Viscardi, G. Acc. Chem. Res.**1991**, 24, 98.

(58) Suradkar, Y. R.; Bhagwat, S. S. J. Chem. Eng. Data **2006**, 51, 2026.

(59) Khamis, M.; Bulos, B.; Jumean, F.; Manassra, A.; Dakiky, M. Dyes Pigments **2005**, 66, 179.

(60) Basu Ray, G.; Chakraborty, I.; Moulik, S. P. J. Colloid Interf. Sci.**2006**, 294, 248.

(61) Bakshi, M. S.; Thakur, P.; Sachar, S.; Kaur, G.; Banipal, T. S.; Possmayer, F.; Petersen, N. O. J. Phys.Chem.C **2007**, 111, 18087.

(62) Göktürk, S.; Tunçay, M. Spectrochim. Acta A**2003**, 59, 1857.

(63) Aoki, M.; Iwayama, Y. YAKUGAKU ZASSHI **1959**, 79, 522.

(64) Robinson, B. H.; White, N. C.; Mateo, C. Adv. Mol. Relax. Processes **1975**, 7, 321.

(65) Acharya, S.; Rebery, B. Arabian J. Chem.**2009**, 2, 7.

(66) Painter, P. C.; Coleman, M. M. Fundamentals of Polymer Science: An Introductory Text; Technomic Pub. Co., 1997.

(67) McCrum, N. G.; Buckley, C. P.; Bucknall, C. B. Principles of polymer engineering.; Oxford University Press, 1997.

(68) Baeurle, S. A. J. Math. Chem. **2009**, 46 363.

(69) Yu, M.; Bozukov, M.; Voigt, W.; Thomas, H.; Moeller, M. Springer Proc. Phys. **2008**, 124, 525.

(70) Kam, S.-k.; Gregory, J. Colloids Surfaces A **1999**, 159, 165.

(71) Neimo, L. Papermaking chemistry; Jyvaskyla, Finland: Fapet Oy, 1999; Vol. 4.

(72) Durand-Piana, G.; Lafuma, F.; Audebert, R. J. Colloid Interf. Sci. **1987**, 119, 474.

(73) Bagai, S.; Sun, C.; Tang, T. J. Phys. Chem. B **2012**, 117, 49.

(74) Toma, A. C.; de Frutos, M.; Livolant, F. o.; Raspaud, E. Biomacromolecules **2009**, 10, 2129.

(75) Lowe, T. L.; Virtanen, J.; Tenhu, H. Polymer **1999**, 40, 2595.

(76) Daoud-Mahammed, S.; Ringard-Lefebvre, C.; Razzouq, N.; Rosilio, V.; Gillet, B.; Couvreur, P.; Amiel, C.; Gref, R. J. Colloid Interf. Sci. **2007**, 307, 83.

(77) Bai, G.; Nichifor, M.; Bastos, M. J. Phys. Chem. B **2010**, 114, 16236.

(78) Sakkayawong, N.; Thiravetyan, P.; Nakbanpote, W. J. Colloid Interf. Sci. **2005**, 286, 36.

(79) Libert, C.; Marechal, E. Eur. Polym.J.**1980**, 16, 1121.

(80) Guthrie, J. T. Review of Progress in Coloration and Related Topics **1990**, 20, 40.

(81) Nath, R. K.; Singh, T. C.; Dasgupta, S.; Mitra, A.; Panda, A. K. Mater. Sci. Eng. C **2010**, 30, 549.

(82) Orchard, B. J.; Tan, J. S.; Hopfinger, A. J. Macromolecules **1984**, 17, 169.

(83) Jang, M.; Min, S.-H.; Park, J. K.; Tlachac, E. J. Environ.Sci.Technol.**2007**, 41, 3322.

(84) Mitra, A.; Nath, R. K.; Biswas, S.; Chakraborty, A. K.; Panda, A. K. J.Photochem. Photobiol. A **2006**, 178, 98.

(85) Jana-Sur, P.; Chakraborty, A. K. J. Photochem.Photobiol. A **2005**, 173, 64.

(86) Yamaki, S. B.; Oliveira, M. G. d.; Atvars, T. D. Z. J. Brazilian Chem. Soc.**2004**, 15, 253.

(87) Zwier, J. M.; Van Rooij, G. J.; Hofstraat, J. W.; Brakenhoff, G. J. J. Microscopy **2004**, 216, 15.

(88) Yunus, W. M. M.; Sheng, C. K. J. Sci. Technol. **2004**, 11.

(89) Talhavini, M.; Atvars, T. D. Z. J. Photochem. Photobiol. A **1998**, 114, 65.

(90) Kolaric, B.; Sliwa, M.; Vallée, R. A. L.; Van der Auweraer, M. Colloids Surfaces A **2009**, 338, 61.

(91) Zhang, W.; Bian, S.; Kim, S. I.; Kuzyk, M. G. Opt. Lett. **2002**, 27, 1105.

(92) Kang, J.-W.; Kim, E.; Kim, J.-J. Opt. Mater. **2003**, 21, 543.

(93) Singh, S.; Kanetkar, V. R.; Sridhar, G.; Muthuswamy, V.; Raja, K. J.Lumines. **2003**, 101, 285.

(94) Robinson, T.; McMullan, G.; Marchant, R.; Nigam, P. Biores. technol. **2001**, 77, 247.

(95) Crini, G. Biores. technol. **2003**, 90, 193.

(96) Wood, P. J. Carbohyd. Res. **1980**, 85, 271.

(97) Stone, A. L.; Bradley, D. F. Biochim. biophys. acta **1967**, 148, 172.

(98) Peyratout, C.; Donath, E.; Daehne, L. J. Photochem. Photobiol. A **2001**, 142, 51.

(99) Panda, A. K.; Chakraborty, A. K. J. Photochem. Photobiol. A **1997**, 111, 157.

(100) Kamat, P. V.; Fox, M. A. J. Phys.Chem.**1984**, 88, 2297.

(101) Seery, M. K.; Fay, N.; McCormac, T.; Dempsey, E.; Forster, R. J.; Keyes, T. E. Phys. Chem. Chem. Phys. **2005**, 7, 3426.

(102) Sarkar, D.; Das, P.; Basak, S.; Chattopadhyay, N. J. Phys. Chem. B **2008**, 112, 9243.

(103) Levine, I. N. Physical Chemistry (5th ed.). (5th ed.) ed.; McGraw-Hill, 2001.

(104) Nakajima, A. Bull. Chem. Soc. Jpn. **2013**, 86, 414.

(105) Buzea, C.; Pacheco, I.; Robbie, K. Biointerphases **2007**, 2, MR17.

(106) Rao, B. S.; Kumar, B. R.; Reddy, V. R.; Rao, T. S.; Chalapathi, G. V. Chalcogenide Lett. **2011**, 8, 39

(107) Buffat, P.; Borel, J. P. Phys. Rev. A **1976**, 13, 2287.

(108) Sapra, S.; Sarma, D. D.; Sanvito, S.; Hill, N. A. Nano Letters **2002**, 2, 605.

(109) Losurdo, M.; Giangregorio, M. M.; Bianco, G. V.; Suvorova, A. A.; Kong, C.; Rubanov, S.; Capezzuto, P.; Humlicek, J.; Bruno, G. Phys. Rev. B **2010**, 82, 155451.

(110) Kodama, R. H. J.Mag. Mag. Mater. **1999**, 200, 359.

(111) Gubin, S. P. Mag. nanoparticles; Wiley-VCH, 2009.

(112) Ko, S. H.; Park, I.; Pan, H.; Grigoropoulos, C. P.; Pisano, A. P.; Luscombe, C. K.; Fréchet, J. M. J. Nano Letters **2007**, 7, 1869.

(113) Hawker, C. J.; Wooley, K. L. Science **2005**, 309, 1200.

(114) Brigger, I.; Dubernet, C.; Couvreur, P. Adv. Drug Deliv. Rev. **2002**, 54, 631.

(115) Jackson, J. B.; Halas, N. J. J. Phys.Chem. B **2001**, 105, 2743.

(116) Ozbay, E. Science **2006**, 311, 189.

(117) Potara, M.; Gabudean, A.-M.; Astilean, S. J.Mater. Chem.**2011**, 21, 3625.

(118) Lal, S.; Grady, N. K.; Kundu, J.; Levin, C. S.; Lassiter, J. B.; Halas, N. J. Chem. Soc. Rev.**2008**, 37, 898.

(119) Bruchez, M.; Moronne, M.; Gin, P.; Weiss, S.; Alivisatos, A. P. Science **1998**, 281, 2013.

(120) Pantarotto, D.; Partidos, C. D.; Hoebeke, J.; Brown, F.; Kramer, E.; Briand, J.-P.; Muller, S.; Prato, M.; Bianco, A. Chem. biol. **2003**, 10, 961.

(121) Edelstein, R. L.; Tamanaha, C. R.; Sheehan, P. E.; Miller, M. M.; Baselt, D. R.; Whitman, L. J.; Colton, R. J. Biosens Bioelectron **2000**, 14, 805.

(122) Nam, J.-M.; Thaxton, C. S.; Mirkin, C. A. Science **2003**, 301, 1884.

(123) Mahtab, R.; Rogers, J. P.; Murphy, C. J. J. Amer. Chem. Soc.**1995**, 117, 9099.

(124) Harrison, B. S.; Atala, A. Biomaterials **2007**, 28, 344.

(125) Molday, R. S.; Mackenzie, D. J. Immun. Methods **1982**, 52, 353.

(126) Weissleder, R.; Elizondo, G.; Wittenberg, J.; Rabito, C. A.; Bengele, H. H.; Josephson, L. Radiology **1990**, 175, 489.

(127) Parak, W. J.; Boudreau, R.; Le Gros, M.; Gerion, D.; Zanchet, D.; Micheel, C. M.; Williams, S. C.; Alivisatos, A. P.; Larabell, C. Adv.Mater. **2002**, 14, 882.

(128) Wong, A. L.; Hunnicutt, M. L.; Harris, J. M. Anal. Chem.**1991**, 63, 1076.

(129) Emmerling, A.; Petricevic, R.; Beck, A.; Wang, P.; Scheller, H.; Fricke, J. J. Non-Crystall. Solids **1995**, 185, 240.

(130) Zhao, X.; Bagwe, R. P.; Tan, W. Adv. Mater.**2004**, 16, 173.

(131) Goloub, T. P.; Koopal, L. K.; Bijsterbosch, B. H.; Sidorova, M. P. Langmuir **1996**, 12, 3188.

(132) Bonacchi, S.; Genovese, D.; Juris, R.; Montalti, M.; Prodi, L.; Rampazzo, E.; Sgarzi, M.; Zaccheroni, N. Top Curr. Chem. **2011**, 300, 93.

(133) Knopp, D.; Tang, D.; Niessner, R. Anal. Chim. Acta **2009**, 647, 14.

(134) Chen, G.; Song, F.; Wang, X.; Sun, S.; Fan, J.; Peng, X. Dyes Pigments **2012**, 93, 1532.

(135) Johnson, S. A.; Ollivier, P. J.; Mallouk, T. E. Science **1999**, 283, 963.

(136) Payne, C. C. Surfactant Sci. Ser. **2006**, 131, 713.

(137) Roberts, W. O. Surfactant Sci. Ser. **2006**, 131, 131.

(138) Boettcher, L. CFI, Ceram. Forum Int. **2009**, 86, D25.

(139) Liong, M.; Lu, J.; Kovochich, M.; Xia, T.; Ruehm, S. G.; Nel, A. E.; Tamanoi, F.; Zink, J. I. ACS Nano **2008**, 2, 889.

(140) Overbeek, J. T. G. Adv. Colloid Interf. Sci.**1982**, 15, 251.

(141) Han, S.; Lee, K. T.; Oh, S. M.; Hyeon, T. Carbon **2003**, 41, 1049.

(142) Collinson, M. M.; Moore, N.; Deepa, P. N.; Kanungo, M. Langmuir **2003**, 19, 7669.

(143) Iler, R. K. The Chemistry of Silica; Wiley, 1979.

(144) Tsai, M.-S.; Huang, P. Y.; Wu, W.-C. Mater. Res. Bull. **2005**, 40, 1609.

(145) Stöber, W.; Fink, A.; Bohn, E. J. Colloid Interf. Sci. **1968**, 26, 62.

(146) Lee, Y.-K.; Rock Yoon, Y.; Rhee, H.-K. Colloids Surfaces A **2000**, 173, 109.

(147) Guo, J.; Liu, X.; Cheng, Y.; Li, Y.; Xu, G.; Cui, P. J. Colloid Interf. Sci. **2008**, 326, 138.

(148) Lim, H. M.; Lee, J.; Jeong, J.-H.; Oh, S.-G.; Lee, S.-H. Engineering **2010**, 2, 998.

(149) Pont, D. In Reg. U.S. Pat. & T.M. off.; Ltd., C. C. a. C., Ed. Canada.

(150) van Blaaderen, A.; Vrij, A. J. Colloid Interf. Sci. **1993**, 156, 1.

(151) Van Blaaderen, A.; Vrij, A. Langmuir **1992**, 8, 2921.

(152) Konovalova, V. V.; Bryk, M. T.; Nigmatullin, R. R.; Gvozdyak, P. I.; Udilova, O. F. Bioproc.Biosys. Eng. **2000**, 23, 651.

(153) Lepp, A.; Siiman, O. J. Phys. Chem.**1985**, 89, 3494.

(154) Bae, E.; Choi, W. Environ. Sci. Technol.**2003**, 37, 147.

(155) Arabatzis, I. M.; Stergiopoulos, T.; Andreeva, D.; Kitova, S.; Neophytides, S. G.; Falaras, P. J.Catal. **2003**, 220, 127.

(156) Imhof, A.; van Blaaderen, A.; Maret, G.; Mellema, J.; Dhont, J. K. G. J. Chem. Phys.**1994**, 100, 2170.

(157) Van Blaaderen, A.; Imhof, A.; Hage, W.; Vrij, A. Langmuir **1992**, 8, 1514.

(158) Bagwe, R. P.; Yang, C.; Hilliard, L. R.; Tan, W. Langmuir **2004**, 20, 8336.

(159) Ha, S.-W.; Camalier, C. E.; Beck Jr, G. R.; Lee, J.-K. Chem. Commun. **2009**, 2881.

(160) Bringley, J. F.; Penner, T. L.; Wang, R.; Harder, J. F.; Harrison, W. J.; Buonemani, L. J. Colloid Interf. Sci. **2008**, 320, 132.

(161) Sharma, S.; Mohan, D.; Singh, N.; Sharma, M.; Sharma, A. K. Optik - Int. J. Light Electr. Opt. **2010**, 121, 11.

(162) Ren, T.-Z.; Yuan, Z.-Y.; Su, B.-L. Colloids Surfaces A **2007**, 300, 79.

(163) Parida, S. K.; Dash, S.; Patel, S.; Mishra, B. K. Adv. Colloid Interf. Sci. **2006**, 121, 77.

(164) Messina, P. V.; Schulz, P. C. J. Colloid Interf. Sci.**2006**, 299, 305.

(165) Krysztafkiewicz, A.; Binkowski, S.; Jesionowski, T. Appl. Surf. Sci.**2002**, 199, 31.

(166) Cardelli, A.; Ricci, L.; Ruggeri, G.; Borsacchi, S.; Geppi, M. Eur.Polym. J.**2011**, 47, 1589.

(167) Lacey, D.; Holder, S. J. Chem. Technol. Biotechnol.**1992**, 54, 201.

(168) Zhavnerko, G. K.; Agabekov, V. E.; Gallyamov, M. O.; Yaminsky, I. V.; Rogach, A. L. Colloids Surfaces A **2002**, 202, 233.

(169) Lattuada, M.; Hatton, T. A. Nano Today **2011**, 6, 286.

(170) Serra, A.; Genga, A.; Manno, D.; Micocci, G.; Siciliano, T.; Tepore, A.; Tafuro, R.; Valli, L. Langmuir **2003**, 19, 3486.

(171) López-Quintela, M. A. Curr. Opin. Colloid Interf. Sci.**2003**, 8, 137.

(172) Wongwailikhit, K.; Horwongsakul, S. Mater. Lett. **2011**, 65, 2820.

(173) Lee, M. S.; Park, S. S.; Lee, G.-D.; Ju, C.-S.; Hong, S.-S. Catal. Today **2005**, 101, 283.

(174) Capek, I. Adv. Colloid Interf. Sci.**2004**, 110, 49.

(175) Mehta, S. K.; Chaudhary, S.; Gradzielski, M. J. Colloid Interf. Sci. **2010**, 343, 447.

(176) Liu, X.-H.; Luo, X.-H.; Lu, S.-X.; Zhang, J.-C.; Cao, W.-L. J. Colloid Interf. Sci. **2007**, 307, 94.

(177) Chakraborty, I.; Moulik, S. P. J. Surface Sci. Technol. **2005**, 21, 195.

(178) Chakraborty, I.; Malik, P.; Moulik, S. J. Nanoparticle Res. **2006**, 8, 889.

(179) Zhang, H.; Mostafavi, M. J. Phys. Chem. B **1997**, 101, 8443.

(180) Suzuki, M.; Sato, T.; Sato, K.; Ishii, Y.; Naruse, H.; Shimada, Y.; Google Patents: 1993.

(181) Kakuta, N.; Goto, N.; Ohkita, H.; Mizushima, T. J. Phys.Chem. B **1999**, 103, 5917.

(182) Gosheger, G.; Hardes, J.; Ahrens, H.; Streitburger, A.; Buerger, H.; Erren, M.; Gunsel, A.; Kemper, F. H.; Winkelmann, W.; von Eiff, C. Biomaterials **2004**, 25, 5547.

(183) Zang, Y.; Farnood, R.; Currie, J. Chem. Eng. Sci. **2009**, 64, 2881.

(184) Sambhy, V.; MacBride, M. M.; Peterson, B. R.; Sen, A. J. Amer. Chem. Sc. **2006**, 128, 9798.

(185) Pourahmad, A.; Sohrabnezhad, S.; Kashefian, E. Spectrochim. Acta A **2010**, 77, 1108.

(186) Husein, M. M.; Rodil, E.; Vera, J. H. Langmuir **2006**, 22, 2264.

(187) He, C.; Sasaki, T.; Zhou, Y.; Shimizu, Y.; Masuda, M.; Koshizaki, N. Adv. Funct. Mater. **2007**, 17, 3554.

(188) Li, Y.; Qian, F.; Xiang, J.; Lieber, C. M. Mater. Today **2006**, 9, 18.

(189) Hosono, H. Thin Solid Films **2007**, 515, 6000.

(190) Wang, C.; Ao, Y.; Wang, P.; Hou, J.; Qian, J.; Zhang, S. Mater. Lett. **2010**, 64, 439.

(191) Syoufian, A.; Satriya, O. H.; Nakashima, K. Catal. Commun. **2007**, 8, 755.

(192) Bell, S. E. J.; Sirimuthu, N. M. S. J. Amer. Chem. Soc. **2006**, 128, 15580.

(193) Stoermer, R. L.; Keating, C. D. J. Amer. Chem.Soc.**2006**, 128, 13243.

(194) Jeunieau, L.; Verbouwe, W.; Rousseau, E.; Van der Auweraer, M.; B.Nagy, J. Langmuir **2000**, 16, 1602.

(195) Rossetti, R.; Hull, R.; Gibson, J. M.; Brus, L. E. J. Chem. Phys. **1985**, 83 1406.

(196) Ohde, H.; Rodriguez, J. M.; Ye, X.-R.; Wai, C. M. Chem. Commun. **2000**, 0, 2353.

(197) Koh, J. H.; Kang, S. W.; Park, J. T.; Seo, J. A.; Kim, J. H.; Kang, Y. S. J. Membrane Sci. **2009**, 339, 49.

(198) Eyal, O.; Shemesh, D.; Katzir, A. Appl. Opt. **1997**, 36, 1185.

(199) Miglietta, M. L.; Rametta, G.; Francia, G.; Bruno, A.; Lisio, C.; Leter, G.; Mancuso, M.; Pacchierotti, F.; Buono, S.; Manzo, S. Sensors Microsys. **2010**, 54, 67.

(200) Lahtinen, R. M.; Mertens, S. F. L.; East, E.; Kiely, C. J.; Schiffrin, D. J. Langmuir **2004**, 20, 3289.

(201) Sui, Z. M.; X.Chen; Wang, L. Y.; Xu, L. M.; Zhuang, W. C.; Y.C.Chai; C.J.Yang Phys. E **2006**, 33.

(202) Sui, Z.; Chen, X.; Wang, L.; Chai, Y.; Yang, C.; Zhao, j. Chem. Lett. **2005**, 34.

(203) Jana, N. R.; Gearheart, L.; Murphy, C. J. Chem. Commun. **2001**, 617.

(204) Bai, J.; Li, Y.; Zhanga, C.; Lianga, X.; Yanga, Q. Colloids Surfaces A **2008**, 329 165.

(205) Chen, S.; Carroll, D. L. J. Phys. Chem. B **2004**, 108, 5500.

(206) Husein, M.; Rodil, E.; Vera, J. H. J. Colloid Interf. Sci. **2004**, 273, 426.

(207) Husein, M. M.; Rodil, E.; Vera, J. H. J. Colloid Interf. Sci. **2005**, 288, 457.

(208) Xue, C.-H.; Chen, J.; Yin, W.; Jia, S.-T.; Ma, J.-Z. Appl. Surface Sci. **2012**, 258, 2468.

(209) Betancourt-Galindo, R.; Cabrera Miranda, C.; Puente Urbina, B. A.; Casta; eda-Facio, A.; nchez-Vald; s, S.; Mata Padilla, J.; Garc; a Cerda, L. A.; Perera, Y. A.; Rodr; guez-Fern; ndez, O. S. ISRN Nanotechnol. **2012**, 2012, 5.

(210) Wang, Y.-S.; Liu, L.-R.; Jiang, Q.; Zhang, Q.-Q. Eur. Polym. J. **2007**, 43, 43.

(211) Nguyen, T. T.-B.; Chang, H.-C.; Wu, V. W.-K. Diamond Related Mater. **2007**, 16, 872.

(212) Martínez, J. C.; Chequer, N. A.; González, J. L.; Cordova, T. Nanosci. Nanotechnol. **2012**, 2, 184.

(213) Sohrabnezhad, S.; Pourahmad, A. Spectrochim. Acta A **2012**, 86, 271.

(214) Urban, C.; Schurtenberger, P. J. Colloid Interf. Sci. **1998**, 207, 150.

(215) Komalam, A.; Muraleegharan, L.; Subburaj, S.; Suseela, S.; Babu, A.; George, S. Int. Nano Lett. **2012**, 2, 1.

(216) Gill, P.; Moghadam, T. T.; Ranjbar, B. J. Biomol. Tech. **2010**, 21, 167.

(217) Kim, N. D.; Yun, H. J.; Nam, I.; Song, I. K.; Yi, J. Curr. App. Phys. **2012**, 12, 1139.

(218) Moulik, S. P.; De, G. C.; Panda, A. K.; Bhowmik, B. B.; Das, A. R. Langmuir **1999**, 15, 8361.

(219) Dadosh, T. Mater.Lett. **2009**, 63, 2236.

(220) O'Keefe, M. A.; Hetherington, C. J. D.; Wang, Y. C.; Nelson, E. C.; Turner, J. H.; Kisielowski, C.; Malm, J.-O.; Mueller, R.; Ringnalda, J.; Pane, M.; Thust, A. Ultramicroscopy **2001**, 89, 215.

(221) Acharya, K. R.; Bhattacharya, S. C.; Moulik, S. P. J. Photochem. Photobiol. A **1997**, 109, 29.

(222) Ghoreishi, S. M.; Behpour, M.; Farsani, A. G. Dyes Pigments **2007**, 74, 585.

(223) Forte-Tavcer, P. Dyes Pigments **2004**, 63, 181.

(224) Tanaka., F.; Harada, Y.; Todoroki, N.; Aratono, M.; Motomura, K. Bull. Chem. Soc. Japan **1993**, 66, 1929.

(225) Bhowmik, B. B.; Ganguly, P. Spectrochim. Acta A **2005**, 62, 808.

(226) Akbas, H. Colloid Journal **2008**, 70, 541.

(227) Rentería, V.M.; Macedo, J. García Colloids Surfaces A **2006**, 278, 1.

(228) Honda, C.; Kamizono, H.; Matsumoto, K. I.; Endo, K. J. Colloid Interf. Sci. **2004**, 278, 310.

(229) Gille, K.; Knoll, H.; Quitzsch, K. Int. J.Chem. Kinetics **1999**, 31, 337.

(230) Abou-Sekkina; Morsy, M. Mater. Lett. **2000**, 42, 297.

(231) Sreethawong, T.; Junbua, C.; Chavadej, S. J. Power Sour. **2009**, 190, 513.

(232) Hosseinzadeh, R.; Bordbar, A. K.; Matina, A. A.; Maleki, R. J. Brazil.Chem. Soc. **2007**, 18, 359.

(233) Chakrabarty, A.; Mallick, A.; Haldar, B.; Das, P.; Chattopadhyay, N. Biomacromolecules **2007**, 8, 920.

(234) Mukhopadhyay, S.; Maity, S. S.; Roy, A.; Chattopadhyay, D.; Ghosh, K. S.; Dasgupta, S.; Ghosh, S. Biochimie **2010**, 92, 136.

(235) Correa, N. M.; Levinger, N. E. J. Phys. Chem. B **2006**, 110, 13050.

(236) Baker, S. N.; Baker, G. A.; Bright, F. V. Green Chemistry **2002**, 4, 165.

(237) Kosower, E. M. J. Amer. Chem. Soc. **2002**, 80, 3253.

(238) Banerjee, P.; Chatterjee, S.; Pramanik, S.; Hossain, S. U.; Bhattacharya, S.; Bhattacharya, S. C. Spectrochim. Acta A **2007**, 66, 1110.

(239) Retter, U.; Koch, M.; Nehls, I. Fresenius' J. Anal. Chem. **1999**, 364, 777.

(240) Gargi Ghosh, P. K. B. Chem. Eng. J. **2006**, 119, 45.

(241) SenVarma, C.; Bhowmik, B. B. J. Photochem. Photobiol. B **1991**, 8, 295.

(242) Bhowmik, B. B.; Chatterjee, I.; Nandy, P. Chem. Phys. Lipids **1986**, 39, 271.

(243) Rose, N. J.; Drago, R. S. J. Amer. Chem. Soc. **1959**, 81, 6138.

(244) Mahltig, B; Fielder, D; Fischer, A.; Simon, P. J. Sol-Gel Sci. Technol. **2010**, 55, 269.

(245) Hait, S. K.; Moulik, S. P. Langmuir **2002**, 18, 6736.

(246) Aaron, J. J.; Gaye, M. D.; Parkanyi, C.; Boniface, C.; Bieze, T. W. N.; Atik, S. S.; RaghuVeer, K. S.; Von Szentpaly, L.; Ghosh, R. Pteridines **1992**, 3, 153.

(247) Biradar, D. S.; Siddlingeshwar, B.; Hanagodimath, S. M. J. Mol. Struc. **2008**, 875, 108.

(248) Raikar, U. S.; Tangod, V. B.; Mastiholi, B. M.; Sreenivasa, S. **2010**, 4 188.

(249) Buwalda, R. T.; Jonker, J. M.; Engberts, J. B. F. N. Langmuir **1999**, 15, 1083.

(250) Chakrabarty, A.; Das, P.; Mallick, A.; Chattopadhyay, N. J. Phys. Chem. B **2008**, 112, 3684.

(251) Mahata, A.; Sarkar, D.; Bose, D.; Ghosh, D.; Girigoswami, A.; Das, P.; Chattopadhyay, N. J. Phys. Chem. B **2009**, 113, 7517.

(252) Caruso, F.; Schüler, C.; Kurth, D. G. Chem.Mater.**1999**, 11, 3394.

(253) Schlüter, A. D. In Synthesis of Polymers; Wiley-VCH Verlag GmbH: 2008, p 459.

(254) Butters, A.; Clifton, A.; Imperial Chemical Industries Plc, UK . 2000, p 25 pp.

(255) Slark, A. T.; Hadgett, P. M. Polymer **1999**, 40, 1325.

(256) Ball, V. Materials **2012**, 5, 2681.

(257) Karsli-Ceppioqlu, S.; Yurdun, T. Marmara Univ. Saglik Bilimleri Enst. Derg. **2012**, 2, 108.

(258) Milikli, G.; Ramachandra, R. C. S. V. Int. J. Integr. Sci., Innovation Technol. **2012**, 1, 32.

(259) Salima, A.; Ounissa, K.-S.; Lynda, M.; Mohamed, B. Procedia Eng. **2012**, 33, 38.

(260) Ramesh , B.; Parande, A. K.; Raghu, S.; Prem Kumar, T. J.Cotton Sci. **2007**, 11, 141.

(261) Rahbar, M. S.; Alipour, E.; Sedighi, R. E. Int. J. Environ. Sci. Technol. **2006**, 3, 79.

(262) Chakraborty, M.; Panda, A. K. Spectrochim. Acta A **2011**, 81, 458.

(263) Archut, A.; Azzellini, G. C.; Balzani, V.; Cola, L.; Voegtle, F. J. Amer. Chem. Soc. **1998**, 120, 12187.

(264) Fouassier, J. P.; Chesneau, E. Makromol. Chem. **1991**, 192, 245.

(265) Zipfel, E.; Grezes, J. R.; Naujok, A.; Seiffert, W.; Wittekind, D. H.; Zimmermann, H. W. Histochemistry **1984**, 81, 337.

(266) Mukherjee, S.; Chakraborty, M.; Panda, A. K.; Bhattacharya, S. C.; Moulik, S. P. Colloids Surfaces A **2011**, 388, 1.

(267) Desenne, P.; Bebot, C.; Laurent, F.; L'oreal, Fr. . 2003, p 35 pp.

(268) Jacquier, I.; L'Oreal, Fr. . 2012, p 44pp.

(269) Bai, G.; Nichifor, M.; Lopes, A.; Bastos, M. J. Phys. Chem. B **2005**, 109, 518.

(270) Schulze, z. W. E.; Hoting, E.; Poppe, E.; Henkel Kommanditgesellschaft auf Aktien, Germany . 2008, p 52 pp.

(271) Ghosh, S. K.; Khatua, P. K.; Bhattacharya, S. C. J. Colloid Interf. Sci. **2004**, 279, 523.

(272) Batchelor, E. K.; Gadde, S.; Kaifer, A. E. Supramol. Chem. **2010**, 22, 40.

(273) Kunisawa, T.; Sato, T.; Yonezawa, Y.; Sluch, M. I.; Vitukhnovsky, A. G. Nippon Shashin Gakkaishi **1996**, 59, 465.

(274) Nandini, R.; Vishalakshi, B. E-J. Chem. **2011**, 8, S253.

(275) Korenman, Y. I.; Sannikova, N. Y.; Sukhanov, P. T.; Gusev, A. V.; Churilina, E. V.; Shatalov, G. V. Izv. Vyssh. Uchebn. Zaved., Khim. Khim. Tekhnol. **2011**, 54, 82.

(276) Park, J.-Y.; Hirata, Y.; Hamada, K. Color. Technol. **2012**, 128, 184.

(277) Jocic, D.; Vílchez, S.; Topalovic, T.; Navarro, A.; Jovancic, P.; Julià, M. R.; Erra, P. Carbohyd. Polym. **2005**, 60, 51.

(278) de Deus, J. F.; Cirpan, A.; Karasz, F.; Akcelrud, L. Curr. App. Phys. **2010**, 10, 365.

(279) Paul, S.; Panda, A. K. Colloids Surfaces A **2012**, 404, 1.

(280) Anderson, L. J. E.; Mayer, K. M.; Fraleigh, R. D.; Yang, Y.; Lee, S.; Hafner, J. H. J. Phys. Chem. C **2009**, 114, 11127.

(281) Schlachter, I.; Höweler, U.; Iwanek, W.; Urbaniak, M.; Mattay, J. Tetrahedron **1999**, 55, 14931.

(282) Liu, X.; Gu, Y.; Huang, J. Chem. A **2010**, 16, 7730.

(283) Paul, S.; Panda, A. J. Surfact. Deterg. **2011**, 14, 473.

(284) Aaron, J. J.; Maafi, M.; Kersebet, C.; PÃ¡rkÃ¡nyi, C.; Antonious, M. S.; Motohashi, N. J. Photochem. Photobiol. A **1996**, 101, 127.

(285) Caselli, M.; Daniele, V.; Mangone, A.; Paolillo, P. J. Colloid Interf. Sci. **2000**, 221, 173.

(286) Viswanathan, K. Colloids Surfaces A **2011**, 386, 11.

(287) Vinod, K.; Varghese, N.; Roy, S. B.; Syamaprasad, U. Supercond. Sci. Technol. **2009**, 22, 1.

(288) Guo, S.; Hailstone, R. K. J. Imaging Sci. Technol. **1996**, 40, 210.

(289) Caruso, R. A.; Susha, A.; Caruso, F. Chem. Mater. **2001**, 13, 400.

(290) Vasconcelos, J. F.; Teixeira, M. M.; Barbosa-Filho, J. M.; Agra, M. F.; Nunes, X. P.; Giulietti, A. M.; Ribeiro-dos-Santos, R.; Soares, M. B. P. Eur. J. Pharmacol. **2009**, 609, 126.

(291) Ramesh, B.; Pugalendi, K. V. J. Med. Food **2006**, 9, 562.

(292) Hoult, J.; Paya, M. Gen. Pharmacol. **1996**, 27, 713.

(293) Giese, A. C.; Christensen, E.; Jeppson, J. J. Amer. Pharm. Assoc. **1950**, 39, 30.

(294) Paulsen, E.; Otkjær, A.; Andersen, K. E. Cont.Dermat. **2010**, 62, 338.

(295) Berret, J. F.; Cristobal, G.; Herve, P.; Oberdisse, J.; Grillo, I. Eur.Phys. J. E **2002**, 9, 301.

(296) Akbas, H.; Kartal, C. Dyes Pigments **2007**, 72, 383.

(297) Colombano, C. G.; Troccoli, O. E. Anal. Chem.**1985**, 57, 1907.

(298) Banerjee, S.; Datta, A. Langmuir **2009**, 26, 1172.

(299) Glinka, Y. D.; Lin, S.-H.; Chen, Y.-T. Appl. Phys. Lett. **1999**, 75, 778.

(300) Geng, Q.; Cui, W. Ind. Eng. Chem. Res. **2010**, 49, 11321.

(301) Aaron, J. J.; Buna, M.; Parkanyi, C.; Antonious, M. S.; Tine, A.; Cisse, L. J. Fluores. **1995**, 5, 337.

(302) McDonagh, C.; Stranik, O.; Nooney, R.; MacCraith, B. D. Nanomedicine-UK **2009**, 4, 645.

(303) Herz, E.; Burns, A.; Bonner, D.; Wiesner, U. Macromol. Rapid Comm. **2009**, 30, 1907.

(304) Pawley, e.; B., J. Handbook of biological confocal microscopy; Third ed.; Springer: New York, NY, 2006.

(305) Sirotkin, V. A.; Solomonov, B. N.; Faizullin, D. A.; Fedotov, V. D. J. Struct.Chem. **2000**, 41, 997.

(306) Wang, J.; Wen, F. Y.; Zhang, Z. H.; Zhang, X. D.; Pan, Z. J.; Zhang, G.; Zhao, G.; Kang, P. L.; Zhang, P. Huanjing Kexue/Environ. Sci. **2006**, 27, 1133.

(307) Jinlian, H.; Woong, L.; Weiping, C.; Liuniu, T.; Haibo, Z. Nanotechnol. **2007**, 18, 185710.

(308) Hosseinzadeh, R.; Maleki, R.; Matin, A. A.; Nikkhahi, Y. Spectrochim. Acta A **2008**, 69, 1183.

(309) Serpone, N.; Khairutdinov, R. F.; Prashant, V. K. a. D. M. Stud. Surface Sci. Catal. **1997**, 103, 417.

(310) Grieve, K.; Mulvaney, P.; Grieser, F. Curr.Opin. Colloid Interf. Sci. **2000**, 5, 168.

(311) Snezhko, A.; Prozorov, T.; Prozorov, R. Phys. Rev. B **2005**, 71, 024527.

(312) Ramírez-Ortiz, J.; Ogura, T.; Medina-Valtierra, J.; Acosta-Ortiz, S. E.; Bosch, P.; Antonio de los Reyes, J.; Lara, V. H. App. Surface Sci. **2001**, 174, 177.

(313) Vinod, K.; Varghese, N.; Syamaprasad, U.; Shipra; Sundaresan, A. Supercond. Sci. Technol. **2008**, 21, 1.

(314) Kruis, F. E.; Fissan, H.; Peled, A. J. Aerosol Sci. **1998**, 29, 511.

(315) Bhattacharya, S.; Lelong, G.; Saboungi, M.-L. J. Exp. Nanosci. **2006**, 1, 375.

(316) Tanabe, K. Mater. Lett. **2007**, 61, 4573.

(317) Muller, J.; Sonnichsen, C.; von Poschinger, H.; von Plessen, G.; Klar, T. A.; Feldmann, J. App. Phys. Letters **2002**, 81, 171.

(318) Allen, N. S. E., MicheleSandoval, GonzaloVerran, JoStratton, JohnMaltby, Julie Photochem. Photobiol. **2005**, 81, 279.

(319) Lanz, M.; Schürch, D.; Calzaferri, G. J. Photochem.Photobiol. A **1999**, 120, 105.

(320) Halford, B. Chem. Eng. News **2006**, 84, 8.

(321) Oloffs, A.; Grosse-Siestrup, C.; Bisson, S.; Rinck, M.; Rudolph, R.; Gross, U. Biomaterials **1994**, 15, 753.

(322) Rao, C. N. R.; Muller, A.; Cheetham, A. K. Nanomaterials Chemistry: Recent Developments and New Directions; Wiley-VCH, 2007.

(323) Rogez, J.; Garnier, A.; Knauth, P. J. Phys. Chem. Solid **2002**, 63, 9.

(324) Calandra, P.; Longo, A.; Marciano, V.; Turco Liveri, V. J. Phys. Chem. B **2003**, 107, 6724.

(325) Pfanner, K.; Gfeller, N.; Calzaferri, G. J. Photochem.Photobiol. A **1996**, 95, 175.

(326) Yamashita, Y.; Aoyama, N.; Takezawa, N.; Yoshida, K. Environ.Sci. Technol. **2000**, 34, 5211.

(327) Proudfoot, C. N. Hand book of Photographic Science and Engineering; second Ed. IS &T ed., 1997.

(328) Bhowmik, B. B.; Sil, A.; Basu, S.; Moulik, S. P. J. Surface Sci. Technol. **2001**, 17, 169.

(329) Nikoobakht, B.; El-Sayed, M. A. Langmuir **2001**, 17, 6368.

(330) Gazzaz, H. A.; Robinson, B. H. Langmuir **2000**, 16, 8685.

(331) Chen, C. C.; Lu, C. S.; Chung, Y. C.; Jan, J. L. J. Hazard. Mater.**2007**, 141, 520.

(332) Kuai, L.; Geng, B.; Chen, X.; Zhao, Y.; Luo, Y. Langmuir **2010**, 26, 18723.

(333) Chattopadhyay, A.; Mukherjee, S.; Raghuraman, H. J.Phys.Chem. B **2002**, 106, 13002.

(334) Kreke, P. J.; Magid, L. J.; Gee, J. C. Langmuir **1996**, 12, 699.

(335) Terrill, R. H.; Postlethwaite, T. A.; Chen, C.-h.; Poon, C.-D.; Terzis, A.; Chen, A.; Hutchison, J. E.; Clark, M. R.; Wignall, G. J. Amer.Chem. Soc. **1995**, 117, 12537.

(336) Ríos, H. E.; Sepúlveda, L. N.; Gamboa, C. I. J. Polym. Sci. B **1990**, 28, 505.

(337) Almgren, M.; Rydholm, R. J. Phys.Chem. **1979**, 83, 360.

(338) Brice, B. A. Phys. Rev. **1931**, 38, 658.

(339) Gaikwad, P.; Rao, B. S. M. J. Indian Chem. Soci. **2010**, 87, 159.

(340) Madelung, O. Semiconductors: data handbook; Springer, 2004.

(341) Fosse, N.; Brohan, L. J. Solid State Chem. **1999**, 145, 655.

(342) De, S.; Girigoswami, A. J. Colloid Interf. Sci. **2004**, 271, 485.

BASIC DATA

BASIC DATA

OF

CHAPTER 1

Table 1. Absorbance of EY in water and in presence of different solvents at 298 K.

λ / nm	**Abs. of EY in water at different concentrations (in μM)**					**Abs. of 10 *μM EY in different solvents***						
	2	**6**	**10**	**14**	**18**	**Water**	**MeOH**	**EtOH**	**PrOH**	**DMF**	**DMSO**	**ButOH**	**PentOH**
425	0.005	0.011	0.018	0.024	0.027	0.018	0.018	0.015	0.013	0.008	0.015	0.002	0.000
435	0.006	0.014	0.024	0.032	0.036	0.024	0.021	0.016	0.013	0.008	0.016	0.004	0.000
445	0.009	0.024	0.040	0.054	0.061	0.040	0.032	0.024	0.019	0.013	0.021	0.010	0.000
455	0.014	0.039	0.065	0.090	0.102	0.065	0.055	0.044	0.037	0.024	0.030	0.026	0.014
465	0.023	0.066	0.110	0.153	0.173	0.110	0.083	0.073	0.066	0.044	0.045	0.052	0.036
475	0.042	0.121	0.202	0.281	0.320	0.202	0.150	0.119	0.105	0.068	0.063	0.087	0.064
485	0.061	0.177	0.295	0.411	0.467	0.295	0.261	0.225	0.207	0.127	0.103	0.171	0.129
495	0.076	0.221	0.369	0.516	0.586	0.369	0.318	0.334	0.332	0.240	0.173	0.269	0.207
505	0.121	0.356	0.593	0.828	0.940	0.593	0.427	0.388	0.378	0.299	0.195	0.308	0.236
515	0.177	0.521	0.867	1.211	1.373	0.867	0.756	0.603	0.553	0.350	0.237	0.461	0.352
525	0.140	0.411	0.683	0.956	1.084	0.683	0.937	0.980	1.002	0.628	0.432	0.817	0.634
535	0.052	0.147	0.243	0.339	0.383	0.243	0.528	0.969	1.136	0.992	0.642	0.891	0.705
545	0.013	0.030	0.049	0.068	0.076	0.049	0.145	0.445	0.617	0.842	0.421	0.454	0.359
555	0.005	0.006	0.008	0.010	0.010	0.008	0.028	0.106	0.165	0.306	0.124	0.119	0.095
565	0.003	0.001	0.001	0.000	0.001	0.001	0.005	0.018	0.031	0.068	0.025	0.023	0.018
575	0.003	0.001	0.001	0.002	0.001	0.001	0.001	0.002	0.005	0.013	0.005	0.004	0.002

Table 2. Absorbance of 10μM EY in presence of different surfactants in aqueous media at 298K.

λ / nm	CTAB						CPC					DDAB				
	[S]/ μM =0	5	10	20	35	80	0	4	10	25	30	0	2	20	25	40
425	0.026	0.027	0.018	0.015	0.012	0.012	0.021	0.028	0.027	0.028	0.002	0.026	0.036	0.064	0.046	0.034
435	0.031	0.032	0.022	0.017	0.013	0.013	0.026	0.028	0.027	0.024	0.001	0.032	0.034	0.057	0.043	0.033
445	0.048	0.046	0.034	0.026	0.020	0.020	0.043	0.033	0.031	0.024	0.005	0.048	0.039	0.049	0.042	0.037
455	0.075	0.070	0.055	0.045	0.038	0.038	0.069	0.045	0.042	0.032	0.018	0.074	0.053	0.046	0.049	0.050
465	0.122	0.111	0.091	0.075	0.064	0.065	0.115	0.071	0.063	0.049	0.041	0.120	0.081	0.052	0.064	0.073
475	0.219	0.197	0.165	0.129	0.108	0.109	0.210	0.123	0.108	0.074	0.073	0.214	0.131	0.065	0.086	0.103
485	0.318	0.283	0.245	0.213	0.198	0.206	0.306	0.180	0.157	0.129	0.144	0.309	0.192	0.100	0.140	0.178
495	0.397	0.355	0.317	0.306	0.306	0.320	0.383	0.235	0.206	0.210	0.249	0.385	0.269	0.151	0.226	0.295
505	0.634	0.565	0.494	0.417	0.373	0.383	0.616	0.361	0.315	0.265	0.314	0.614	0.395	0.180	0.273	0.353
515	0.925	0.817	0.708	0.583	0.530	0.560	0.902	0.499	0.432	0.314	0.408	0.896	0.505	0.201	0.315	0.424
525	0.732	0.645	0.590	0.630	0.695	0.763	0.709	0.411	0.358	0.423	0.592	0.711	0.460	0.268	0.447	0.621
535	0.262	0.242	0.271	0.469	0.613	0.677	0.249	0.204	0.183	0.485	0.628	0.255	0.349	0.323	0.536	0.713
545	0.056	0.065	0.109	0.249	0.331	0.351	0.049	0.114	0.107	0.435	0.441	0.055	0.317	0.315	0.486	0.557
555	0.012	0.023	0.051	0.087	0.101	0.099	0.007	0.090	0.084	0.297	0.189	0.011	0.311	0.236	0.303	0.261
565	0.005	0.013	0.024	0.026	0.023	0.020	0.000	0.074	0.067	0.158	0.063	0.004	0.252	0.151	0.155	0.093
575	0.003	0.009	0.014	0.010	0.007	0.004	0.000	0.058	0.051	0.090	0.026	0.002	0.148	0.112	0.099	0.047

Table 3. Fluorescence intensity of EY in water and in presence of different solvents at 298K.

λ / nm	**F.I. (a.u.) of EY in water at different concentrations (*in μM*)**					**F.I.(a.u) of 10 *μM EY in different solvents***							
	2	**6**	**10**	**14**	**18**	**Water**	**MeOH**	**EtOH**	**PrOH**	**DMF**	**DMSO**	**ButOH**	**PentOH**
500	0.286	0.229	0.193	0.245	0.308	0.360	0.327	0.169	0.048	0.048	0.080	0.073	0.068
510	1.283	1.001	0.811	0.909	1.387	0.815	0.784	0.433	0.097	0.101	0.189	0.173	0.163
520	4.695	4.175	3.691	2.557	4.517	3.492	3.529	2.171	0.485	0.599	1.111	1.036	0.962
530	9.848	9.876	9.543	4.343	8.486	9.204	11.694	7.150	1.997	2.383	4.619	4.032	3.937
540	12.760	13.775	14.086	4.795	10.146	10.966	19.174	15.534	8.298	7.180	13.793	11.040	10.875
550	11.312	12.829	13.574	3.844	8.574	8.473	17.930	18.225	19.021	16.265	19.072	16.564	15.470
560	8.061	9.330	9.969	2.628	5.987	5.801	13.329	14.939	19.951	18.778	16.499	15.024	13.623
570	5.672	6.556	7.039	1.815	4.192	4.271	9.650	10.808	15.563	15.645	11.939	10.957	9.770
580	4.152	4.807	5.177	1.316	3.052	3.284	7.611	8.122	11.251	11.484	8.578	7.781	6.934
590	3.004	3.507	3.750	0.953	2.196	2.377	5.913	6.399	8.811	8.613	6.719	6.003	5.341
600	2.026	2.366	2.544	0.641	1.488	1.572	4.085	4.680	6.958	6.782	5.043	4.560	4.032
610	1.293	1.522	1.633	0.409	0.954	0.986	2.590	3.105	4.981	5.055	3.403	3.165	2.760
620	0.836	0.974	1.041	0.263	0.613	0.635	1.621	1.961	3.287	3.433	2.123	2.047	1.762
630	0.549	0.638	0.686	0.174	0.402	0.429	1.058	1.239	2.067	2.210	1.313	1.277	1.103
640	0.370	0.428	0.462	0.118	0.272	0.293	0.722	0.819	1.329	1.388	0.842	0.814	0.703
650	0.250	0.288	0.312	0.080	0.185	0.198	0.487	0.555	0.886	0.905	0.554	0.544	0.475

λ_{ex} = 500 nm.

Table 4. Fluorescence intensity of 10μM EY in presence of different surfactants in aqueous media at 298K.

λ / *nm*	CTAB				CPC						DDAB			
	[S]/ μM = 0	**0.01**	**0.02**	**5.00**	**0**	**0.01**	**0.02**	**0.03**	**1.00**	**3.00**	**0**	**0.002**	**0.20**	**0.40**
502	0.229	0.315	0.159	0.100	0.218	2.920	2.060	0.783	0.061	0.097	0.229	0.448	0.153	0.100
510	0.829	0.848	0.386	0.324	0.794	0.717	0.267	0.064	0.104	0.021	0.827	0.857	0.125	0.172
520	3.630	3.349	1.265	1.665	3.443	2.688	0.830	0.163	0.591	1.202	3.625	3.677	0.760	0.970
530	9.700	7.215	2.255	6.538	9.689	5.065	1.272	0.241	2.585	4.987	10.066	9.398	3.110	3.983
540	11.746	7.925	2.551	14.848	11.967	5.050	1.194	0.301	7.855	13.417	12.277	10.961	7.653	10.694
550	9.113	6.074	2.223	16.772	9.358	3.672	0.941	0.375	10.967	16.724	9.537	8.347	9.909	13.917
560	6.275	4.195	1.660	13.487	6.417	2.545	0.765	0.339	8.993	13.646	6.504	5.679	8.234	11.643
570	4.575	3.103	1.219	9.660	4.689	1.959	0.599	0.246	6.154	9.569	4.721	4.193	5.649	8.212
580	3.531	2.394	0.916	7.209	3.621	1.509	0.459	0.168	4.335	6.964	3.655	3.267	4.054	5.949
590	2.553	1.698	0.648	5.562	2.600	1.073	0.323	0.120	3.310	5.399	2.628	2.333	3.115	4.618
600	1.680	1.112	0.427	4.023	1.708	0.699	0.212	0.086	2.441	3.963	1.730	1.529	2.291	3.403
610	1.053	0.697	0.273	2.671	1.075	0.445	0.135	0.060	1.620	2.623	1.094	0.962	1.517	2.281
620	0.677	0.450	0.179	1.705	0.694	0.289	0.090	0.039	1.021	1.642	0.700	0.621	0.948	1.443
630	0.455	0.304	0.121	1.082	0.463	0.195	0.061	0.028	0.636	1.026	0.467	0.417	0.599	0.909
640	0.311	0.208	0.084	0.716	0.317	0.133	0.043	0.020	0.415	0.669	0.319	0.286	0.392	0.604
650	0.208	0.138	0.058	0.485	0.212	0.088	0.030	0.015	0.279	0.451	0.213	0.189	0.267	0.404

λ_{ex} = 500 nm.

BASIC DATA
OF
CHAPTER 2

Table 1. Absorbance of 10μM EY in presence of polymers at different polymer / dye ([P] / [D]) molar ratio at 298K.

λ / nm	**Absorbance**												
	PDMDAAC					**LM200**				**JR400**			
	[P]/[D]=0	**0.2**	**0.4**	**0.7**	**0.9**	**0.4**	**1.1**	**1.4**	**1.8**	**0.4**	**1.1**	**1.4**	**1.8**
425	0.042	0.041	0.038	0.036	0.033	0.041	0.019	0.010	0.006	0.056	0.045	0.036	0.031
435	0.047	0.045	0.041	0.039	0.035	0.047	0.024	0.016	0.010	0.061	0.049	0.041	0.036
445	0.063	0.059	0.053	0.049	0.044	0.062	0.038	0.029	0.023	0.076	0.064	0.055	0.049
455	0.088	0.081	0.074	0.069	0.062	0.084	0.060	0.051	0.045	0.100	0.088	0.078	0.071
465	0.132	0.121	0.111	0.103	0.094	0.126	0.100	0.090	0.083	0.144	0.130	0.120	0.112
475	0.223	0.2	0.182	0.165	0.149	0.206	0.178	0.165	0.156	0.230	0.214	0.201	0.192
485	0.314	0.289	0.271	0.256	0.239	0.281	0.251	0.238	0.229	0.312	0.296	0.281	0.270
495	0.388	0.369	0.358	0.349	0.337	0.355	0.323	0.310	0.301	0.389	0.371	0.355	0.343
505	0.603	0.544	0.5	0.458	0.418	0.555	0.515	0.494	0.480	0.602	0.578	0.555	0.535
515	0.861	0.751	0.663	0.579	0.504	0.765	0.717	0.692	0.672	0.830	0.803	0.773	0.747
525	0.696	0.628	0.578	0.531	0.488	0.579	0.545	0.533	0.526	0.635	0.615	0.595	0.579
535	0.253	0.272	0.292	0.309	0.323	0.198	0.199	0.205	0.213	0.224	0.224	0.223	0.222
545	0.056	0.098	0.135	0.167	0.193	0.045	0.048	0.053	0.058	0.058	0.058	0.060	0.060
555	0.011	0.036	0.057	0.076	0.091	0.007	0.005	0.007	0.008	0.019	0.019	0.019	0.019
565	0.003	0.012	0.018	0.024	0.028	0.006	0.005	0.003	0.002	0.011	0.010	0.010	0.010
575	1E-3	0.004	0.005	0.006	0.007	0.002	0.002	0.001	0.001	0.009	0.009	0.009	0.008

Table 2. Absorbance of 10μM EY in presence of polymers at higher polymer / dye ([P] / [D]) molar ratio at 298K.

λ / nm	Absorbance															
	PDMDAAC						LM200					JR400				
	[P]/[D]=0	2	4	6	8	10	2	4	6	8	10	2	4	6	8	10
425	0.014	0.010	0.013	0.025	0.017	0.018	0.012	0.011	0.011	0.01	0.009	0.002	0.005	0.009	0.037	0.010
435	0.020	0.014	0.017	0.028	0.020	0.021	0.016	0.014	0.014	0.012	0.011	0.003	0	0.003	0.041	0.005
445	0.036	0.021	0.025	0.036	0.028	0.030	0.029	0.026	0.023	0.021	0.019	0.018	0.014	0.009	0.053	0.007
455	0.060	0.042	0.045	0.055	0.049	0.051	0.05	0.047	0.042	0.039	0.037	0.043	0.039	0.033	0.075	0.030
465	0.104	0.076	0.080	0.087	0.080	0.082	0.088	0.082	0.073	0.069	0.066	0.086	0.079	0.071	0.110	0.065
475	0.190	0.127	0.130	0.141	0.135	0.138	0.162	0.151	0.131	0.123	0.118	0.168	0.154	0.142	0.175	0.131
485	0.278	0.238	0.237	0.249	0.239	0.241	0.246	0.231	0.208	0.199	0.196	0.256	0.246	0.235	0.266	0.226
495	0.348	0.370	0.372	0.376	0.355	0.353	0.321	0.307	0.288	0.282	0.282	0.341	0.334	0.325	0.352	0.315
505	0.551	0.394	0.411	0.435	0.428	0.432	0.497	0.468	0.416	0.399	0.39	0.525	0.486	0.450	0.459	0.419
515	0.811	0.428	0.481	0.557	0.582	0.600	0.722	0.678	0.598	0.57	0.557	0.741	0.689	0.645	0.642	0.609
525	0.657	0.484	0.548	0.633	0.662	0.682	0.624	0.605	0.592	0.591	0.604	0.585	0.585	0.584	0.617	0.594
535	0.247	0.413	0.428	0.445	0.440	0.445	0.285	0.299	0.355	0.381	0.412	0.239	0.269	0.293	0.319	0.320
545	0.060	0.276	0.252	0.223	0.196	0.192	0.091	0.106	0.15	0.169	0.189	0.063	0.079	0.091	0.112	0.104
555	0.014	0.129	0.106	0.084	0.068	0.065	0.018	0.023	0.037	0.043	0.048	0.011	0.016	0.019	0.035	0.023
565	0.003	0.038	0.032	0.026	0.019	0.020	0.003	0.001	0.002	0.003	0.003	0	0	0	0.014	0.001
575	0.000	0.011	0.010	0.009	0.005	0.006	0.007	0.006	0.005	0.005	0.006	0.003	0.003	0.002	0.002	0.001

Table 3. Absorbance of 10μM EY in aqueous polymer solution at different temperature recorded at 517 nm.

Polymers	$C_S x 10^5 M$	Absorbance at different temp.(K) at 517 nm				
		303	308	313	318	323
PDAC	5	0.614	0.598	-	0.63	-
	6	0.636	0.624	0.618	0.631	0.619
	8	0.651	0.639	0.632	0.66	0.643
	9	0.665	0.648	0.648	0.663	0.649
	10	0.667	0.666	0.653	0.679	0.665
	11	0.677	0.667	0.665	0.685	-
	12	0.685	-	0.666	0.706	0.675
	13	0.693	-	0.67	0.71	0.685
	14	0.697	-	-	-	0.692
LM200	7	0.59	0.59	0.59	0.59	0.60
	8	0.58	0.57	0.58	0.57	0.58
	9	0.56	0.55	0.55	0.55	0.55
	10	0.54	0.54	0.54	0.53	0.53
	11	0.53	0.51	0.52	0.51	0.52
	12	0.51	0.50	0.50	0.50	0.50
	13	0.50	0.49	0.49	0.49	0.49
JR400	10	0.55	0.56	0.56	0.56	0.56
	12	0.54	0.54	0.55	0.55	0.54
	14	0.53	0.54	0.54	-	0.53
	16	0.52	0.52	0.52	0.52	0.52
	18	0.51	0.51	0.52	0.51	0.51

Table 4. Fluorescence intensity of 10μM EY in presence of polymers at different polymer / dye ([P] / [D]) molar ratio at 298K.

λ / nm	**Fluorescence intensity**												
	PDMDAAC					**LM200**				**JR400**			
	[P]/[D]=0	**0.2**	**0.4**	**0.7**	**0.9**	**0.4**	**1.1**	**1.4**	**1.8**	**0.4**	**1.1**	**1.4**	**1.8**
500	0.044	0.054	0.067	0.077	0.084	0.187	0.187	0.186	0.182	0.142	0.145	0.141	0.143
510	0.182	0.175	0.161	0.144	0.124	0.389	0.385	0.379	0.375	0.303	0.305	0.303	0.304
520	0.768	0.716	0.633	0.559	0.457	1.332	1.308	1.286	1.269	1.221	1.199	1.175	1.149
530	2.063	1.759	1.463	1.210	0.935	2.325	2.275	2.229	2.191	2.390	2.299	2.243	2.183
540	2.489	2.056	1.669	1.347	1.020	2.058	2.017	1.981	1.934	2.153	2.071	2.032	1.986
550	1.944	1.592	1.300	1.052	0.793	1.394	1.375	1.341	1.323	1.436	1.401	1.378	1.340
560	1.342	1.100	0.902	0.734	0.561	0.944	0.928	0.910	0.899	0.983	0.954	0.931	0.919
570	0.979	0.811	0.668	0.542	0.415	0.708	0.693	0.689	0.677	0.738	0.715	0.703	0.691
580	0.755	0.622	0.510	0.414	0.316	0.526	0.518	0.512	0.504	0.546	0.529	0.519	0.509
590	0.543	0.446	0.365	0.293	0.226	0.367	0.361	0.358	0.350	0.375	0.363	0.353	0.347
600	0.357	0.294	0.238	0.192	0.147	0.239	0.235	0.230	0.228	0.237	0.230	0.230	0.222
610	0.226	0.185	0.151	0.121	0.093	0.161	0.157	0.155	0.153	0.153	0.149	0.147	0.145
620	0.147	0.120	0.098	0.079	0.060	0.110	0.111	0.109	0.107	0.103	0.102	0.098	0.098
630	0.098	0.081	0.067	0.053	0.041	0.083	0.081	0.081	0.078	0.074	0.072	0.071	0.069
640	0.068	0.056	0.045	0.036	0.028	0.062	0.060	0.061	0.059	0.052	0.052	0.051	0.049
650	0.045	0.037	0.030	0.025	0.019	0.046	0.046	0.046	0.045	0.037	0.035	0.036	0.036

λ_{ex} = 500nm

Table 5. Fluorescence intensity of 10μM EY in presence of polymers at higher polymer / dye ([P] / [D]) molar ratio at 298K.

λ / nm	**Fluorescence intensity**												
	PDMDAAC					**LM200**				**JR400**			
	[P]/[D]=0	**4**	**10**	**20**	**40**	**10**	**40**	**60**	**90**	**10**	**40**	**60**	**90**
505	0.066	0.009	0.025	0.035	0.044	0.034	0.013	0.013	0.012	0.092	0.090	0.083	0.040
510	0.145	0.019	0.058	0.086	0.109	0.060	0.020	0.020	0.017	0.184	0.192	0.179	0.080
520	0.622	0.080	0.283	0.409	0.509	0.126	0.055	0.062	0.049	0.621	0.663	0.609	0.248
530	1.766	0.238	0.901	1.327	1.658	0.177	0.159	0.180	0.127	1.256	1.338	1.122	0.414
540	2.128	0.347	1.405	2.119	2.666	0.186	0.287	0.288	0.171	1.302	1.371	1.100	0.378
550	1.577	0.295	1.182	1.799	2.268	0.168	0.259	0.253	0.135	0.922	0.957	0.755	0.255
560	1.037	0.195	0.776	1.177	1.492	0.127	0.171	0.164	0.087	0.601	0.622	0.482	0.167
570	0.738	0.131	0.514	0.782	0.990	0.092	0.115	0.109	0.058	0.433	0.441	0.345	0.118
580	0.568	0.098	0.383	0.588	0.741	0.068	0.084	0.081	0.047	0.323	0.335	0.264	0.093
590	0.402	0.072	0.281	0.429	0.540	0.051	0.068	0.065	0.037	0.230	0.232	0.186	0.068
600	0.263	0.049	0.184	0.281	0.359	0.037	0.049	0.048	0.028	0.151	0.155	0.127	0.048
610	0.167	0.031	0.114	0.171	0.219	0.027	0.034	0.033	0.021	0.098	0.100	0.082	0.033
620	0.109	0.020	0.071	0.109	0.136	0.021	0.024	0.023	0.017	0.066	0.067	0.054	0.025
630	0.073	0.014	0.046	0.070	0.088	0.016	0.017	0.018	0.014	0.046	0.047	0.040	0.020
640	0.050	0.010	0.032	0.048	0.060	0.014	0.015	0.015	0.012	0.034	0.035	0.030	0.017

λ_{ex} = 500nm.

Table 6. Fluorescence anisotropy values (r) of 10μM EY at different polymer concentrations.

PDAC		**LM200**		**JR400**	
Conc. ($1E^{-5}M$)	Anisotropy(r)	Conc. ($1E^{-5}M$)	Anisotropy(r)	Conc. ($1E^{-5}M$)	Anisotropy(r)
0	0.06	0	0.06	0	0.06
1	0.08	10	0.07	10	0.12
2	0.12	20	0.04	20	0.13
4	0.15	30	0.04	30	0.13
6	0.16	40	0.04	40	0.14
8	0.16	50	0.04	50	0.15
10	0.16	60	0.06	60	0.15
20	0.16	70	0.06	70	0.14
30	0.15	80	0.06	80	0.13
40	0.16				
50	0.16				
60	0.16				
70	0.15				
80	0.16				

BASIC DATA
OF
CHAPTER 3

Table 1 A. Absorbance of 7HC in water in different concentrations at 298K.

λ /	Absorbance							
nm	**[7HC]/μM=2**	**4**	**6**	**10**	**12**	**14**	**16**	**20**
200	0.109	0.134	0.191	0.272	0.323	0.389	0.444	0.514
210	0.056	0.051	0.071	0.092	0.112	0.137	0.151	0.179
220	0.043	0.041	0.057	0.072	0.088	0.106	0.116	0.136
230	0.020	0.017	0.023	0.028	0.037	0.046	0.051	0.064
240	0.013	0.011	0.015	0.018	0.025	0.031	0.035	0.046
250	0.011	0.008	0.011	0.013	0.019	0.023	0.026	0.036
260	0.010	0.006	0.008	0.007	0.013	0.016	0.018	0.026
270	0.011	0.009	0.012	0.014	0.02	0.025	0.028	0.037
280	0.013	0.014	0.020	0.025	0.033	0.040	0.046	0.057
290	0.014	0.019	0.028	0.037	0.047	0.056	0.065	0.078
300	0.016	0.025	0.036	0.049	0.061	0.072	0.084	0.103
310	0.020	0.034	0.049	0.069	0.084	0.100	0.116	0.139
320	0.024	0.041	0.060	0.085	0.103	0.121	0.141	0.167
330	0.023	0.040	0.058	0.082	0.099	0.118	0.137	0.163
340	0.017	0.030	0.043	0.06	0.074	0.088	0.102	0.124
350	0.009	0.015	0.022	0.029	0.037	0.044	0.051	0.067
360	0.003	0.005	0.006	0.005	0.009	0.011	0.013	0.026
370	0.003	0.000	0.000	0.014	0.001	0.000	0.001	0.041
380	0.003	0.000	0.000	0.014	0.000	0.000	0.001	0.040
390	0.003	0.000	0.000	0.014	0.000	0.000	0.001	0.039
400	0.003	0.000	0.000	0.014	0.000	0.000	0.000	0.038

Table 1 B. Fluorescence intensity of 7HC in water at different concentrations at 298K.

λ /	Fluorescence intensity							
nm	**[7HC]/μM=2**	**4**	**6**	**10**	**12**	**14**	**16**	**20**
400	0.144	0.183	0.224	0.258	0.266	0.272	0.294	0.360
410	0.237	0.371	0.539	0.716	0.649	0.712	0.891	1.194
420	0.415	0.773	1.283	1.818	1.607	1.843	2.419	3.270
430	0.770	1.526	2.481	3.559	3.193	3.647	4.766	6.496
440	1.011	2.170	3.573	5.109	4.487	5.253	6.867	9.367
450	1.133	2.376	3.987	5.694	5.034	5.920	7.700	10.574
460	1.061	2.231	3.701	5.377	4.692	5.542	7.181	9.818
470	0.896	1.846	3.077	4.425	3.891	4.534	5.975	8.125
480	0.725	1.441	2.417	3.459	3.048	3.575	4.671	6.350
490	0.576	1.107	1.787	2.594	2.282	2.659	3.474	4.749
500	0.436	0.823	1.329	1.879	1.668	1.977	2.499	3.429
510	0.335	0.611	0.968	1.381	1.211	1.417	1.823	2.478
520	0.262	0.448	0.709	0.989	0.871	1.011	1.297	1.753
530	0.220	0.361	0.521	0.729	0.639	0.731	0.919	1.222
540	0.172	0.292	0.398	0.522	0.481	0.543	0.627	0.864
550	0.132	0.229	0.295	0.399	0.356	0.412	0.468	0.607
560	0.127	0.204	0.241	0.305	0.267	0.316	0.349	0.457
570	0.136	0.175	0.188	0.247	0.225	0.251	0.263	0.344
580	0.120	0.168	0.175	0.214	0.186	0.186	0.224	0.264
590	0.109	0.166	0.162	0.190	0.159	0.169	0.189	0.217
600	0.100	0.134	0.137	0.168	0.165	0.147	0.165	0.185

λ_{ex} = 375 nm.

Table 2. Absorbance of silica-7HC system with different wt.% of Silica at 298K.

λ /	Absorbance							
nm	**0**	**0.004**	**0.008**	**0.012**	**0.016**	**0.02**	**2**	**3**
200	0.469	0.448	0.398	0.359	0.333	0.296	2.391	2.919
210	0.154	0.168	0.144	0.141	0.157	0.146	2.326	2.938
220	0.112	0.123	0.103	0.100	0.110	0.103	1.855	2.559
230	0.050	0.057	0.052	0.056	0.070	0.072	1.396	1.921
240	0.038	0.042	0.038	0.043	0.056	0.058	1.104	1.506
250	0.029	0.033	0.029	0.033	0.045	0.047	0.925	1.251
260	0.020	0.024	0.019	0.023	0.034	0.036	0.710	0.946
270	0.032	0.034	0.027	0.028	0.035	0.035	0.515	0.669
280	0.051	0.050	0.040	0.038	0.041	0.039	0.369	0.471
290	0.070	0.068	0.055	0.051	0.050	0.045	0.278	0.351
300	0.091	0.085	0.071	0.062	0.058	0.051	0.213	0.266
310	0.125	0.116	0.097	0.084	0.075	0.064	0.185	0.228
320	0.150	0.138	0.116	0.099	0.088	0.074	0.179	0.213
330	0.142	0.130	0.110	0.094	0.085	0.071	0.190	0.216
340	0.103	0.095	0.079	0.069	0.066	0.057	0.210	0.227
350	0.047	0.044	0.036	0.033	0.039	0.035	0.232	0.240
360	0.010	0.010	0.007	0.008	0.020	0.020	0.242	0.244
370	0.000	0.001	0.007	0.007	0.003	0.002	0.228	0.233
380	0.001	0.000	0.008	0.010	0.005	0.005	0.192	0.200
390	0.001	0.001	0.008	0.009	0.002	0.003	0.135	0.149
400	0.000	0.000	0.007	0.008	0.000	0.000	0.083	0.102

[7HC] = 10μM.

Table 3. Fluorescence intensity (a.u.) of 2 wt. % colloidal silica in water.

λ / *nm*	F.I.	λ / *nm*	F.I.
400	0.743	510	0.226
410	0.616	520	0.179
420	0.718	530	0.144
430	0.869	540	0.124
440	0.794	550	0.105
450	0.769	560	0.089
460	0.700	570	0.079
470	0.588	580	0.071
480	0.475	590	0.062
490	0.368	600	0.053
500	0.285		

λ_{ex} = 375.

Table 4. Fluorescence intensity of silica-7HC system with different wt.% of Silica. [7HC]=10μM; λ_{ex}= 375nm.

λ /	F.I. (a.u.)													
nm	**0**	**0.004**	**0.008**	**0.012**	**0.016**	**0.02**	**2**	**3**	**4**	**5**	**6**	**7**	**8**	**9**
400	0.036	0.042	0.059	0.088	1.109	1.359	0.044	0.308	0.284	0.249	0.224	0.195	0.157	0.128
410	0.091	0.137	0.214	0.358	0.464	0.571	0.090	1.301	1.152	0.998	0.858	0.706	0.553	0.398
420	0.224	0.371	0.603	1.044	1.355	1.666	0.211	3.710	3.321	2.869	2.425	2.007	1.570	1.104
430	0.452	0.739	1.215	2.102	2.716	3.326	0.409	7.164	6.452	5.633	4.820	3.983	3.142	2.210
440	0.655	1.085	1.777	3.056	3.972	4.802	0.587	9.993	9.066	7.999	6.888	5.709	4.526	3.205
450	0.750	1.228	2.027	3.441	4.464	5.404	0.663	11.081	10.069	8.883	7.693	6.412	5.095	3.610
460	0.696	1.148	1.916	3.226	4.211	5.109	0.625	10.455	9.508	8.416	7.337	6.055	4.807	3.399
470	0.579	0.954	1.603	2.707	3.566	4.300	0.520	8.969	8.102	7.147	6.189	5.101	4.038	2.843
480	0.453	0.744	1.249	2.121	2.823	3.402	0.411	7.195	6.503	5.702	4.908	4.029	3.174	2.248
490	0.338	0.557	0.934	1.583	2.133	2.567	0.317	5.518	4.989	4.350	3.717	3.058	2.386	1.683
500	0.248	0.405	0.671	1.141	1.558	1.852	0.230	4.052	3.646	3.159	2.708	2.221	1.736	1.213
510	0.179	0.289	0.477	0.809	1.103	1.322	0.170	2.913	2.618	2.266	1.931	1.572	1.232	0.857
520	0.134	0.205	0.334	0.558	0.772	0.915	0.126	2.043	1.831	1.595	1.357	1.110	0.862	0.606
530	0.097	0.145	0.229	0.387	0.532	0.638	0.098	1.423	1.270	1.104	0.938	0.759	0.595	0.417
540	0.072	0.101	0.153	0.266	0.368	0.437	0.073	0.980	0.877	0.758	0.646	0.531	0.406	0.287
550	0.054	0.076	0.109	0.185	0.257	0.301	0.045	0.457	0.414	0.358	0.304	0.247	0.193	0.136
560	0.042	0.054	0.076	0.126	0.173	0.203	0.045	0.457	0.414	0.358	0.304	0.247	0.193	0.136
570	0.036	0.043	0.058	0.090	0.119	0.141	0.037	0.321	0.288	0.249	0.212	0.172	0.134	0.096
580	0.030	0.034	0.043	0.065	0.082	0.098	0.033	0.224	0.198	0.176	0.149	0.123	0.093	0.071
590	0.026	0.027	0.031	0.051	0.063	0.070	0.030	0.160	0.143	0.123	0.110	0.087	0.067	0.051
600	0.024	0.022	0.027	0.036	0.043	0.051	0.026	0.114	0.107	0.088	0.078	0.061	0.048	0.037

BASIC DATA
OF
CHAPTER 4

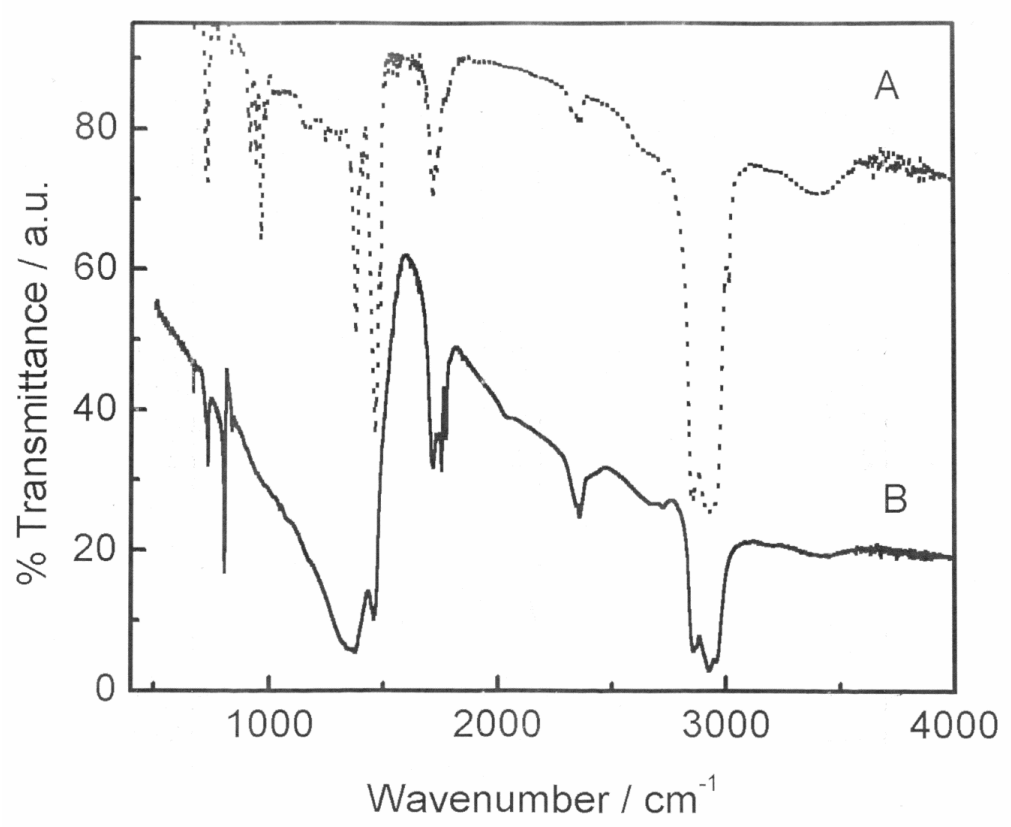

Figure 1. FTIR spectra of (A) pure CTAB and (B) aqueous extract of CTAB stabilized AgBr nanoparticles.

Table 1. Absorbance of CTAB coated AgBr nanoparticles at different AgBr concentration in aqueous medium at 298K.

λ / nm	Absorbance		
	[AgBr] / μM = 20	30	50
200	0.135	0.169	0.205
210	0.489	0.386	0.462
220	0.245	0.314	0.377
230	0.142	0.174	0.232
240	0.109	0.130	0.179
250	0.095	0.116	0.159
260	0.086	0.108	0.147
270	0.085	0.107	0.144
280	0.081	0.104	0.138
290	0.077	0.100	0.130
300	0.074	0.096	0.124
310	0.071	0.094	0.120
320	0.066	0.088	0.110
330	0.060	0.081	0.100
340	0.054	0.075	0.092
350	0.051	0.071	0.086

Table 2. Variation in the size of AgBr nanoparticles with respect to concentration.

Time / hr	d_h / nm			
	[AgBr]/μM = 10	**20**	**30**	**40**
0	56	48	56	53
6	133	154	120	119
24	168	196	172	196
30	172	189	182	208
48	189	199	185	211
52	189	201	185	206

Table 3. TGA data of pure CTAB, CTAB coated AgBr nanoparticles isolated from water, and chloroform.

Temp./°C	**Weight of CTAB coated AgBr nps in gms**		
	CTAB	**isolated from water**	**isolated from $CHCl_3$**
70	0.03	0.05	0.02
80	0.03	0.05	0.02
90	0.03	0.05	0.02
100	0.03	0.05	0.02
110	0.03	0.05	0.02
120	0.03	0.05	0.02
130	0.03	0.05	0.02
140	0.03	0.05	0.02
150	0.03	0.05	0.02
160	0.03	0.05	0.02
170	0.03	0.05	0.02
180	0.03	0.05	0.02
190	0.03	0.05	0.02
200	0.02	0.05	0.02
210	0.02	0.05	0.02
220	0.02	0.05	0.02
230	0.01	0.05	0.01
240	0.00	0.05	0.01
250	0.00	0.04	0.01
260	0.00	0.04	0.01
270	0.00	0.04	0.01
280	0.00	0.04	0.01
290	0.00	0.02	0.01
300	0.00	0.02	0.01
310	0.00	0.02	0.01
320	0.00	0.02	0.01

Table 4. The enthalpy change for the formation of AgBr nanoparticles.

[$AgNO_3$] / mM	**ΔH_f / kCalmol^{-1}**
0.06	-19.41
0.04	-17.66
0.03	-16.28
0.02	-15.45
0.015	-14.80

Table 5. Conductance of CTAB and KBr against concentration of $AgNO_3$.

[$AgNO_3$] / µM	Sp. Conductance/µS of CTAB	Sp. Conductance/µS of KBr	[$AgNO_3$] / µM	Sp. Conductance/µS of CTAB	Sp. Conductance/µS of KBr
0	42.9	89.7	1.71E-4	40.9	85.1
4.99E-6	42.9	89.7	1.83E-4	40.7	84.9
9.98E-6	42.8	89.4	1.95E-4	40.7	84.7
1.49E-5	42.8	89.1	2.06E-4	40.5	84.5
1.99E-5	42.8	88.9	2.17E-4	40.4	84.3
2.49E-5	42.8	88.6	2.29E-4	40.2	84.1
2.98E-5	42.6	88.4	2.40E-4	40.0	83.9
3.47E-5	42.6	88.2	2.52E-4	40.0	83.7
3.97E-5	42.4	88.1	2.63E-4	39.8	83.3
4.46E-5	42.4	87.9	2.74E-4	39.8	83.2
4.95E-5	42.4	87.7	2.85E-4	39.6	83.0
5.44E-5	42.4	87.3	2.96E-4	39.6	82.8
5.93E-5	42.4	87.1	3.07E-4	39.4	82.6
7.15E-5	42.2	86.9	3.18E-4	39.3	82.4
8.36E-5	42.2	86.8	3.29E-4	39.3	82.2
9.56E-5	41.9	86.4	3.40E-4	39.1	82.0
1.08E-4	41.7	86.3	3.51E-4	39.7	81.9
1.12E-4	41.7	86.1	3.62E-4	40.6	81.7
1.24E-4	41.5	85.9	3.66E-4	41.1	81.5
1.36E-4	41.5	85.7	3.70E-4	41.8	81.3
1.48E-4	41.3	85.5	3.75E-4	42.3	81.3
1.60E-4	41.1	85.3	3.79E-4	42.9	82.0

REPRINTS

Spectrochimica Acta Part A 81 (2011) 458–465

Contents lists available at ScienceDirect

Spectrochimica Acta Part A: Molecular and Biomolecular Spectroscopy

journal homepage: www.elsevier.com/locate/saa

Spectral behaviour of eosin Y in different solvents and aqueous surfactant media

Moumita Chakraborty, Amiya Kumar Panda*

Department of Chemistry, University of North Bengal, Darjeeling 734013, West Bengal, India

ARTICLE INFO

Article history:
Received 16 March 2011
Received in revised form 11 June 2011
Accepted 16 June 2011

Keywords:
Eosin Y
Cationic surfactants
Solvent polarity
Interaction constant
Stokes shift
Anisotropy

ABSTRACT

Photophysical behaviour of the anionic xanthene dye, eosin Y (EY) was investigated in solvents of different polarities as well as in the presence of aqueous cationic surfactants. From the correlation between $E_T(30)$ and Kosower Z values of EY in different solvents, subsequent parameters for EY were determined in the presence of surfactants. A red shift, both in the absorption and emission spectra of EY, was observed with decreasing solvent polarity. Dimerisation of EY was found to be dependent on solvent polarity. Cationic surfactants retarded the process of dimerisation, which were evident from the lower dimerisation constant (K_D) values, compared to that of in pure water. Dye–surfactant interaction constants were determined at different temperatures (298–318 K) and subsequently the thermodynamic parameters, viz., ΔG°, ΔH° and ΔS° were evaluated using the interaction constant values. The fluorescence spectra of EY followed the same trend as in the absorption spectra, although with lesser extents. Stokes shifts were calculated and correlated with the polarity of the medium. Fluorescence of EY was initially quenched by the cationic surfactants in their pre-micellar region, which then followed a red shift with intensity enhancement. Fluorescence quenching was found to be of Stern–Volmer type where the excited state lifetime of EY remained unchanged in different surfactant media. However, the anisotropy value of EY was changed in the post micellar region of surfactants.

1. Introduction

Surfactants have a tendency to accumulate at the air–liquid interface and thus they can change the properties of interface. In addition, because of their amphipathic structures, they can congregate to form a stabilized entity, called micelle, after the attainment of critical micelle concentration (CMC) [1]. Among the different industrial applications, surfactants are used in dye industry as they can wet [2] and help in the dispersion of dyes, especially which are poorly soluble. Examples include industrial cleaners, cosmetics, plasticizers in cements and concretes, etc. [3,4]. Thus the study of dye–surfactant interaction is important from the fundamental understanding point of view as well as industrial applications. Photophysical studies of dyes in aqueous surfactant solution are also important to understand the mimicking bio-membranous interfaces [5]. According to Bhowmik and Ganguly [6], dye molecules form 1:1 charge transfer complex with oppositely charged surfactants. Surfactants are also used as solubilizers for water insoluble dyes, as disaggregating agent for dyes, which accelerates the adsorption of dye on fibres [7]. Besides, dye–surfactant interaction studies can effectively determine the critical micelle concentration of surfactants [8,9].

Eosin Y (EY) belongs to the xanthene group of dyes and studies on the interaction of surfactant with different xanthene dyes have been performed for a substantial period of time [5,10–12]. EY is a xanthene derivative and finds many applications, viz., in solvent polarity determination [10], lasers, CMC determination [9], the characterization of super conductors, etc. [13]. EY sensitized nanoparticles can produce hydrogen by photocatalytic decomposition of water [14]. Although several studies have been made involving dye–surfactant interactions, yet this particular field of research is still important for improvised dyeing process in terms of theoretical, technological, environmental as well as economic point of view [15]. According to Göktürk and Tunçay [16], a dye molecule exhibits spectral changes in the presence of varying amount of surfactants consistently and there exist sequential equilibria between surfactant monomers, micelles, dye aggregates and pre-micellar dye–surfactant complex, etc. Solvents also play important role on the spectral and aggregation behaviour of dye molecules, which subsequently find many applications as described by De et al. [10]. Effect of solvent polarity on the aggregation behaviour of EY has been studied by De et al. [10], where a significantly high concentration of dye was used (as high as 10^{-3} M). However, practical applications, which count for economy, environmental issues and lesser usage of dye molecule, photophysical studies of EY in the dilute region, are believed to be more important. In addition to this, a systematic investigation on the photophysical behaviour of EY in a variety of solvents is also not common in literature. Photophys-

* Corresponding author. Tel.: +91 943334710; fax: +91 3532699001.
E-mail address: akpanda1@yahoo.com (A.K. Panda).

1386-1425/$ – see front matter © 2011 Elsevier B.V. All rights reserved.
doi:10.1016/j.saa.2011.06.038

ical studies of EY in the presence of different surfactants are also not very common [5,10].

The present study deals with the photophysical behaviour of EY in solvents of different polarities and cationic surfactants. The endeavour was to undertake a physico-chemical investigation on the effects of different solvents (protic and aprotic) on EY. The solvents used were water, methanol, ethanol, n-propanol, n-butanol, n-pentanol, DMF and DMSO. Also, systematic studies on the interaction between EY and different cationic surfactants were undertaken with the variation of surfactant head group, chain length, as well as the number of hydrocarbon chains. The surfactants used were hexadecyltrimethylammonium bromide, hexadecylpyridinium chloride, didodecyldimethylammonium bromide and didecyldimethylammonium bromide. As the polarity of a solvent controls the photophysical characteristics of a dye at the molecular level, hence such studies are assumed to provide information involving the solvation capacity of the dye molecules and their aggregation behaviour. These parameters could directly be estimated using the Kosower *Z* values, dielectric constants and the refractive indices of the media. Effect of solvent polarity on the self-aggregation of dye molecules can also be estimated from such studies. Dye–surfactant interaction studies are believed to shed information on the polarity of the medium (governed by added surfactants), nature and extent of interactions between dye and surfactant molecules as well as the self-aggregation behaviour of dye in the presence of the surfactants.

2. Materials and methods

2.1. Materials

The anionic xanthene dye, 2-(2,4,5,7-tetra bromo-6-oxido-3-oxo-3H-xanthen-9-yl) benzoate, disodium salt (eosin Y, EY) was a product from Sigma–Aldrich, USA. The cationic surfactants, hexadecyltrimethylammonium bromide (CTAB, Aldrich, Germany), hexadecylpyridinium chloride (CPC, SRL, India), didodecyldimethylammonium bromide (DDAB) and didecyldimethylammonium bromide (DeDAB, Fluka, Switzerland) of >99% purity were used. Solvents used, viz., methanol (MeOH), ethanol (EtOH) and n-butanol (ButOH) (SD Fine Chem. Ltd., India); n-propanol (PrOH) (SRL, India); n-pentanol (PentOH) (Lobe Chemie Pvt. Ltd. India); dimethyl formamide (DMF) and dimethyl sulphooxide (DMSO) (E. Merck, India) were of HPLC grade. A.R. grade glycerol was a product from SRL, India. Water used in this study was deionised and doubly distilled.

2.2. Methods

A stock solution of 1.0 mM EY was prepared to perform the experimental works after proper dilution as per requirement. The visible absorption spectra were recorded on a UVD-2950 spectrophotometer (Labomed Inc., USA). Spectra were recorded in the range 400–600 nm using a matched pair of quartz cuvette of 1.0 cm path length. The fluorescence spectroscopic measurements were performed using a bench-top spectrofluorimeter (Quantamaster-40, Photon Technology International Inc., NJ, USA). Fluorescence data were recorded at controlled room temperature. The excitation wavelength for EY was set at 500 nm (λ_{ex}) and the emission spectra were recorded in the range of 500–650 nm. Fluorescence anisotropy measurements were performed at an emission wavelength of 540 nm (λ_{em}^{max}). Steady state fluorescence anisotropy (r) was determined according to the expression:

$$r = \frac{I_{VV} - G.I_{VH}}{I_{VV} + 2G.I_{VH}} \quad (1)$$

where $G = I_{VV}/I_{HH}$. I_{VV} corresponds to the intensity obtained when the excitation and the emission polarizers are oriented vertically. I_{VH} is the intensity obtained for vertical excitation polarizer and horizontal emission polarizer. I_{HV} and I_{HH} refer to similar parameters as above for the horizontal positions of the excitation polarizer [17].

Fluorescence lifetime measurements of EY were recorded with the same fluorimeter where a nano LED (Photon Technology International Inc.) of 505 nm wavelength was used to excite the dye. Fluorescence decays were obtained by Ströbe technique [18].

3. Results and discussion

3.1. Absorption spectra of EY

3.1.1. Effect of dye concentration on the absorption spectra of EY

Fig. 1A describes the visible absorption spectra of aqueous EY at different concentrations (2–20 μM). The aqueous solution of EY exhibits an intense band at 517 nm with a shoulder at 496 nm. The present observation was found to be comparable with previous reports [9,10]. The band at 517 nm corresponds to the monomeric form of EY while the shoulder at 496 nm is due to the dimeric form of EY. According to De et al. [10], EY dimerizes through the stacking of two monomers (Type A), alternately known as H-aggregates. With the increasing concentration of the dye in water, intensity of both the bands increased. However, the relative enhancement in the intensity of 496 nm shoulder was found to be higher than that of the 517 nm peak. Results clearly suggest that with increasing EY concentration in water the process of dimerisation through the stacking of monomers increases. Thus the ground state population of the dimeric form increases with increase in dye concentration [19–21]. As in the present study, the maximum concentration of dye in water was 20 μM, therefore, no higher aggregates, other than the dimers were expected [10]. The absorption spectra of EY were resolved using principal component analysis method, as detailed in different publications of Estelrich et al. [20,21] and De et al. [10]. Briefly, the spectra were fitted to two overlapping Gaussian

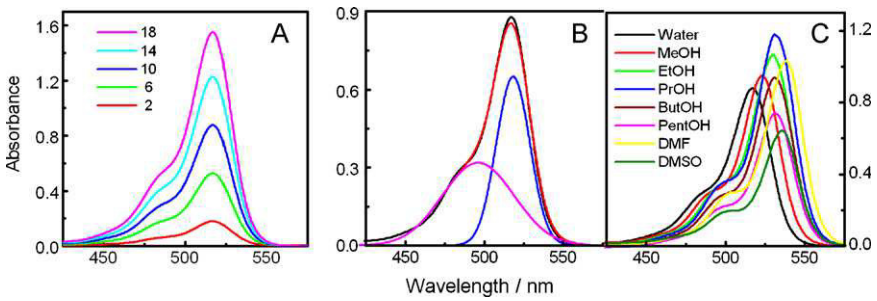

Fig. 1. (A) Absorption spectra of EY in water at different concentrations (in μM, mentioned inside the figure). (B) Resolved absorption spectra of 10 μM EY in H_2O (purple and blue), the red and black lines represent the reconstituted and original spectra of EY respectively. (C) Absorption spectra of 10 μM EY in different solvents (as mentioned in the figure). Temperature 298 K. (For interpretation of the references to color in this figure legend, the reader is referred to the web version of the article.)

curves with the help of Gaussian curve fitting, as shown in Fig. 1B. As already stated, the resolved spectra of EY in water comprise of two peaks. Therefore, it could be assumed that there exists equilibrium between the monomer (M) and the dimer (D) at a particular temperature. If we consider the following equilibrium (ignoring the existence of higher aggregates other than the dimer):

$$2M \Leftrightarrow D \tag{2}$$

then the equilibrium constant (K_D) could be expressed as:

$$K_D = \frac{C_D}{C_M^2} \tag{3}$$

where C_D and C_M stand for molar concentration of dimeric and monomeric form of EY.

Thus, the total absorbance of EY at a particular wavelength $A(\lambda)$ is contributory effect of both the monomeric and dimeric form of EY. Therefore one can make a following expression:

$$A(\lambda) = \varepsilon_M(\lambda)C_M + \varepsilon_D(\lambda)C_D \tag{4}$$

The term '$\varepsilon(\lambda)$' stands for the molar absorption co-efficient at a particular wavelength (λ). The ultimate solution for resultants of equation takes the following form as:

$$A(\lambda) = \varepsilon_D(\lambda)\left(\frac{C}{2} - \frac{-1 \pm \sqrt{1 + 8.K_D.C}}{8.K_D}\right) + \varepsilon_M(\lambda)\left(\frac{-1 \pm \sqrt{1 + 8.K_D.C}}{4.K_D}\right) \tag{5}$$

K_D can suitably be determined by iterative method as described by Estelrich et al. [20]. If one plots the molar absorbance, $A(\lambda)$, as a function of dye concentration (C) at any wavelength, one can determine the molar absorptivity of monomer, ε_M (λ), dimer, ε_D (λ) and the dimerisation constant, K_D. The non-linear least square regression analysis of the above equation was done using Microsoft Excel (Solver)^{TM} program. Initially, some hypothetical value of $\varepsilon_M(\lambda)$ and $\varepsilon_D(\lambda)$ were provided to the solver. The molar absorptivity of the lowest concentration of the dye was approximated for the monomeric form while that of the dimeric form was considered as highest concentration. The iterative method of using MS Excel (Solver)^{TM} minimises all the values and hence K_D can be determined. K_D value of aqueous EY in the studied concentration range (2–20 μM) was found to be 9.7×10^4 M^{-1}. The present result for the K_D value was found to be higher than that reported by De et al. [10] (3.0×10^4 M^{-1}). In their study, the concentration range of EY was much higher than the present concentration range, where the probability of higher aggregate formation was less than the reported systems of De et al. [10].

3.1.2. Effect of solvent polarity

Solvent polarity plays a great role on the spectral behaviour of a dye molecule. Therefore, by suitably analysing the spectral behaviour of a dye molecule, a solvent can be characterized in terms of its polarity and solvation power. Spectra of EY were recorded in a number of solvents of different polarities. Two categories of solvents were used, viz., protic (water, methanol, ethanol, n-propanol, n-butanol and n-pentanol) and aprotic (DMF and DMSO). It may be mentioned that due to its ionic nature, EY was insoluble in solvents like n-alkanes, cyclo-alkanes, chloroform, carbon tetrachloride, etc. The absorption maximum (λ_{max}^{abs}) of EY was shifted to higher wavelength (red shift) with the decrease in solvent polarity. The λ_{max}^{abs} for EY followed the order: water < methanol < ethanol < n-propanol ≈ n-butanol ≈ n-pentanol < DMSO < DMF. Spectra of EY in different solvents have also been shown in Fig. 1C.

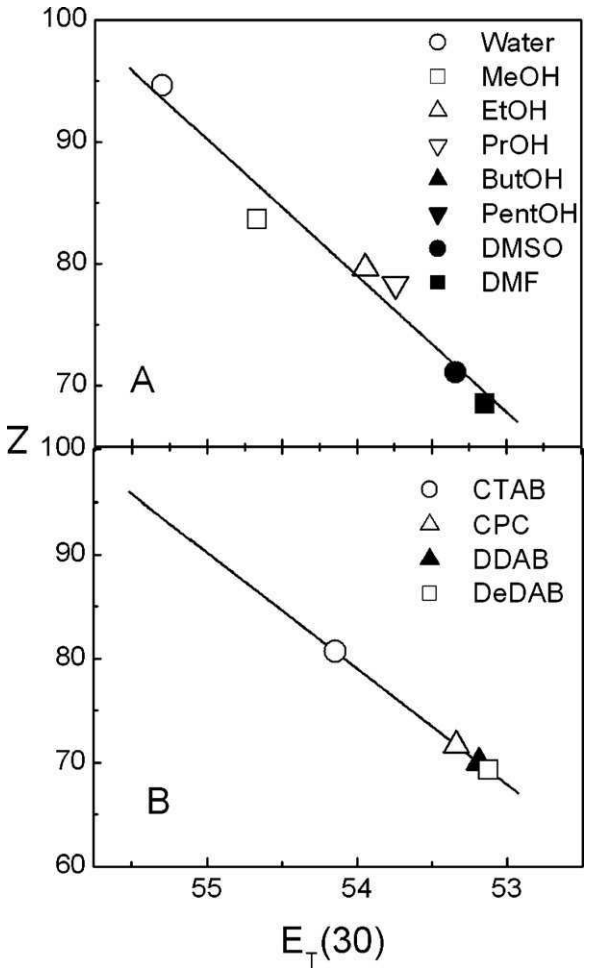

Fig. 2. Kosower Z vs. $E_T(30)$ profile for 10 μM EY in (A) solvents of different polarities and (B) surfactants at 298 K. Solvents and surfactants are mentioned inside the figure.

The solvent polarity parameter, $E_T(30)$, of EY was evaluated using the following formula [23,24]:

$$E_T(30) = \frac{28591}{\lambda_{max}^{abs}} \tag{6}$$

Another parameter called Kosower Z value is also used as standard of solvent polarity [25], which are readily available in the literature. It was found that the Kosower Z value decreases linearly with the decrease in solvent polarity as shown in Fig. 2A. $E_T(30)$ values of EY in the presence of different surfactants were also calculated using Eq. (6) (spectral behaviour of EY in the presence of surfactants will be discussed later). A good linear co-relation between the Kosower Z and $E_T(30)$ values for EY and different surfactants were also observed as shown in Fig. 2B. Table 1 summarises the results of the spectral analyses of EY in different solvents and aqueous surfactant solutions.

While considering the process of dimerisation (the method of K_D determination has previously been described in detail), it was found that the K_D value decreased with the decrease in solvent polarity. This was as predicted. It is expected that with the decrease in solvent polarity the process of dimerisation (formation of H-aggregates) will be hindered. As surfactant in water also lead to the decrease in polarity, hence the K_D value of EY in surfactant medium should decrease compared to the K_D value in pure water. Besides, Coulombic interaction of EY with oppositely charged surfactant retards the process of dimerisation. Analysis of Table 1 reveals that the dimerisation constant of EY was almost the same in water and

Table 1
Spectral parameters of EY in the presence of different solvents and surfactants at 298 K.

Solvent/system	$E_T(30)$	Z	$K_D \times 10^4/M^{-1}$	$\bar{\nu}_a/cm^{-1}$	$\bar{\nu}_f/cm^{-1}$	$\Delta\bar{\nu}/cm^{-1}$
Water	55.3	94.6	9.7	19342.4	18518.5	823.9
MeOH	54.7	83.6	9.8	19120.5	18416.2	704.3
EtOH	53.9	79.6	9.1	18867.9	18248.2	619.7
PrOH	53.7	78.3	7.1	18797.0	18018.0	779.0
ButOH	53.7	77.7	6.8	18797.0	18115.9	681.1
PentOH	53.7	77.6	5.5	18797.0	18115.9	681.1
DMSO	53.3	71.1	7.5	18656.7	17921.2	735.5
DMF	53.1	68.5	5.5	18587.4	18148.8	438.6
CTAB (15)	54.1	80.7	7.9	18939.4	18248.2	691.2
CPC (15)	53.8	77.3	6.1	18832.4	18214.9	617.5
DDAB (0.03)	53.3	71.7		18656.7	18115.9	540.8
DeDAB (0.2)	53.1	69.4		18587.4	18115.9	471.4

Parentheted values indicate the surfactant concentration in mM. 10 μM EY was used for study.

methanol. Protic solvents favoured the process of dimerisation than the aprotic solvents. The trend leads to the conclusion that the dielectric constant of the medium plays an important role in dye aggregation. Thus, hydrophobic interaction of dye molecules will be strong enough to overcome the electrostatic repulsion between the anions. Also, the –OH group present in water and alcohols promote aggregation, as hydrogen bonding plays an important role which is revealed by near similarity of K_D values for water, methanol and ethanol.

3.1.3. Effect of surfactants

Fig. 3 describes the effect of the surfactants (CTAB, CPC and DDAB) on the absorption spectra of 10 μM EY in water. The intensity of EY absorption decreased and subsequently the absorption maximum of EY was also shifted to higher wavelengths with the progressive addition of cationic surfactants. After a certain concentration of the surfactant was attained, there was no shift in the peak position (except didodecyldimethylammonium bromide). However, there was increase in the absorbance value which eventually attained maximum. Such spectral shift in the presence of surfactants is not uncommon [5,10] in the presence of CTAB, CPC and DDAB, the absorption maxima were red shifted to 528, 531 and 536 nm respectively (for pure EY in water the value was at 517 nm), indicating electrostatic interaction between EY and oppositely charged cationic surfactants [6,22]. Between CTAB and CPC, CPC exhibited stronger interaction with EY, as it required lesser amount to cause significant spectral change. Both CPC and CTAB have similar hydrocarbon chain length, but the hydrophilic–lipophilic balance (HLB) value of CPC being higher [26,27], its hydrophilic interaction (which was prevalently electrostatic in nature) with the dye is higher. A surfactant having higher HLB value implies its stronger affinity towards water and vice versa. Besides, the presence of a planar pyridinium ring favours better stacking of the dye with CPC. A significant spectral change was also observed in case of the doubled tailed surfactant, DDAB. In fact, the hydrophobic interaction is definitely higher in case of DDAB compared to the other single tailed surfactants. Also, vesicle formation could play some role in this case [28–30]. Similar were the observations for DeDAB (spectra not shown). The spectral data with a fixed concentration of EY and varying concentrations of the cationic surfactants (CTAB, CPC, DDAB and DeDAB) have been utilized to calculate the binding constant (K_b) of the dye with the surfactants using Rose and Drago's absolute method [31]:

$$\frac{(C_D.C_S)}{(A-A_0)} = \frac{1}{[K_b.L(\varepsilon_{DS}-\varepsilon_D)]} + \frac{C_S}{[L(\varepsilon_{DS}-\varepsilon_D)]} \quad (7)$$

where C_D is the initial concentration of the dye, C_S is the initial concentration of the surfactant, A_0 is the absorbance of the pure dye solution at λ_{max}^{abs}, A is the absorbance of the dye–surfactant solution at λ_{max}^{abs}, K_b is the binding constant of the dye with surfactant,

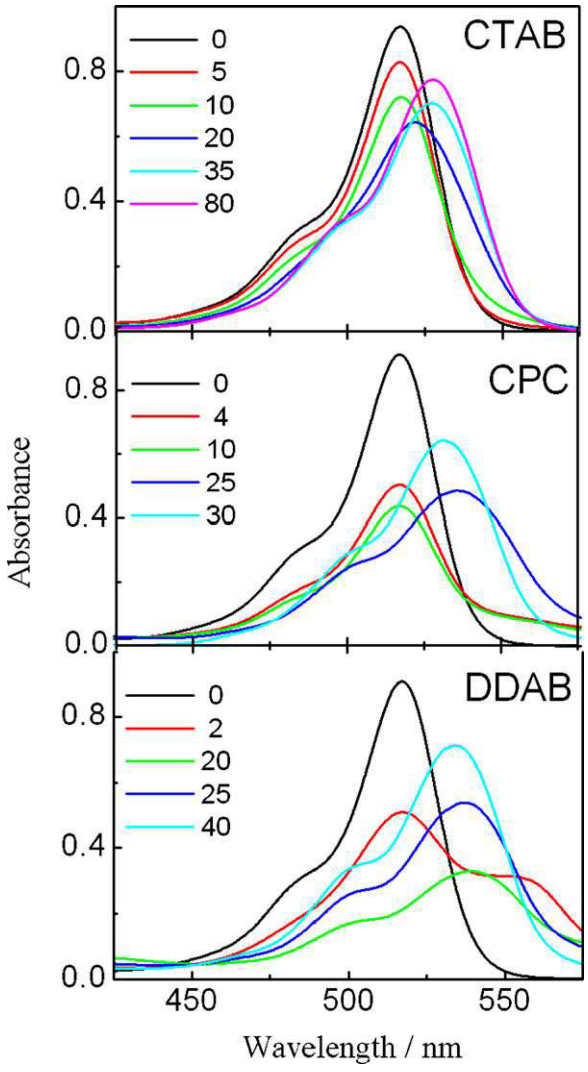

Fig. 3. Absorption spectra of 10 μM EY in water in the presence of different concentrations of surfactants at 298 K. Surfactants and their concentrations (in μM) are mentioned in the figure.

ε_D is the molar absorption coefficient of the dye, ε_{DS} is the molar absorption coefficient of the dye–surfactant complex, and L is the optical path length of the solution. The values of $(C_D.C_S)/(A-A_0)$ were plotted against C_S and a straight line was constructed (figure not shown to save space). From the slope and intercept of the linear plots, the binding constant, K_b was calculated. The K_b values for the surfactants were calculated at five different temperatures (298,

Table 2
Thermodynamic parameters for the interaction of EY with different surfactants.

Surfactants	T/K	$K_b \times 10^4$/M^{-1}	$(-)\Delta G^\circ$/kJ mol^{-1}	ΔH°/kJ mol^{-1}	ΔS° /J K^{-1} mol^{-1}
CTAB	298	4.62	26.69	−16.38	34.62
	303	3.67	26.56	−35.28	−28.77
	308	2.94	26.43	−54.49	−91.12
	313	1.94	25.77	−74.02	−154.16
	318	1.15	24.80	−93.87	−217.19
CPC	298	13.52	29.36	−78.54	−165.03
	303	7.16	28.25	−63.74	−117.12
	308	6.69	28.54	−48.69	−65.41
	313	3.99	27.65	−33.39	−18.33
	318	3.83	27.99	−17.85	31.90
DDAB	298	6.75	27.06	−37.08	−31.70
	303	5.70	27.67	−11.30	54.03
	308	4.57	27.56	14.91	137.90
	313	8.73	29.70	41.55	227.64
	318	8.53	30.11	68.62	310.48
DeDAB	298	2.35	25.02	−53.48	−95.53
	303	1.68	24.59	−35.87	−37.21
	308	1.48	24.67	−17.96	21.79
	313	1.38	24.88	00.25	80.27
	318	1.45	25.41	18.74	138.86

10 μM EY was used for study.

303, 308, 313 and 318K). From the K_b values, the thermodynamic parameters like the standard Gibbs free energy change (ΔG°), the standard enthalpy change (ΔH°) and the standard entropy change (ΔS°) for the dye–surfactant complex formation were determined using standard thermodynamic expressions [32]:

$$\Delta G^\circ = -RT \ln K_b \tag{8}$$

Changes in the standard enthalpy, ΔH°, were evaluated by the van't Hoff equation:

$$\left[\frac{\partial(\Delta G^\circ)}{\partial(1/T)}\right] = \Delta H^\circ \tag{9}$$

In the present study, ΔG° vs. T profile was found to follow a 2^0 polynomial equation as [33]:

$$\Delta G^\circ = a + bT + cT^2 \tag{10}$$

where a, b and c are the polynomial coefficients.

The polynomial coefficients thus helped in determining the ΔH° values described in the following expression:

$$\left[\frac{d(\Delta G^\circ/T)}{d(1/T)}\right] = a - cT^2 = \Delta H^\circ \tag{11}$$

The standard entropy change (ΔS°) for the dye–surfactant complex formation was then evaluated according to the following expression:

$$\Delta S^\circ = \frac{\Delta H^\circ - \Delta G^\circ}{T} \tag{12}$$

Thermodynamic parameters for the formation of the dye–surfactant complexes have been summarised in Table 2. Analysis of the table reveals that with the increase in the temperature, the binding constant (K_b) values decrease, revealing the binding process to be exothermic in nature. Negative ΔH° values also support this, although few exceptions were observed in case of DDAB and DeDAB at higher temperatures. ΔG° values reveal that the spontaneity of the dye–surfactant binding process is maximum at 298 K in case of single tailed surfactants. Also, the higher values of free energy change indicate the dye–surfactant interaction process to be governed both by electrostatic and hydrophobic forces [5,6,22].

3.2. Fluorescence spectral studies

3.2.1. Effect of dye concentration

When excited at 500 nm, an aqueous solution of 2 μM EY emits maximum radiation at 535 nm (λ_{em}^{max}). Unlike the absorption spectra EY did not exhibit any significant shoulder in its emission spectra. Fig. 4A reveals that with the increasing EY concentration in water, the fluorescence intensity was enhanced and the λ_{em}^{max} was progressively shifted to higher wavelengths up to 545 nm. However, in case of absorption spectra no spectral shift occurred with increasing dye concentration. The enhancement in the fluorescence intensity (F.I.) with increasing dye concentration and the absence of any significant dimeric band in the emission spectra proves that the excited state is predominantly populated with the monomeric form of EY and therefore, excited state aggregation is not permitted. In the case of absorption spectra, absorbance vs. concentration profile for EY at λ_{max}^{abs} was linear. But in aqueous medium, F.I. vs. [EY] plot was linear up to 10 μM, beyond which a negative deviation from linearity was noted in all the cases. Such phenomenon was probably due to the self quenching of the dye molecules.

3.2.2. Effect of solvent and surfactant on the emission spectra of EY

Emission spectral shift in different solvents followed the same sequence as in the absorption spectra. Emission spectra of EY in different solvents have been present in Fig. 4B.

Stokes shift ($\Delta\bar{\nu} = \bar{\nu}_a - \bar{\nu}_f$, where, $\bar{\nu}_a$ and $\bar{\nu}_f$ are the frequencies of the corresponding absorption and fluorescence maximum respectively) for EY in different environments was also evaluated using the standard procedure [34–36]. In the present case, Stokes shift has been found to increase with increasing solvent polarity. Results are summarised in Table 1 alongwith other spectral data. In case of alcohols, behaviour of n-propanol, n-butanol and n-pentanol did not follow the generalization. Stokes shift value decreased for methanol, compared to water, which also decreased further in case of ethanol. In case of n-propanol, the value was increased. The value did not change systematically among n-propanol, n-butanol and n-pentanol. The results indicate that the increasing hydrophobicity of the higher alcohols could not significantly and systematically control the spectral shift of EY. The anomalous behaviour in the presence of higher alcohols could also be due to the limited solubility. However further studies are warranted to make a final conclusion in this regard. Increase in Stokes shift with increas-

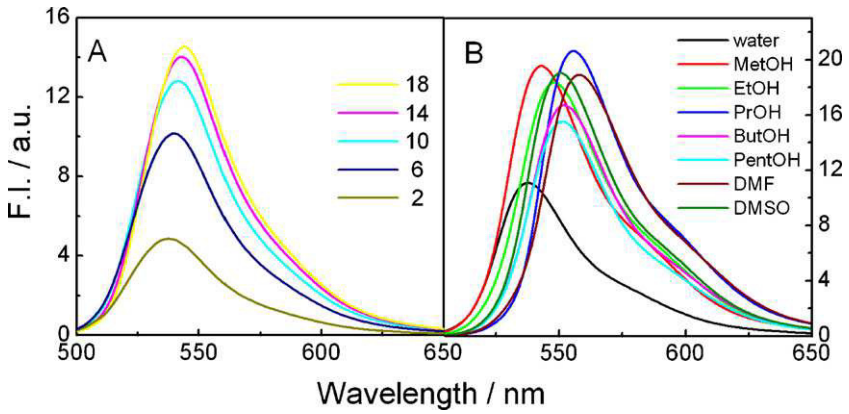

Fig. 4. (A) Emission spectra of EY in water at different concentrations (in μM, as mentioned in the figure). (B) Emission spectra of 10 μM EY in different solvents (mentioned inside the figure). Temperature: 298 K; λ_{ex} = 500 nm.

ing solvent polarity indicates stronger solvation of EY. EY, being ionized, is expected to be better solvated with a solvent of higher polarity (exceptions being n-propanol and DMF). Results also suggest that excited state dipole moment was increased in solvents of higher polarity. Larger magnitudes of Stokes shift also indicate the difference between the excited state and the ground state geometry [36].

Similar to the absorption spectroscopic studies, effect of cationic surfactants on the fluorescence spectra of 10 μM EY were also undertaken. Results are graphically presented in Fig. 5 for CTAB, CPC and DDAB. Unlike the absorption spectra, the emission spectral shift was less induced by cationic surfactants. Emission maximum of EY was only significantly shifted above the critical micelle concentration of all the four surfactants. Surfactants quenched the fluorescence of EY in their pre-micellar region. The cationic surfactants could bind to the anionic dye by way of electrostatic interaction, which finally led to the decrease in fluorescence. Quenching was found to be of Stern–Volmer type, assuming that the fluorescence quenching of EY is due to the formation of the excited state complex with the oppositely charged surfactants. Stern-Volmer constant (the interaction constant between dye and surfactant in the excited state) has been calculated using standard method [10] and also the relation $K_{SV} = k_q \cdot \tau_0$ (k_q = quenching constant and τ_0 = lifetime of the fluorophore), was found to be valid for all the four studied surfactants. As, τ_0 did not significantly change within the studied concentration range for a particular surfactant, hence the product of k_q and τ_0 remained constant, i.e., K_{SV} could easily be calculated from the slope of F_0/F vs. [Q] plot. Stern–Volmer plot for CTAB and DDAB have been shown in Fig. 6 as representative. Related results for all the surfactants are summarised in Table 3. Although the excited state lifetime did not change significantly among the four different surfactants, however, the dynamic quenching constants (k_q) varied among the surfactants significantly. For CPC, the value was higher than that of CTAB. Due to the presence of pyridinium ring in CPC there occurred better stacking of EY over CPC, which was not so favourable in case of CTAB. For the double tailed surfactants, the values of k_q were found

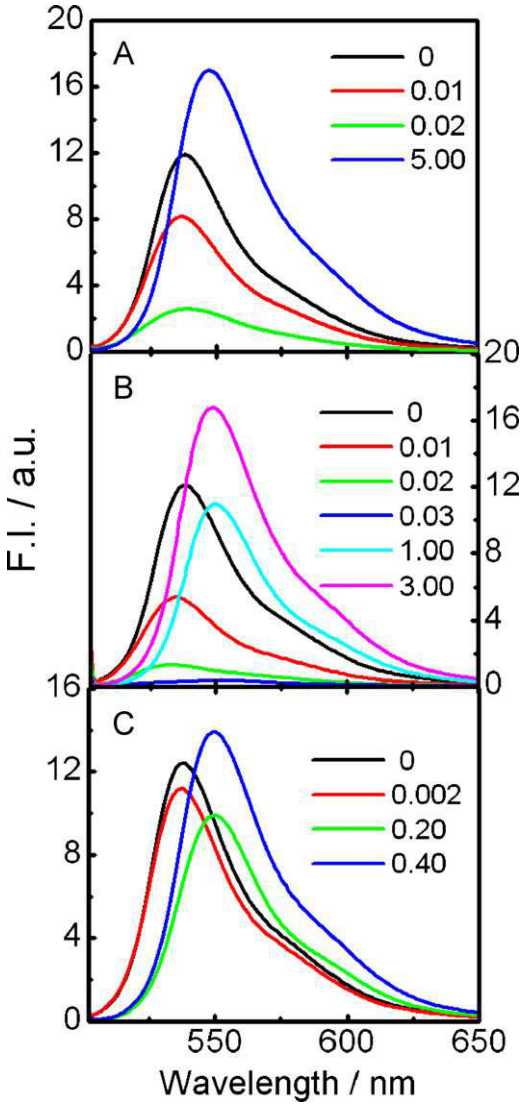

Fig. 5. Fluorescence spectra of 10 μM EY in the presence of different concentrations of (A) CTAB, (B) CPC, and (C) DDAB at 298 K. Surfactant concentrations (in mM) have been mentioned in the figure.

Table 3
Fluorescence data of aqueous EY solution in the presence of different cationic surfactants at 298 K.

Surfactants	$10^{-4} \times K_{sv}$ /M^{-1}	τ_0/ns	$10^{-13} \times k_q$/M^{-1} s^{-1}
CTAB	8.81	2.50	3.52
CPC	9.41	2.52	3.73
DDAB	4.68	2.60	1.80
DeDAB	4.85	2.54	1.90

10 μM EY was used for study. λ_{ex} = 500 nm. λ_{em}^{max} = 540 nm.

to be lower even than CTAB. Results indicate retarded interaction between the surfactant head group and EY. Presence of two hydrocarbon tails may hinder the surfactants to be in the proximity of EY. It, therefore, could clearly be concluded that the excited state

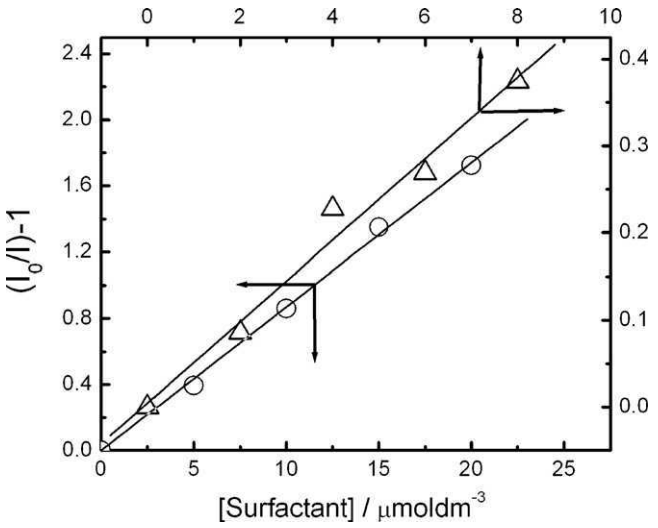

Fig. 6. Stern–Volmer plot for the fluorescence quenching of 10 μM EY in water by (○) CTAB and (△) DDAB at 298 K. λ_{ex} = 500 nm.

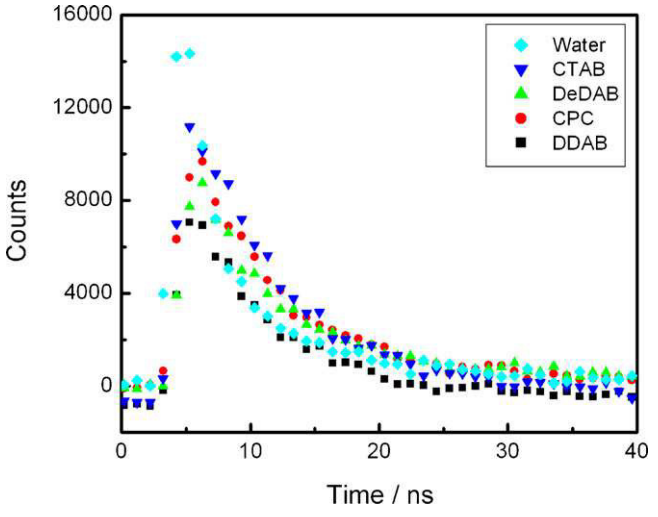

Fig. 7. Fluorescence decay curves of 10 μM EY in water and different surfactants (mentioned in the figure). λ_{ex} = 500 nm.

interaction between dye and oppositely charged surfactants were governed by Coulombic interactions [6,37].

3.2.3. *Fluorescence lifetime measurements*

Time-resolved fluorescence studies were carried out to determine the emission decay parameters for EY in different solvents and surfactants. 10 μM EY exhibited a lifetime 2.50 ns. The lifetime did not change significantly with the variation of solvent polarity and surfactant concentration. Similar results were observed by other researchers [10]. The fluorescence decay curve of EY was found to be single exponential in water and in the presence of all the surfactants used (as shown in Fig. 7).

3.2.4. *Steady-state fluorescence anisotropy*

Fluorescence anisotropy provides important information about the micro-viscosity of the medium around a fluorescent dye molecule [38,39]. When a dye molecule binds to oppositely charged micelle, the micro-viscosity of the dye–micelle interface gets significantly changed [40]. Variation of fluorescence anisotropy with the surfactant concentration has been shown in Fig. 8. Pure EY in water has an anisotropy value of 0.057. A mild increase in the anisotropy value was observed in aqueous salt solution (0.057 in water to 0.067 in 1.0 mM NaCl solution). The increase in the fluorescence anisotropy with increasing salt concentration was a direct consequence of viscosity enhancement of aqueous salt solution. Among the different alcohols, anisotropy increased with increasing alcohol chain length (data not shown). DMF and DMSO exhibited similar behaviour as that of water. Surfactants could significantly alter the anisotropy value of EY in water. A significant increase in the fluorescence anisotropy of EY was noted in the post-micellar region. Hence, one could employ the anisotropy measurement technique as a tool to determine the critical micellar concentration of surfactant. As already have been mentioned that there is a direct correlation between the fluorescence anisotropy and viscosity of the medium [17,40], therefore, one needs to correlate the anisotropy with viscosity. In the inset of Fig. 8, anisotropy dependence of EY on glycerol concentration in water has been shown as reference. It is believed that EY could electrostatically bind at the micellar interface, which restricts the segmental motion of the dye molecule. Hence, the micro viscosity around dye–micelle interface becomes significant than the viscosity when the dye just binds electrostatically to a surfactant in its pre-micellar region.

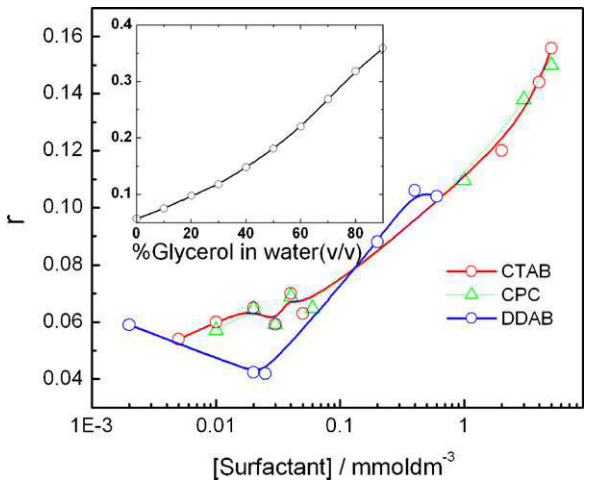

Fig. 8. Variation of fluorescence anisotropy (r) of EY with the concentration of surfactant [surfactant] in water at 298 K. A 10 μM EY in water was used. λ_{ex} = 500 nm and λ_{em} = 540 nm. Inset: anisotropy–concentration profile of EY in glycerol–water mixture is shown for comparison. Surfactants are mentioned inside the figure.

4. Summary and conclusions

Absorption and emission spectral behaviour of the anionic xanthene dye, EY was investigated in the solvents of different polarities as well as in different aqueous cationic surfactant solution. By suitably analysing the spectral data of EY in the presence of surfactants in their pre-micellar region, dye–surfactant interaction constant values were determined both in the ground and excited states. Stokes shifts were calculated and correlated with the polarity of the medium. Steady state fluorescence anisotropy values were evaluated in the pre- and post-micellar regions of surfactants in aqueous medium. A significant change in the anisotropy values was observed for EY.

Based on the experimental results the following conclusions could be drawn:

(1) The ground state is predominantly populated with the dimeric form of EY as revealed from the absorption spectra On the contrary, emission spectra of EY prove that the excited state is predominantly populated with the monomeric form of EY and hence excited state aggregation is not permitted.

(2) Dimerisation constant (K_D) values in different media reveal that the process is more favoured in protic solvents than the aprotic solvents. The solvent-dye hydrogen bonding plays an important role in the aggregation of the dye molecules.
(3) The dye–surfactant binding process is exothermic in nature and is controlled both by electrostatic and hydrophobic forces, as revealed from the thermodynamic parameters.
(4) A red shift in the absorption spectra of EY with the decrease in solvent polarity was observed. Stokes shifts were found to be correlated with the polarity of the medium. Larger magnitudes of Stokes shift indicate that the excited state geometry could be different from that of the ground state.
(5) The excited state interaction between EY and surfactants is dependent the nature of the surfactant head group, type and number of hydrocarbon chains, although it is primarily governed by Coulombic forces.
(6) Important information regarding the micro-viscosity of the medium around EY could be obtained from the fluorescence anisotropy measurements. Also, this measurement technique could be used as a tool to determine the critical micellar concentration of surfactants.

Acknowledgements

The work has been financially supported by the University Grants Commission (UGC), New Delhi, India. MC acknowledges fellowship from UGC.

References

[1] S.P. Moulik, Micelles: self-organized surfactant assemblies, Curr. Sci. 71 (1996) 368–376.
[2] S.M. Ghoreishi, M. Behpour, A.G. Farsani, Study of interaction between a cationic surfactant and two anionic azo dyes by ion-selective electrode technique and spectrophotometry, Dyes Pigments 74 (2007) 585–589.
[3] P. Forte-Tavcer, Interactions between some anionic dyes and cationic surfactants with different alkyl chain length studied by the method of continuous variations, Dyes Pigments 63 (2004) 181–189.
[4] F. Tanaka, Y. Harada, N. Todoroki, M. Aratono, K. Motomura, Interaction of sodium 4′-(butylamino)azobenzene-4-sulfonate with 2-(octylsulfinyl)ethanol in adsorbed film and micelle, Bull. Chem. Soc. Jpn. 66 (1993) 1929–1933.
[5] B.B. Bhowmik, P. Ganguly, Photophysical studies of some dyes in aqueous solution of triton X-100, Spectrochim. Acta A 62 (2005) 808–813.
[6] B.B. Bhowmik, P. Ganguly, Photophysics of xanthene dyes in surfactant solution, Spectrochim. Acta A 61 (2005) 1997–2003.
[7] H. Akbas, Micellization of dodecylpyridinium chloride in water–ethanol solutions, Colloid J. 70 (2008) 541–548.
[8] M. Khamis, B. Bulos, F. Jumean, A. Manassra, M. Dakiky, Azo dyes interactions with surfactants. Determination of the critical micelle concentration from acid–base equilibrium, Dyes Pigments 66 (2005) 179–183.
[9] Y.R. Suradkar, S.S. Bhagwat, CMC determination of an odd carbon chain surfactant (C13E20) mixed with other surfactants using a spectrophotometric technique, J. Chem. Eng. Data 51 (2006) 2026–2031.
[10] S. De, S. Das, A. Girigoswami, Environmental effects on the aggregation of some xanthene dyes used in lasers, Spectrochim. Acta A 61 (2005) 1821–1833.
[11] M.A.J. Rodgers, Picosecond fluorescence studies of xanthene dyes in anionic micelles in water and reverse micelles in heptane, J. Phys. Chem. 85 (1981) 3372–3374.
[12] A. Seret, A. Van de Vorst, Solubility properties of Eosin Y and Rose Bengal triplet state in sodium dodecyl sulfate micellar solutions, J. Phys. Chem. 94 (1990) 5293–5299.
[13] M.M. Abou-Sekkina, Exploration of a cuprate superconductor $YBa_2Cu_3O_7$ as a catalyst and industrial antipollutant, Mater. Lett. 42 (2000) 297–304.
[14] T. Sreethawong, C. Junbua, S. Chavadej, Photocatalytic H_2 production from water splitting under visible light irradiation using Eosin Y-sensitized mesoporous-assembled Pt/TiO_2 nanocrystal photocatalyst, J. Power Sources 190 (2009) 513–524.
[15] A.R. Tehrani Bagha, H. Bahrami, B. Movassagh, M. Arami, F.M. Menger, Interactions of gemini cationic surfactants with anionic azo dyes and their inhibited effects on dyeability of cotton fabric, Dyes Pigments 72 (2007) 331–338.
[16] S. Göktürk, M. Tunçay, Spectral studies of safranin-O in different surfactant solutions, Spectrochim. Acta A 59 (2003) 1857–1866.
[17] A. Chakrabarty, A. Mallick, B. Haldar, P. Das, N. Chattopadhyay, Binding interaction of a biological photosensitizer with serum albumins: a biophysical study, Biomacromolecules 8 (2007) 920–927.
[18] S. Mukhopadhyay, S.S. Maity, A. Roy, D. Chattopadhyay, K.S. Ghosh, S. Dasgupta, S. Ghosh, Characterization of the structure of the phosphoprotein of Chandipura virus, a negative stranded RNA virus probing intratryptophan energy transfer using single and double tryptophan mutants, Biochimie 92 (2010) 136–146.
[19] K. Manna, A.K. Panda, Spectral studies on the interaction of pinacyanol chloride with binary surfactants in aqueous medium, Spectrochim. Acta A 74 (2009) 1268–1274.
[20] R. Sabaté, J. Estelrich, Determination of the dimerization constant of pinacyanol: role of the thermochromic effect, Spectrochim. Acta A 70 (2008) 471–476.
[21] R. Sabate, M. Gallardo, A. de la Maza, J. Estelrich, A spectroscopy study of the interaction of pinacyanol with n-dodecyltrimethylammonium bromide micelles, Langmuir 17 (2001) 6433–6437.
[22] S. Biswas, S.C. Bhattacharya, P.K. Sen, S.P. Moulik, Absorption and emission spectroscopic studies of fluorescein dye in alkanol, micellar and microemulsion media, J. Photochem. Photobiol. A: Chem. 123 (1999) 121–128.
[23] C. Reichardt, Solvatochromic dyes as solvent polarity indicators, Chem. Rev. 94 (2002) 2319–2358.
[24] S.N. Baker, G.A. Baker, F.V. Bright, Temperature-dependent microscopic solvent properties of 'dry' and 'wet' 1-butyl-3-methylimidazolium hexafluorophosphate: correlation with (30) and Kamlet-Taft polarity scales, Green Chem. 4 (2002) 165–169.
[25] E.M. Kosower, The effect of solvent on spectra. I. A new empirical measure of solvent polarity: Z-values, J. Am. Chem. Soc. 80 (2002) 3253–3260.
[26] U. Retter, M. Koch, I. Nehls, Investigation of the optimization of the recovery of mineral oil from water, Fresen. J. Anal. Chem. 364 (1999) 777–779.
[27] P.K.B. Gargi Ghosh, Chem. Eng. J. 119 (2006) 45–53.
[28] C. SenVarma, B.B. Bhowmik, Photoinduced interaction of thionine with phospholipid and cholesterol in artificial membranes, J. Photochem. Photobiol. B: Biol. 8 (1991) 295–305.
[29] B.B. Bhowmik, A. Sil, Photoinduced interaction of riboflavin dye with different reducing agents in aqueous and liposome media, Chem. Phys. Lipids 127 (2004) 189–197.
[30] B.B. Bhowmik, I. Chatterjee, P. Nandy, Liposome formation of egg lecithin and its interaction with iodine, Chem. Phys. Lipids 39 (1986) 271–277.
[31] N.J. Rose, R.S. Drago, Molecular addition compounds of iodine. I. An absolute method for the spectroscopic determination of equilibrium constants, J. Am. Chem. Soc. 81 (1959) 6138–6141.
[32] M. De, S. Bhattacharya, S.P. Moulik, A.K. Panda, Interfacial composition, structural and thermodynamic parameters of water/(surfactant + n-butanol)/n-heptane water-in-oil microemulsion formation in relation to the surfactant chain length, J. Surfact. Deterg. 13 (2010) 475–484.
[33] S.K. Hait, S.P. Moulik, Interfacial composition and thermodynamics of formation of water/isopropyl myristate water-in-oil microemulsions stabilized by butan-1-ol and surfactants like cetyl pyridinium chloride, cetyl trimethyl ammonium bromide, and sodium dodecyl sulfate, Langmuir 18 (2002) 6736–6744.
[34] J.J Aaron, M.D. Gaye, C. Parkanyi, C. Boniface, T.W.N. Bieze, S.S. Atik, K.S. Raghu-Veer, L. Von Szentpaly, R. Ghosh, Solvent effects upon the electronic absorption and fluorescence spectra of pteridines and riboflavin and their ground and first excited singlet-state dipole moments, Pteridines 3 (1992) 153–163.
[35] D.S. Biradar, B. Siddlingeshwar, S.M. Hanagodimath, Estimation of ground and excited state dipole moments of some laser dyes, J. Mol. Struct. 875 (2008) 108–112.
[36] U.S. Raikar, V.B. Tangod, B.M. Mastiholi, S. Sreenivasa, Solvent effects and photophysical studies of ADS560EI laser dye, Afr. J. Pure Appl. Chem. 4 (2010) 188–197.
[37] R.T. Buwalda, J.M. Jonker, J.B.F.N. Engberts, Aggregation of azo dyes with cationic amphiphiles at low concentrations in aqueous solution, Langmuir 15 (1999) 1083–1089.
[38] A. Chakrabarty, P. Das, A. Mallick, N. Chattopadhyay, Effect of surfactant chain length on the binding interaction of a biological photosensitizer with cationic micelles, J. Phys. Chem. B 112 (2008) 3684–3692.
[39] A. Mallick, B. Haldar, N. Chattopadhyay, Spectroscopic investigation on the interaction of ICT probe 3-acetyl-4-oxo-67-dihydro-12H indolo-[2,3-a] quinolizine with serum albumins, J. Phys. Chem. B 109 (2005) 14683–14690.
[40] A. Mahata, D. Sarkar, D. Bose, D. Ghosh, A. Girigoswami, P. Das, N. Chattopadhyay, Photophysics and rotational dynamics of a Î²-carboline analogue in nonionic micelles: effect of variation of length of the headgroup and the tail of the surfactant, J. Phys. Chem. B 113 (2009) 7517–7526.

Spectrochimica Acta Part A: Molecular and Biomolecular Spectroscopy 97 (2012) 722–727

Contents lists available at SciVerse ScienceDirect

Spectrochimica Acta Part A: Molecular and Biomolecular Spectroscopy

journal homepage: www.elsevier.com/locate/saa

Effect of colloidal silica on the spectral behaviour of 7-hydroxycoumarin in aqueous medium

Moumita Chakraborty, Soumik Bardhan, Swapan K. Saha *, Amiya K. Panda *

Department of Chemistry, University of North Bengal, Darjeeling 734 013, West Bengal, India

HIGHLIGHTS

- Imperfections in colloidal silica were incorporated by thermal heating.
- Interaction of silica and 7HC was studied by absorption, emission and FTIR spectroscopy.
- Mechanism on the effect of H-bonding on excited state energy transfer process was rationalized.

GRAPHICAL ABSTRACT

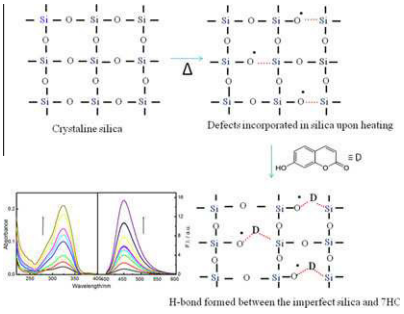

ARTICLE INFO

Article history:
Received 4 May 2012
Received in revised form 10 July 2012
Accepted 11 July 2012
Available online 25 July 2012

Keywords:
Ludox®
7-Hydroxycoumarin
Excited state hydrogen bonding
HFRET

ABSTRACT

Absorption and emission spectroscopic studies, in combination with FTIR measurements, were carried out for 7-hydroxycoumarin (7HC) and nanocolloidal dispersion of silica. Attempt has been made to identify the characteristics of excited state H-bond formed between colloidal silica and 7HC in aqueous medium. Both the absorption and emission spectra of 7HC was found to be dependent on the concentration of silica. At lower silica concentrations, the absorption spectra decreases with increasing silica concentration, on the other hand, at higher concentration a bathochromic shift occurs in the absorption spectra of 7HC. Fluorescence behaviour followed the opposite trend in comparison to the absorption spectra. It is proposed that at lower silica concentration, excited state H-bond was formed between 7HC and silica dispersions. At higher concentration, the decrease in fluorescence intensity is attributed to the self quenching of adsorbed dye molecules over silica surface following the mechanism of Homo Förster resonance energy transfer (HFRET). Results were correlated with the size and surface charge of colloidal silica as measured by dynamic light scattering and zeta potential studies.

Introduction

Semiconductor nanoparticles have gained importance for their multifarious applications as they posses favourable optical properties, viz., high quantum yield, enhanced photostability, capability of cell imaging [1], etc. Among different semiconductor nanocrystals, silica has got special importance because it can be used in different forms for solute pre-concentration and immobilization of analytical reagents [2]. Besides, silica has got special attention for other specific properties like optical transparency [3], high hydrophilicity [4] and negative surface charge in aqueous media [5]. According to Bonacchi et al. [6], silica nanoparticles have some fascinating properties compared to other conventional nanosystems which include its photophysical inertness, absence of intrinsic toxicity, capability to host a large number of photochemically active species and also to protect the active material segregated inside its pore. These specific properties have additional advantages for silica nanoparticles in the field of bioanalysis and disease diagnostics [7]. According to Parida et al. [8], silica surface can be modified

* Corresponding authors. Tel.: +91 943334710; fax: +91 3532699001 (A.K. Panda), tel.: +91 9434045491; fax: +91 3532699001 (S.K. Saha).
E-mail addresses: ssahanbu@hotmail.com (S.K. Saha), akpanda1@yahoo.com (A.K. Panda).

1386-1425/$ - see front matter © 2012 Elsevier B.V. All rights reserved.
http://dx.doi.org/10.1016/j.saa.2012.07.059

into various functionalities because of the presence of active –OH groups which make silica suitable for different purposes as mentioned above. Traditional organic fluorophores are usually photosensitive which could be overcome by conjugating with silica nanoparticles [9]. However, the process of conjugation between an organic dye and silica nanoparticles is not straightforward. While silica is highly hydrophilic, organic dyes are usually hydrophobic, which makes the aggregation process less favourable. There are several reports on the synthesis and characterization of silica coated fluorescent nanoparticles [6,10]. Although, fluorescent/fluorescent doped/fluorescent conjugated silica nanoparticles have several advantages, however, such systems suffer some limitations which are strongly dependent on their size and concentration [7]. According to Ha et al. [11] and Bringley [12] in some cases, fluorescence could even be quenched, compared to the free dye molecules. Therefore, a detailed spectral investigation on the absorption and fluorescence spectra of dye-silica aggregates are warranted for better technological applications as well as from the fundamental understanding point of view. Towards this initiative we have undertaken the spectroscopic investigations on colloidal silica-7HC aggregates in a wide concentration range of silica. In addition to the aforementioned point of interest, it is believed that physicochemical studies on dye-colloidal aggregates would have been equally important in the field of waste water treatment [13], lasing property [14], dye-sensitized solar cells [15], photocatalytic reactions [16], etc. Ludox® is commercially available spherical shaped silica particles suspended in aqueous medium which find different applications [17–22]. Therefore, colloidal silica in the form of Ludox® can be considered as an appropriate model system in investigating its capability to alter (both enhancement and quenching) the absorbance and fluorescence intensity of fluorophores in aqueous medium. The dye 7-hydroxycoumarin, commonly known as "Umbelliferone", is a natural product of the coumarin family [23]. It is known to have antioxidant properties [24,25]. The ultraviolet activity of 7-hydroxycoumarin led to its use as a sunscreen agent and an optical brightener for textiles [26–29]. It is used as laser dyes and also as fluorescent indicator [27,30]. Although several reports are available in the literature which include the interaction between silica and a number of dyes [8,31–36], however, reports involving the interaction of Ludox® with 7-hydroxycoumarin are not common in literature. The occurrence of excited state H-bonding between silica and 7-hydroxycoumarin is supposed to be understood in a better way through fluorescence spectroscopic analysis, which could further be investigated via FTIR measurements.

The present study aimed at understanding the extent of interaction between 7-hydroxycoumarin and Ludox® (commercial form colloidal silica) through absorption and fluorescence spectroscopy, fluorescence lifetime and FTIR studies. Finally, size and zeta potential measurements using dynamic light scattering technique were carried out in order to understand the stacking behaviour of dye molecules over the silica surface.

Experimental

Materials

The dye, 7-hydroxychromen-2-one (7-hydroxycoumarin, 7HC), was a product from Chem Service, West Chester, USA (99% pure) and was used as received. Colloidal dispersion of silica (Ludox AM-30 colloidal silica, 30 wt.% suspension in water) was procured from M/S Sigma Aldrich, USA. HPLC grade acetonitrile from E. Merck, Germany was used for FTIR measurements. Double distilled water with a conductance of 2–4 μS/cm was used in preparing the solutions.

Methods

A stock solution of 7HC (1.0 mM) was prepared as described elsewhere [37] using double distilled water. This stock solution was diluted within the range 1–20 μM. Thirty weight percent of the supplied Ludox® solution was diluted to 10 wt.%, which was used as the stock solution. This stock solution was heated at 80 °C for 2 h. The heating is supposed to cause defects/imperfections in the microcrystalline silica particles as reported by Banerjee et al. [38]. This solution was then diluted to required concentrations. This preheated colloidal suspension was used throughout all the experiments unless specifically mentioned. Henceforth, colloidal silica means silica microcrystalline suspensions comprising imperfections/defects.

DLS and zeta potential measurements of Ludox®, the dye (7HC) and the dye–Ludox® system were carried out by a Nano ZS 90 (Malvern, UK). A He–Ne laser of 632.8 nm wavelength was used and the data were recorded at a scattering angle of 90°. Steady state electronic absorption spectra were recorded on a UVD-2950 spectrophotometer (Labomed Inc., USA). Spectra were recorded within the range 200–400 nm using a matched pair of quartz cuvette of 1 cm path length, while the steady state fluorescence spectra were recorded in a bench-top spectrofluorometer (Quantamaster-40, Photon Technology International Inc., NJ, USA). The dye, in the presence and absence of Ludox®, was excited at 375 nm while the emission spectra were recorded in the range 400–600 nm. Fluorescence lifetime of the dye in the absence and presence of Ludox® was recorded at 450 nm using 310 nano LED as the light source. The fluorescence decay was found to be single exponential in nature and the χ^2 value was found to be greater than 1.0.

FTIR absorption spectra were recorded in the range of 400–4000 cm^{-1} with a Shimadzu 83000 spectrometer (Japan) using a CaF_2-IR crystal window (Sigma–Aldrich) equipped with presslock holder with 100 number scans and spectral resolution of 4 cm^{-1}. All the measurements were carried out at ambient but controlled temperature.

Results and discussion

Characterization of Ludox® in the absence and presence of 7HC

Dynamic light scattering (DLS) and zeta potential measurements

Pure Ludox® within the range 0.004–0.02 wt.% exhibited an average particle size of 27 nm as obtained by dynamic light scattering measurement. Effect of heating was insignificant on the size of Ludox suspension. The size variation in the presence of 7HC was found to be insignificant. Zeta potential measurements were carried out to understand the electrostatic interactions between 7HC and Ludox® in aqueous medium. If there occurs such an electrostatic interaction, it is expected that the zeta potential of Ludox® would change with the addition of 7HC. Pure silica exhibited an average zeta potential of −35 mV in aqueous medium in absence of 7HC. Ludox suspension, without heating possesses a lower zeta potential value (−14 mV) compared to the thermally treated Ludox suspension. The increase in negative zeta potential value was due to the formation of defects which led to the generation of electron rich centres [39]. However, when Ludox® was added progressively to 10 μM 7HC, a variation in the zeta potential was noted as summarized in Table 1. At lower concentration (within 0.004–0.02 wt.%) with the progressive addition of Ludox® to the dye, initially the zeta potential value was found to be −23 mV, which eventually attained the value for pure Ludox®. When Ludox® is heated above 80 °C it leads to the formation of defects, which are rich in electrons. These point defects are capable of forming H-bonds with 7HC. Thus 7HC, through the process of adsorption on the defective sites, can delocalize the electron density on Ludox®

Table 1
Hydrodynamic diameter and zeta potential data for thermally treated colloidal silica nanoparticles, Ludox®, in the absence and presence of 10 μM 7HC at 298 K.

Wt.% of colloidal silica	d_h/nm		Z.P./mV	
	Silica	Silica-7HC	Silica	Silica-7HC
0.004	25	25	−35	−23
0.008	27	27	−35	−29
0.012	25	27	−34	−33
0.016	–	26	–	−35
0.02	–	28	–	−35

surface. As a result, there occurs a decrease in the zeta potential for Ludox® on the addition of 7HC. After the complete adsorption of all the dye molecules over the silica surface, no variation in the zeta potential value occurred. Variations and subsequent attainability of the constancy followed the same trend as observed in the absorption and emission spectroscopic measurements. The explanation for the constancy of the size in the presence and absence of 7HC remains unexplored. This needs further experiments which could be considered as future perspective.

Absorption and fluorescence spectral studies

Absorption and emission studies of 7HC within the range 2–20 μM are shown in Fig. 1. Upon increasing the concentration of the dye, both absorption and emission intensities increased linearly in the studied concentration range. The molar absorption coefficient of 7HC at 324 nm was found to be $1.035 \times 10^4\ M^{-1}\ cm^{-1}$. This linear increment in the absorption and emission spectra revealed that no aggregation occurred in the studied concentration range. No spectral shifts were also recorded, confirming the absence of dimer or higher aggregates in the solution.

While considering the spectral behaviour of Ludox® it is noted that the absorption and emission spectra are featureless for Ludox® up to 0.02 wt.% in water. However, Ludox® at higher concentration range up to 2 wt.% exhibited an absorption peak at 205 nm which is due to the oxygen free radical present in defective SiO_2 moiety. Above this concentration the absorption spectra of Ludox® became noisy with progressive red shifts (spectra not shown). This was due to the scattering of aggregated silica at higher concentration range. Effect of Ludox® on the spectral behaviour of 7HC is shown in Fig. 2. The present study on the interaction of Ludox® and 7HC are divided into two parts: (a) lower concentration range, i.e., 0–0.02 wt.% of silica and (b) higher concentration range, i.e., 0.02–9.00 wt.% of silica. In the dilute range of Ludox®, the spectra of pure Ludox® were featureless. However, on the progressive addition of Ludox® to 10 μM 7HC solution, absorbance of 7HC is suppressed. Absorbance at 324 nm, characteristic of 7HC, decreased linearly with Ludox® concentration (Fig. 2A). The linearity is not observed when the Ludox® concentration exceeds the concentration of 0.02 wt.%. The systematic linear decrease at 324 nm on progressive addition of Ludox® at lower concentration range was due to uniform adsorption of 7HC over the colloidal Ludox® surface whereby monolayer of dye molecules were formed [40]. The noisy and non-systematic decrease in the absorption spectra of 7HC in the presence of higher amount (<0.02 wt.%) of Ludox® was due to the irregular adsorption of the dye over Ludox® surface. While considering the absorption spectra in the higher concentration range (Fig. 2B), the spectra of 7HC was red shifted to 360 nm due to the irregular stacking of dye molecules over the silica surface whereby fine precipitates were found to settle down at the bottom of the vial, visible through naked eye. The complete adsorption of 7HC leads to the featureless spectra and the formation of precipitates. In Fig. 2B, the same spectra of 7HC (spectrum 7), as shown in Fig. 2A (spectrum 1), has also been presented for comparison. Due to the large difference in the absorbance values for two different systems (for panel A the absorbance scale is 0–0.17 while for panel B it is 0–3.25), the spectra of 7HC (as shown in panel B) appears insignificant compared to that of Ludox® at higher concentration. A 2 wt.% silica, when excited at 375 nm, emits at 430 nm. Another shoulder appeared at 450 nm (Fig. 3). Again, at higher concentration the spectra became noisy which is due to the irregular scattering of the colloidal aggregates. Contrary to the absorption spectra of silica-dye system in the low concentration range, the fluorescence intensity (F.I.) of 7HC increased linearly with the increasing Ludox® concentration up to 0.02 wt.% as shown in Fig. 4A. Upon further increase in the concentration of Ludox® the F.I. decreased in a non-linear fashion (shown in Fig. 4B). The significant enhancement in the F.I. of 7HC in the lower concentration range of Ludox® was due to the excited state H-bonding between the defects incorporated into silica nanoparticle (resulted by heating) and the OH group of 7HC as shown in Scheme 1 [41]. The formation of H-bond was further established by FTIR measurements (to be discussed and shown in the subsequent section). The non-linear decrease in the F.I. of 7HC at higher concentration range was due to the irregular adsorption and subsequent precipitation of 7HC over the Ludox® surface. According to Chen et al. [7],

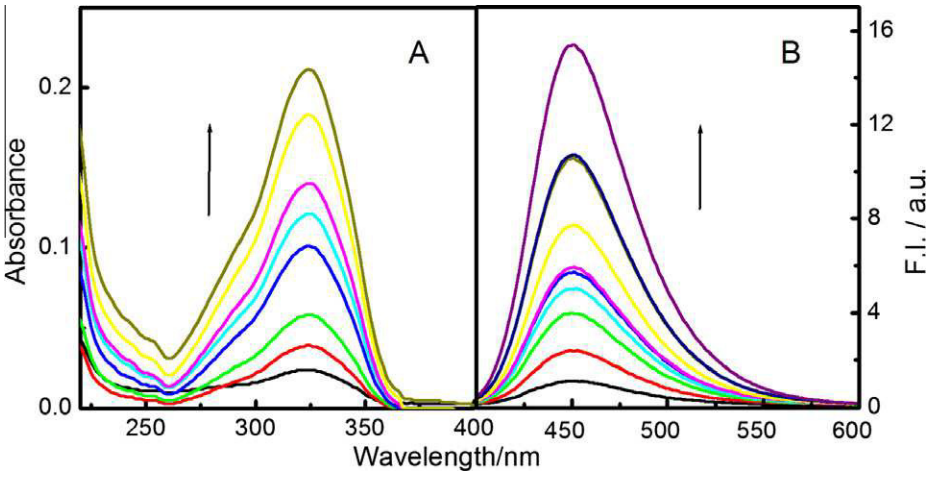

Fig. 1. (A) Absorption and (B) emission spectra of 7HC in water at different concentrations at 298 K. Concentration of 7HC/μM: 1,2; 2,4; 3,6; 4,10; 5,12; 6,14; 7,16 and 8,20: λ_{ex} = 375 nm.

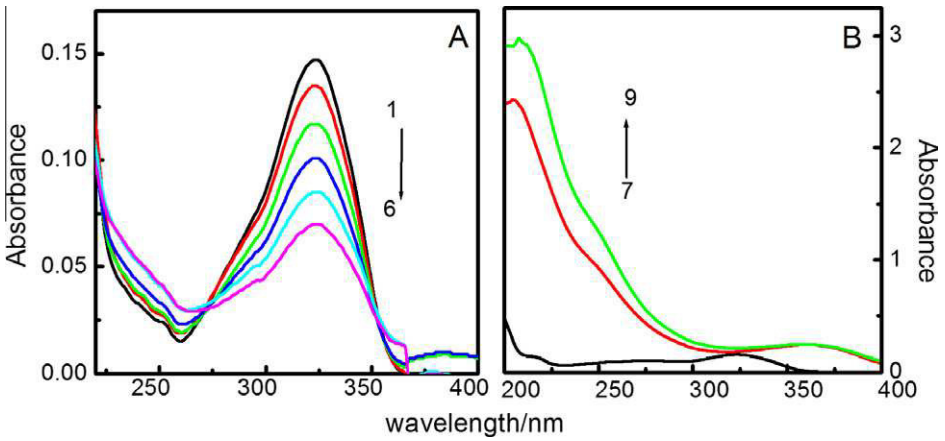

Fig. 2. Absorption spectra 10 μM 7HC in the presence of varying amount of Ludox® at 298 K. Ludox® was used in the two different concentration (wt.%) ranges. (A) 1, 0; 2, 0.004; 3, 0.008; 4, 0.012; 5, 0.016 and 6, 0.02. In panel (B) spectra of 7HC is shown in the presence of 7, 0.0; 8, 2; and 9, 3 wt.% of Ludox®. Note the differences in the units of absorbance axis in two panels.

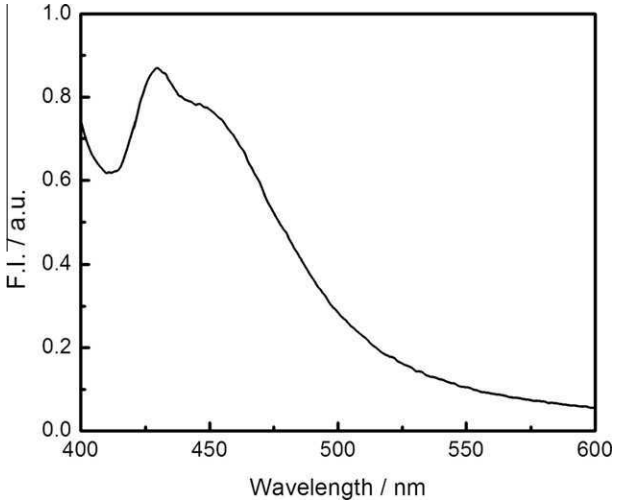

Fig. 3. Emission spectra of 2 wt.% colloidal silica in water. Temperature: 298 K; λ_{ex} = 375 nm.

the quenching mechanism was due to the involvement of non-radiative processes. When the fluorophores are closely packed within the solid matrix of Ludox®, the intermolecular energy transfer process becomes more favourable. In the present study, a fast Homo Förster resonance energy transfer (HFRET) among the fluorophores (herein 7HC) become significant, which eventually lead to self quenching process [42,43]. The process becomes remarkable when no prominent Stokes shift occur for the fluorophores in the absence and presence of silica [44]. The change in fluorescence of a dye molecule in close proximity to a second molecule is attributed to Förster resonance energy transfer (FRET). FRET is a mechanism which describes energy transfer between two chromophores, one in the excited state and the other in its ground state [45]. When the transfer of energy occurs between two identical molecules the phenomenon is known as Homo Förster resonance energy transfer (HFRET) [42,43]. In the present study, at higher Ludox® concentration, the dye molecules are very rigidly bound around the silica surface for which there are possibilities of energy transfer from an excited dye molecule to another dye molecule in the ground state. It is to be mentioned that the lifetime of 7HC (5.35 ns) was not significantly changed in presence of Ludox®. The Stern–Volmer quenching phenomena help in understanding the kinetics of a photophysical intermolecular deactivation process. Stern–Volmer quenching process is usually valid for the systems where the lifetime of a probe does not change significantly in the presence of quencher [46]. However, in the present case, the decrease in the F.I. with added Ludox® did not follow Stern–Volmer equation [46]:

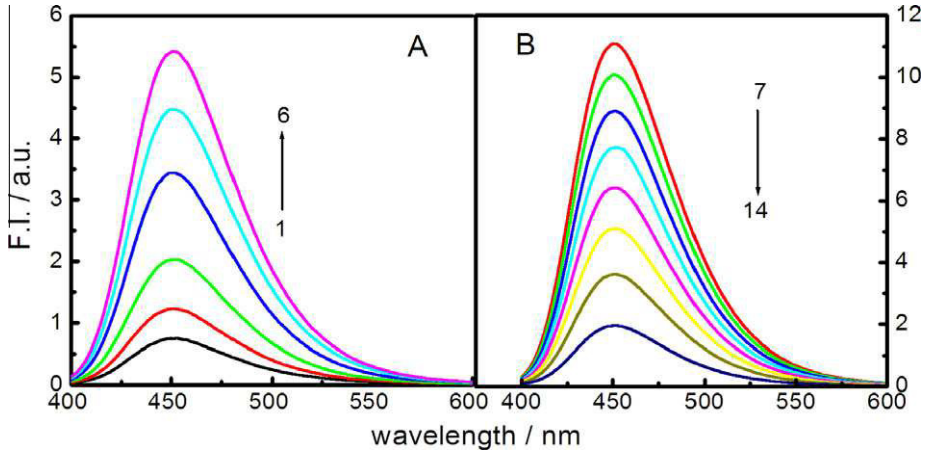

Fig. 4. Emission spectra of 10 μM 7HC in the presence of (A) lower wt.% (1, 0; 2, 0.004; 3, 0.008; 4, 0.012; 5, 0.016 and 6, 0.02) and (B) higher wt.% (2, 3, 4, 5, 6, 7, 8 and 9 wt.%) of Ludox® at 298 K. *Note:* in the lower concentration range of Ludox®, fluorescence of 7HC increased (Panel A) while the fluorescence of 7HC was quenched in the presence of higher amount of Ludox® (Panel B).

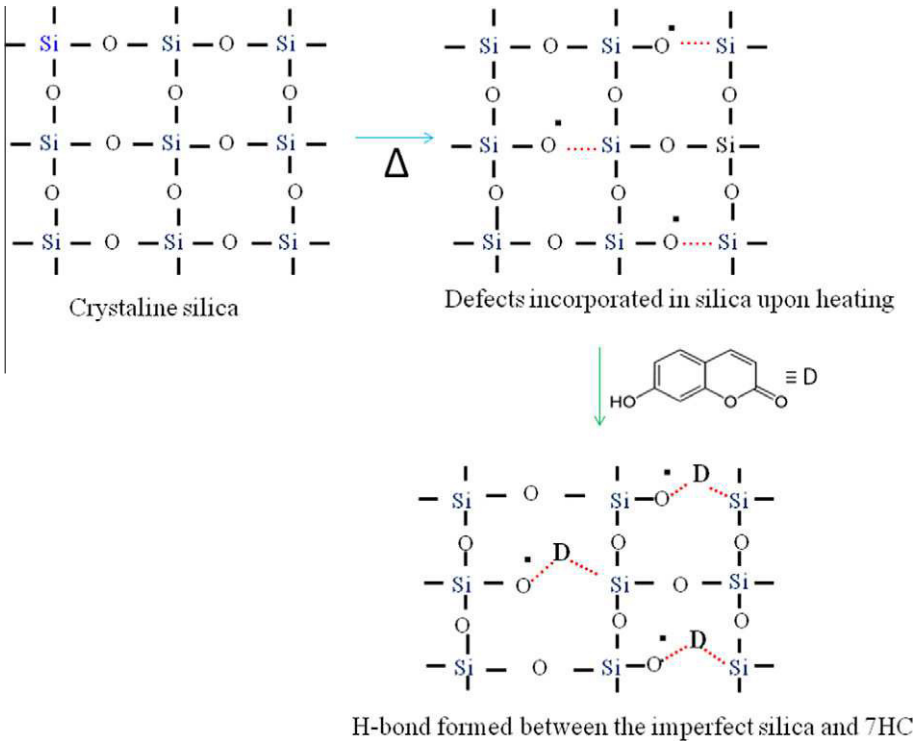

Scheme 1. H-bond formation between the imperfect silica and 7HC.

$$\frac{F_0}{F} = 1 + K_{sv}[Q] \quad (1)$$

where, F_0 and F are the fluorescence intensities of 7HC in the absence and presence of quencher, Q; [Q] = Quencher concentration. Had there been a quenching of 7HC by Ludox®, the plot of F_0/F vs [Q] would be a straight line, which was not observed in the present case.

Infrared spectroscopic study

The IR spectral band of water in the OH stretching frequency region (~3100 to 3750 cm^{-1}) is usually very broad and structureless due to the continuum water structures with varying hydrogen bond strength. Anticipating that neat water, therefore, may not provide precise information of the dynamics of water via conventional IR spectroscopy, dilute water is employed for measurement in the present study. Assuming the concentration of neat water to be 55.5 M, sufficient amount of CH_3CN was added to water to make it 1.0 M because under this condition, water molecules are mostly solvated by CH_3CN and no water aggregates (even low order aggregates) are present [47]. Fig. 5 shows the IR spectra of 7HC (1.0 M) and water (1.0 M) in CH_3CN on CaF_2 plates. The peaks corresponding to the vibration of OH symmetric stretching of the weakly hydrogen bonded (3542 cm^{-1}) and nonbonded (3627 cm^{-1}) species of 7HC with CH_3CN are resolved. These peaks are exactly superimposed on the peaks of dilute water (1.0 M) in CH_3CN as observed previously (not shown here) [47]. On the other hand, Ludox® in dilute water yields a broad OH stretching band at 3602 cm^{-1}. The IR spectra of the mixture of 7HC (1.0 M), water (1.0 M) and SiO_2 (1.0 M) in CH_3CN is interesting. For the quantitative evaluation,

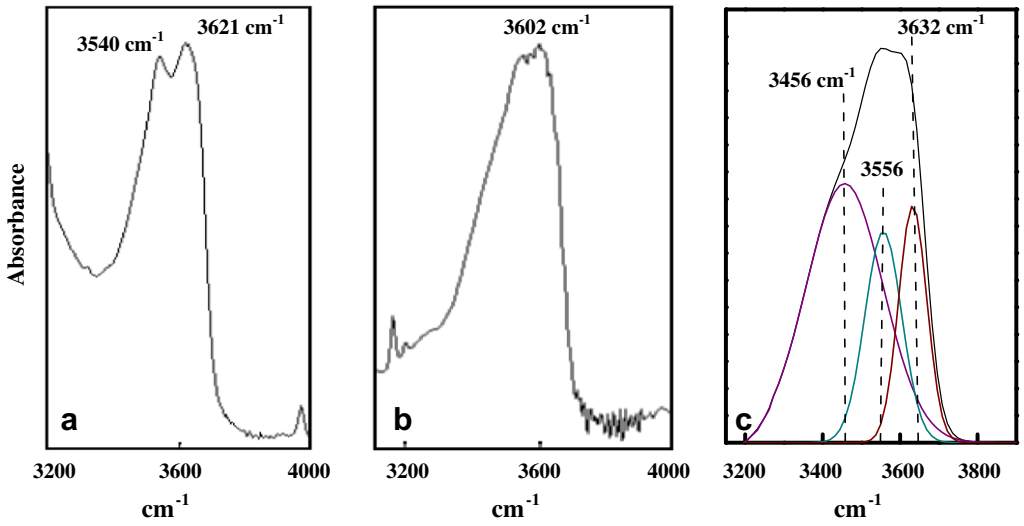

Fig. 5. (a) IR spectra of 7-HC (1.0 M) and H_2O (1.0 M) in acetonitrile, (b) IR spectra of SiO_2 (1.0 M) and H_2O (1.0 M) in acetonitrile, (c) IR spectra of 7-HC (1.0 M), H_2O (1.0 M) and SiO_2 (1.0 M) in acetonitrile and Gaussian components from least squares fitting.

the spectra are deconvoluted into Gaussian profiles, which clearly yield three peaks at 3456 cm^{-1}, 3556 cm^{-1} and 3632 cm^{-1}, respectively [48]. It seems apparent that both the components of the OH stretching mode of 7HC are only slightly shifted to 3556 cm^{-1} and 3632 cm^{-1}, respectively, while that of the hydrated silica is blue shifted to a great extent and resonate at 3456 cm^{-1}. This shows that silica–OH donates proton to the OH oxygen of 7HC acceptor site in forming strong hydrogen bond between the two [49]. However, to make final conclusion on the morphology of Ludox® in the absence and presence of 7HC through electron microscopic measurements are narrated. Besides, the adsorption kinetics of 7HC over silica surface, as measured by quartz crystal micro balance (QCM) studies would further highlight the detailed mechanism. These above mentioned components are considered to be the future perspectives of the present work.

Summary and conclusions

Physico-chemical studies on the interactions of the imperfect nanocolloidal dispersion of silica (Ludox®) with 7HC have been undertaken with the aid of electronic absorption, emission and vibrational spectroscopic measurements. While the absorption and emission intensities of 7HC were increased with increasing dye concentration in the range of 0–20 μM, the enhancement of fluorescence intensity is brought about at the low concentration of silica. This enhancement of the fluorescence intensity of 7HC has been related to the strengthening of excited state H-bonds formed between Ludox® and 7HC. It may be noted that the radiationless deactivation can dramatically influence the regulation of electronic states by H-bonding interactions and the fluorescence of chromophores in H-bonded surroundings may be quenched or enhanced by H-bonds [50]. At high concentration range of silica, strong and irregular adsorption of 7HC onto silica surface led to a red shift in the absorption spectra. The intermolecular fluorescence quenching, under the prevailing condition, is governed by the Homo Förster resonance energy transfer formalism. The size of the colloidal dispersion was independent of the concentration of silica and 7HC. Due to the stacking of dye molecules onto silica surface, negative zeta potential values of Ludox® was suppressed compared to the systems without the dye. The adsorption kinetics of 7HC over silica surface, as measured by quartz crystal microbalance (QCM) studies would further highlight the detail mechanism. Besides, Raman spectroscopic studies are considered to more informative in understanding the exact nature of H-bonding between Ludox® and 7HC in aqueous medium. These components are considered to be the future perspectives of the present work.

Acknowledgements

The work has been financially supported by the Department of Science and Technology, Govt. of India. M.C. acknowledges the receipt of INSPIRE Fellowship from DST.

References

[1] F.F. Michalet, L.A. Pinaud, J.M. Bentolila, S. Tsay, J.J. Doose, G. Li, A.M. Sundaresan, S.S. Wu, S. Gambhir, Weiss, Science 28 (2005) 538–544.
[2] A.L. Wong, M.L. Hunnicutt, J.M. Harris, Anal. Chem. 63 (1991) 1076–1081.
[3] A. Emmerling, R. Petricevic, A. Beck, P. Wang, H. Scheller, J. Fricke, J. Non-Cryst. Solids 185 (1995) 240–248.
[4] X. Zhao, R.P. Bagwe, W. Tan, Adv. Mater. 16 (2004) 173–176.
[5] T.P. Goloub, L.K. Koopal, B.H. Bijsterbosch, M.P. Sidorova, Langmuir 12 (1996) 3188–3194.
[6] S. Bonacchi, D. Genovese, R. Juris, M. Montalti, L. Prodi, E. Rampazzo, M. Sgarzi, N. Zaccheroni, Top. Curr. Chem. 300 (2011) 93–138.
[7] G. Chen, F. Song, X. Wang, S. Sun, J. Fan, X. Peng, Dyes Pigments 93 (2012) 1532–1537.
[8] S.K. Parida, S. Dash, S. Patel, B.K. Mishra, Adv. Colloid Interface Sci. 121 (2006) 77–110.
[9] X. Wang, O. Ramstrom, M. Yan, Chem. Commun. 47 (2011) 4261–4263.
[10] K. Viswanathan, Colloids Surf. A. 386 (2011) 11–15.
[11] S.W. Ha, C.E. Camalier, G.R. Beck Jr, J.K. Lee, Chem. Commun. (2009) 2881–2883.
[12] J.F. Bringley, T.L. Penner, R. Wang, J.F. Harder, W.J. Harrison, L. Buonemani, J. Colloid Interface Sci. 320 (2008) 132–139.
[13] V.V. Konovalova, M.T. Bryk, R.R. Nigmatullin, P.I. Gvozdyak, O.F. Udilova, Bioprocess Biosystem Eng. 23 (2000) 651–656.
[14] A. Lepp, O. Siiman, J. Phys. Chem. 89 (1985) 3494–3502.
[15] E. Bae, W. Choi, Environ. Sci. Technol. 37 (2003) 147–152.
[16] I.M. Arabatzis, T. Stergiopoulos, D. Andreeva, S. Kitova, S.G. Neophytides, P. Falaras, J. Catal. 220 (2003) 127–135.
[17] J.Th.G. Overbeek, Adv. Colloid Interface Sci. 15 (1982) 251–277.
[18] M.M. Collinson, N. Moore, P.N. Deepa, M. Kanungo, Langmuir 19 (2003) 7669–7672.
[19] S. Han, K.T. Lee, S.M. Oh, T. Hyeon, Carbon 41 (2003) 1049–1056.
[20] M. Liong, J. Lu, M. Kovochich, T. Xia, S.G. Ruehm, A.E. Nel, F. Tamanoi, J.I. Zink, ACS Nano 2 (2008) 889–896.
[21] S.W. Keller, S.A. Johnson, E.S. Brigham, E.H. Yonemoto, T.E. Mallouk, J. Am. Chem. Soc. 117 (1995) 12879–12880.
[22] R.A. Caruso, A. Susha, F. Caruso, Chem. Mater. 13 (2001) 400–409.
[23] J.F. Vasconcelos, M.M. Teixeira, J.M. Barbosa-Filho, M.F. Agra, X.P. Nunes, A.M. Giulietti, R. Ribeiro-dos-Santos, M.B.P. Soares, Eur. J. Pharmacol. 609 (2009) 126–131.
[24] B. Ramesh, K.V. Pugalendi, J. Med. Food 9 (2006) 562–566.
[25] J. Hoult, M. Paya, Gen. Pharmacol. 27 (1996) 713–722.
[26] A.C. Giese, E. Christensen, J. Jeppson, J. Am. Pharm. Assoc. 39 (1950) 30–36.
[27] C. Párkányi, M.S. Antonious, J.-J. Aaron, M. Buna, A. Tine, L. Cissá, Spectrosc. Lett. 27 (1994) 439–449.
[28] Y. Hu, C. Yuan, J. Mater. Sci. Technol. 22 (2006) 239–244.
[29] E. Paulsen, A. Otkjær, K.E. Andersen, Contact Dermatitis 62 (2010) 338–342.
[30] S. Kumar, V.C. Rao, R.C. Rastogi, Spectrochim. Acta A. 57 (2001) 41–47.
[31] A. Krysztafkiewicz, S. Binkowski, T. Jesionowski, Appl. Surf. Sci. 199 (2002) 31–39.
[32] P.V. Messina, P.C. Schulz, J. Colloid Interface Sci. 299 (2006) 305–320.
[33] A.R. Cestari, E.F.S. Vieira, G.S. Vieira, L.E. Almeida, J. Colloid Interface Sci. 309 (2007) 402–411.
[34] T.Z. Ren, Z.Y. Yuan, B.L. Su, Colloids Surf. A. 300 (2007) 79–87.
[35] S. Sharma, D. Mohan, N. Singh, M. Sharma, A.K. Sharma, J. Light Elec. Optic 121 (2010) 11–18.
[36] A. Cardelli, L. Ricci, G. Ruggeri, S. Borsacchi, M. Geppi, Eur. Polym. J. 47 (2011) 1589–1600.
[37] C.G. Colombano, O.E. Troccoli, Anal. Chem. 57 (1985) 1907–1910.
[38] S. Banerjee, A. Datta, Langmuir 26 (2009) 1172–1176.
[39] Y.D. Glinka, S.-H. Lin, Y.-T. Chen, Appl. Phys. Lett. 75 (1999) 778–780.
[40] Q. Geng, W. Cui, Ind. Eng. Chem. Res. 49 (2010) 11321–11330.
[41] Z. Li, S.C. Rutan, Anal. Chim. Acta 312 (1995) 127–139.
[42] C. McDonagh, O. Stranik, R. Nooney, B.D. MacCraith, Nanomedicine-UK 4 (2009) 645–656.
[43] R.I. Nooney, C.M.N. McCahey, O. Stranik, X.L. Guevel, C. McDonagh, B.D. MacCraith, Anal. Bioanal. Chem. 393 (2009) 1143–1149.
[44] E. Herz, A. Burns, D. Bonner, U. Wiesner, Macromol Rapid Comm. 30 (2009) 1907–1910.
[45] J.B. Pawley, in: Handbook of Biological Confocal Microscopy, third ed., Springer, NY, 2006.
[46] M. Chakraborty, A.K. Panda, Spectrochim. Acta A 81 (2011) 458–465.
[47] V.A. Sirotkin, B.N. Solomonov, D.A. Faizullin, V.D. Fedotov, J. Struct. Chem. 41 (2000) 997–1003.
[48] S.K. Mehta, G. Kaur, R. Mutneja, K.K. Bhasin, J. Colloid Interface Sci. 338 (2009) 542–549.
[49] J. Joseph, E.D. Jemmis, J. Am. Chem. Soc. 129 (2007) 4620–4632.
[50] G.-J. Zhao, K.-L. Han, Accounts Chem. Res. 45 (2011) 404–413.

Langmuir

Article

pubs.acs.org/Langmuir

Surfactant-Assisted Synthesis and Characterization of Stable Silver Bromide Nanoparticles in Aqueous Media

Moumita Chakraborty,[†] Fang-Wei Hsiao,[‡] Bappaditya Naskar,[§] Chien-Hsiang Chang,[‡] and Amiya Kumar Panda*,[†]

[†]Department of Chemistry, University of North Bengal, Darjeeling 734 013, W.B., India

[‡]Department of Chemical Engineering, National Cheng Kung University, Tainan 701,Taiwan

[§]Centre for Surface Science, Department of Chemistry, Jadavpur University, Kolkata 700 032, W.B., India

Supporting Information

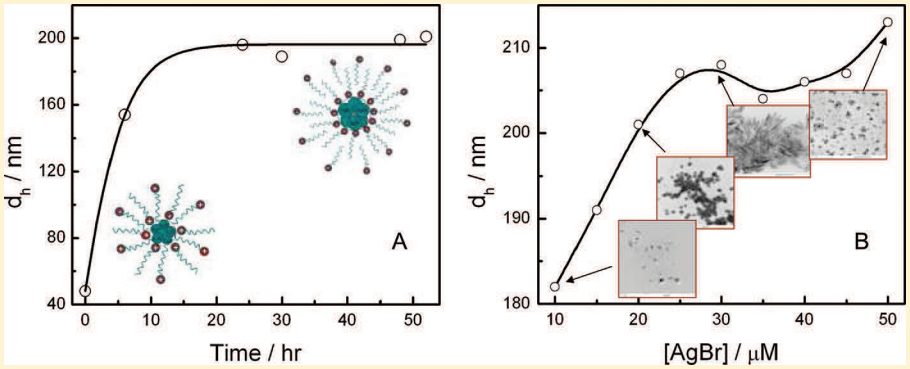

ABSTRACT: Colloidal dispersions of silver bromide (AgBr) in aqueous surfactant medium have been prepared using a surfactant-assisted synthesis approach with hexadecyltrimethylammonium bromide (CTAB). The surfactant acts both as source of bromide ion as well as the stabilizing agent. Upon progressive addition of silver nitrate to aqueous CTAB solution, stable AgBr dispersions were obtained. Formation of surfactant cation (CTA^+) stabilized AgBr was confirmed by way of XRD, FTIR and NMR studies. Thermal behavior of the isolated nanoparticles was investigated by differential scanning calorimetry (DSC) and thermal gravimetric analysis (TGA), where the occurrence of phase transition in the surfactant-stabilized nanoparticles was observed. Kinetics of the particle growth was investigated by dynamic light scattering measurements, which predicted the formation of surfactant bilayered structures associated with the nanoparticles of AgBr. Band gap of the nanoparticles was determined by suitably analyzing the UV−visible spectral data, which concluded that the particles behaved like insulators. Morphology of the particles, studied by TEM measurements, was found to be spherical. Finally, enthalpy of formation of surfactant-stabilized AgBr, determined calorimetrically, was found to be dependent on the concentration of the precursors.

INTRODUCTION

Because of their fascinating properties and multifaceted application potentials, research interests in the physicochemical investigations on synthesis and characterizations of nanoparticles are ever increasing since last few decades.[1−3] Nanoparticles find applications in various fields, viz., semiconductor,[4−7] superconductor,[8−12] magnetic materials,[13,14] opto-electronic devices,[7,15−17] catalysts,[18−20] paint,[21,22] electrochemistry,[1−3,23] biomedical devices,[24,25] etc. As the nanomaterials have larger surface area than the bulk material, they become more reactive. The nanoparticles can be considered as a bridge between the bulk material and atomic/molecular entities.[26]

There has been a significant increase in the synthesis and characterization of silver halide (AgX) nanoparticles due to their specific properties.[1−3] Silver halides are being used as photographic material for a long time.[1,12,24,27] According to Sambhy et al.,[24] AgBr nanoparticles have microbicidal activity. Composite materials of AgCl and poly(methyl methacrylate) can be used as separation membranes.[27] Because of their high conductivity, AgX are used as solid ionic conductors.[28] However, the most important property of silver halides is their enhanced band gap emission in the nano range compared to the bulk material.[29] Besides the aforementioned properties silver halides are also used as catalysts.[30−32] Taking into account of different application potentials of nanoparticles of AgX, it is worth pursuing to study the convenient ways to prepare a stable dispersion of AgX. It has been reported that when present in pure crystalline form, silver halide salts are unstable.[33] Detailed mechanism for the degradation of Ag^+ ions into metallic silver has been explained by Proudfoot.[34] However, if AgX salts are in a dispersed state, they become

Received: February 11, 2012
Revised: March 28, 2012
Published: April 18, 2012

   dx.doi.org/10.1021/la300615b | *Langmuir* 2012, 28, 7282−7290

stable.[31] This has motivated the authors to undertake the investigations on the synthesis and characterization of colloidal silver bromide in aqueous surfactant medium. It has been reported by Lahtinen et al.[35] that quaternary ammonium ion comprising a long hydrocarbon chain could stabilize the synthesized AgBr nanoparticle with a protective coating. Hexadecyltrimethylammonium bromide (CTAB) is one of the cationic surfactants that has been used by many researchers as stabilizers or templates for the synthesis of various novel materials.[1−3,36] Sui et al.[2,3] have used CTAB as a stabilizer in preparing positively charged silver nanoparticles. Chen et al.[37] have used CTAB as a stabilizer, where seed mediated growth of silver nanodisks in aqueous media has been reported. Reports of Sui et al.[2,3] and Nikhoobakt et al.[38] have suggested that CTAB could act as a passivating agent in stabilizing the colloidal nanoparticles. Likewise, Liu et al.[1] have proposed that hexadecyltrimethylammonium ion could form a bilayer like structure around colloidal AgBr particles, which was very much mimetic to vesicles.

Because of the manifold applications of AgBr nanoparticles, a number of reports are available in the literature.[24,31,33,39−41] He et al.[41] have prepared novel layered AgBr-based nanocomposite stabilized by CTAB. Lahtinen et al.[35] have reported the preparation of surfactant monolayer protected silver bromide nanoparticles. Bai et al.[42] have prepared and characterized AgBr nanoparticles in poly(vinylpyrrolidone) matrix. Photocatalytic activity of the synthesized AgBr nanoparticles as polymer composites has been reported by different authors.[33,43] Preparation of AgBr nanoparticles has also been reported in water-in-oil microemulsion media by Husein et al.[39] They have prepared AgBr nanoparticles in water-in-oil microemulsion where the existence of bulk water was possible for which the nanoparticles got precipitated in that water pool. In their case, basically formation of AgBr nanoparticles occurred in the confined water pool of water-in-oil microemulsion. However, in the present case, our proposition is different. We believe that AgBr nanoparticles are formed in aqueous medium first which then get stabilized by surfactant monolayers/bilayers. However, in all the cases, the wide applications of AgBr were not convenient because of the limited stability of AgBr nanoparticles as colloidal dispersions. Moreover, reports on the use of AgBr nanoparticles in the dilute concentration range (of the order of milli to micromolar) are not plenty in literature.

As already mentioned, although AgBr nanoparticles have many application potentials, it is difficult to obtain stable colloidal dispersions of AgBr, especially in the aqueous medium.

In this paper, the synthesis and characterization of colloidal dispersions of silver bromide using a very simple but novel approach are reported. Upon progressive addition of silver nitrate to aqueous CTAB solution, colloidal dispersions of AgBr are formed in the aqueous medium. The surfactant acts both as a stabilizing agent as well as the source for bromide ion. The colloidal dispersions of AgBr were stabilized by the layered structured surfactant cation assemblies. Although there are previous reports on the synthesis and characterization of AgBr nanoparticles, the studies in solution phase are not so common, which are essential for practical purposes. In the present case, the nanocolloidal dispersions of AgBr were found to be stable in the studied concentration range (10^{-6}−10^{-5} M) up to a year. Formation of nanoparticles of AgBr was confirmed by the way of XRD, FTIR, and NMR studies. Band gap of the nanoparticles in the dispersed state was investigated by UV−visible spectral measurements. Growth kinetics of the surfactant-protected nanoparticles (SPN) was studied by dynamic light scattering method. Thermal behavior of SPN was also studied by DSC/TGA analysis. Morphological studies were performed by TEM measurements. Our endeavor was to undertake a simple but novel one-pot synthesis of stable AgBr nanoparticles and its application in aqueous media.

EXPERIMENTAL SECTION

Materials. The cationic surfactant hexadecyltrimethylammonium bromide (CTAB) was a product from Sigma-Aldrich, USA. The surfactant was stated to be >99% pure and was used as such. A.R grade silver nitrate ($AgNO_3$) was purchased from SD. Fine Chemical Ltd., India. All the chemicals were used as received. Double distilled water with a specific conductance of 2−4 μS cm^{-1} at 298 K was used for preparing the solutions.

Methods. A stock solution of 1 mM $AgNO_3$ was prepared in water with which experimental works were carried out. 5.0 mL of colloidal dispersions of AgBr particles were prepared in 0.4 mM CTAB solution at five different concentrations (10, 20, 30, 40, and 50 μM). Quantitative amount of 1 mM $AgNO_3$ was added in 100 steps with constant stirring to obtain AgBr in the above-mentioned concentrations. It may also be mentioned that we had prepared and studied the AgBr nanoparticles in the concentration range of 10−50 μM with an interval of 5 μM. By the method of trial and error it was found that a 0.4 mM CTAB solution was the optimum concentration in obtaining a stable dispersion of AgBr up to 50 μM (shelf life = 1 year). Above the 0.4 mM concentration there is excess of Br^- ions which would cross the solubility limit and thus failed to stabilize the system despite of large amount of CTAB. On the contrary, there is deficiency of CTA^+ ions to stabilize the system when the concentration of CTAB solution is below 0.4 mM. Henceforth, all the preparations would mean for a 0.4 mM CTAB solution in water. A stock solution of 1 mM CTAB was used for the study.

Surfactant-stabilized nanoparticles of AgBr were isolated in two ways. First, the method of Liu et al.[1] was adapted to isolate AgBr from its aqueous dispersion. A 10 mL 20 mM aqueous $AgNO_3$ solution was added dropwise to 100 mL 6 mM CTAB solution under rigorous stirring and the dispersion thereby obtained, which was not as stable as the aforesaid preparation (stable up to 2 h), was centrifuged at 10000 rpm and the sediment was washed with water. It was then vacuum-dried at 80 °C. This isolate was termed as "aqueous extract". In another method, surfactant-stabilized AgBr colloidal dispersion was extracted into chloroform layer and then the organic layer was dried under vacuum. The second category was termed as "chloroform extract". XRD, FTIR, DSC, and TGA analyses were done on both the extracts.

The diffraction patterns of the isolated nanoparticles and the precursors were recorded in a RINT 2000, Rigaku diffractometer (Japan) using Cu$K\alpha_1$ (0.15418 nm) radiation operated at 40 kV and 40 mA in the range of 5° to 70° at the rate of 3°/min. The FTIR spectral data were recorded in a Shimadzu 8300 FT-IR spectrometer (Japan) by taking the samples in the form of KBr pellets using standard procedure.[1] ^{1}H NMR spectra were recorded in a 300 MHz FT-NMR by Bruker-Advance (5 mm BBO Probe) spectrometer (Switzerland) using tetramethylsilane (TMS) as an internal standard. The conductance measurements were undertaken by Eutech Instruments con 510 conductivity/TDS/°C/°F meter. The UV−visible absorption spectra were recorded on a UVD-2950 spectrophotometer (Labomed Inc., USA) using a matched pair of quartz cuvette of 1 cm path length. Size of nanoparticles was determined by dynamic light scattering method using a dynamic light scattering spectrometer Nano ZS 90 (Malvern, U.K.). A He−Ne laser of 632.8 nm wavelength was used and the data were recorded at a scattering angle of 90°. Samples were filtered using Millipore hydrophobic membrane filter of 0.25 μm pore size. Thermal gravimetric analysis (TGA) of the isolated nanoparticles as well as CTAB was carried out on Mettler H10, Neo-Pharma Instruments Corp. from 50 to 325 °C and the differential scanning calorimetry (DSC) measurements were done on Pyris 6 DSC

dx.doi.org/10.1021/la300615b | Langmuir 2012, 28, 7282−7290

(Perkin-Elmer, USA). The samples were heated at a rate of 10 °C/min from 50 to 140 °C and the cooling was done at 5 °C/min. The instrument was calibrated with Indium before each experiment. The enthalpy changes for the formation of nanoparticles were measured in an OMEGA isothermal titration calorimeter (ITC) (Microcal Inc., Northampton, MA, USA). 1.8 and 1.325 mL CTAB solutions were taken in the reference and reaction cell, respectively. In the ITC experiment, enthalpy change associated with the interaction process was calculated under constant temperature accurately within 0.01 °C. As prepared samples of AgBr nanoparticles in surfactant medium were used for morphological studies by TEM. TEM images were recorded with an H-7500, transmission electron microscope (Hitachi, Japan), with an acceleration voltage of 80 kV. A drop of nanocolloidal dispersion of AgBr was dried on carbon-coated copper grid using the standard procedure.[3]

RESULTS AND DISCUSSION

X-ray Diffraction Studies. Characteristic X-ray diffraction patterns of CTA^+-stabilized AgBr nanoparticles, isolated in two different ways, along with the precursors CTAB and $AgNO_3$ are shown in Figure 1. X-ray diffractograms of CTAB and

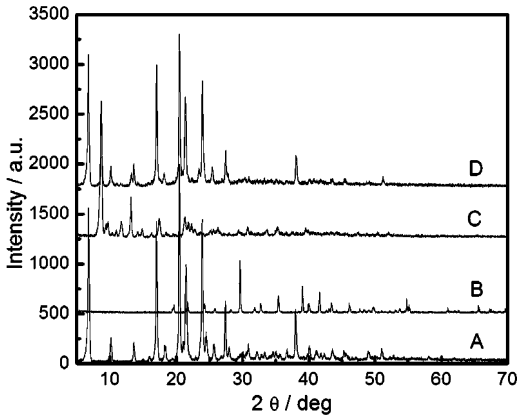

Figure 1. XRD patterns of (A) CTAB, (B) silver nitrate, (C) CTA^+-coated silver bromide nanoparticles isolated from water and (D) CTA^+-coated silver bromide nanoparticles isolated using chloroform.

chloroform extracted CTA^+-stabilized AgBr bear the same features. Aqueous extract exhibited differences, although not so significantly. Pure CTAB bearing higher crystalinity exhibited sharp and intense peaks at 2θ values of 10.1, 13.4, 18.2, 20.3, 21.4, 23.9, 27.4, 30.8, and 38.1 degrees, respectively. Nanoparticles extracted by two different methods did not exhibit any characteristic peak for $AgNO_3$. This suggests the complete conversion of $AgNO_3$ to AgBr, which was not unexpected. Maximum concentration of added $AgNO_3$ was 50 μM in presence of 0.4 mM CTAB. Therefore, it could be expected that all the Ag^+ ions would be in the form of AgBr. Diffractograms of the nanoparticles isolated directly from aqueous media did not exhibit distinct, specific and intense peak for AgBr. The less intense diffractograms of any nanoparticle is not uncommon.[1,24,44] Particles in the nanodimensions are less crystalline and hence their X-ray diffractograms have fewer features than the corresponding bulk materials.[26] Additionally, formation of lesser amount of AgBr compared to the amount of CTAB present resulted in the masking of AgBr diffractograms by CTAB. CTA^+-coated AgBr nanoparticles exhibited its characteristic peaks at 32.0, 49.0, and 67.5 deg, respectively. The results mildly deviated from the reported values[24,31,42] which is possibly due to the differences in the experimental conditions. In the present case, while obtaining the representative peaks for AgBr nanoparticles, we performed the analysis by expanding the corresponding zones. Individually expanded zones are presented in the supplementary section (Figure S1, Supporting Information). The interplanar distances corresponding to the above-mentioned peaks were 2.9, 2.0, and 1.7 Å respectively. Corresponding crystal planes (*hkl*) were (200), (220), and (400) respectively.[42] Results confirmed the formation of crystals bearing the same structure as of cubic face centered bromargyrite (www.webmineral.com/MySQL/xray.php). Formation of AgBr was therefore established from the X-ray analysis.

Fourier Transform Infrared Spectra. In order to further establish the formation of CTA^+-coated AgBr nanoparticles, FTIR spectral measurements were carried out. The representative results are shown in Figure 2. The symmetric and

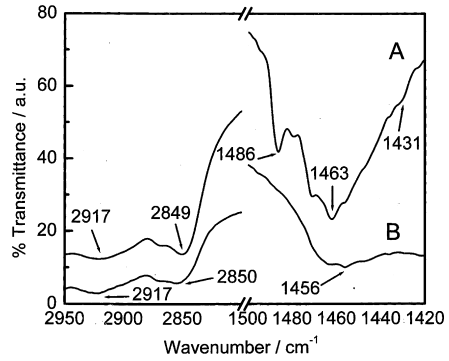

Figure 2. FTIR spectra of (A) pure CTAB and (B) aqueous extract of CTAB-stabilized AgBr nanoparticles.

asymmetric $-(CH_2)-$ vibrations of pure CTAB appear at 2849 and 2917 cm^{-1} respectively. Isolated nanoparticles also bear the same fingerprint, which indicates the direct noninvolvement of hydrocarbon chains in stabilizing the AgBr nanoparticles. The observed peaks at 1486 and 1431 cm^{-1} for pure CTAB were due to the asymmetric and symmetric $-C-H$ vibration of the quarternary ammonium moiety.[1−3] In case of isolated nanoparticles the peak at 1486 cm^{-1} was broadened and shifted to 1456 cm^{-1} and the peak at 1431 cm^{-1} was not present. Results suggest that AgBr clusters influenced the $(CH_3)_3N^+$ vibration.

NMR Spectroscopic Studies. Coating ability of CTA^+ over AgBr clusters was further evidenced through ^1H NMR measurements.[3,45−47] Spectral data of NMR studies are summarized in Table 1 and spectra are shown in Figure S2, Supporting Information. Peaks for pure CTAB appeared as follows: δ = 3.6 ppm (α-CH_2-), δ = 3.47 ppm ($(CH_3)_3N^+$), δ = 1.8 ppm (β-CH_2-), δ = 1.36 ppm (γ-CH_2-), δ = 1.25 ppm ($-(CH_2)_n-$) and at δ = 0.88 ppm (terminal $-CH_3$). For surfactant-stabilized nanoparticles, no shift in the terminal $-CH_3$ and $-(CH_2)_n-$ protons occurred, which indicates that AgBr clusters could not perturb the terminal $-CH_3$ protons. All the other proton signals were down shifted (approximately 0.13 ppm) indicating the partial attachment of the surfactant headgroup to AgBr nanoparticle.[3,45−47]

Conductometric Titration. Conductometric titration of an aqueous solution of 0.4 mM CTAB by $AgNO_3$ is graphically presented in Figure S3, Supporting Information. Similar titration with 0.4 mM KBr is also shown for comparison. With the progressive addition of silver nitrate into the aqueous KBr solution, conductivity monotonously decreased. After the neutralization point, a further increase in conductance was

dx.doi.org/10.1021/la300615b | Langmuir 2012, 28, 7282−7290

Table 1. ^{1}HNMR Data of CTAB and CTA^+-Coated AgBr Nanoparticles[a]

system	terminal-CH_3	$-(CH_2)-_n$	γ-$(CH_2)-$	β-$(CH_2)-$	$(CH_3)_3N^+-CH_2-$
CTAB	0.88 (3H, m)	1.26 (24H, s)	1.36 (2H, s)	1.8 (2H, br)	3.47–3.6 (11H, m)
aqueous extract of CTA^+-coated AgBr	0.88 (3H, m)	1.26 (24H, s)	1.36 (2H, s)	1.76 (2H, br)	3.46–3.54 (11H, m)
$CHCl_3$ extract of CTA^+-coated AgBr	0.88 (3H, m)	1.25 (24H, s)	1.34 (2H, s)	1.76 (2H, br)	3.38–3.47 (11H, m)

[a]Here, s, m and br, s denote singlet, multiplet, and broad singlet. $CDCl_3$ was used as solvent.

noted. When $AgNO_3$ solution was progressively added to KBr solution, instantaneous formation of AgBr particles occurred which remained as suspension. Usually, such titration leads to the replacement of Br^- ions with the NO_3^- ions alongwith the formation of insoluble component, AgBr. Conductivity of NO_3^- ions is almost similar to that of Br^- ions.[48] Therefore, there should not be any significant change in the conductance before the neutralization point. However, suspended AgBr colloids might hinder the mobility of the ions present in solution, which ultimately led to the decrease in conductance.

Conductance profile for CTAB solution followed the similar trend, although to lesser extent. The appearance of neutralization point at a lower concentration and also lesser conductance in the preneutralization point, compared to KBr, was not unexpected. CTA^+ ions are involved in stabilizing the AgBr nanoparticles in the form of layers (to be discussed in detail later on). The conductivity of CTA^+ ions is less compared to the K^+ ions. Therefore, the conductometric titration curves for CTAB would always maintain a lower profile than KBr. According to Almgren and Rydholm,[49] CTAB micelles have much higher surface charge and hence a larger electric field for which Br^- ions can bind strongly as counterions to the micelles. Subsequently, the average mobility of the ionic species is decreased. In the previously published report,[2] surfactant ions could stabilize the nanoparticles through the formation of bilayer structures around them. Br^- ions would thus act as counterions, which lessen their availability compared to KBr solution of identical strength. However, it is to be mentioned that due to the formation of vesicle like entities the fraction of counterion dissociation would be higher compared to the CTAB micelles.

UV–Visible Spectroscopy. UV–visible spectra of colloidal AgBr, dispersed and stabilized in/by aqueous CTAB solution, were recorded in the range 200–350 nm at different concentrations of AgBr (viz., 10, 20, 30, 40, and 50 μM, some of which are shown in Figure 3). Colloidal dispersions exhibited a strong and intense peak at 212 nm against CTAB as blank. Absorbance at 212 nm increased with increasing AgBr concentration. The peak at 212 nm corresponds to the absorption of CTA^+-coated AgBr in aqueous solution. Increase in intensity with increasing AgBr concentration implies the accumulation of CTA^+ around AgBr nanoparticles. Results clearly indicate the clustering of the surfactant molecules which eventually stabilizes the nanoparticles. The exact orientation of surfactant molecules around AgBr nanoparticles will be discussed later on. Although not so sharp, another faint shoulder appeared at 270 nm which corresponds to AgBr nanoparticles.[1,39] The shoulder at 270 nm appeared faint in comparison to previously published reports[1,39] because in the present case lower concentrations were used. It is also to be mentioned that pure AgBr in bulk state or in its vapor state appears light green.[50] However, in the present case we have failed to detect the corresponding peak in the visible region as the concentration of AgBr was in the micromolar range. Besides, the existence of larger amount of CTAB could have masked the greenish appearance of AgBr. The stabilizing agent, CTAB also protects the AgBr colloids from reduction to Ag metals, which is otherwise common for silver halides in their bulk state.

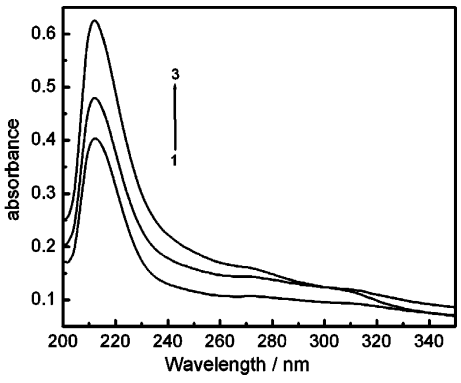

Figure 3. UV–visible absorption spectra of CTA^+-coated AgBr nanoparticles in aqueous medium at 25 °C. Concentrations of AgBr [in μM]: (1) 20, (2) 30, and (3) 50. A 0.4 mM CTAB solution was used as blank.

The absorbance-concentration profile at 212 nm obeyed Beer's law and the molar absorption coefficient of CTA^+-stabilized AgBr was found to be 6.88×10^{-3} $M^{-1}cm^{-1}$ at 212 nm. Such kind of report for AgBr is not available in the literature. The spectral data were further analyzed to determine the optical band gap (ε_g) of CTA^+-stabilized AgBr nanoparticles in aqueous medium using the Tauc relation:[51]

$$(\varepsilon h\nu)^n = C(h\nu - \varepsilon_g) \quad (1)$$

where ε, h, and ν are the molar absorption coefficient, Planck's constant, and frequency of light respectively and C is a constant. The exponent depends on the type of transition for direct allowed transition (here $n = 1/2$). Liu et al.[1] have prepared AgBr nanoparticles using the present approach where the concentration of AgBr was fairly high, for which, the colloidal suspension exhibited peaks in the range 250–320 nm. According to them, the spectra correspond to the direct band gap of AgBr. We also have extended this approach to determine the direct band gap in the range 219–226 nm. From the linear portion of the plot of $(\varepsilon h\nu)^2$ against $h\nu$ (as shown in Figure 4), the band gap was determined from the ratio of the intercept and slope of the linear part. On an average, the band gap was found to be 5.35 eV for a 30 μM AgBr dispersion. With increasing AgBr concentration the band gap decreased, attained a minima at 40 μM AgBr (inset of Figure 4) which again increased up to 50 μM AgBr. Dispersions comprising higher than 60 μM AgBr became unstable. For bulk AgBr, the reported direct band gap is 4.29 eV.[52] Higher band gap value for AgBr nanoparticles was attributed to the size confinement effect. It is not unexpected for the band gap to increase with the decrease in particle size.[51] The decrease in band gap with increasing AgBr concentration was due to the formation of larger particles.

dx.doi.org/10.1021/la300615b | Langmuir 2012, 28, 7282–7290

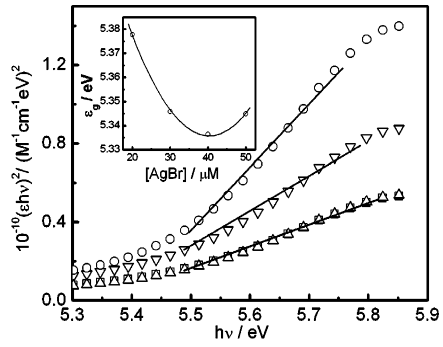

Figure 4. Plot of $(\varepsilon h\upsilon)^2$ vs hυ for the determination of the band gap of silver bromide nanoparticles. Concentrations of AgBr (μM): (○) 20; (▽) 30; (□) 40; (△) 50. Inset: Band gap−silver bromide concentration profile.

After the attainment of 40 μM AgBr concentration, smaller clusters are formed for which a further increase in the band gap occurred.

DLS Studies and ζ Potential Measurements. The kinetics for the growth in particle size as functions of $AgNO_3$ concentration and time were studied by dynamic light scattering method. Also, during the same studies, surface charges of the colloidal dispersions of CTA^+-coated AgBr were investigated through ζ potential measurements. Results are summarized in Figure 5. With the increase in time, particles

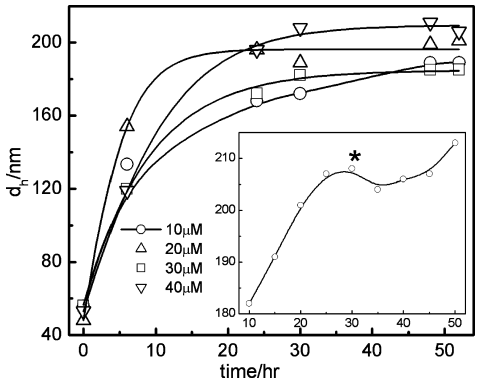

Figure 5. d_h vs time profiles for silver bromide nanoparticles. Inset: d_h vs [AgBr] profile after52 h of the particle formation.

grew up to 24 h and then the size attains constancy. This implies that the growth process is completed within 24 h. Initially the size was around 50 nm. Within 6 h, there occurred a 2-fold increase in size. It is believed that initially randomly oriented CTA^+ ions stabilized the colloidal particles of AgBr through the formation of monolayer, in the manner as shown in the Scheme1A. However, the kind of orientation, as shown in Scheme1A, is not stable from both the thermodynamic and kinetic point of view, for which an enlarged bilayer like structure is formed around the AgBr nanoparticle (shown in Scheme 1B), which becomes stable. The CTA^+ bilayer formation in stabilizing nanoparticles has been reported earlier.[1,2,38] Therefore, the increase in the hydrodynamic diameter of CTA^+-stabilized nanoparticles is a contribution of colloidal growth of AgBr as well as the size enhancement due to the bilayer structure formation. Additionally, the increase in the bilayer density could contribute to the size enhancement of the surfactant-stabilized dispersion of silver bromide. The ζ potential values were found to increase with increasing time which subsequently attained constancy (data not shown to save space). Initially, the nanoparticles were stabilized by surfactant molecules through a monolayer coating with an irregular orientation (as shown in the Scheme 1A), with lower ζ potential value. However, after the bilayer-like structures were formed, the extent of dissociation of the counterions (bromide) increased and hence the ζ potential also increased. When the formation of the bilayer-like structures was completed, the ζ potential values attained constancy (data not shown). The formation of bilayer-like structures would lead to the creation of bigger entities as shown in Scheme 1. Hence, overall charge density would be less compared to the pure micelles. Accordingly, the extent of dissociation would be higher for the bilayer-like entities than the pure micelles of CTAB. As a result, the ζ potential for the bilayer-stabilized nanoparticle system will be higher than the corresponding micellar entities.

The size of the AgBr colloids stabilized by CTA^+ was also found to be dependent on the concentration of $AgNO_3$, as shown in the inset of Figure 5. An increase in the size of the particle was observed up to 25 μM AgBr dispersion, which then decreased mildly, followed by a further linear increase after 45 μM. Precipitation occurred when the final AgBr concentration exceeded 60 μM. It is therefore evident that the optimum concentration to get a stable colloidal dispersion of AgBr in 0.4 mM aqueous CTAB solution is 30 μM as marked with an asterisk in the inset of Figure 5. With increasing concentration of AgBr initially the particles grow bigger with a smaller number of nuclei. This is possible because of the presence of relatively larger amount of stabilizing agent CTAB. When a certain concentration is reached (25−30 μM) formation of a larger number of nuclei of nanoparticles of AgBr supersedes the growth processes. The growth rates of smaller nuclei were thus smaller than the growth rate of AgBr at lower concentration. At lower concentrations, number density of nanoparticles was low; the stabilizing agent was relatively abundant compared to the formed nanoparticles which results in the formation of fairly stable and larger aggregates. When the concentration of AgBr exceeds 40 μM, there would not be enough supply of the stabilizing agent for the growth of so many nuclei, resulting in smaller nanoparticle formation. Hence, number density of nuclei would increase. Subsequently, collision probability and formation of localized clusters would increase.

The rate of the particle growth was evaluated as the rate process followed a first order kinetics. As the concentration of CTAB was much higher than the $AgNO_3$ concentration, use of first order kinetics is justified. The following first order rate expression could therefore be used:[53]

$$t = \frac{2.303}{k} \log \frac{d_f - d_i}{d_f - d_t} \qquad (2)$$

Here t = time, k = first order rate constant, d_i = initial particle size, d_t = particle size at time t, d_f = final particle size.

There was no significant difference in the growth rate for different concentrations of $AgNO_3$. The average rate constant for the particle growth was found to be 5.63×10^{-3} h^{-1}.

DSC−TGA Analysis. Figure 6A denotes the TGA curves for pure CTAB, aqueous and chloroform extracts of CTA^+-stabilized AgBr nanoparticles. For pure CTAB, two weight loss steps were observed at 160−170 and 170−240 °C of 10 and 77%, respectively.[3] The thermal decomposition of aqueous extract of CTA^+-stabilized AgBr was reflected through four

dx.doi.org/10.1021/la300615b | Langmuir 2012, 28, 7282−7290

Scheme 1. Schematic Diagrams for (A) Surfactant Monolayer Protected AgBr NPs and (B) AgBr NPs Stabilized by CTA^+ Bilayer

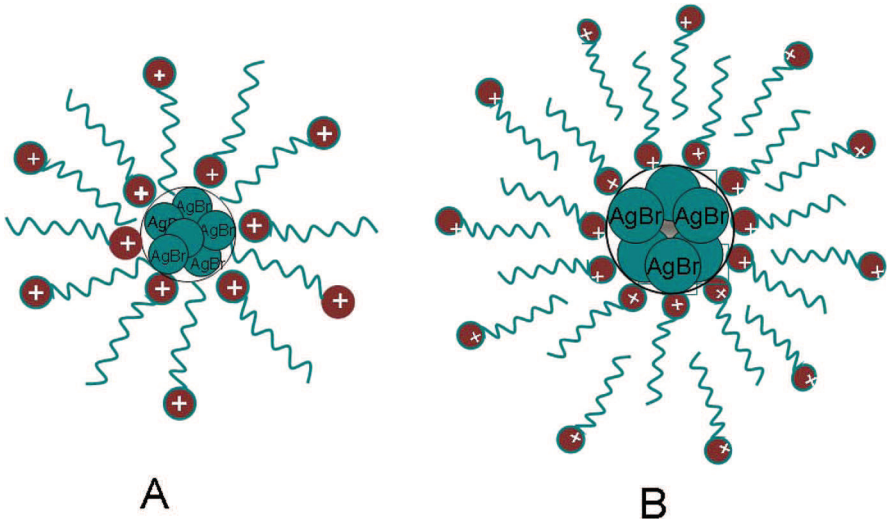

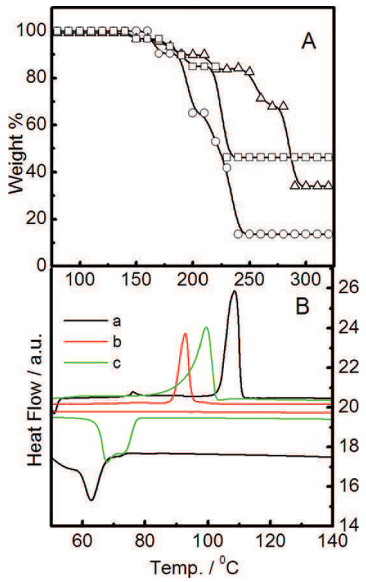

Figure 6. (A) TGA data of pure CTAB (*o*), CTA^+-coated AgBr nanoparticles isolated from water (Δ) and chloroform (□). (B) DSC curves of pure CTAB (a), CTA^+-coated AgBr nanoparticles isolated from water (b) and chloroform (c). Upper curves indicate heating while the lower curves were obtained during cooling.

weight loss steps at 140−190, 190−220, 220−270 and 270−290 °C of 10,6,16 and 24%, respectively. On the contrary, the chloroform extract of CTA^+-coated AgBr was decomposed through two weight loss steps of 15 and 39% at 140−200 and 200−230 °C, respectively. The weight loss for the aqueous extract was higher than that for the corresponding chloroform extract, which was obvious; for the nanoparticles stabilized by bilayered structures, there would be a larger number of surfactant molecules than the corresponding monolayer protected systems (chloroform extract). The weight losses are due to the thermal decomposition of CTAB (150−300 °C)[54] by a self-combustion process.[53] According to Mukherjee et al.[53] and others[55] when CTAB undergoes thermal decomposition there occurs formation of some solid carbon for which the attainment of 0 wt % in TGA analysis was not observed. In case of aqueous extract there is a bilayer of CTA^+ around the AgBr nanoparticles, which makes the system more stable compared to chloroform extract and hence the weight loss takes place at higher temperature. Also, the % weight loss in case of surfactant-coated AgBr nanoparticles was less than pure CTAB. Pure CTAB undergoes thermal decomposition in this range of temperature whereas the surfactant-coated AgBr decomposes at a much higher temperature. The results suggest two different states of CTA^+ around AgBr nanoparticles and the formation of CTA^+ bilayers on the AgBr clusters. The two different states of CTA^+ ion around the AgBr nanoparticles correspond to the two different orientations: first kind includes the CTA^+ ions where the head groups are oriented toward the nanoparticles while for the other, the surfactant head groups are protruding out of the nanoparticles. It is believed that extracting the CTA^+-coated nanoparticles in chloroform eliminates the bilayer structure and the CTAB molecules contributing to the second layer will be collected as part of the solid phase when the chloroform is evaporated.

DSC profiles for heating and cooling of the pure CTAB and isolated nanoparticles in the temperature range of 40−140 °C are shown in Figure 6B. In the studied temperature range, pure CTAB exhibited a sharp endothermic peak at 108 °C, whereas, the endothermic peaks for the aqueous and chloroform extracts appeared at 93 and 100 °C. These endothermic peaks, in the three cases, are not the result of any weight losses. Rather, these very observations attribute to the melting of the ordered regions of hydrocarbon chains in free CTAB and CTA^+ bilayers.[2,56] The AgBr nanoparticles isolated from chloroform showed the endothermic peak in between pure CTAB and aqueous extract. The reason could be the formation of monolayer-protected nanoparticles, which make them more rigid, compared to those isolated from the aqueous media, thereby having a higher melting point than the aqueous extract but lower than pure CTAB. On the other hand, during cooling, only pure CTAB and chloroform extracted nanoparticles exhibited peaks within the temperature range of 60−80 °C.

Isothermal Titration Calorimetry (ITC). Isothermal titration calorimetry has been found to be a very sensitive tool in estimating the enthalpy of formation of nanoparticles. It has previously been reported[53] that when otherwise water

dx.doi.org/10.1021/la300615b | *Langmuir* 2012, 28, 7282−7290

insoluble materials were synthesized in nano dimension using compartmentalized system, the problem of precipitation could easily be avoided. Not many reports are available in literature on these aspects of nanomaterials. Advantage of ITC studies to estimate the formation of nanoparticles at different precursor concentrations lies in the fact that, with suitable processing, the parameters related to the precipitation could easily be avoided. Results of the microcalorimetric titration of aqueous $AgNO_3$ (taken in the syringe against aqueous CTAB solution) for different initial $AgNO_3$ concentrations are shown graphically in Figure 7. It has been observed that with the increasing concentration of AgBr, there is a decrease in the enthalpy change. The decrease is attributed to the formation of a larger number of crystals. ΔH_f vs $[AgNO_3]$ profile was linear in nature. The study was carried out at five different concentrations and then the plot was extrapolated to zero. The enthalpy change for formation of AgBr nanoparticles was thus found to be 13.24 kcal mol^{-1}. The exothermic nature of the reaction is proved by the negative values of the enthalpy change.

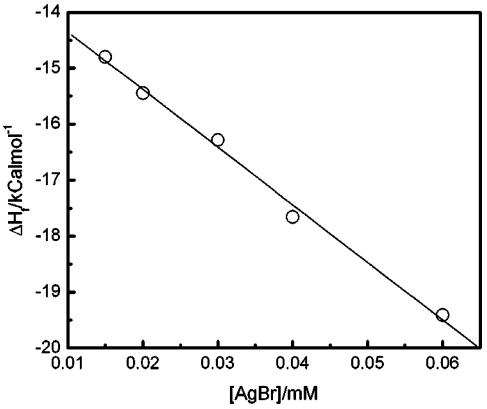

Figure 7. Plot of ΔH_f vs $[AgNO_3]$ for the formation of AgBr in presence of 0.4 mM CTAB solution.

Transmission Electron Microscopy. Representative TEM images of the nanocolloidal dispersions of silver bromide, stabilized by CTAB, are shown in Figure 8. Particle morphology was found to be strongly dependent on the concentration of AgBr. Particles were spherical in shape although in some cases rice grains like morphologies were also observed (at 10 and 30 μM AgBr concentrations). Particles were mostly clustered whereby the size increased with increasing AgBr concentration up to 30 μM, beyond which a decrease in the particle size was again observed. In case of 50 μM AgBr dispersion, smaller particles were found to be clustered. The observation in dynamic light scattering studies was thus further confirmed by TEM studies. It is to be mentioned here that EDX measurements carried out on the same spot exhibited the absence of artifacts.

At very low concentrations of AgBr, particle density was low, as observed in Figure 8A. With increased AgBr concentration, particles grew bigger. However, beyond 30 μM AgBr concentrations, a size constriction effect was observed. When AgBr concentration was sufficiently high, the surfactants failed to provide proper protection. Additionally, with the increased $AgNO_3$ concentration, the rate of AgBr formation became faster. These two combined effects led to the formation of smaller particles in the higher concentration range. Size analysis of Figure 8B reveals the particle to be about 60 nm. The shape of the 30 μM AgBr was like rice grains. As shown in Figure 8E, the particles were clustered together, suggesting their formation following the same mechanism as in Figure 8D, but with a higher rate. The clustering of smaller particles (as in Figure 8E)

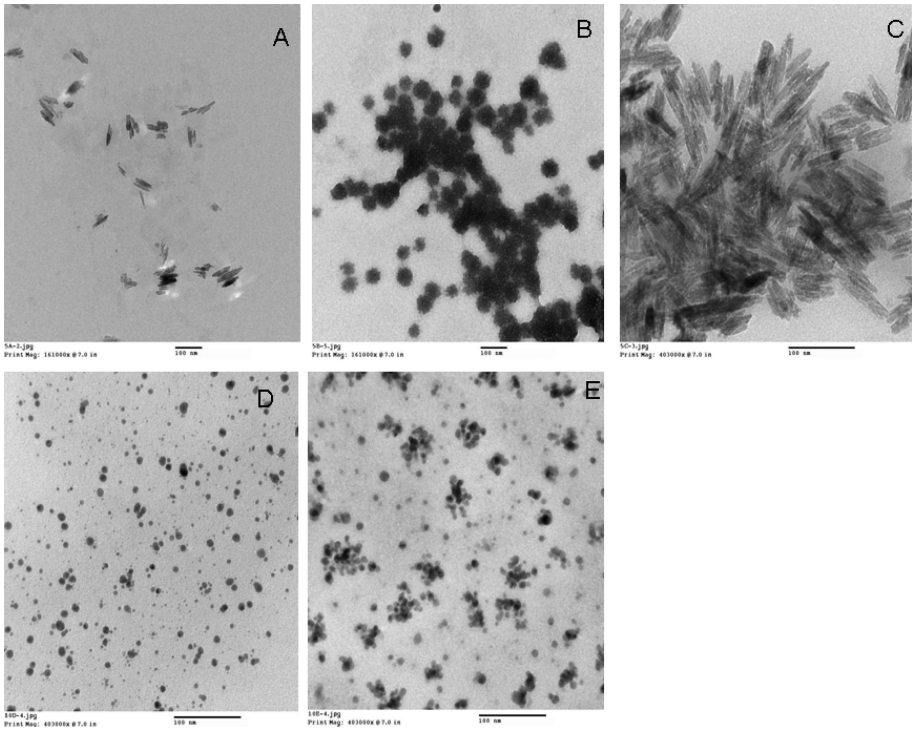

Figure 8. TEM images of different concentrations: *A* = 10 μM, *B* = 20 μM, *C* = 30 μM, *D* = 40 μM and *E* = 50 μM of silver bromide nanoparticles. Scale bars: 100 nm.

dx.doi.org/10.1021/la300615b | *Langmuir* 2012, 28, 7282−7290

was due to the process of Ostwald ripening. When the samples were irradiated with high energy electron beam some Ag^+ ions could have been reduced to Ag^0. However, this reduction did not lead to any significant morphological changes. In the present case, chances of decomposition of AgBr by electron beam radiation are less, as AgBr particles enjoy additional protection from the surfactant bilayer-like entity. Similar method of TEM measurements has previously been reported by Liu et al.[1] However, it is noteworthy that the morphological characterization by low energy SEM would have been more reliable, which is considered as the future perspective.

CONCLUSIONS

Surfactant-stabilized colloidal dispersions of AgBr have been prepared and characterized. The optimum concentration of CTAB used was 0.4 mM. To obtain the stable colloidal dispersions, the molar ratio of $AgNO_3$ to CTAB was maintained in the range of 1:40−1:8. The formation of the nanocolloidal dispersions has been supported by the conductometric and the calorimetric studies. The formation process was found to be exothermic in nature. The complete conversion of $AgNO_3$ to AgBr has been established from the XRD measurements. Formation of CTA^+-coated AgBr nanoparticles was established from XRD, TEM, FTIR, NMR and UV−visible spectral studies. The DSC−TGA analysis confirms two different states of CTA^+ around AgBr nanoparticles and the formation of the CTA^+ bilayer like structure was thus ensured. The formation of the bilayer like structure was further confirmed from the DLS results, where a 2-fold increase in size occurred within few hours from the time of the formation of the nanocolloidal dispersions. The morphology of the nanocolloidal dispersions was examined by TEM measurement and the particles were mostly found to be spherical in shape except for 10 and 30 μM AgBr solutions where the shape is rice-grain like.

ASSOCIATED CONTENT

Supporting Information

Expanded X-ray diffractograms, NMR spectra, and conductance profiles. This material is available free of charge via the Internet at http://pubs.acs.org.

AUTHOR INFORMATION

Corresponding Author

*Telephone: +919433334710. Fax: +913532699001. E-mail: akpanda1@yahoo.com.

Notes

The authors declare no competing financial interest.

ACKNOWLEDGMENTS

The work has been financially supported by the University Grants Commission (UGC), New Delhi, India. M.C. acknowledges the receipt of INSPIRE Fellowship from the Department of Science and Technology, Govt. of India. C.-H.C. and A.K.P acknowledge the financial assistance from the Confederation of Indian Industries, India and National Science Council, Taiwan (NSC100-2923-E-006-003-MY3) for sponsoring academic exchange program. We are grateful to CSS, JU for allowing us to carry out the calorimetric measurement. Valued guidance and suggestions from Prof. S. P. Moulik, CSS, JU is gratefully acknowledged.

REFERENCES

(1) Liu, X.-H.; Luo, X.-H.; Lu, S.-X.; Zhang, J.-C.; Cao, W.-L. A novel cetyltrimethyl ammonium silver bromide complex and silver bromide nanoparticles obtained by the surfactant counterion. *J. Colloid Interface Sci.* **2007**, *307*, 94−100.

(2) Sui, Z.; Chen, X.; Wang, L.; Chai, Y.; Yang, C.; Zhao, j. An Improved Approach for synthesis of Positively Charged Silver Nanoparticles. *Chem. Lett.* **2005**, *34*, 100−101.

(3) Sui, Z. M.; Chen, X.; Wang, L. Y.; Xu, L. M.; Zhuang, W. C.; Chai, Y. C.; Yang, C. J. Capping effect of CTAB on positively charged Ag nanoparticles. *Physica E* **2006**, 33.

(4) Serpone, N.; Khairutdinov, R. F.; Prashant, V. K. a. D. M. Application of nanoparticles in the photocatalytic degradation of water pollutants. *Stud. Surf. Sci. Catal.* **1997**, *103*, 417−444.

(5) Luo, X.; Morrin, A.; Killard, A. J.; Smyth, M. R. Application of Nanoparticles in Electrochemical Sensors and Biosensors. *Electroanalysis* **2006**, *18*, 319−326.

(6) Grieve, K.; Mulvaney, P.; Grieser, F. Synthesis and electronic properties of semiconductor nanoparticles/quantum dots. *Curr. Opin. Colloid Interface Sci.* **2000**, *5*, 168−172.

(7) Hosono, H. Recent progress in transparent oxide semiconductors: Materials and device application. *Thin Solid Films* **2007**, *515*, 6000−6014.

(8) Snezhko, A.; Prozorov, T.; Prozorov, R. Magnetic nanoparticles as efficient bulk pinning centers in type-II superconductors. *Phys. Rev. B* **2005**, *71*, 024527.

(9) Ramírez-Ortiz, J.; Ogura, T.; Medina-Valtierra, J.; Acosta-Ortiz, S. E.; Bosch, P.; Antonio de los Reyes, J.; Lara, V. H. A catalytic application of Cu2O and CuO films deposited over fiberglass. *Appl. Surf. Sci.* **2001**, *174*, 177−184.

(10) Louis, C. N.; Iyakutti, K.; Malarvizhi, P. Pressure dependence of metallization and superconducting transition in AgCl and AgBr. *J. Phys. Condens. Matter* **2004**, *16*, 1577−1592.

(11) Vinod, K.; Varghese, N.; Roy, S. B.; Syamaprasad, U. Significant enhancement of the in-field critical current density of the MgB_2 superconductor through codoping of nano-TiC with nano-SiC. *Supercond. Sci. Technol.* **2009**, *22*, 055009.

(12) Lee, T. G.; Ranot, M.; Seong, W. K.; Jung, S.-G.; Kang, W. N.; Joo, J. H.; Kim, C.-J.; Jun, B.-H.; Kim, Y.; Zhao, Y.; Dou, S. X. Fabrication of superconducting MgB_2 thin films on textured Cu(100) tape by hybrid physical and chemical vapor deposition. *Supercond. Sci. Technol.* **2009**, *22*, 045006.

(13) Lee, S.-J.; Jeong, J.-R.; Shin, S.-C.; Kim, J.-C.; Chang, Y.-H.; Chang, Y.-M.; Kim, J. D. J.-D. Nanoparticles of magnetic ferric oxides encapsulated with poly(D,L latide-*co*-glycolide) and their applications to magnetic resonance imaging contrast agent. *J. Magn. Magn. Mater.* **2004**, *272*−*276*, 2432−2433.

(14) Kruis, F. E.; Fissan, H.; Peled, A. Synthesis of nanoparticles in the gas phase for electronic, optical and magnetic applications--a review. *J. Aerosol Sci.* **1998**, *29*, 511−535.

(15) Li, Y.; Qian, F.; Xiang, J.; Lieber, C. M. Nanowire electronic and optoelectronic devices. *Mater. Today* **2006**, *9*, 18−27.

(16) Tanabe, K. Optical radiation efficiencies of metal nanoparticles for optoelectronic applications. *Mater. Lett.* **2007**, *61*, 4573−4575.

(17) Muller, J.; Sonnichsen, C.; von Poschinger, H.; von Plessen, G.; Klar, T. A.; Feldmann, J. Electrically controlled light scattering with single metal nanoparticles. *Appl. Phys. Lett.* **2002**, *81*, 171−173.

(18) Wang, C.; Ao, Y.; Wang, P.; Hou, J.; Qian, J.; Zhang, S. Controlled synthesis in large-scale of CdS mesospheres and photocatalytic activity. *Mater. Lett.* **2010**, *64*, 439−441.

(19) Zhao, S.; Su, D.; Che, J.; Jiang, B.; Orlov, A. Photocatalytic properties of TiO2 supported on SBA-15 mesoporous materials with large pores and short channels. *Mater. Lett. 65*, 3354−3357.

(20) Syoufian, A.; Satriya, O. H.; Nakashima, K. Photocatalytic activity of titania hollow spheres: Photodecomposition of methylene blue as a target molecule. *Catal. Commun.* **2007**, *8*, 755−759.

(21) Kumar, A.; Vemula, P. K.; Ajayan, P. M.; John, G. Silver-nanoparticle-embedded antimicrobial paints based on vegetable oil. *Nat. Mater.* **2008**, *7*, 236−241.

(22) Allen, N. S. E.; MicheleSandoval, GonzaloVerran; JoStratton; JohnMaltby; Julie. Photocatalytic Coatings for Environmental Applications. *Photochem. Photobiol.* **2005**, *81*, 279−290.
(23) Lanz, M.; Schürch, D.; Calzaferri, G. Photocatalytic oxidation of water to O2 on AgCl-coated electrodes. *J. Photochem. Photobiol. A: Chem.* **1999**, *120*, 105−117.
(24) Sambhy, V.; MacBride, M. M.; Peterson, B. R.; Sen, A. Silver Bromide Nanoparticle/Polymer Composites: Dual Action Tunable Antimicrobial Materials. *J. Am. Chem. Soc.* **2006**, *128*, 9798−9808.
(25) Oloffs, A.; Grosse-Siestrup, C.; Bisson, S.; Rinck, M.; Rudolph, R.; Gross, U. Biocompatibility of silver-coated polyurethane catheters and silvercoated Dacron material. *Biomaterials* **1994**, *15*, 753−758.
(26) Rao, C. N. R. *Nanomaterials Chemistry: Recent Developments and New Directions*; Wiley-VCH: New York, 2007.
(27) Shen, J.-N.; Zheng, X.-C.; Ruan, H.-M.; Wu, L.-G.; Qiu, J.-H.; Gao, C.-J. Synthesis of AgCl/PMMA hybrid membranes and their sorption performance of cyclohexane/cyclohexene. *J. Membr. Sci.* **2007**, *304*, 118−124.
(28) Rogez, J.; Garnier, A.; Knauth, P. Solution calorimetric investigation of AgCl-AgI ionic conductor composites at 298 K: observation of metastable AgI modifications. *J. Phys. Chem. Solids* **2002**, *63*, 9−14.
(29) Calandra, P.; Longo, A.; Marciano, V.; Turco Liveri, V. Physicochemical Investigation of Lightfast AgCl and AgBr Nanoparticles Synthesized by a Novel Solid-Solid Reaction. *J. Phys. Chem. B* **2003**, *107*, 6724−6729.
(30) Pfanner, K.; Gfeller, N.; Calzaferri, G. Photochemical oxidation of water with thin AgCl layers. *J. Photochem. Photobiol. A: Chem.* **1996**, *95*, 175−180.
(31) Kakuta, N.; Goto, N.; Ohkita, H.; Mizushima, T. Silver Bromide as a Photocatalyst for Hydrogen Generation from CH_3OH/H_2O Solution. *J. Phys. Chem. B* **1999**, *103*, 5917−5919.
(32) Yamashita, Y.; Aoyama, N.; Takezawa, N.; Yoshida, K. Characterization of Highly Active AgCl/Al2O_3 Catalyst for Photocatalytic Conversion of NO. *Environ. Sci. Technol.* **2000**, *34*, 5211−5214.
(33) Pourahmad, A.; Sohrabnezhad, S.; Kashefian, E. AgBr/nanoAlMCM-41 visible light photocatalyst for degradation of methylene blue dye. *Spectrochim. Acta, Part A* **2010**, *77*, 1108−1114.
(34) Proudfoot, C. N. *Handbook of Photographic Science and Engineering*, 2nd ed.; IS&T: Springfield, VA, 1997.
(35) Lahtinen, R. M.; Mertens, S. F. L.; East, E.; Kiely, C. J.; Schiffrin, D. J. Silver Halide Colloid Precursors for the Synthesis of Monolayer-Protected Clusters. *Langmuir* **2004**, *20*, 3289−3296.
(36) Jana, N. R.; Gearheart, L.; Murphy, C. J. Wet chemical synthesis of silver nanorods and nanowires of controllable aspect ratio. *Chem. Commun.* **2001**, 617−618.
(37) Chen, S.; Carroll, D. L. Silver Nanoplates: Size Control in Two Dimensions and Formation Mechanisms. *J. Phys. Chem. B* **2004**, *108*, 5500−5506.
(38) Nikoobakht, B.; El-Sayed, M. A. Evidence for Bilayer Assembly of Cationic Surfactants on the Surface of Gold Nanorods. *Langmuir* **2001**, *17*, 6368−6374.
(39) Husein, M. M.; Rodil, E.; Vera, J. H. A Novel Approach for the Preparation of AgBr Nanoparticles from Their Bulk Solid Precursor Using CTAB Microemulsions. *Langmuir* **2006**, *22*, 2264−2272.
(40) Hubert, F.; Testard, F.; Spalla, O. Cetyltrimethylammonium Bromide Silver Bromide Complex as the Capping Agent of Gold Nanorods. *Langmuir* **2008**, *24*, 9219−9222.
(41) Chun He, T. S.; Zhou, Y.; Shimizu, Y.; Masuda, M.; Koshizaki, N. Surfactant-Assisted Preparation of Novel Layered Silver Bromide-Based Inorganic/Organic Nanosheets by Pulsed Laser Ablation in Aqueous Media. *Adv. Funct. Mater* **2007**, *17*, 3554−3561.
(42) Jie Bai, Y. L.; Zhanga, C.; Lianga, X.; Yanga, Q. Preparing AgBr nanoparticles in poly(vinyl pyrrolidone) (PVP) nanofibers. *Colloids Surf., A* **2008**, *329*, 165−168.
(43) Kuai, L.; Geng, B.; Chen, X.; Zhao, Y.; Luo, Y. Facile Subsequently Light-Induced Route to Highly Efficient and Stable Sunlight-Driven Ag-AgBr Plasmonic Photocatalyst. *Langmuir* **2010**, *26*, 18723−18727.
(44) Wang, Z.; Liu, J.; Chen, X.; Wan, J.; Qian, Y. A Simple Hydrothermal Route to Large-Scale Synthesis of Uniform Silver Nanowires. *Chem.−Eur. J.* **2005**, *11*, 160−163.
(45) Chattopadhyay, K.; Das, T. K.; Majumdar, A.; Mazumdar, S. NMR studies on interaction of lauryl maltoside with cytochrome c oxidase: a model for surfactant interaction with the membrane protein. *J. Inorg. Biochem.* **2002**, *91*, 116−124.
(46) Kreke, P. J.; Magid, L. J.; Gee, J. C. 1H and 13C NMR Studies of Mixed Counterion, Cetyltrimethylammonium Bromide/Cetyltrimethylammonium Dichlorobenzoate, Surfactant Solutions: The Intercalation of Aromatic Counterions. *Langmuir* **1996**, *12*, 699−705.
(47) Terrill, R. H.; Postlethwaite, T. A.; Chen, C.-h.; Poon, C.-D.; Terzis, A.; Chen, A.; Hutchison, J. E.; Clark, M. R.; Wignall, G. Monolayers in Three Dimensions: NMR, SAXS, Thermal, and Electron Hopping Studies of Alkanethiol Stabilized Gold Clusters. *J. Am. Chem. Soc.* **1995**, *117*, 12537−12548.
(48) Ríos, H. E.; Sepúlveda, L. N.; Gamboa, C. I. Electrical conductivity of cationic polyelectrolytes in aqueous solution. *J.Polym. Sci., B: Polym. Phys.* **1990**, *28*, 505−511.
(49) Almgren, M.; Rydholm, R. Influence of counterion binding on micellar reaction rates. Reaction between p-nitrophenyl acetate and hydroxide ion in aqueous cetyltrimethylammonium bromide. *J. Phys. Chem.* **1979**, *83*, 360−364.
(50) Brice, B. A. Absorption Band Spectra of Silver Bromide and Silver Iodide Vapors. *Phys. Rev.* **1931**, *38*, 658−669.
(51) Rao, B. S.; Kumar, B. R.; Reddy, V. R.; Rao, T. S.; Chalapathi, G. V. Influence on optical properties of nickel doped cadmium sulphide. *Chalcogen Lett.* **2011**, *8*, 39−44.
(52) Madelung, O., *Semiconductors: data handbook*. Springer: Berlin, 2004.
(53) Mukherjee, S.; Chakraborty, M.; Panda, A. K.; Bhattacharya, S. C.; Moulik, S. P. Physicochemistry of Bis-alkyltrimethylammonium Dichromate, Tungstate and Molybdate amphiphiles: Synthesis, Characterization, Behaviors at the Air-water Interface and Self-aggregation in Aqueous Medium. *Colloids Surf. A: Physicochem. Eng. Aspects* **2011**, *388*, 1−11.
(54) Xia, Y.; Mokaya, R. On the synthesis and characterization of ZSM-5/MCM-48 aluminosilicate composite materials. *J. Mater. Chem.* **2004**, *14*, 863−870.
(55) Fosse, N.; Brohan, L. Thermal and Structural Investigations of the Bis-Dihexadecyldimethylammonium Dichromate. *J. Solid State Chem.* **1999**, *145*, 655−667.
(56) Swami, A.; Kumar, A.; Sastry, M. Formation of Water-Dispersible Gold Nanoparticles Using a Technique Based on Surface-Bound Interdigitated Bilayers. *Langmuir* **2003**, *19*, 1168−1172.